DOKUZ EYLUL UNIVERSITY
GRADUATE SCHOOL OF NATURAL AND APPLIED SCIENCES

INVESTIGATION OF SENSOR CHARACTERISTICS OF SOME CHROMOIONOPHORE STRUCTURES IN POLYMER AND SOL-GEL MATRICES

by

Özlem ÖTER

May, 2007

İZMİR

INVESTIGATION OF SENSOR CHARACTERISTICS OF SOME CHROMOIONOPHORE STRUCTURES IN POLYMER AND SOL-GEL MATRICES

A Thesis Submitted to the
Graduate School of Natural and Applied Sciences of Dokuz Eylul University
In Partial Fulfillment of the Requirements for the Degree of Doctor of Chemistry in
Chemistry, Applied Chemistry Program

by

Özlem ÖTER

May, 2007

İZMİR

Ph.D. THESIS EXAMINATION RESULT FORM

We have read the thesis entitled **"INVESTIGATION OF SENSOR CHARACTERISTICS OF SOME CHROMOIONOPHORE STRUCTURES IN POLYMER AND SOL-GEL MATRICES"** completed by **ÖZLEM ÖTER** under supervision of **ASSOCIATED PROFESSOR KADRİYE ERTEKİN** and we certify that in our opinion it is fully adequate, in scope and in quality, as a thesis for the degree of Doctor of Chemistry.

Doç. Dr. Kadriye Ertekin

Supervisor

Prof. Dr. Berrin Yenigül	Doç. Dr. Ünsal Gemici
Committee Member	Committee Member
Prof. Dr. Emür Henden	Prof. Dr. Kadir Pekmez
Jury Member	Jury Member

Prof.Dr. Cahit HELVACI
Director
Graduate School of Natural and Applied Sciences

ACKNOWLEDGMENTS

I would like to express sincere gratitute to my supervisor Associated Professor Dr. Kadriye Ertekin for providing the fascinating subject, for her valuable support during this thesis and for the great working conditions at our laborotory.

I gratefully acknowledge the extensive help of my colleagues Sibel Derinkuyu and Sevinç Zehra Yıldız.

Finally, I want to thank to my parents, my husband and my son for their tolerant attitude to my working effort during the elaboration of this dissertation and for their incessant support during all the years of my studies.

INVESTIGATION OF SENSOR CHARACTERISTICS OF SOME CHROMOIONOPHORE STRUCTURES IN POLYMER AND SOL-GEL MATRICES

ABSTRACT

In the first part of this work, two original optical CO_2 sensors were designed in very new matrix materials. The pH indicator dyes, bromothymol blue (BTB) and 8-hydroxypyrene-1,3,6-trisulfonic acid trisodium salt (HPTS) have been characterized in the ionic liquids of 1-methyl-3-butylimidazolium tetrafluoroborate (RTIL-I) and 1-methyl-3-butylimidazolium bromide (RTIL-II). The acidity constants (pKa) of the dyes have been determined and the spectral response of the sensor composition to gaseous and dissolved CO_2 has been evaluated.

In the second part, two original Fe^{3+} sensor designs were proposed. The photoluminescent properties of Fe^{3+} selective organic fluoroionophores, bis(7-methoxybenzofuran-2-il)ketoxime (BFK) and N-(4-dimethylaminophenyl)-3,5-di-t-butyl salicylaldimine (DBS) were investigated in different solvents (dichloromethane, tetrahydrofuran, toluene and ethanol) and in polymer matrices of polyvinylchloride (PVC) and ethyl cellulose (EC) by using absorption and emission spectrometry. The response to Fe^{3+} ions was evaluated in terms of the effect of pH, ionic strength and cross sensitivity to other cations.

In the third part, the oxygen sensitive dye of tris (2, 2'-bipyridyl) ruthenium (II) chloride was characterised in conventional and ionic liquid modified sol-gel matrices. The effect of sol-gel composition and ionic liquid amount to oxygen sensitivity were studied.

In all sensor designs, the response time, long-short term stabilities, reversibility, limit of detection, linear concentration range and repeatability characteristics also have been studied.

Keywords: optical sensors**,** ionic liquids, polyvinyl chloride, ethyl cellulose, sol-gel, carbon dioxide, iron

BAZI KROMOİYONOFOR YAPILARIN POLİMER VE SOL JEL MATRİKSLERDE SENSÖR ÖZELLİKLERİNİN İNCELENMESİ

ÖZ

Bu çalışmanın birinci bölümünde, çok yeni matriks materyaller kullanılarak iki orijinal CO_2 sensörü geliştirildi. pH indikatör boyalarından bromo timol mavisi (BTB) ve 8-hidroksipiren-1,3,6-trisülfonic asit trisodyum tuzu (HPTS) ilk defa olarak, 1-metil-3-butilimidazolyum tetrafloroborat (RTIL-I) ve 1-metil-3-butilimidazolyum bromür (RTIL-II) iyonik sıvıları içerisinde karakterize edildi. Boyaların asitlik sabitleri ve sensör bileşiminin gaz ve çözünmüş CO_2'e olan yanıtları değerlendirildi.

İkinci bölümde ise, iki orijinal Fe^{3+} sensörü geliştiridi. Fe^{3+}'e seçimli organik floroiyonoforlar, bis(7-metoksibenzofuran-2-il)ketoksim (BFK) ve N-(4-dimetilaminofenil)-3,5-di-t-butil salisilaldimin (DBS), farklı çözücülerde (diklorometan, tetrahidrofuran, toluen ve etanol) ve polivinilklorür (PVC) ve etil selüloz (EC) polimer matrikslerinde, absorpsiyon ve emisyon spektroskopisi kullanılarak araştırıldı.

Üçüncü bölümde ise, oksijene duyarlı boya, tris (2, 2'-bipiridil) rutenyum (II) klorür, konvensiyonel ve iyonik sıvı modifiye sol-jel matrikslerde karakterize edildi. Sol-jel içeriğinin ve iyonik sıvı miktarının oksijen duyarlılığına olan etkisi çalışıldı.

Tüm sensör tasarımlarında, sensör yanıtı, uzun-kısa dönem kararlılığı, rejenere edilebilirliği, tayin limiti, doğrusal çalışma aralığı ve tekrarlanabilirlik özellikleri belirlendi.

Anahtar kelimeler: optik sensörler, iyonik sıvılar, polivinil klorür, etil selüloz, sol-jel, karbon dioksit, demir

CONTENTS

Sayfa

CHAPTER ONE

INTRODUCTION

Chemical sensors

Different definitions of sensors are given in the literature and the discussion about the features and the requirements of sensors is still going on. The following definition is given by an IUPAC commission on sensors.

"A chemical sensor is a device that transforms chemical information ranging from the concentration of a spesific sample component to total composition analysis into analytical usefull signal. The chemical information mentioned above may originate from a chemical reaction of the analyte or from a physical property of the system invesitigated. A chemical sensor is an essential component of an analyser. In addition to the sensor, the analyser may contain that perform the following functions: sampling, sample transport, signal processing, data processing" (Wolfbeis, 1991).

Chemical sensors have been widely used in such applications as critical care, safety, industrial hygiene, process controls, product quality controls, human comfort controls, emissions monitoring, automotive, clinical diagnostics, home safety alarms, and, more recently, homeland security. In these applications, chemical sensors have resulted in both economic and social benefits. Chemical sensors have a chemical or molecular target to be measured. Sensors can be classified in many different ways. They may be classified according to the principle of operation of the transducer in two main groups as "physical" and "chemical" sensors. They also can be divided into sub groups as optical, electrochemical, electrical, mass sensitive, magnetic and thermometric devices. They can also be classified as direct and indirect sensors or as reversible or non-reversible ones and respect of their applications or sizes.

So many different kinds of sensors are commercially available; some of them are listed below.

Semiconducting oxide sensors

The heated metal oxide sensor is probably the most investigated and widely produced chemical sensor. The working principle of this type of sensor is that the resistance of the metal oxide semiconductor changes when it is exposed to the target gas because the target gas reacts with the metal oxide surface and changes its electronic properties. New materials such as the rare earth oxides or gallium oxide are being used as the active sensor elements. Recent reviews include many examples of this type of gas sensors (Göpel & Schierbaum, 1995; Shimizu & Egashira, 1999).

Electrochemical sensors (liquid electrolyte)

There are two major sensor classes that use liquid electrolytes: amperometric and potentiometric sensors. The earliest example of an amperometric gas sensor, the Clark oxygen sensor used for the measurement of oxygen in the blood is more than 40 years old. The amperometric sensor produces current signal, which is related to the concentration of the analyte by Faraday's law and the laws of mass transport (Cao, Shakin & Sun, 1992).

Ion-selective electrodes

Ion-selective electrodes (ISEs) belong to potentiometric chemical sensor group and are most often based on the measurement of the interfacial potential at an electrode surface caused by a selective ion exchange reaction. The wellknown glass pH electrode is a typical ISE (Galster, 1991).

1.1.4 Solid electrolyte sensors

Using a solid electrolyte to replace the liquid electrolyte in an electrochemical sensor, one can construct a solid electrolyte electrochemical sensor. Solid electrolyte sensors are typically designed to operate at high temperature and can operate in either a potentiometric or amperometric mode. Over the past ten years, two potentiometric designs have evolved: surface-modified solid electrolyte gas sensors and mixed potential gas sensors (Göpel, Reinhardt & Rösch, 2000; Mukundan, Brosha, Brown & Garzon, 1999; Yamazoe & Miura, 1996; Weppner, 1996).

1.1.5 Optical chemical sensors and optodes

They have become an important area of research since their introduction two decades ago. Optical sensors are compact and ideally suited to miniaturization while at the same time they are resisting to electrical interference and utilize the simplicity of photometric measurements. Many optical chemical sensors utilize color complexing or redox reagents immobilized in suitable polymeric membrane (Ensafi & Bakhshi, 2003; Ensafi & Aboutalebi, 2005). Optical chemical sensors can be classified in three groups: Probes, fiber-optic chemical sensors and non fiber optic chemical sensors. Sensors which produce an irreversible response to the presence of analytes are referred to as ‘probes’. If the signal is reversible and continuous then it is called as sensor. Fiber optic sensors are based on optical spectroscopy performed on sites inaccessible to conventional spectroscopy, over large distances, or even on several spots along the fiber.

1.1.5.1 Advantages of chemical optical sensors

There are numerous advantages of chemical optical sensors described below.

- Optical sensors do not require a reference signal as in potentiometry which increases the cost and causes perturbations.

- The ease of miniaturization allows the development of very small, light and flexible sensors much smaller than any electrochemical sensor especially for sensing in clinical chemistry and medicine.
- Low loss optical fibers allow transmittance of optical signals over wide distances. Remote sensing makes it possible to perform analyses when samples are hard to reach, dangereous, too hot or too cold, in harsh environments or radioactive.
- They are not influenced from electrical interferences, strong magnetic fields and surface potentials. On the other hand fibers do not present a risk for health since they do not disperse any electrical signal.
- Analyses can be performed in almost real time without any need of sampling.
- Since several fiber sensors placed in different sites can be coupled to one fluorimeter, the method allows multiple analyses with a single control instrument.
- Coupling of small sensors for different analytes to produce a sensor bundle of small size allows simultaneous monitoring of various analytes without any interference.
- Extremely small sample volume is not a disadvantage as in polarographic electrodes.
- Fiber optical sensing is a non-destructive analytical method.
- Fibers are manufactured from nonrusting materials, so that they have excellent stability. They are also resistant to radiation.
- In practice, a single fiber may be used to assay several analytes at the same time.
- Especially sensors based on dynamic fluorescence quenching have a useful dynamic range often larger than that of electrochemical sensors.
- Most fiber sensors can be employed over a wider temperature range than electrodes.

1.1.5.2 Disadvantages of chemical optical sensors

Besides these advantages optical sensors also have some disadvantages:

- Ambient light can interphere so optical isolation is nesessary.
- They have limited long term stability because of photobleaching and wash out. The signal drifts due to these reasons can be compensated by using ratiometric method or time resolved measurements.
- The fiber optics used at present have impurities that can give background absorption, fluorescence and Raman Scatter. Low-priced (plastic) fibers are confined to visible range, whereas UV light is transmitted by rather expensive quartz fibers only. Because of this sensing dyes that can be excited at visible range are preferred in sensor designs.
- More selective indicators have to be found for various important analytes and the immobilization techniques have to be improved.

In summary, optical sensors offer a variety of new aspects. Despite several limitations, they have the potential of becoming an attractive alternative to other sensing methods and to perform diognastic, environmental or clinical functions beter, faster, more accurate or less expensive than existing approaches (Wolfbeis, 1991).

1.1.5.3 Fiber optic sensors (FOS)

Fiber optic sensors are a class of sensors that use optical fibers (Figure 1.1) to detect anaytes. Fiber-optic cable consists of a plastic or glass core surrounded by a layer of cladding material. Principle of optical fibre is total internal reflection of light through the core of the fiber. Light is generated by a light source and is sent through an optical fiber. Total internal reflection is the complete transmission of light through fiber optics, which states that all the light striking a boundary between two media will be totally reflected. That is, no light energy will ever be lost across the boundary. This principle pertains only when two conditions are met:

- The critical angle is less than the angle of incidence for the particular combination of materials (see Figure 1.1). The materials in this case are the core and the cladding of the optical fiber.
- The light is in the denser medium and approaching the less dense medium. The cladding material is less dense than the core material, and as a result has a lower index of refraction.

The light then returns through the optical fiber and is captured by a photo detector. Some optical fiber sensors use a single optical fiber while others use separate optical fibers for the light source and for the detector.

Optical fiber can be made of either glass or plastic. Glass optical fibers consist of a bundle of very thin glass strands, each typically measuring 0.051 mm (0.002 inches) diameter. A flexible stainless steel–armored sheath is usually added to protect the bundle of cladded fibers, but for some applications a polyvinyl-chloride jacket (PVC) is used. Plastic fiber-optic cable usually consists of a single strand typically 0.254–1.52 mm diameter. These fibers are flexible, and excellent for applications that require repeated flexing as well as for use in extremely tight areas.

There are three general classes of fiber optic sensors (Figure 1.2). The first type is completely passive.

A spectroscopic method can be used to detect individual types of analytes. This method involves sending a light source directly through the optical fiber and analyzing the light that is reflected or emitted by the anayte. The refractive index of the material at the tip of the optical fiber can be used to determine what phases (vapor, water, or NAPL) are present.

A second class of fiber optic sensors consists of a fiber optic sensor with a chemically interacting thin film attached to the tip. This film is formulated to bind with certain types of chemicals. Analyte concentration can be found by measuring

the color of the thin film, the change in refractive index, or by measuring the flourescing of the film.

The third type of fiber optic sensors involves injecting a reagent near the sensor. This reagent reacts either chemically or biologically with the anayte. The reaction products are detected to give an estimate of the analyte concentration.

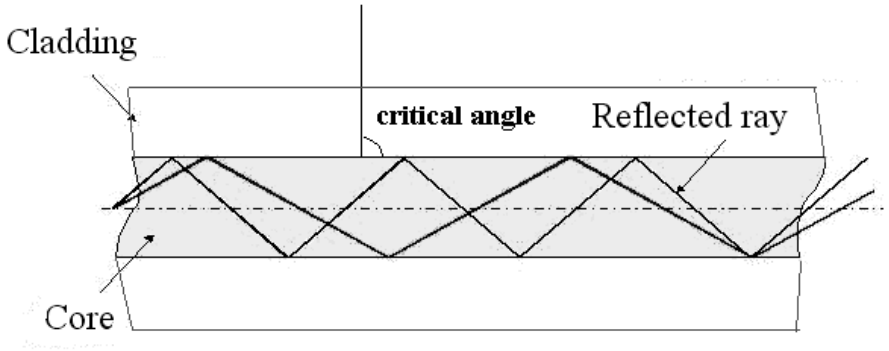

Figure 1.1 Structure of an optical fiber.

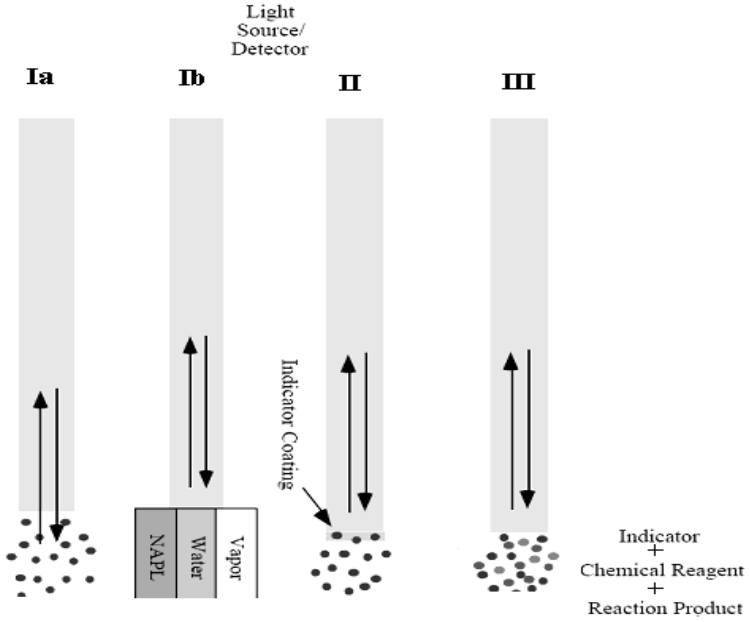

Figure 1.2 Three types of fiber optic sensors Ia: spectroscopic measurement of fluorescent or phosphorescent anayte; Ib: refractive index changes due to vapor, water and NAPL; II: indicator is coated at the tip of the optic fiber and changes color due to the binding with analyte; III: a chemical reaction is considered between the added reagent and the analyte. Reaction product is measured.

The fiber-optic assemblies are either in individual or bifurcated form. Fiber-optic through-beam mode requires two cables. One is attached to the emitter of the fiber optic sensor and is used to transmitte light energy to a sensing location. The other is attached to the receiver of the remote sensor and is used to transmitte light energy from the sensing location back to the remote sensor. As with standard through-beam photoelectric sensing, the emitter and detector cables are positioned opposite each other.

In constrast to an individual cable, a bifurcated cable combines the emitter and the receiver cable assemblies into one assembly. The emitter and receiver strands are laid side-by-side along the length of the cable and are randomly mixed at the sensing point, an ideal configuration for applications that require a compact sensing tip. When an object is in front of the sensing tip of the bifurcated cable, light from the emitter cable reflects off the object and back into the receiver of the remote sensor via the receiver cable, and detection is achieved.

Fiber optics serves analytical sciences in several ways. First, they enable optical spectroscopy to be performed on sites inaccessible to conventional spectroscopy, over large distances, or even on several spots along the fiber. Second, fiber optics, in being waveguides, enables less common methods of interrogation, in particular evanescent wave spectroscopy. Fibers are available now with transmissions over a wide spectral range.

Major fields of applications are in medical and chemical analysis, molecular biotechnology, marine and environmental analysis, industrial production monitoring and bioprocess control, and the automotive industry.

1.1.5.4 Optical measurement techniques

- Amplitude change based ones
  - absorption
  - fluorescence, luminescence
  - spectral-dependent variations of absorption/fluorescence

  - refractive index
  - scattering
- Time resolved changes (luminescence, absorption)
- Polarization changes
- Phase changes – interferometry

1.1.5.4.1 Spectroscopic methods (Absorption and fluorescence method. Most optical and fiber-optic sensors are based on absorption and fluorescence methods. Absorption method is simple and easy to use but it is not very sensitive, requiring the use of a high concentration of the indicator and/or a thick sensing layer. Fiber-optic sensors based on absorption method are difficult to miniaturize, especially for transmission mode in which a sensing element has to be placed between two face to face fibers. Reflection configuration, sometimes using a reflector, is often employed to overcome this problem (Motellier, Michels, Dureault & Toulhoat, 1993). In addition, evanescentwave (EW) or attenuated total reflection modes can also be used (Egami, Suzuki, Sugihara, Fujimura & Okamoto, 1997; Yang & Saavedra, 1995). In contrast, fluorescence method is more sensitive and can be used for small-size sensors and/or low concentration of indicators (Tan, Shi & Kopelman, 1992; Tan, Shi, Smith, Birnbaum & Kopelman, 1992). Fiber-optic sensors, based on distal end or EW excitation, are easier to design and miniaturize (Song, Parus & Kopelman, 1997).

Measurement with fiber-optic sensors often suffers from instabilities resulting from decrease in the concentration of the indicator due to leaching and photobleaching, fluctuations in the intensity of light source and variations in light attenuation through the optical fiber due to changes in the degree of bending. For absorption method, such instabilities can be accounted for by measuring absorbance at multiple wavelengths, e.g. at peak absorption (to respond to analyte at isosbestic point to account for indicator concentration) and at zero absorption (as the baseline to account for light intensity) (Motellier et al., 1993). For fluorescence sensors, the ratiometric method (i.e. the use of the ratio of two fluorescence intensities) continued to be used to overcome the above problem (Grant & Glass, 1997; Leiner & Wolfbeis,

1991; Song et al., 1997; Xu, Rollins, Alcala & Marchant, 1998). The problem can also be solved by measuring fluorescence lifetime as the analytical signal since the decay of fluorescence is insensitive to both the concentration of indicator and the intensity of excitation light (Draxler, Lippitsch & Leiner 1993; Szmacinski & Lakowicz, 1993; Thompson & Lakowicz, 1993).

1.2 Sensors for gases

The use of simple optical technology to devise reflective sensor devices for the monitoring of dissolved and atmospheric gases and vapours are under investigation. Current investigations include the detection of traces of toxic gases such as NH_3, H_2S, Cl_2, SO_2, HCHO, HCl, etc. and also other gases such as O_2 using chemically-sensitive matrices that can be interfaced to the optical fibres to produce devices that will have probe configurations and employ reflectance or fluorescence detection techniques at the chemical transducer. Recent works include the investigation into organic and organometallic optical thin films for gas sensors. Thin film devices are produced by sputtering, vacuum sublimation and Langmuir-Blodgett techniques. Multi-gas and vapour sensing systems are being studied which utilise differences in spectra and chemical kinetics, in conjunction with novel signal processing techniques.

1.2.1 Optical oxygen sensors

Optical sensors for oxygen based on dynamic quenching of luminescence have had particular success in the past years, and they are now being improved and adapted to specific problems. A plastic fiber-based optical sensor array has been introduced for the in situ measurement of ground air oxygen concentrations in a lignite mine tailing affected by acid mine drainage formation (Koelling, Hecht & Holst, 2002). The instrument evaluates the oxygen dependent change of the luminescence lifetime of an oxygen indicator using a phase modulation technique. Optical oxygen sensors generally are based on the fluorescence of a ruthenium complex in a polymer matrix to measure the partial pressure of oxygen. This kind of sensors generally uses the below working mechanism:

1. The pulsed LED lamp sends light to an optical fiber.
2. The optical fiber carries the light to the probe. The distal end of the probe tip consists of a thin layer of a hydrophobic polymer material. A ruthenium complex is trapped in the matrix, effectively immobilized and protected from water.
3. The light from the LED excites the ruthenium complex at the probe tip.
4. The excited ruthenium complex fluoresces, emitting energy.
5. If the excited ruthenium complex encounters an oxygen molecule, the excess energy is transferred to the oxygen molecule in a non-radiative transfer, decreasing or quenching the fluorescence signal. The degree of quenching correlates to the level of oxygen concentration or to oxygen partial pressure in the film, which is in dynamic equilibrium with oxygen in the sample.
6. The energy is collected by the probe and carried through the optical fiber to the spectrometer. The analog data will be converted to digital data that the PC can understand.

1.2.2 Optical CO_2 sensors

The present CO_2 sensing techniques are based on infrared (IR) absorptiometry, electrochemical Severinghouse electrode and optical sensors. However, in spite of the sensitiveness of the IR absorptiometry sensor, it is subject to strong interference from water vapour and is an expensive, bulky and not particularly robust system. On the other hand, Severinghouse electrode detects CO_2 due to the changes in the pH of the solution and is markedly affected from electromagnetic disturbances, from interferent asidic and basic gases and from osmotic pressure in the sample. Recently, the optical CO_2 sensors based on the absorbance or fluorescence change of pH indicator have been developed. They offer several attractive features which include electrical isolation, reduced noise interference, ability of miniaturization and remote sensing. Amao & Nakamura (2004) designed an optical CO_2 sensor based on the overlay of the CO_2 induced absorbance change of pH indicator dye α-naphtolphytalein with the fluorescence of tetraphenylporphyrin using ethyl cellulose and polystyrene membrane and obtained 53.9 % signal change from 100 % N_2 to 100 % CO_2. Müller & Hauser (1996) performed an optode for measurements of low

concentrations of dissolved CO_2. The usefull measuring range was found from 10^{-5} up to 10^{-3} M H_2CO_3 which contributes to 10^{-3}-10^{-1} M $NaHCO_3$ concentration and the response and recovery times were found as 6 and 20 minutes respectively.

Neurauter, Klimant & Wolfbeis (1999) measured dissolved and gaseous CO_2 with ethyl cellulose made sensor films and found the detectable CO_2 level between 0-30 hPa. The cross sensitivity to oxygen was the most crucial factor in this sensors performance. If stored in air and exposed to sunlight the sensors were destroyed within a few days.

Water-dissolved carbon dioxide was quantified with a reservoir type capillary microsensor (Ertekin, Klimant, Neurauter & Wolfbeis, 2003). A pH indicator in the form of its ion pair with a quaternary ammonium base and a buffer in an ethyl cellulose matrix, all placed at the tip of an optical fiber, served as the sensing chemistry. The dynamic range was between 1 and 20 hPa pCO_2. The response time is 15 s, and the detection limit is 1 hPa pCO_2. The sensitivity of fiber-optic CO_2 sensors utilizing indicator dyes was studied once more. Gastric CO_2 can be monitored with optical fibers of similar design (Baldini et al., 2003) and the results compare favorably with those obtained with a commercial (non-fiber-optic) instrument. A sol-gel-based optical carbon dioxide sensor that employs dual luminophore internal referencing and is intended for application in food packaging technology was described (Bueltzingsloewen et al., 2002). A fluorescent pH indicator was immobilized in a hydrophobic organically modified silica matrix, along with cetyltrimethylammonium hydroxide as an internal buffer. Fluorescence is measured in the phase domain by means of the dual luminophore referencing scheme. The resolution is <1%, and the limit of detection is 0.08% CO_2. Oxygen cross-sensitivity is minimized by immobilizing the reference luminophore in polymer nanobeads.

1.3 Optical Chemical Sensors for the Determination of Heavy Metal Ions

(Kuswandi, 2000)

Recent years, chemical sensors for heavy metal ions have seen an increasing interest. A ‘metal sensor’ is described as a device which is capable of responding to

the presence of a heavy metal ion in a reversible and continuous manner. Sensors which produce an irreversible response to the presence of heavy metal ions are referred to as 'metal probes'. The optical properties of a material may be measured by the conventional methods of absorbance, fluorescence and reflectance spectroscopy, and in various formats such as test strips and disposable tips, while employing optical waveguides such as optical fibres, integrated optics and capillary-type devices (Oehme & Wolfbeis, 1997).

1.3.1 Sensors based on intrinsic optical properties

So far, the optical sensors discussed have been based on an immobilised reagent which acts as a chemical transducer for the desired analyte. However, there are sensors which rely on the intrinsic optical properties of heavy metal ions. In this case, quantification is achieved via the measurement of the absorbance (UV-visible) or luminescence of the sample solution. Suitable analytes for this mode of measurement include the transition metal ions Fe (II), Co (II), Cu (II), Cr (III), Ni (II) (Andrew & Worsfold, 1994), the lanthanide ions europium and terbium, and the radionuclides uranium and plutonium. Such sensors lack specificity since they are subject to interference from any species absorbing at the same wavelength as the analyte, and sample turbidity and changes in refractive index will also have a significant effect. Absorbance based analysis is applicable only at relatively high concentrations of heavy metal ions because their molar absorptivities are low, typically 10-100 mol^{-1} dm^3 cm^{-1}.

1.3.2 Sensors based on chromophores

The majority of heavy metal ion sensors are based on the use of an indicator dye which undergoes a binding reaction with the ions. This reaction is accompanied by a change in the absorbance or fluorescence of such chelators. In other words, an indicator acts as a transducer for the chemical species that cannot be determined directly by optical means. This has an important implication in that it is the concentration of the indicator species that is quantified rather than the analyte itself.

Many indicators cannot be used in optical sensors because of unfavourable analytical wavelengths, poor photostability, low molar absorptivity or the need for additional reagents. Most of them bind with the metal ion irreversibly or only at low or high pH so they can not be used for continuous sensing at near neutral pH. Upon binding with the metal ion, most indicators undergo a change in colour, with one band appearing as the other disappears, rather than an intensity change of one single band.

1.3.3 Sensors based on fluorophores

In contrast to chromogenic reagents, fluorescent indicators are of the yes/no type in that only one of the species (the complexed or the noncomplexed) is fluorescent. Fluorescent indicators frequently provide improved sensitivity (which is important in miniature sensors) and also selectivity because it is unlikely that an interfering species would have the same absorbance and emission as the analyte complex. Fluorimetry (and luminescence spectrometry in a wider sense) also offers a broad variety of spectroscopic techniques including the measurement of lifetime, polarisation and energy transfer. An important group of indicators is based on the quenching of luminescence by heavy metals and transition metals. In the case of static quenching, the quencher interacts with the fluorophore in its ground state. In dynamic (collisional) quenching, the interaction between the metal ion (quencher) and the fluorophore occurs in the excited state only and leads to a reduction in both the emission intensity and the decay time. The photophysical process of dynamic quenching is fully reversible, that is, the indicator is not consumed. Hence, quenchable fluorophores comprise an important class of indicators for reversible sensors. Most heavy metals quench by virtue of the heavy atom effect, and the quenching efficiency of many transition metals, in particular Fe (III), Co (II) and Ni (II) is thought to be due to their numerous unpaired spins.

1.3.4 Sensors based on ionophores

Due to limitations of conventional reagents (mainly caused by their high stability constants) there has been an increase in the use of ionophores in optical chemical sensors. Ionophores are non-coloured ion-complexing organic molecules, or lipophilic ion carriers, which are capable of reversibly binding to ions and transporting them across organic membranes by carrier translocation. Their most widespread application so far is in ion-selective membranes for alkali and alkaline earth metal ions, the best example being valinomycin, a highly specific neutral carrier for potassium ions (Hisamoto, Miyashita *et al.*, 1995; Wolfbeis & Schaffar, 1987). Several sensing schemes are used in which ionophore selectivity is combined with an optical readout, namely (a) the introduction of chromogenic or fluorogenic moieties into ionophores to obtain so-called chromoionophores or fluoroionophores, (b) the combination of ionophores with potentially sensitive indicators, (c) the extraction of ions into membranes using neutral ion carriers (ion exchange), and (d) the extraction of an ion along with a counterion into a membrane phase (coextraction). Recognition of heavy metals is accomplished by neutral ionophores capable of binding the metal ion, while the optical signal is provided by a proton selective chromoionophore. On extraction of a heavy metal ion (of charge n) into the membrane, n protons are released by the chromoionophore, resulting in a change in its colour or fluorescence. The interesting feature of this approach is that it is only the carrier for a specific heavy metal ion that needs to be varied, while the chromoionophore can remain the same.

1.4 Luminescence

1.4.1 Mechanism of Luminescence (Lakowicz, 1993; Parker, 1968; Schmidt, 1994)

Luminescence means emission of light by electronically excited atoms or molecules. Electronic excitation requires the supply of energy. Various kinds of luminescence, such as electroluminescence, chemiluminescence, thermoluminescence and photoluminescence, are known and called by the source from which energy is derived. In the case of photoluminescence (fluorescence and

phosphorescence) the energy is provided by the absorption of infra-red, visible or ultra-violet light. Two models are necessary to describe the interaction of light with matter: In the one light is regarded as a succession of waves, in the other as a collection of particles. The latter was introduced by Planck, who showed that radiant energy can only be absorbed in definite unites or quanta. The energy quantum E, is defined as

$$E = h\nu = h\frac{c}{\lambda} \qquad (1.1)$$

where ν is the frequency, h is Planck's constant ($6.626 \cdot 10^{-34}$ Js), λ the wavelength, and c the constant velocity of light in vacuum ($2.998 \cdot 10^{8}$ ms^{-1}). The absorption and emission of light is illustrated by Jablonski level diagram, shown in Figure 1.3. According to the Boltzmann distribution, at room temperature the valance electrons are in the lowest vibration level (ν=0) of the ground electronic state. A transition of these electrons from the ground state (level 0 of S_0) to higher energy levels takes place on absorption (a) of light. The Franck-Condon principle states that there is approximately no change in nuclear position and spin orientation, because absorption of light occurs in about 10^{-15} s. Therefore, the electronic transition is represented by a vertical line. Molecules excited to an upper vibrational level of any excited state rapidly lose their excess of vibrational energy by collision with solvent molecules, and falls to the lowest vibrational level. Molecules in the upper excited states (S_2, S_3, ...) relax by internal conversion (IC), radiationless to the lowest excited singlet state (S_1) within 10^{-12} s. Transition from this level to the vibration levels of the ground state can take place by emitting photons (f). A portion of the excited molecules may return to the ground state by other mechanisms, such as electron transfer, collision, intersystemcrossing (ICS), internal conversion or chemical reaction. Fluorescence emission occurs spontaneously, again in accordance with the Franck-Condon principle, if the radiationless transition lifetime is sufficiently long. The radiative lifetime of fluorescence lies between 10^{-9} s for spin allowed transitions ($\pi^* \pi$) to 10^{-6} for less probable transitions (π^* n). Molecules in the lowest excited state (S_1) can also undergo conversion to the first triplet state (T_1) by intersystem crossing (ISC).

This process requires a time of the same order of magnitude as fluorescence radiation lifetime and therefore competes with fluorescence. Although radiative transitions between states of different multiplicity are spin forbidden, these transitions do take place with low probability compared with singlet-singlet, or triplet-triplet transitions. Emission from the first triplet state (T_1) to the ground state is termed phosphorescence, and usually shifted to higher wavelengths than fluorescence. The radiation lifetime for this transition is about 10^{-2} to 10^{+2} s.

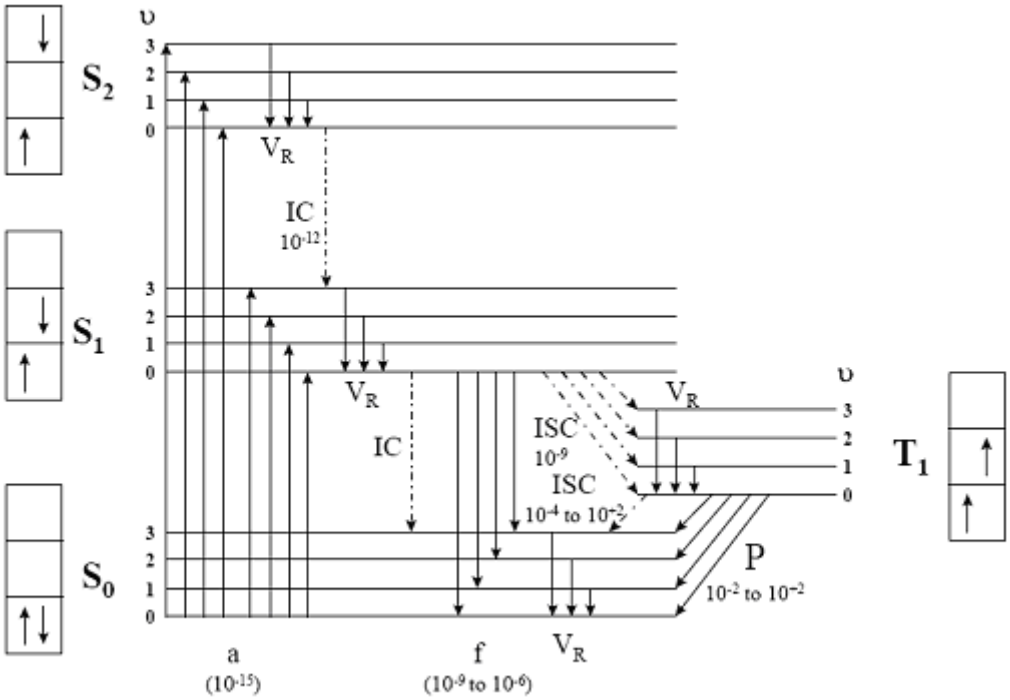

Figure 1.3 Jablonski diagram with the reciprocal rates of transition in [s] (taken from Mayr, 1999)

1.4.2 Stoke's Shift (Lakowicz, 1993; Parker, 1968; Schmidt, 1994)

The law of Stokes states that the fluorescence and phosphorescence is shifted to higher wavelengths relatively to absorption (Stoke's Shift). The explanation is provided by the Jablonski diagram. As already mentioned, emission usually occurs form the lowest excited state, but higher excited state are reached by absorption. The radiationless vibrational relaxation (V_R) and internal conversion (IC) involves a loss

of energy which is reflected in a shift to emission bands of lower energy. Furthermore, molecules generally decay to excited vibrational levels of S_0.

1.4.3 Quantum Yield (Lakowicz, 1993; Parker, 1968; Schmidt, 1994)

A molecule in the relaxed state S_1 (the lowest excited state) can return to the ground state, radiationless or by the emission of fluorescence. The fluorescence quantum yield is the ratio of the number of photons emitted to the number absorbed expressed by the rate constants Γ and k, respectively. Hence, the quantum yield can be written as

$$\Phi = \frac{\Gamma}{\Gamma + k} \qquad (1.2)$$

The quantum yield can be close to unity if the radiationless rate of deactivation (k) is much smaller than the rate of radiative emission ($k << \Gamma$).

1.4.4 Solvatochromism (Lakowicz, 1993; Schmidt, 1994; Reichardt, 1988)

The excitation and emission spectra of many chromophores are sensitive to the polarity of their surrounding environment. A hypsochromic (or blue) shift of the absorption band, with increasing solvent polarity is called negative solvatochromism. The corresponding bathochromic (or red shift) is entitled positive solvatochromism. Obviously, solvatochromism depends on the solvation of the ground and first excited state of the chromophore. If the ground state is better stabilised by increasing solvent polarity than the excited state, negative solvatochromism is observed. Better stabilisation of the excited molecule relative to that in the ground state, with increasing polarity, leads to positive solvatochromism. The solvent polarity does not only affect the absorption spectra, but also the emission spectra. The mechanism is illustrated in Figure 1.4. According to the Franck-Condon principle nuclei do not move during the timespan of an electronic transition (10^{-15} s). Therefore, the excited molecule (B) has the same solvation pattern as the molecule in the ground state. Excited molecules have a lifetime in order of about 10^{-8} s. The solvent molecules re-orientate within 10^{-10} s resulting in relaxed excited state, with a solvation shell in

equilibrium to this state. From this relaxed excited state (C) light is emitted. By analogy, the orientation of the solvent molecules does not change during the emission (D), due to Franck-Condon principle. Re-orientation of the solvent molecules follows, resulting in an equilibrium ground state (A). The interaction of a molecule with solvent upon excitation and emission, can be described by a change of the molecule´s dipole moment in the ground (μ) and excited state (μ*). A positive solvatochromism is observed if the dipole moment is increased during excitation, while decreasing dipole moment results in negative solvatochromism.

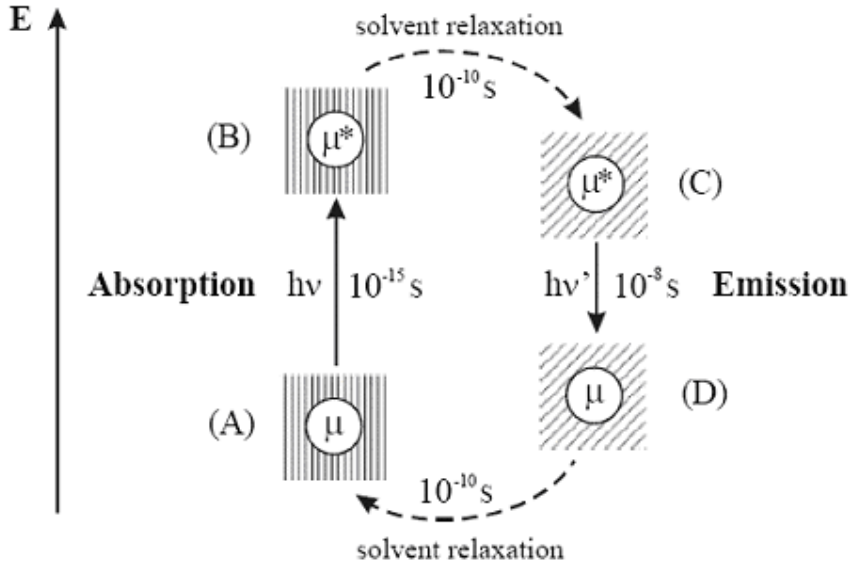

Figure 1.4 Effect of the solvent on the energy of a dipole (μ) upon excitation and emission. Different solvatation shells are illustrated by squares filled with different patterns (taken from Mayr, 1999).

1.5 Materials and Polymers in Optical Sensing (Mohr, G. J., 2006)

1.5.1 Requirements for Sensor Polymers/Materials

Requirements of sensor matrix materials can be listed as follows:

- Solubility of indicator chemistry in polymer matrix
- Selectivity and sensitivity (solubility of the analyte, free analyte diffusion)
- Good operational lifetime and shelf-life
- No crystallisation/migration/reorientation of components
- No ageing effects

- Stability at elevated temperatures (sterilisability)
- Stability against ambient light
- Stability against chemicals (acids, bases, oxidants)
- Mechanical stability
- Transparency for light
- No intrinsic colour/luminescence of the polymer matrix
- Biocompatibility (no toxicity of components)

1.5.2 Types of Polymers Used in Optical Sensing

1.5.2.1 Lipophilic Polymers and Plasticizers

Polymers that have a high glass transition temperature (Tg) are brittle (Figure 1.5). They require plasticizers to make them flexible. Furthermore, the high density/rigidity of the polymer chains (without plasticizers) hinders diffusion of ions and gases in the polymer matrix. Therefore, plasticizer to polymer ratios of up to 2:1 is required. While polyvinylchloride (PVC) is soluble in tetrahydrofuran and cyclopentanone, polymers such as methacrylate, polystyrene and polyvinyl acetate are also soluble in ethyl acetate, ethylmethyl ketone, dichloromethane, etc.

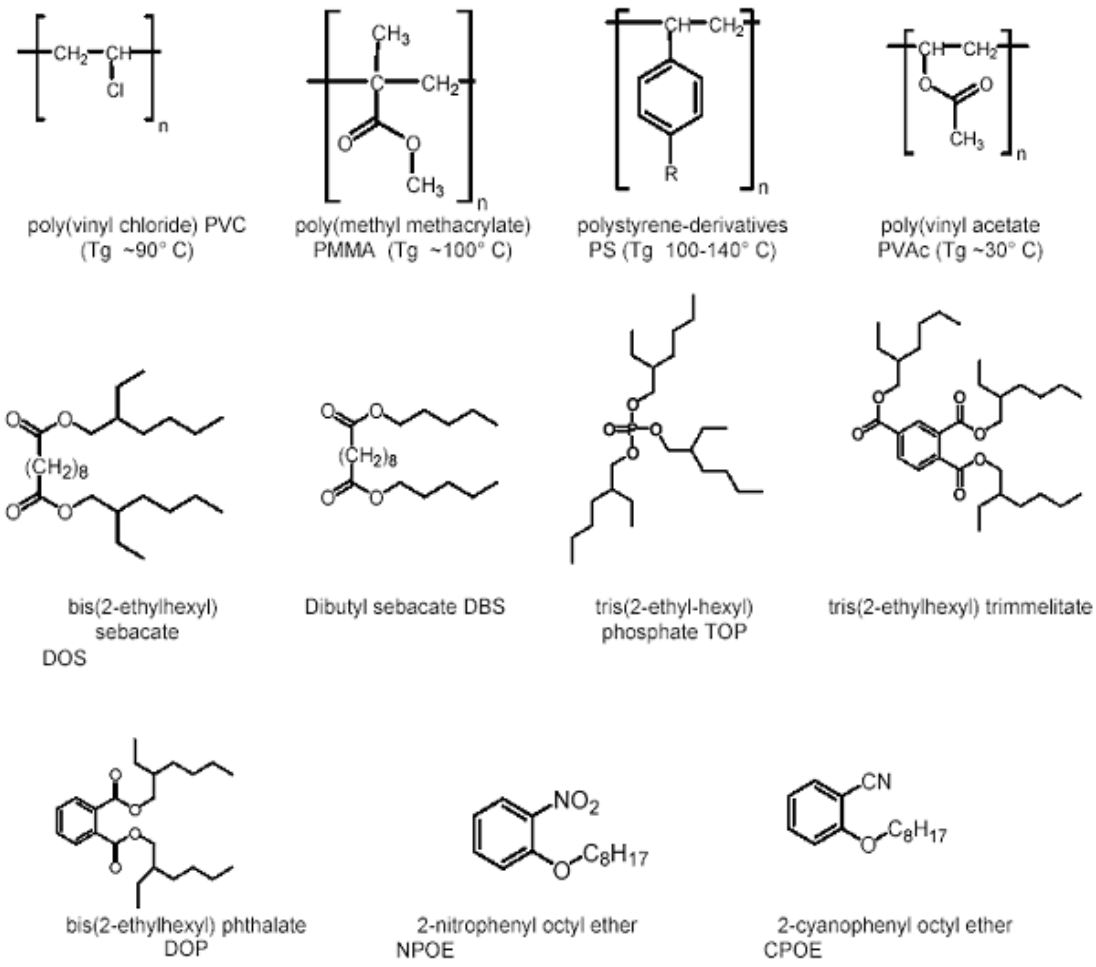

Figure 1.5 Lipophilic Polymers and Plasticizers that have a high glass transition temperature (taken from http://www2.uni-jena.de/~c1moge/Mohr/ASCOS2002.pdf).

Polymers with low glass transition do not require plasticizers (Figure 1.6). However, these compounds are often apolar and, consequently, bad solvents for polar ligands, ionophores, dyes, and analytes.

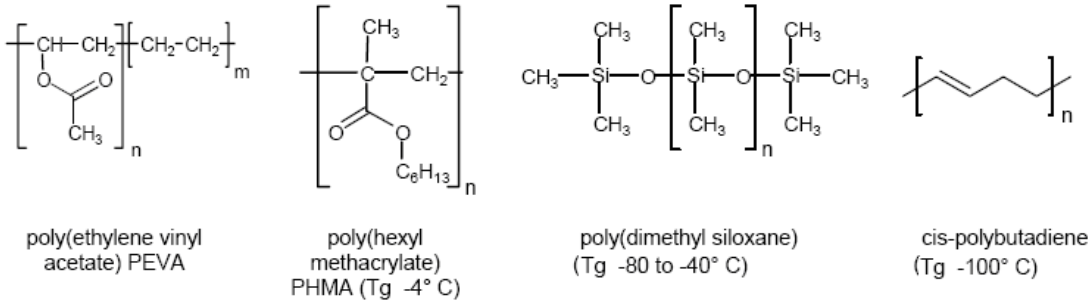

Figure 1.6 Polymers with low glass transition
(taken from http://www2.uni-jena.de/~c1moge/Mohr/ASCOS2002.pdf).

Gankema, Lugtenberg, Engbersen, Reinhoudt & Moller (1994) have presented siloxane copolymers with reactive methacrylate groups and polar substituents which exhibit a behaviour and polarity similar to plasticized PVC but have the advantage that all components can be covalently linked to the polymer matrix (by copolymerisation).

1.5.2.2 Hydrophilic Polymers

Hydrophilic polymers provide a matrix which corresponds to an aqueous environment (Figure 1.7). Ions can diffuse quite freely, but the possible water uptake (10-1000%) can cause significant swelling of the polymer. Swelling of the matrix affects the optical properties of the sensors and, consequently, the signal changes.

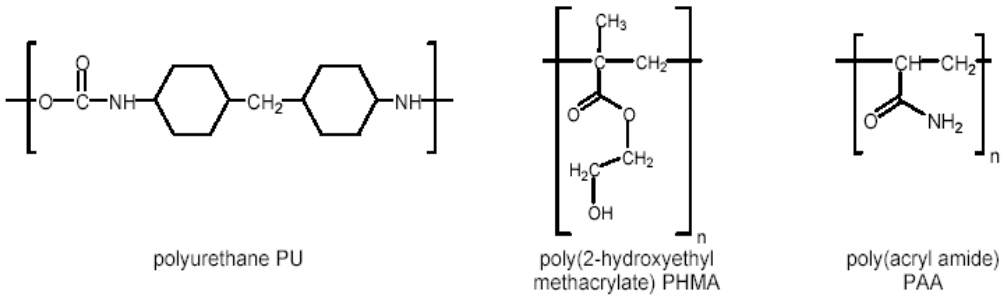

Figure 1.7 Hydrophilic polymers
(taken from http://www2.uni- jena.de/~c1moge/Mohr/ASCOS2002.pdf).

1.5.2.3 Ionic Polymers (polyelectrolytes)

Polyelectrolytes exhibit a large amount of dissociable groups. These compounds are often used for ion exchange chromatography. They can also be used to exchange their counterions with indicator ions (Figure 1.8).

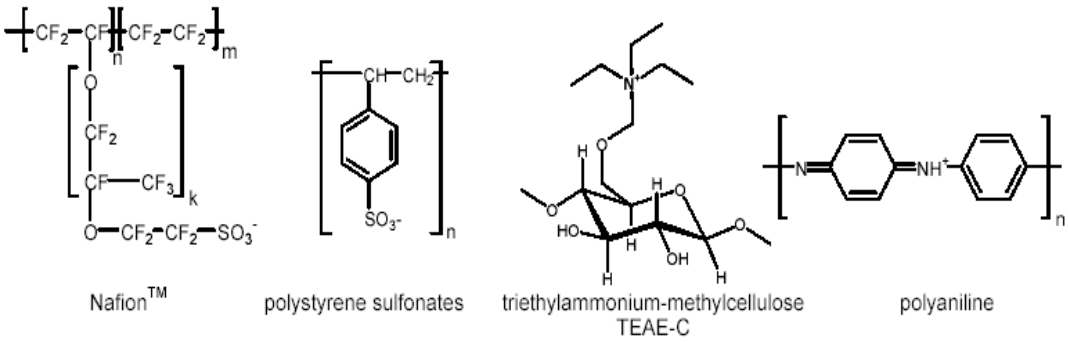

Figure 1.8 Ionic Polymers.

(taken from http://www2.uni-jena.de/~c1moge/Mohr/ASCOS2002.pdf)

.

1.5.3 Immobilisation of Indicators in Polymers

1.5.3.1 Hydrophobic interactions

Most indicator chemistry is adapted to aqueous solution (for titration in water). Therefore, the molecules are water-soluble and if dissolved in lipophilic polymers, they are washed out immediately. In order to make dyes, ionophores and ligands soluble in polymers and to avoid leaching of the components, they have to be made lipophilic (Figure 1.9). Lipophilic molecules can be obtained by introduction of long alkyl chains. However, the chemical synthesis involved can be tedious. Therefore, another possibility is to obtain lipophilic compounds by ion-pairing. Ion pairs are mostly obtained by dissolving both components (water-soluble ionic indicator and water-soluble ionic surfactant of opposite charge) separately in water, pouring both solutions together and filtering the precipitated product.

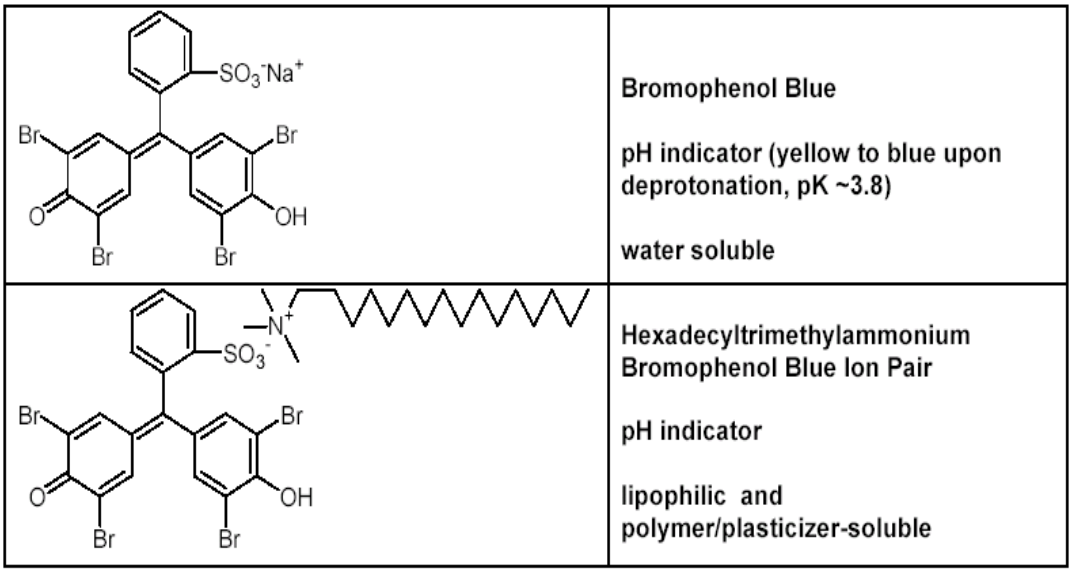

Figure 1.9 Bromophenol blue and its lipophilic ion pair form
(taken from http://www2.uni-jena.de/~c1moge/Mohr/ASCOS2002.pdf).

1.5.3.2 Ion-exchange

Indicators can be made lipophilic by ion-pairing with surfactants. However, they can also be directly immobilised on the polymer by ion-pairing with ionic polymers (polyelectrolytes) (Figure 1.10). Solutions or suspensions of the polymers are usually mixed with aqueous or alcoholic solutions of the dyes.

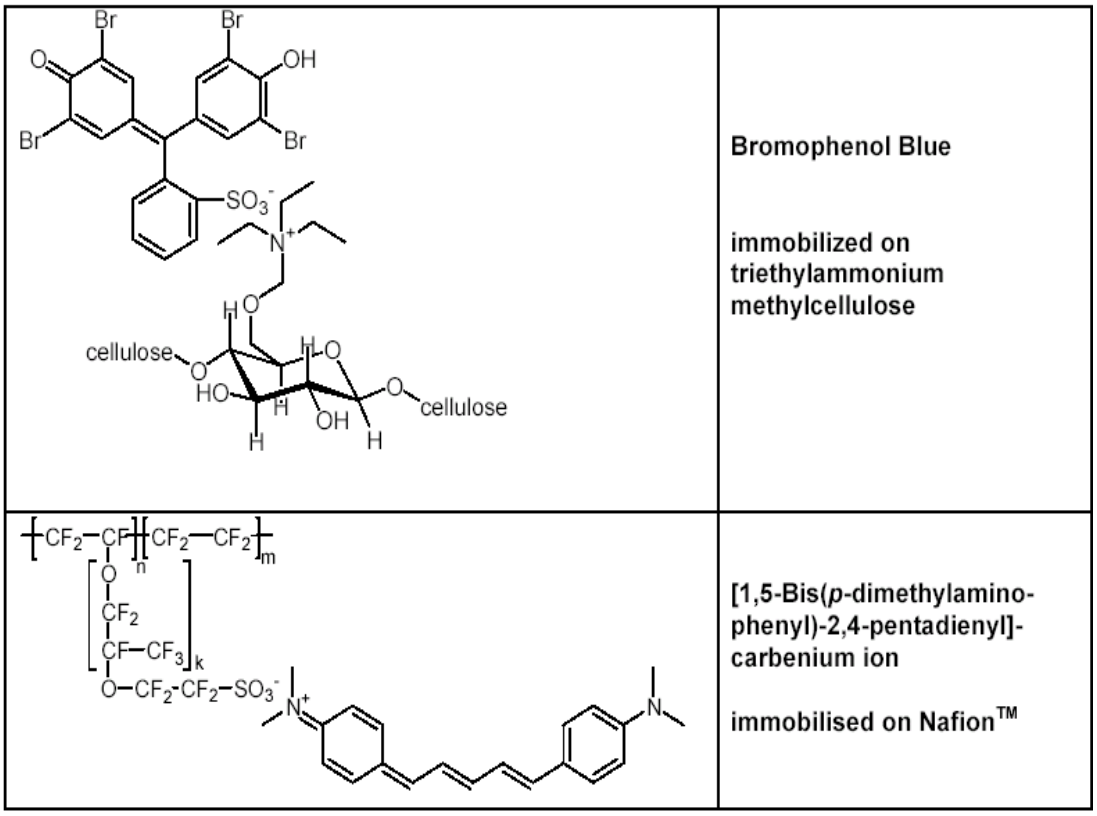

Figure 1.10 Bromophenol blue immobilized on triethylammoniummethylcellulose and Nafion (taken from http://www2.uni-jena.de/~c1moge/Mohr/ASCOS2002.pdf).

1.5.3.3 Covalent immobilization

Covalent immobilisation of the indicator chemistry to the polymer matrix is the best of all immobilisation methods. The operational stability and shelf life is superior (no leaching, crystallisation, evaporation of components). However, to obtain indicators and polymers with functional groups is inevitably linked with significant synthetic effort. Very often, chemical modification of dyes negatively affects their selective and sensitive analyte recognition. In principal two different ways of immobilisation are possible, namely (a) to bind a reactive dye (e.g. fluorescein succinimidyl ester) to a reactive polymer matrix (e.g. aminocellulose), or (b) to polymerise a reactive dye (e.g. a dye with a methacrylate group) with common monomers (e.g. methyl methacrylate) to give a copolymer. Several indicator dyes are available in a reactive form (primarily for labelling of peptides). These reactive molecules with isothiocyanate groups, sulfonyl chloride groups, vinylsulfonyl groups, or succinimidyl groups (fluorescein isothiocyanate, dabcyl succinimidyl

ester, hydroxypyrene trisulfonyl chloride) can be covalently attached to aminoethylcellulose or amino-PVC. Indicator dyes with amino or hydrazino groups (aminofluorescein, Texas Red hydrazide) can be coupled to carboxy-PVC or carboxymethylcellulose (Figure 1.11).

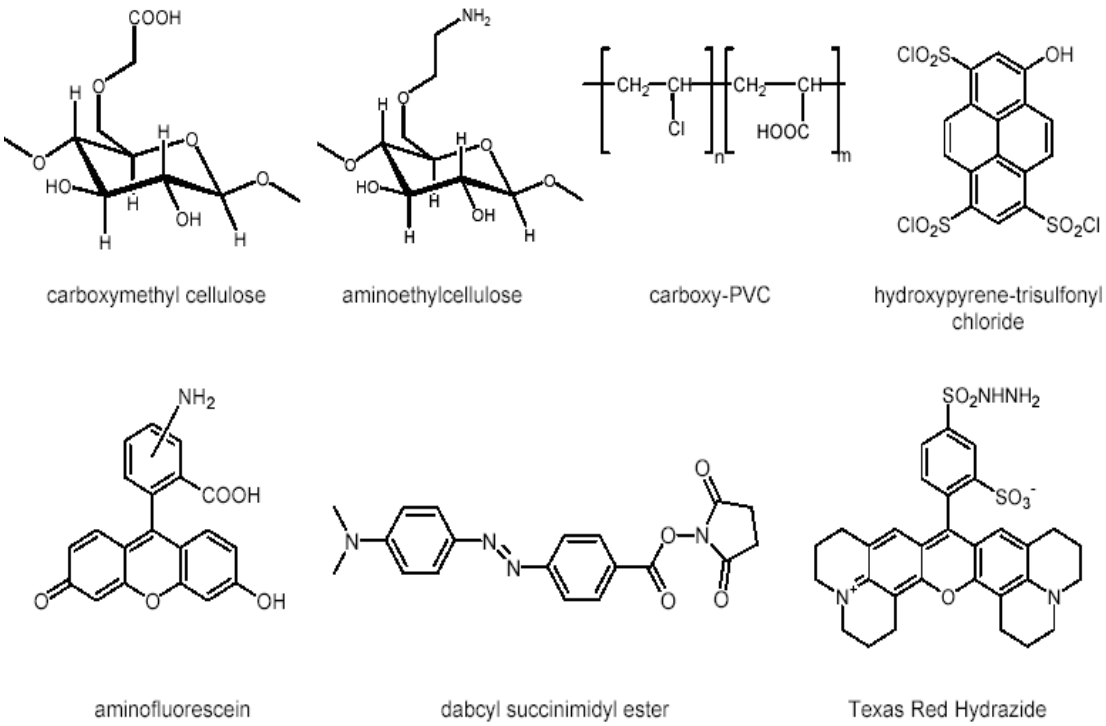

Figure 1.11 Indicators and polymers with functional groups.

1.6 Effect of Polymers on Indicator Chemistry

Dependent on whether a hydrophilic or lipophilic polymer matrix is used, the recognition process of analytes by the indicator chemistry can be completely different. In the case of lipophilic polymers, analyte ions can only be transported into a polymer membrane if, simultaneously, another ion is released or co-extracted (see below). This restriction is not valid for hydrophilic polymers, and clearly not for neutral analytes.

1.6.1 Co-extraction and ion-exchange

The optical sensors are composed of ion-selective carriers (ionophores), pH indicator dyes (chromoionophores), and lipophilic ionic additives dissolved in thin layers of plasticized PVC. Ionophores extract the analyte from the sample solution into the polymer membrane. The extraction process is combined with co-extraction or exchange of a proton in order to maintain *electroneutrality* within the unpolar polymer membrane. This is optically transduced by a pH indicator dye (chromoionophore). The preparation of sensor layers is relatively simple. It only requires to dissolve the components (pH indicator dye, ionophore, ionic additive) together with polyvinyl chloride and a plasticizer in tetrahydrofuran (similar to ion-selective electrode membranes) (Figure 1.12, 1.13). The solutions are then spin-coated on transparent support materials and fixed in flow-through cells, or they are applied onto optical fibers as well as planar wave guides by dip-coating. Since the recognition element (ionophore) and the optical transducer are different molecules, almost any available ionophore can be combined with one appropriate pH-indicator. Furthermore, it is possible to tailor the properties of the sensor by using plasticizers of different polarity. The mechanism is mathematically well-defined and allows predicting the dynamic range and selectivity of the sensor membrane. A severe disadvantage is the intrinsic cross-sensitivity to pH because sensors based on ionexchange measure the ratio of activities between analyte ion and the proton, and sensors based on coextraction measure the product of activities of analyte and protons. Consequently, the pH of the sample solution has to be determined or to be adjusted by addition of buffer.

1.6.1.2 Measurement of Cations

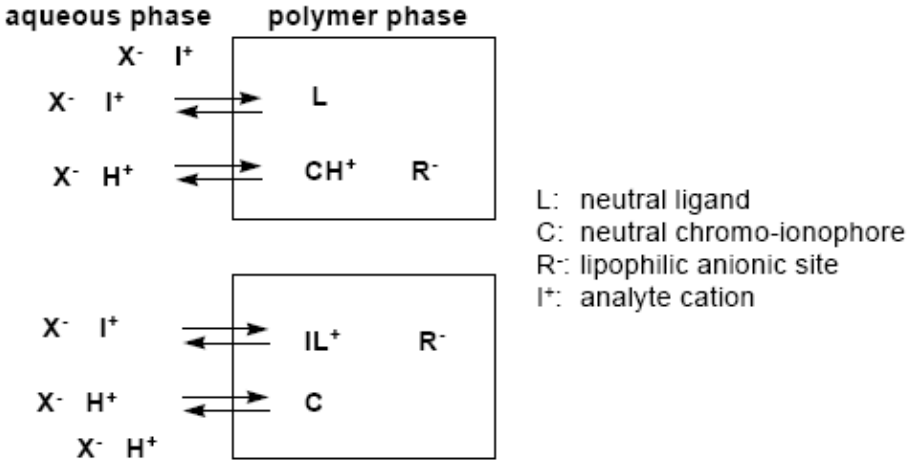

Figure 1.12 Mechanism of ion-exchange of an analyte ion and a proton between a sensor membrane (composed of a neutral pH indicator dye, a neutral ligand and a lipophilic anionic site) and the aqueous phase
(taken from http://www2.uni-jena.de/~c1moge/Mohr/ASCOS2002.pdf).

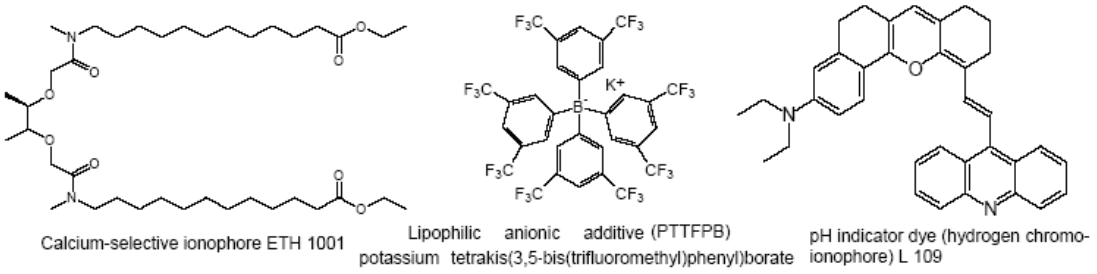

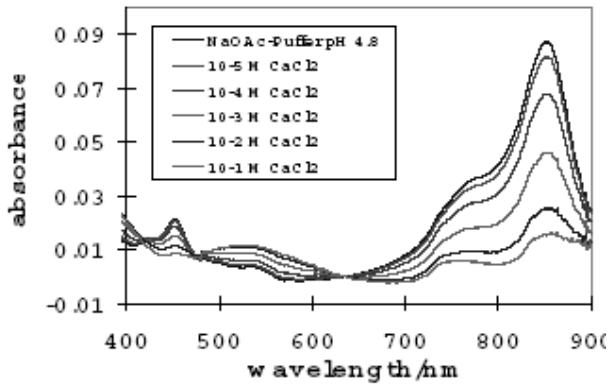

Figure 1.13 Decreasing absorbance of a calcium-sensitive ion-exchange membrane at 850 nm (composed of L109, ETH 1001 and PTTFPB in plasticized PVC) upon exposure to increasing concentrations of calcium ion at pH 4.8 (taken from http://www2.uni-jena.de/~c1moge/Mohr/ASCOS2002.pdf).

1.6.2 Potential-sensitive Dyes (PSDs)

Potential-sensitive or polarity-sensitive dyes are known to optically respond to changes in their microenvironment such as changes in polarity or lipophilicity. In sensor membranes based on PSDs, these changes are induced by selective carriers, which, similar to the mechanisms of co-extraction and ion exchange, extract analyte ions from the sample solution into the polymer membrane. However, the response to the increase of analyte ions in the polymer phase is different. In the case of ion exchange or co-extraction, electroneutrality in the membrane is maintained via protonation/deprotonation of pH indicator dyes. PSDs usually do not posses functional groups that are protonable or deprotonable. Therefore, electroneutrality can only be established if the PSD moves between the aqueous and the polymer phase. As a consequence of the motion of the PSD between phases of different polarity, optical signal changes are induced which can result from aggregation, but also from solvatochromism. The sensors exhibit significantly lower crosssensitivity to pH than optical sensors based on the ion-exchange/co-extraction mechanism.

1.6.2.1 Measurement of Cations

The selective ionophore (e.g. valinomycin) extracts potassium from the aqueous into the organic polymer phase (Figure 1.14). The presence of potassium in the membrane phase causes a separation of the dye-borate ion pair (due to reasons of electroneutrality), which results in accumulation of the dye cations at the plasticizer/water interface. Without lipophilic counter ion, the solubility of the dye in a plasticizer is relatively poor, and it tends to form weakly fluorescent multimers or aggregates. Consequently, a decrease in fluorescence is observed.

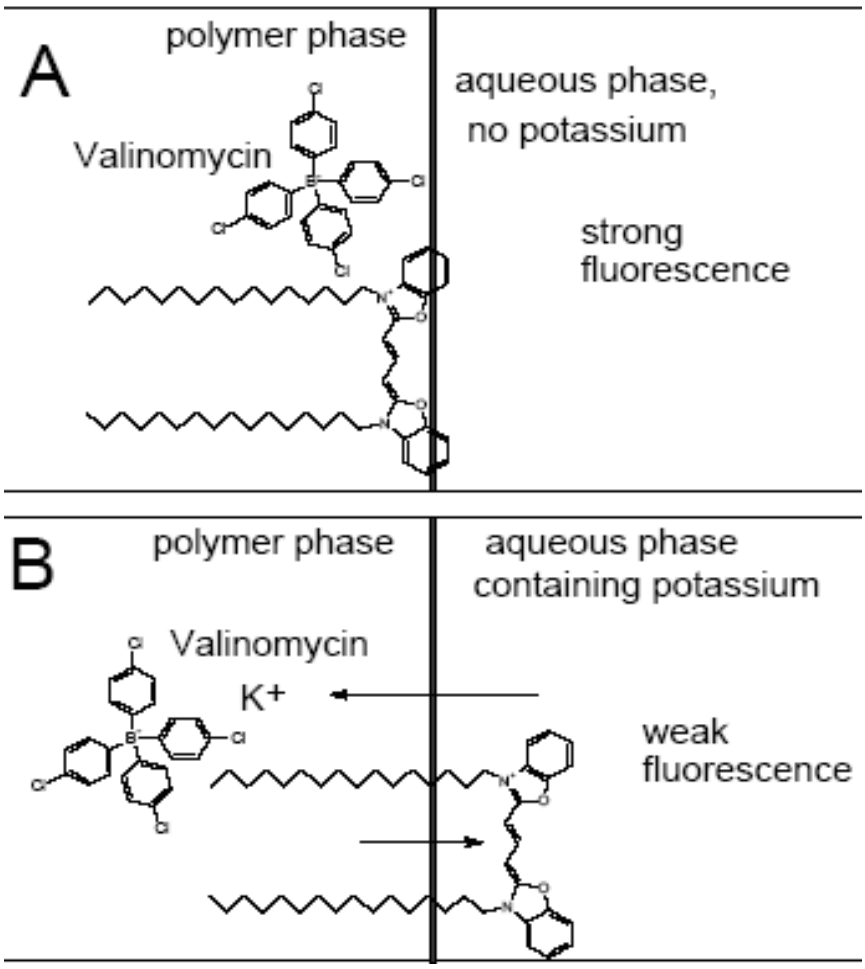

Figure 1.14 Schematic representation of the microenvironment of a cationic PSD (diOC16(3)) in a potassium sensor before (A) and after (B) extraction of potassium from the aqueous into the lipophilic membrane phase. The sensor membrane is composed of valinomycin, diOC16(3) and a lipophilic borate salt dissolved in plasticized PVC
(taken from http://www2.uni-jena.de/~c1moge/Mohr/ASCOS2002.pdf).

1.6.3 Chromogenic and Fluorogenic Indicators

1.6.3.1 Measurement of Ions

The response of optical sensors based on chromogenic and fluorogenic indicators is completely different to the sensing schemes discussed above. The above schemes (ion-exchange, coextraction) make use of nonselective pH indicator dyes and selective ionophores. However, chromogenic and fluorogenic ligands are a combination of selective recognition and optical transduction in one molecule. They consist of a chromophoric part directly connected with the recognition moiety. Whereas the above schemes work best in a lipophilic polymer matrix (mostly

plasticized PVC), indicator dyes should be dissolved in a hydrophilic (aqueous-like) matrix in order to allow rapid diffusion of analyte ions to and from the ligands. Furthermore, due to the facilitated ion diffusion in hydrophilic matrices, a large pH-cross-sensitivity similar to the pH-crosssensitivity of ion-exchange/co-extraction-based sensors is not observed.

Generally, sensors based on chromogenic or fluorogenic indicators are advantageous over sensors based on PSDs or ion-exchange/co-extraction. A specific interaction between a chromophore that already contains the moiety for analyte recognition is simpler than the above mechanisms which require lipophilic ionic sites, specific pH-indicator dyes and selective (uncoloured) ionophores. Furthermore, such ligands are generally less pH-sensitive as long as the recognition process is represented by the equilibrium:

$$\text{ion} + \text{indicator} \leftrightarrow \text{complex (ion-indicator)}$$

If the ion binding process involves the displacement of protons according to:

$$\text{ion} + \text{indicator-H}^+ \leftrightarrow \text{complex(ion-indicator)} + \text{H}^+$$

Then the process is cross-sensitive to pH. In order to provide a rather natural aqueous environment for the indicator dyes, they should be embedded in hydrophilic rather than in lipophilic polymers. This, however, requires significant synthetic effort because the indicator should be covalently linked to the polymer in order to prevent leaching.

1.6.3.1.1 Measurement of Cations. Probably the best optical sensors for pH are based on pH indicator dyes covalently immobilized on transparent cellulose membranes.

The principle can also be used for measurement of cations such as potassium using a selective ligand (crown ether) linked to the chromophore.

Another approach for ion-sensing (here: copper and zinc) is based on the water-soluble ligand Zincon. The ion pair with quaternary ammonium halides can be homogeneously dissolved in polymers such as plasticized polyvinyl acetate, ethyl cellulose, and polyurethane (Figure 1.15). When the Zincon ion-pair is exposed to an aqueous sample containing the analyte, the latter diffuses into the sensor membrane to react with the indicator, and gives a colour transition from pink to blue at near neutral pH. The pKa value of Zincon for the color transition from pink to blue is above 13, therefore, the sensor membrane is virtually insensitive to pH changes. However, due to the high complexation constant of Zincon for copper and zinc, the response of sensor membrane is irreversible and must be evaluated kinetically.

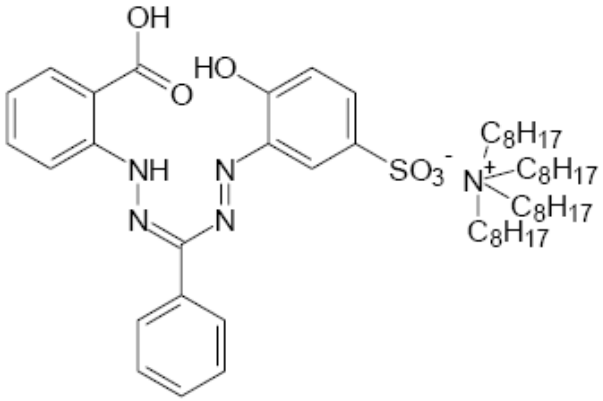

Figure 1.15 Chemical structure of the Zincon-tetraoctylammonium ion pair

1.7 Ionic Liquids (Yang & Pan, 2005)

Ionic liquids are very new matrix materials for sensor design. Unlike traditional solvents, which can be described as molecular liquids, ionic liquids are composed of ions (see Figure 1.16 for the structures of the commonly used ionic liquids). Their unique properties such as nonvolatility, non-flammability, and excellent chemical and thermal stability have made them an environmentally attractive alternative to conventional organic solvents. Ionic liquids have low melting points (<100 °C) and remain as liquids within a broad temperature window (<300 °C).

One of the most special properties for ionic liquids is their high polarity. On the normalized polarity scale (ENT) setting tetramethylsilane at 0.0 and water at 1.0, the polarity of common ionic liquids normally falls in the range of 0.6–0.7, similar to

that of lower alcohols and formamide (Rantwijk, Lau & Sheldon, 2003). A correlation between the decrease in both the chain length of the alkyl substituents on the imidazolium ring of the cation and the anion size with an increase in polarity can be observed (Carmichael & Seddon, 2000). The polarity values of ionic liquids are sometimes sensitive to the temperature and the presence of water (Baker, S.N., Baker G.A. & Bright, 2002). Because of the high polarity, ionic liquids present an ideal reaction melieu for chemical and biochemical reactions due to their ability to dissolve a wide range of different substances including polar and nonpolar organic, inorganic, and polymeric compounds.

Despite of their high polarity, most of ionic liquids are hydrophobic and can dissolve up to 1% of water, and the presence of water may affect the physical properties of the ionic liquids (Seddon, Stark & Torres, 2000). However, the solubility of water in ionic liquids varies unpredictably (Rantwijk et al., 2003). For example, although 1-butyl-3-methylimidazolium tetrafluoroborate ([BMIm][BF_4]), 1-butyl-3-methylimidazolium hexafluorophosphate ([BMIm][PF_6]), and 1-butyl-3-methyl-imidazolium-bis-(trifluoromethylsulphonyl) imide ([BMIm][Tf_2N]) are similar on Reichardt's polarity scale, the former one is completely water-miscible while the latter two are only slightly soluble in water (Park & Kazlauskas, 2003).

Ionic liquids are generally immiscible with many organic solvents especially when the latter are nonpolar, such as hexane; whereas some may be miscible with polar solvents like dichloromethane and tetrahydrofuran (Park & Kazlauskas, 2003). The immiscibility of ionic liquids with either water or organic solvents has made them feasible to be used to form two-phase systems.

Compared to typical organic solvents, ionic liquids are much more viscous (35–500 cP viscosity for commonly used ionic liquids versus 0.6 cP for toluene and 0.9 cP for water at 25 °C) (Park & Kazlauskas, 2003; Brennecke & Maginn, 2001). The viscosity of an ionic liquid represents its tendency to form hydrogen bonding and the strength of its van derWaals interactions, and can be lowered by increasing the

temperature or by adding some organic co-solvents. Normally, an ionic liquid with longer alkyl chains on the cation and a larger anion size presents a higher viscosity.

One obvious advantage of using ionic liquids over the use of normal organic solvents is that the physical and chemical properties of the ionic liquids, including their polarity, hydrophobicity, viscosity, and solvent miscibility, can be finely tuned by altering the cation, anion, and attached substituents. This is important, because by manipulating the solvent properties, one is allowed to design an ionic liquid for specific reaction conditions, such as to increase the substrate solubility, to modify the enzyme selectivity, or to tailor the reaction rate.

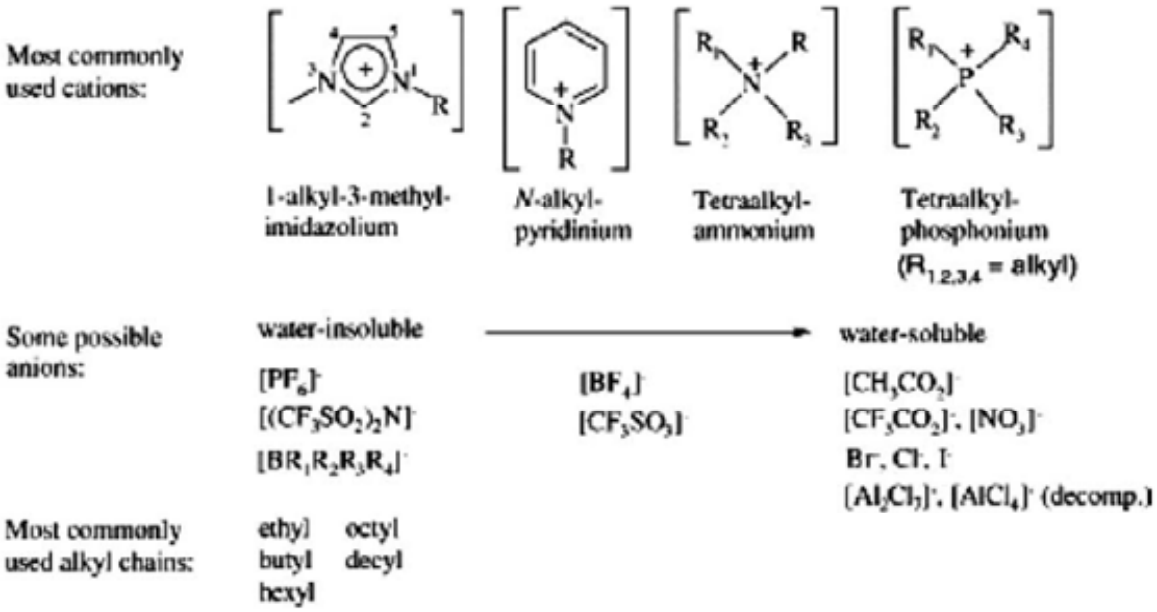

Figure 1.16 The building blocks of ionic liquids (taken from Yang & Pan, 2005).

1.7.1 Usage of ionic liquids in the construction of sensors (Liu, Jönsson & Jiang, 2005)

ILs were employed as the sensing materials of quartz crystal microbalance (QCM) sensor for organic vapors, including toluene, methanol, ethanol, 2-propanol, 1-butanol, acetone, acetonitrile, chloroform, tetrahydrofuran, and ethyl acetate (Liang, Yuan, Warmack, Barnes, & Dai, 2002). This application was based on the fact that the viscosity of the IL membrane decreases rapidly because of solubilization

of analytes and the change in viscosity varies with the chemical species of the vapors and the types of IL. This results in a frequency shift of the corresponding quartz crystal. The liquid status of ILs at room temperature provided fast diffusion of analytes, so the QCM sensor exhibited a rapid response time (average less than 2 s) to organic vapors with an excellent reversibility. Furthermore, the sensor had a long shelf life because of the zero vapor pressure and stable chemical properties of ILs, which eliminate the possibility of loss of these liquids through vaporization and chemical reaction. This sensor was also applied to determine the solubility of carbon dioxide in a series of imidazolium-based ILs at 25 ^{o}C with CO_2 pressures at or less than 1 bar (Baltus, Culbertson, Dai, Luo, & DePaoli, 2004).

A novel solid-state amperometric O_2-gas sensor based on supported 1-methyl-3-ethyl-imidazolium tetrafluoroborate ([C_2MIM][BF_4]) porous polyethylene membrane-coated electrodes has been reported (Wang, Okajima, Kitamura, & Ohsaka, 2004). Compared to solid electrolyte gas sensors and classic Clark-type gas sensors, this proposed O_2-gas sensor possesses the advantages of easy construction and miniaturization, as well as applicability at room temperature. The drawback of this sensor is that it is restricted to detecting O_2 from a dry gas stream, as moisture can be absorbed by the supported [C_2MIM][BF_4] membrane.

It was reported that, when ILs are used in gas sensors, the lower diffusion coefficients of the gaseous analyte in ILs lengthen the response time and limit the attainable steady-state currents (Buzzeo, Hardacre, & Compton, 2004). However, the negligible vapor pressure and robust thermal stability of ILs warrant IL-based gas sensors operating under extreme conditions, such as high temperature and high pressure. Oter, Ertekin, Topkaya & Alp (2006a, 2006b), reported two new and very stable optical CO_2 sensor prepared by simple doping of water-miscible roomtemperature ionic liquids, 1-methyl-3-butylimidazolium tetrafluoroborate (RTIL-I) and 1-methyl-3-butylimidazolium bromide (RTIL-II) with pH indicator dyes of 1-hydroxypyrene-3,6,8-trisulfonic acid (HPTS) and bromothymol blue (BTB).

1.8 Combination of Sensor Materials with Transducers

Sensor layers are mostly attached to a solid support since their mechanical stability is generally quite low. In most cases, all components (polymer, plasticiser, additives and indicator dyes) are dissolved in a common solvent and spin-coated, spray-coated, dip-coated or simply pipetted onto the support material. The solid support can be a glass plate which is mounted in a photometer and exposed to the analyte in a flow-through cell but it can as well be a surface plasmon resonance (SPR) cell, an attenuated total reflection (ATR) crystal or an optical fibre known from communication technology. Immobilisation directly on the light source, e.g. a light emitting diode (LED) is also possible.

Recently, the immobilisation of indicators in tiny beads rather than in polymer layers has provided nanoparticles which can be inserted into cells and measure analytes within a living cell.

CHAPTER TWO

EXPERIMENTAL METHOD AND INSTRUMENTATION

All solvents used in this thesis were of analytical grade and purchased from Merck, Johnson and Mathey, Acros, Fluka and Riedel. Solvents for the spectroscopic studies were used without further purification.

The pH and CO_2 sensitive fluorescent dye, 8-Hydroxypyrene-1,3,6-trisulfonic acid trisodium salt (HPTS) was 98 % purity and from Fluka. The ionic liquids, 1-methyl-3-butylimidazolium tetrafluoroborate (RTIL-I) and 1-methyl-3-butylimidazolium bromide (RTIL-II) were obtained from Professor S. Alp and were synthesized in our laboratories. Tetrabutylammonium hydroxide for titration (in nonaqueous medium) was standard 0.1 M solution in isopropanol/methanol (0.1 N) from Fluka. The solution was concentrated to 1 M with vacuum evaporator before use for the titrations in ionic liquid media. The sodium bicarbonate in powder form was puriss from Riedel (99-100%).

The pH and CO_2 sensitive dye, bromothymol blue (BTB) sodium salt was from Riedel and used either with the original form or modified form by ion pairing. The ion pair was formed by the reagent tetraoctyl ammonium bromide which was obtained from Sigma.

The polymer polyvinyl chloride (PVC) was high molecular weight and obtained from Fluka. The polymer ethyl cellulose was from Organics with an ethoxy content of 48%. The plasticiser, dioctyl phtalate (DOP) was 99 % from Aldrich. The additive potassium tetrakis (4-chlorophenyl) borate was selectophore, 98 % from Fluka. The iron sensitive dye of N-(4-dimethylaminophenyl)-3,5-di-*t*-butyl salicylaldimine (DBS) dye was supplied from Professor B. Çetinkaya and was synthesized in the laborotories of University of Ege. The other iron sensitive dye, Bis(7-metoksi-1-benzofuran-2-il)ketoksim (BFK) was supplied from Dr. C. Kırılmış and was synthesized in the laborotories of University of Fırat.

The standard metal solutions were prepared from their 0.1 M stock solutions by using the metal salts of $Cu(NO_3)_2$, $Co(NO_3)_2$, $NiCl_2.6H_2O$, $Pb(NO_3)_2$, $Hg_2(NO_3)_2$, $Hg(NO_3)_2$, $CrCl_3$, $CdCl_2$, $Fe(NO_3)_3$, ammonium-iron(II) sulphate.hexahydrate, $Al(SO_4)_3.16H_2O$. N-N-Bis-(2-hydroxyethyl)-2-aminoethansulfonic acid (BES buffer) was from Merck. The preparation of buffer solutions was explained in Section 2.7.

The sol-gel precursor tetraethyl orthosilicate (TEOS) was obtained from Merck (98 % purity, for synthesis). The additive Triton X-100 was obtained from Merck (98 % purity, GR). The O_2 sensitive fluorescent dye, tris (2, 2'-bipyridyl) ruthenium (II) chloride ($Ru(bipy)_3^{2+}$) was supplied from Aldrich (99.5% purity). The commercial ionic liquid, 1-ethyl-3-methylimidazolium tetrafluoroborate (RTIL-III) was supplied from Fluka. The ionic liquid of 1-methyl-3-(triethoxysilanebutyl)imidazolium tetrafluoroborate (RTIL-IV) was supplied from Dr. H. Türkmen and was synthesized in the laboratories of University of Ege.

Absorption spectra were recorded using a Shimadzu 1601 UV-Visible spectrophotometer. Steady state fluorescence emission and excitation spectra were measured using Varian Cary Eclipse Spectrofluorometer with a Xenon flash lamp as the light source. The fiber optic components were obtained from Varian and explained in detail in Section 2.1. The emission spectra were corrected using a piece of silica ground on both faces held in a triangular cuvette configuration called the diffuser. The heavy metal analysis studies were executed by fiber optical and flow system. The flow cell is made from polytetrafluoroethylene (PTFE) in the atelier of University of Ege. The flow system was explained in Section 2.2. pH measurements were recorded with a WTW pH meter. In all of the studies ultra pure water of Millipore was used. Cylinders of carbon dioxide, oxygen and nitrogen gases of 99.99% purity were obtained from Gunes or Karbogaz, Izmir, Turkey. The gas mixtures were prepared with a Sonimix 7000 Gas Diluter enstrument and were explained in detail in Section 2.3.

2.1 Construction of fiber optical system

The fiber optical sensor was constructed with the commercial accessories of Varian Cary Eclipse Spectrofluoremeter (Figure 2.1): Eclipse Fibre optic coupler, Fluorescence remote read probe (2 metres), Probe tip for solid measurements and Probe tips for liquid measurements (10 mm and 20 mm length tips). This method also allows the examination of samples remote from the instrument. The installation steps are:

- ***The fibre optic coupler*** is an accessory that enables the use of a fiber optic probe with Carry Eclipse spectrofluoremeter. After the removal of the sample compartment of the Carry Eclipse, the fibre optic coupler was stabilized to the same position by the help of the screws.
- ***The fiber optic probe*** was connected to the coupler accessory by inserting the two connector ends into the two key holds.
- ***The probe tips*** were screwed onto the end of the probe. Due to the phase of the sample (solid or liquid), either a solid sample probe tip or a liquid sample probe tip were used.
- To ensure that the fibre optic system will operate at maximum performance, it is nesessary to optimize the efficiency with which light passes through the coupling device before experimentation begins. The allignment was done by using the software of the instrument.

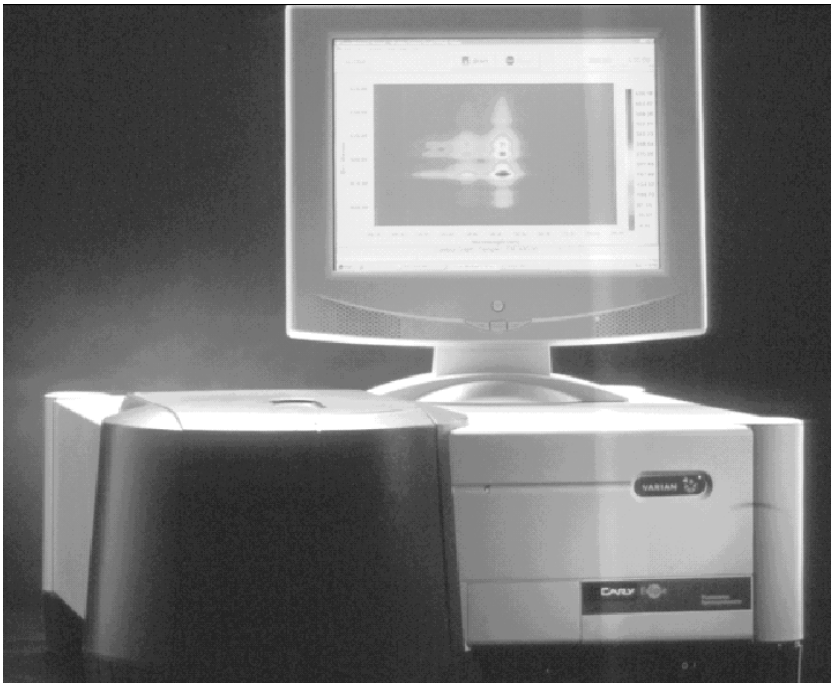

Fluorescence remote read probe

Fibre optic coupler accessory

probe tips

Figure 2.1 Varian Cary Eclipse Spectrofluoremeter and fiber optical system accessories.

2.2 Combination of the flow system with fiber optic system (for metal ion determinations)

Metal response measurements were carried out with fiber optic probe (2m long) and solid sample tip accessories constructed on the spectrofluorometer. For instrumental control, data acquisition and processing the software package of the spectrofluorometer was used.

The tip of the bifurcated fiber optic probe was interfaced with a sensing film in a buffer containing 300 μL flow cell (Figure 2.3). The flow cell was equipped with a four channel Ismatec Reglo Analog peristaltic pump. Analyte solutions or buffers

were transported by the peristaltic pump via tygon tubing of 2.06 mm i.d. (Figure 2.2)

Figure 2.2 Ismatec Reglo Analog peristaltic pump.

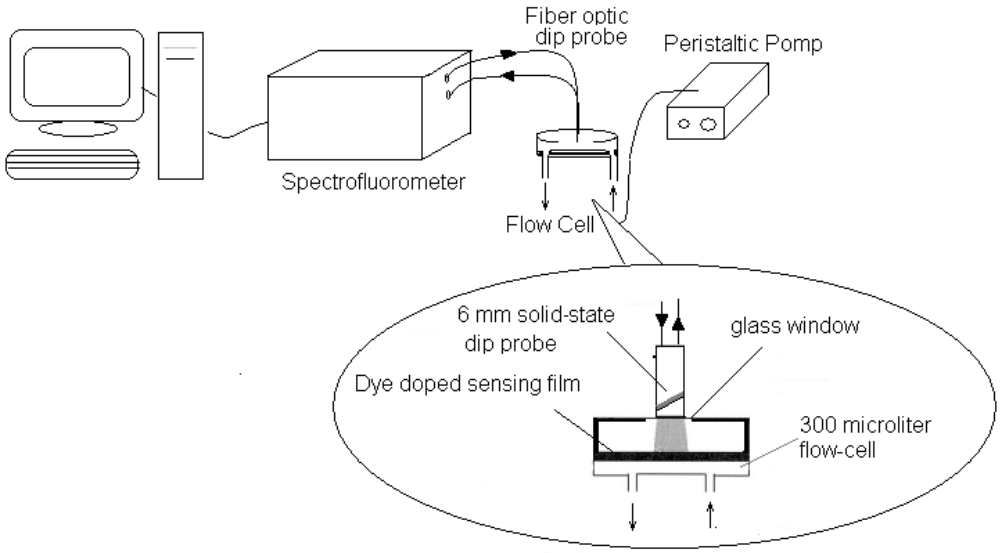

Figure 2.3 Instrumental set-up used for dye-doped thin film evaluation.

2.3 Mixing of the gases

Gaseous CO_2 or O_2 with N_2 were mixed in the concentration range 0–100% either in a gas diluter; Sonimix 7000A gasblending system or in a home made gas mixing chamber by controlling the gas flow rates with sensitive flow-meters (Figure 2.4). Gas mixtures were introduced into the sensor agent containing cuvette via a diffuser needle under ambient conditions either directly or after humidification of the gas by bubbling through water at 25 °C.

Figure 2.4 Sonimix 7000 Gas Diluter.

2.4 Synthesis of ion pairs

In order to convert the water soluble dye into polymer soluble form, ion pair form of the dye must be synthesized. This method provides the immobilization of the dye into the polymer matrix and prevents the leaching of the dye.

The ion pair between the water soluble dye and the tetraoctylammonium counterion (TOA) was prepared by the following method: The appropriate amounts of the dye and the tetraoctylammonium bromide (TOABr) (834 mg) were dissolved in 30 ml of water containing 1% sodium carbonate and 30 ml of CH_2Cl_2 respectively, and mixed in a separatory funnel. The ion pair was completely extracted from the aqueous phase into the organic phase. The organic phase was washed three times

with 0.05 M NaOH and separated. After the evaporation of organic solvent under vacuum, the crystalline ion pair was obtained.

2.5 Construction of the sensing films

The sensing cocktails were prepared due to the analyte type either with PVC, ethyl cellulose, ionic liquid or sol- gel matrix.

2.5.1 PVC cocktail preparation (Seiler & Simon, 1992; Bakker & Simon, 1992; Lerchi, Bakker, Rusterholz & Simon, 1992)

The membranes were prepared to contain the dye, 33% PVC (High molecular weight), 66% plasticizer (Dioctyl phthalate, DOP) by weight and the additive potassium tetrakis-(4-chlorophenil) borate (PTCPB). The chemical structures of PVC, DOP and PTCPB were shown in Figure 2.6. The mixture was dissolved in the solvent of tetrahydrofuran (THF) and mixed by several hours by the help of a magnetic stirrer.

The resulting cocktail was spread on a 125 μm polyester support (Mylar from Du Pont) and dried in a desicator which was saturated with the solvent vapour. The polyester support was optically fully transparent, ion impermeable and exhibited good adhesion to PVC. The most important function of the polyester was to act as a mechanical support because the thin silicon films were impossible to handle. Once dried, the film was insoluble in water and could be cut into pieces of appropriate size. The approximate thickness of the film was 5 μm. Film thicknesses were measured using Tencor Alpha Step 500 Prophylometer. The films were kept in a desiccator in the dark. This way, the photostability of the membrane was ensured and the damage from the ambient air of the laboratory was avoided. For absorbance and steady state fluorescence measurements each sensing film was cut to 1.2 cm width and 2.5 cm length and fixed diagonally into the sample cuvette (Figure 2.5) and the absorption or emission spectra were recorded. For fiber optical and flow system measurements, each sensing film was cut to 1 cm width and 1 cm length and fixed into the flow cell shown in Figure 2.3.

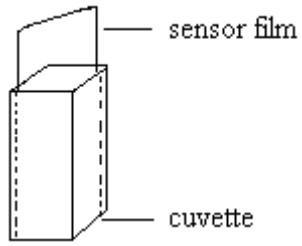

Figure 2.5 The placement of the sensor film in the sample cuvette.

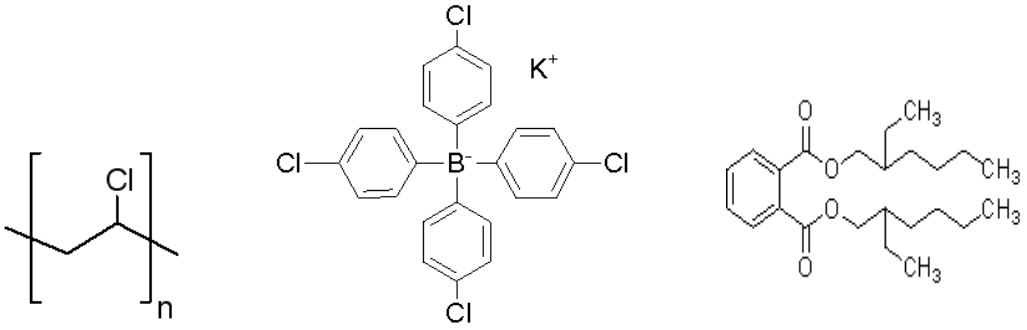

PVC PTCPB DOP

Figure 2.6 Structures of PVC, PTCPB and DOP

2.5.2 Ethyl cellulose cocktail preparation

The membranes were prepared to contain the dye, 33% ethyl cellulose (48-49.5% ethoxy content, EC) and 66% plasticizer (DOP) by weight. The mixture was dissolved in the solvent of tetrahydrofuran and was mixed by several minutes by the help of a magnetic stirrer. The same procedure with the PVC matrix was employed after. The structure of ethyl cellulose is shown in Figure 2.7.

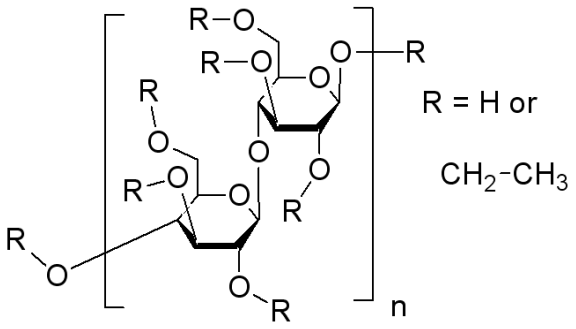

Figure 2.7 Structure of ethyl cellulose

2.5.3 Sol-gel cocktail preparation

The sol-gel components are tetraethyl orthosilicate (tetraethoxysilane, TEOS) and hydrochloric acid or sodium hydroxide whether it is acid catalised or base catalised sol-gel. Triton X-100 was added in order to improve the homogeneity of the silica sol-gel and to give a crack-free monolith. Dye doped silica gel glasses were prepared by hydrolization and condensation of TEOS with acidic water. The sol gel was also prepared by the addition of different ionic liquids with the same method. In all cases the solutions were aged at room temperature in open glass vials. After the manuel coating of the sol-gel to glass slides, the slides were left to dry at room temperature or at 70 ^{o}C in oven. Glass slides were used as solid support onto which the sol-gel was cast by manual dip-coating technique. Prior to casting, the glass surface was activated by treatment with concentrated HNO_3 for 24 h, washed with distilled water, and then ethanol.

2.6 Quantum yield calculations

Fluorescence quantum yield values (Φ_F) of the employed dyes were calculated by using the comparative William's method (Williams, Winfield & Miller, 1983). This is a reliable method for recording Φ_F and involves the use of well characterised standard samples with known Φ_F values.

Essentially, solutions of the standard and test samples with identical absorbance at the same excitation wavelength can be assumed to be absorbing the same number of

photons. Hence, a simple ratio of the integrated fluorescence intensities of the two solutions (recorded under identical conditions) will yield the ratio of the quantum yield values. Since Φ_F for the standard sample is known, it is trivial to calculate the Φ_F for the test sample.

According to this method, the standard samples should be chosen to ensure they absorb at the excitation wavelength of choice for the test sample, and, if possible, emit in a similar region to the test sample. In order to minimise re-absorption effects (Dhami et al., 1995) absorbances in the 10 mm fluorescence cuvette should never exceed 0.1 at and above the excitation wavelength. Above this level, non-linear effects may be observed due to inner filter effects, and the resulting quantum yield values may be perturbed. This maximum allowable value of the recorded absorbance must be adjusted depending upon the path length of the absorption cuvette being used (for example, 10 mm = 0.1 maximum, 20 mm = 0.2 maximum etc).

In this study, standard 10 mm path length fluorescence and absorption cuvettes were used for running the fluorescence and absorbance measurements. The UV-vis absorption (absorbance≤0.10 at the excitation wavelength) and corrected fluorescence emission spectra were recorded for three or more solutions with increasing concentrations of the sample and the standard. The integrated fluorescence intensities (that is, the area of the fluorescence spectrum) were calculated from the fully corrected fluorescence spectrum. Graphs of integrated fluorescence intensity *vs* absorbance were plotted. The gradient of the plots were later used in the quantum yield calculations according to the following equation

.

$$\theta_x = \theta_{st}\left(\frac{Grad_X}{Grad_{ST}}\right)\left(\frac{n_x^2}{n_{ST}^2}\right) \qquad (2.1)$$

Where the subscripts *ST* and *X* denote standard and test respectively, Φ is the fluorescence quantum yield, *Grad* the gradient from the plot of integrated fluorescence intensity *vs* absorbance and n is the refractive index of the solvent.

2.7. Preparation of the employed buffer solutions

2.7.1 Preparation of 0.01 M acetic acid/acetate buffer

0.0034 mol of acetic acid and 0.0065 mol of sodium acetate were dissolved in 950 mL ultra pure water. The solution was titrated to pH 5 at the lab. temperature of 20 ^{o}C either with 0.1 M HNO_3 or 0.1 M NaOH as needed. The resulting solution was made up to 1000 ml with ultra pure water in a volumetric flask. The buffer solutions in the range of pH 3.0-7.0 were prepared by the same way by adjusting to the desired pH.

2.7.2 Preparation of 0.005 M acetic acid/acetate buffer

0.0017 mol of acetic acid and 0.0032 mol of sodium acetate were dissolved in 950 mL ultra pure water. The solution was titrated to pH 5.0 at the lab temperature of 20^{o}C either with 0.1 M HNO_3 or 0.1 M NaOH as needed. The resulting solution was made up to 1000 ml with ultra pure water in a volumetric flask. The buffer solutions in the range of pH 3.0-7.0 were prepared by the same way by adjusting to the desired pH.

2.7.3 Preparation of 0.01 M acetic acid/acetate buffer in the physiological salinity level

0.003 mol of acetic acid and 0.0069 mol of sodium acetate were dissolved in 950 mL ultra pure water. 7.495g of NaCl was added to this solution. The solution was titrated to pH 5.0 at the lab temperature of 20 ^{o}C either with 0.1 M HNO_3 or 0.1 M NaOH as needed. After, it was made up to 1000 ml with ultra pure water in a volumetric flask. The resulting solution was in the physiological salinity level containig 135 mM NaCl (The ionic strength of the solution was 135 mM). The buffer solutions in the range of pH 3.0-7.0 were prepared by the same way by adjusting to the desired pH.

2.7.4 Preparation of 0.005 M acetic acid/acetate buffer in the physiological salinity level

0.0015 mol of acetic acid and 0.0034 mol of sodium acetate were dissolved in 950 mL ultra pure water. 7.699 g of NaCl was added to this solution. The solution was titrated to pH 5.0 at the lab temperature of 20^{o}C either with 0.1 M HNO_3 or 0.1 M NaOH as needed. After, it was made up to 1000 ml with ultra pure water in a volumetric flask. The resulting solution was in the physiological salinity level containig 135 mM NaCl (The ionic strength of the solution was 135 mM). The buffer solutions in the range of pH 3.0-6.0 were prepared by the same way by adjusting to the desired pH.

2.7.5 Preparation of 0.005/0.01 M NaH_2PO_4/Na_2HPO_4 buffer

0.0029/0.0058 mol of NaH_2PO_4 and 0.0020/0.0041 mol of Na_2HPO_4 were dissolved in 950 mL ultra pure water. The solution was titrated to pH 7.0 at the lab temperature of 20 ^{o}C either with 0.1 M HNO_3 or 0.1 M NaOH as needed. The resulting solution was made up to 1000 ml with ultra pure water in a volumetric flask. The buffer solutions in the range of pH 7.0-9.0 were prepared by the same way by adjusting to the desired pH.

2.7.6 Preparation of 0.01 M BES buffer

2.352 g of BES sodium salt (N,N-Bis(2-hydroxyethyl)-2-aminoethanesulfonic acid sodium salt, MW = 235.2, pKa of free acid = 7.1) was dissolved in approx. 950ml of ultra pure water. The solution was titrated to pH 7.0 at the lab temperature of 20 ^{o}C either with 0.1 M HNO_3 or 0.1 M NaOH as needed. The resulting solution was made up to 1000 ml with ultra pure water in a volumetric flask. The buffer solutions in the range of pH 5.0-7.0 were prepared by the same way by adjusting to the desired pH.

CHAPTER THREE

EMISSION-BASED OPTICAL CARBON DIOXIDE SENSING WITH HPTS IN GREEN CHEMISTRY REAGENTS: ROOM-TEMPERATURE IONIC LIQUIDS

3.1 Introduction

The concentration of CO_2, the most potent greenhouse gas, after water vapour, in the atmosphere has increased by more than 30% from the pre-industrial era which increase the average temperature of the earth and result in dramatic changes in climate and the ecosystem. Developed countries are committed to an overall reduction of about 5.2% of all greenhouse gas emissions in the period 2008-2012 compared to 1990 according to Kyoto Protocol. So, the reduce of CO_2 emissions and the continueous and accurate monitoring of CO_2 levels in atmosphere and surface waters such as coastal oceans, deep oceans, estuaries, rivers etc. has a vital importance on global climate and ecosystem and is an exigency for governments. Also the detection of dissolved and gaseous CO_2 is an important feature in industrial applications, in chemical, biochemical, medicine and clinical analysis such as blood gas monitoring, breathe gas analysis, respiration, photosynthesis etc.

The continuous and accurate monitoring of CO_2 levels in the atmosphere is of vital importance because of the threat of global warming. Current CO_2 sensing techniques are mainly based on infrared (IR) absorptiometry, the electrochemical Severinghouse electrode, and optical sensors. Optical CO_2 sensors based on the absorbance or fluorescence changes of pH indicators have several attractive features, including electrical isolation, reduced noise interference, the possibility of miniaturization, and remote sensing. Amao & Nakamura (2004) designed an optical CO_2 sensor based on overlay of the CO_2-induced absorbance change of the pH indicator dye α-naphtholphthalein with the fluorescence of tetraphenylporphyrin using ethyl cellulose and polystyrene membranes, and obtained 53.9% signal change from 100% N_2 to 100% CO_2. Müller & Hauser (1996), constructed an optode for measurement of low concentrations of dissolved CO_2. The useful measurement range

was between 10^{-3} and 10^{-1} mol L^{-1} $NaHCO_3$. They recorded response and recovery times of 6 and 20 min, respectively. Neurauter et al. (1999) measured gaseous CO_2 levels in an ethylcellulose matrix in the concentration range 0–30 hPa. The pH-sensitive fluorescent dye 1-hydroxypyrene-3,6,8-trisulfonic acid (HPTS) has been exploited in many previously described aqueous-phase carbon dioxide optical sensors (Bültzingslöwen et al., 2002; Ertekin et al., 2003; Malins & MacCraith, 1998; Neurauter, Klimant & Wolfbeis, 2000; Weigl & Wolfbeis, 1995; Wolfbeis, Kovacs, Goswami & Klainer, 1998). Weigl & Wolfbeis (1995) proposed a method for lipophilic extraction of the ion pair of HPTS with a quaternary ammonium salt into the membrane phase; this approach has been used many times. Although some investigations of pCO_2 sensor design with HPTS have resulted in commercialization of the products (Adrian, Mark & Novartis, 2002; Alderete, Olstein & Furlong, 1998; Furlong, 1997; Yafuso & Suzuki, 1989), most of the sensors produced using the ion-pair form of HPTS as indicator material have suffer from limited storage lifetimes.

In fact, in most of the optical sensors, indicators are adsorbed or immobilized in a solid matrix and when they are in contact with the sample, leaching can occur. Besides these, there are some problems about the lifetimes of the sensors due to evaporation of water or poisoning by ambient air and interfering gases such as NO_2, SO_2 or O_2 (Amao & Nakamura, 2004; Bültzingslöwen et al., 2002; Ertekin et al., 2003; Malins & MacCraith, 1998; Müller & Hauser, 1996; Neurauter et al., 1999; Neurauter et al., 2000; Weigl & Wolfbeis, 1995; Wolfbeis et al., 1998). To overcome these difficulties, Ertekin et al. (2003) designed a fiber optic sensing device in a capillary reservoir filled with the florescent indicator HPTS in an ethyl cellulose solution. He & Rechnitz (1995) proposed a fiber optic sensor in which a pipet tip was used that was filled with an aqueous indicator solution.

In contrast, several investigations have shown that ionic liquids have better CO_2 adsorption capacity than currently used polymeric materials (Blanchard, Hancu, Beckman & Brennecke, 1999; Blanchard, Gu & Brennecke, 2001; Cadena et al., 2004; Camper, Scovazzo, Koval & Noble, 2004; Scovazzo et al., 2004). CO_2 is reversibly soluble in imidazolium-based ionic liquids (Aki, Mellein, Saurer &

Brennecke, 2004; Anthony, Maginn & Brennecke, 2001; Anthony, Maginn & Brennecke, 2002; Bates, Mayton, Ntai & Davis, 2002; Kamps, Tuma, Xia & Maurer, 2003). Experimental values for the solubility of carbon dioxide, ethane, methane, oxygen, nitrogen, hydrogen, argon, and carbon monoxide in 1-butyl-3-methylimidazolium tetrafluoroborate have been reported to be a function of temperature between 283 ^{o}K and 343 ^{o}K at atmospheric pressure; carbon dioxide has been found to be the most soluble gas, with mole fraction solubilities of the order of 10^{-2} (Jacquemin, Gomes, Husson & Majer, 2006). Because of to the strong coulombic attraction between the ions of these liquids they have no measurable vapor pressure up to their thermal decomposition point, >300 °C. This lack of vapor pressure makes these materials highly attractive for gas processing and they may be regarded as "liquid solids" incorporating some of the most useful physical properties of both phases. Their properties have been widely reported; probably the most important is that room-temperature ionic liquids can be used as "clean solvents" and "catalysts" for green chemistry. Their gas sorption–desorption dynamics are very rapid and desorption by vacuum treatment is completely reversible. These properties make RTILs exceptionally promising as matrix materials for optical sensor design. Lee & Chou (2004) designed an electrochemical sensor and used ionic liquids for the determination of ethanol, but to our knowledge, ionic liquids are used for the first time as a matrix material in the optical CO_2 sensor design.

In this study, a new and very stable optical sensor prepared by simple doping of water-miscible room temperature ionic liquids, 1-methyl-3-butylimidazolium tetrafluoroborate (RTIL-I) and 1-methyl-3-butylimidazolium bromide (RTIL-II), with HPTS have been reported. The first part of this study covers determination of the photophysical properties of HPTS in the RTILs, including calculation of the pKa and excitation–emission related data in the RTILs. In the second part the performance of the sensor for dissolved and gaseous carbon dioxide is reported.

3.2 Choice of matrix material

Water-miscible and room-temperature ionic liquids were chosen as matrix materials and synthesized in our laboratory, in accordance with the conventional

literature method (Bonhote, Dias, Armand, Papageorgiou & Gratzel, 1996; Fuller, Carlin, Delong & Haworth, 1994; Holbrey & Seddon, 1999; Lau, Rantwijk, Seddon & Sheldon, 2000; Sweeny & Peters, 2001; Welton, 1998). The schematic structures of the ionic liquids are shown in Figure 3.1.

The RTIL-based matrix is a highly stable and spectroscopically available microenvironment for the HPTS molecule. Although the imidazolium ionic liquids have non-negligible absorption and intrinsic fluorescence in the visible region of the electromagnetic spectrum, the observed fluorescence of the ionic liquids studied was negligible in the excitation and emission wavelength ranges of the indicator dye and did not limit the sensing ability of HPTS in any way (Figure 3.5). Another important reason for choosing this material is the solubility of CO_2 in water-miscible ionic liquids, which is approximately 10 to 20 times that in conventional solvents, polymer matrices, or water. According to the literature (Anthony et al., 2002; Bates et al., 2002), the high solubility of CO_2 in RTILs results from the formation of weak Lewis acid–base complexes between CO_2 (the electron-pair acceptor) and the RTIL anion (the electron-pair donor). The literature also suggests that free volume within the RTILs affects relative CO_2 solubility. Hydration of CO_2 and subsequent protolysis is also essential for the functionality of the optical CO_2 sensors (Stumm & Morgan, 1981; Mills, Chang & McMurray, 1992). Gaseous carbon dioxide dissolves in the trace amounts of water present in the matrix, forming carbonic acid, which interacts with the deprotonated form of the indicator. The water content of the 1-butyl-3-methylimidazolium tetrafluoroborate has been reported to be 690 ppm after drying of the liquid for 15 h at 343 ^{o}K under vacuum (Jacquemin et al., 2006). The water-miscible RTILs used retain sufficient moisture to facilitate the water-mediated sensor chemistry. It has been reported that the presence of $[F]^{-}$ in hydrated molten ammonium salts results in facilitated transport of CO_2 via a catalyzed bicarbonate reaction (Blanchard et al.,1999; Anthony et al., 2002; Bates et al., 2002).

In the presence of trace amounts of water, $[PF_6]^-$ decomposes into HF and F^- reacts with CO_2 in order to form HCO_3^-:

$$2F^- + H_2O + CO_2 \rightarrow HCO_3^- + HF_2^-$$

Similarly, it is also probable that the $[BF_4]^-$ ion of RTIL-I also catalyzes bicarbonate formation. The different relative signal changes for the two ionic liquids (RTIL-I and RTIL-II) can therefore be attributed to the catalytic action of tetrafluoroborate anion.

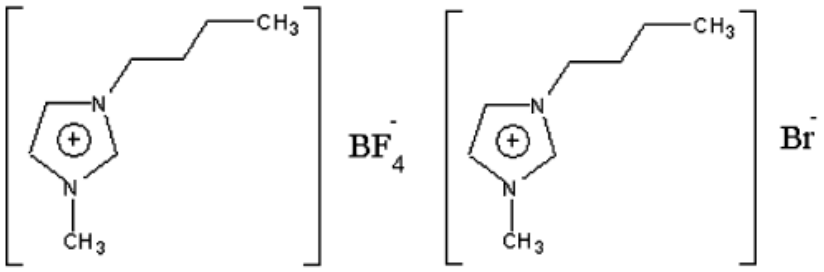

RTIL-I RTIL-II

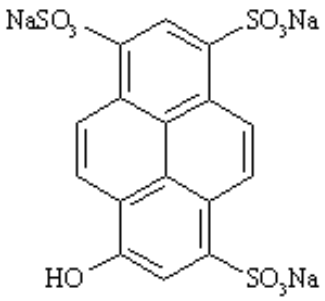

Figure 3.1 The structures of the water-miscible room-temperature ionic liquids (RTIL-I and RTIL-II) and the dye (HPTS)

3.3 Cocktail preparation procedures

Sensing cocktails were prepared by dissolving the sodium salt of the indicator dye in two different ionic liquids. Cocktail 1 contained 2×10^{-5} mol L^{-1} HPTS in 1 mL RTIL-I containing 160 µL 1 mol L^{-1} tetrabutylammonium hydroxide (TBAOH). Cocktail 2 contained 2×10^{-5} mol L^{-1} HPTS in 3 mL ionic liquid but did not contain

TBAOH. Other cocktail compositions are given in Table 3.1. Cocktails 1 and 4 were used for sensing gaseous CO_2 and cocktails 3 and 6 for sensing dissolved CO_2. Cocktails 2 and 5 were used during experiments to determine pK_a.

Table 3.1 Compositions of the cocktails used as CO_2-sensing agents

Cocktail no.	Ionic liquid[a]	Dye[b]	Additive
C1	RTIL I (1 mL)	HPTS (2×10^{-5} mol L^{-1})	TBAOH (1 mol L^{-1}, 160 µL)
C2	RTIL I(3 mL)	HPTS (2×10^{-5} mol L^{-1})	–
C3	RTIL I (1 mL)	HPTS (2×10^{-5} mol L^{-1})	TBAOH (1 mol L^{-1}, 130 µL)
C4	RTIL II (1 mL)	HPTS (2×10^{-5} mol L^{-1})	TBAOH (1 mol L^{-1}, 40 µL)
C5	RTIL-II (3 mL)	HPTS (2×10^{-5} mol L^{-1})	–
C6	RTIL II (1 mL)	HPTS (2×10^{-5} mol L^{-1})	TBAOH (1 mol L^{-1}, 25 µL)
C7	RTIL II (3 mL)	HPTS (2×10^{-5} mol L^{-1})	Perchloric acid (0.5 mol L^{-1}, 190µL)

[a]RTIL-I and RTIL-II are the room-temperature ionic liquids 1-methyl-3-butylimidazolium tetrafluoroborate and 1-methyl-3-butylimidazolium bromide
[b]HPTS is trisodium salt of 8-hydroxypyrene-1,3,6-trisulfonic acid, Na salt

3.4 Results and discussion

3.4.1 Absorption spectra of HPTS in RTILs at different pHs and dissociation constant calculations (pK_a)

Knowledge of the dissociation constant (pK_a) of HPTS in RTILs is of fundamental importance for providing information on the chemical reactivity range of the indicator dye and the suitability of this dye as a CO_2-sensing agent in ionic liquid media. Indicators with pK_a values between 6.8 and 10.0 in aqueous media are essential for sensitive pCO_2 optodes. To evaluate the availability of HPTS in the RTILs for CO_2 sensing, the acidity constant was determined. pH-induced absorption spectra of the cocktails were recorded in the pH ranges 5.5–11.0 and 8.5–12.0 in RTIL-I and II, respectively. Cocktail 2 contains the acidic form of HPTS in RTIL-I and was titrated with 1 mol L^{-1} TBAOH. Cocktail 5 contains the basic form of HPTS in RTIL-II and was titrated with 0.5 mol L^{-1} perchloric acid. After each addition the absorption spectra and pH of the media were recorded. pH-dependent absorption spectra of HPTS in RTIL-I and RTIL-II are shown in Figure 3.2. In RTIL-I, absorption bands of HPTS appeared at 365, 380, 403 and 470 nm and an isobestic

point was formed at 415 nm. In RTIL-II, absorption maxima of HPTS were observed at 403 and 480 nm. The absorption bands of HPTS at 365 and 380 nm in RTIL-I disappeared in RTIL-II. In RTIL-I the resolution of the absorption spectrum of the acidic form of HPTS was better than that of the basic form in RTIL-II. This better resolution can be attributed to the well balanced interaction of the organic HPTS molecule with the imidazolium group and the tetrafluoroborate anion. A significant bathochromic shift of the absorption maximum of the basic form of HPTS (λ_{max}=480 nm) was observed in RTIL-II compared with those in water (λ_{max}=454 nm), in ethylcellulose (λ_{max}=460 nm) or in RTIL-I (λ_{max}=470 nm). This substantial bathochromic shift in RTIL-II can be attributed to the greater polarity of the bromine derivative. pK_a values were calculated by use of absorption spectra related data and α_a and α_b, the ratios of the concentrations of the acidic and basic forms of HPTS, respectively, to the total concentration of HPTS. By the use of Equations 3.1 and 3.2, α_a and α_b for HPTS in RTIL-I and II were calculated from spectral data.

$$\alpha_a = (A-A_b)/(A_a-A_b) \qquad (3.1)$$

$$\alpha_b = (A-A_a)/(A_b-A_a) \qquad (3.2)$$

where A_a and A_b are the absorbance intensities of the acidic and basic forms of HPTS and A is the absorbance at any pH. At low pH α_a was equal to 1 and α_b was 0 when all the HTPS was in the acidic form. Likewise, at high pH α_a was equal to 0 and α_b was 1 when all the HPTS molecules were in the basic form. Table 3.2 shows the absorbance values of 2×10^{-5} mol L^{-1} HPTS at λ_{max} = 470 nm and the calculated α values in RTIL-I.

The acid dissociation constants (pK_a) of HTPS in RTIL-I and RTIL-II can be easily obtained at pH values when α_a and α_b are equal to 0.50. From Figures 3.3 and 3.4, the pK_a values of HPTS in RTIL-I and II were found to be 9.50 and 11.20, respectively.

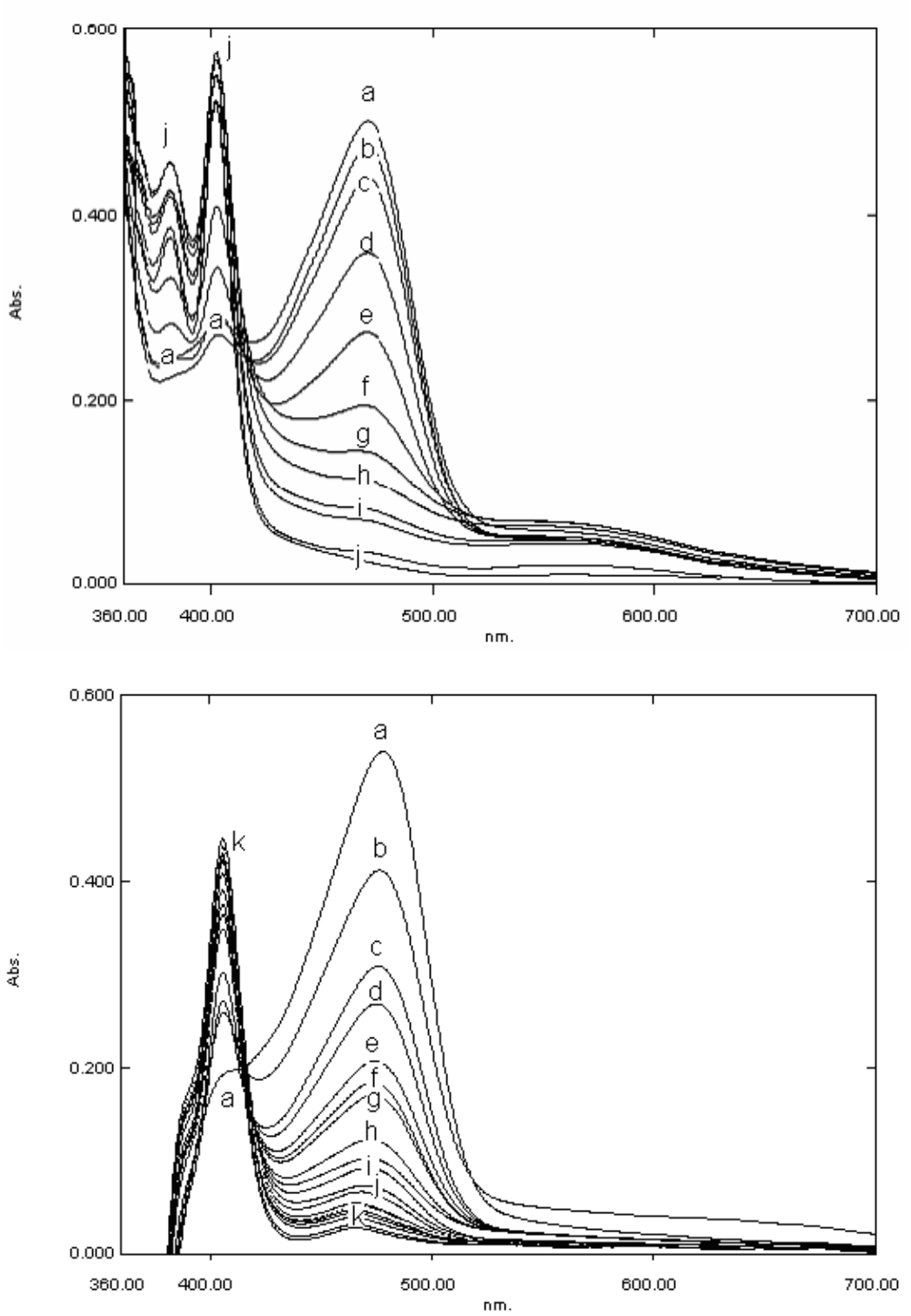

Figure 3.2 Absorption spectra of 2×10^{-5} mol L^{-1} HPTS. I After titration with 1 mol L^{-1} tetrabutylammonium hydroxide in RTIL-I. a, pH 11.06 b, pH 10.68 c, pH 10.37 d, pH 9.93 e, pH 9.63 f, pH 9.10 g, pH 8.74 h, pH 8.45 i, pH 8.00, 7.55 j: pH 6.96 , 5.67; II After titration with 0.5 mol L^{-1} perchloric acid in RTIL-II. a, pH 12.0; b, pH 11.7; c, pH 11.5; d, pH 11.3; e, pH 11.1; f, pH 10.9; g, pH 10.7; h, pH 10.4; i, pH 10.3 and 10.2; j, pH 10.0 and 9.9; k, pH 9.8 and 8.7.

Table 3.2 Absorbance values of 2×10^{-5} mol L^{-1} HPTS at λ_{max} = 470 nm and the calculated α values in RTIL-I.

A (λ_{max} = 470 nm)	A_a	A_b	α_a	α_b
0.000 (pH=0.25)	0	0.5	1.000	0.000
0.015 (pH=3.52)	0	0.5	0.970	0.030
0.024 (pH=5.67)	0	0.5	0.952	0.048
0.029 (pH=5.96)	0	0.5	0.942	0.058
0.029 (pH=6.30)	0	0.5	0.942	0.058
0.035 (pH=6.96)	0	0.5	0.930	0.070
0.069 (pH=7.55)	0	0.5	0.862	0.138
0.081 (pH=8.00)	0	0.5	0.838	0.162
0.113 (pH=8.45)	0	0.5	0.774	0.226
0.126 (pH=8.53)	0	0.5	0.748	0.252
0.144 (pH=8.74)	0	0.5	0.712	0.288
0.193 (pH=9.10)	0	0.5	0.614	0.386
0.227 (pH=9.36)	0	0.5	0.546	0.454
0.272 (pH=9.63)	0	0.5	0.456	0.544
0.360 (pH=9.93)	0	0.5	0.280	0.720
0.439 (pH=10.37)	0	0.5	0.122	0.878
0.472 (pH=10.68)	0	0.5	0.056	0.944
0.500 (pH=11.06)	0	0.5	0.000	1.000

Table 3.3 Absorbance values of 2×10^{-5} mol L^{-1} HPTS at λ_{max} = 470 nm and the calculated α values in RTIL-II.

A (λ_{max} = 470 nm)	A_a	A_b	α_a	α_b
0.543 (pH=12.00)	0.027	0.543	0.000	1.000
0.411 (pH=11.70)	0.027	0.543	0.256	0.744
0.308 (pH=11.48)	0.027	0.543	0.455	0.545
0.268 (pH=11.34)	0.027	0.543	0.533	0.467
0.226 (pH=11.11)	0.027	0.543	0.614	0.386
0.208 (pH=11.10)	0.027	0.543	0.649	0.351
0.185 (pH=11.91)	0.027	0.543	0.694	0.306
0.172 (pH=10.70)	0.027	0.543	0.719	0.281
0.123 (pH=10.40)	0.027	0.543	0.814	0.186
0.104 (pH=10.33)	0.027	0.543	0.851	0.149
0.092 (pH=10.16)	0.027	0.543	0.874	0.126
0.075 (pH=10.00)	0.027	0.543	0.907	0.093
0.067 (pH=9.99)	0.027	0.543	0.923	0.077
0.059 (pH=9.85)	0.027	0.543	0.938	0.062
0.054 (pH=9.80)	0.027	0.543	0.948	0.052
0.051 (pH=9.72)	0.027	0.543	0.953	0.047
0.047 (pH=9.58)	0.027	0.543	0.961	0.039
0.044 (pH=9.46)	0.027	0.543	0.967	0.033
0.039 (pH=9.30)	0.027	0.543	0.977	0.023
0.032 (pH=8.89)	0.027	0.543	0.990	0.010
0.027 (pH=8.70)	0.027	0.543	1.000	0.000

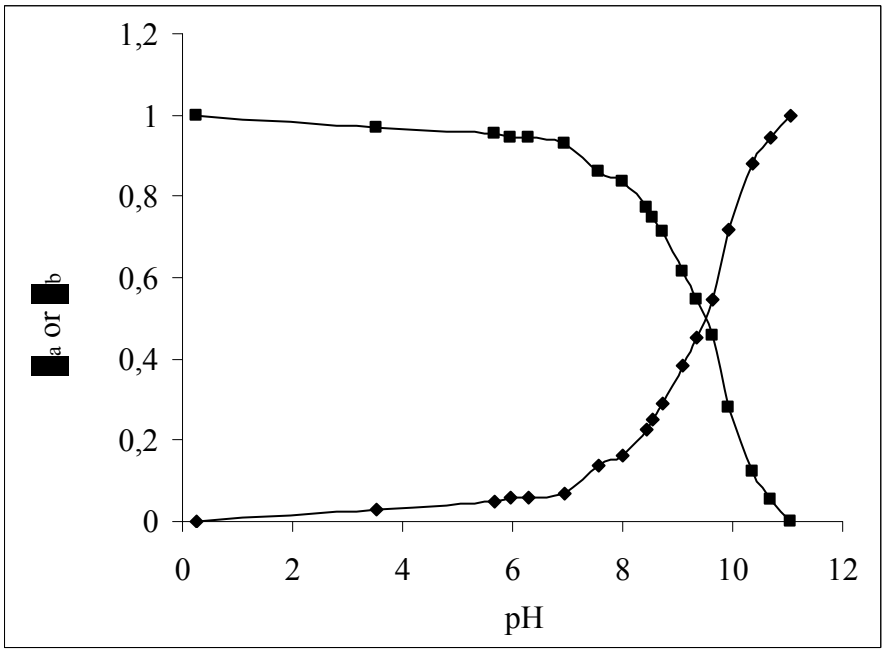

Figure 3.3 Plots of α_a and α_b of HPTS against pH in RTIL-I

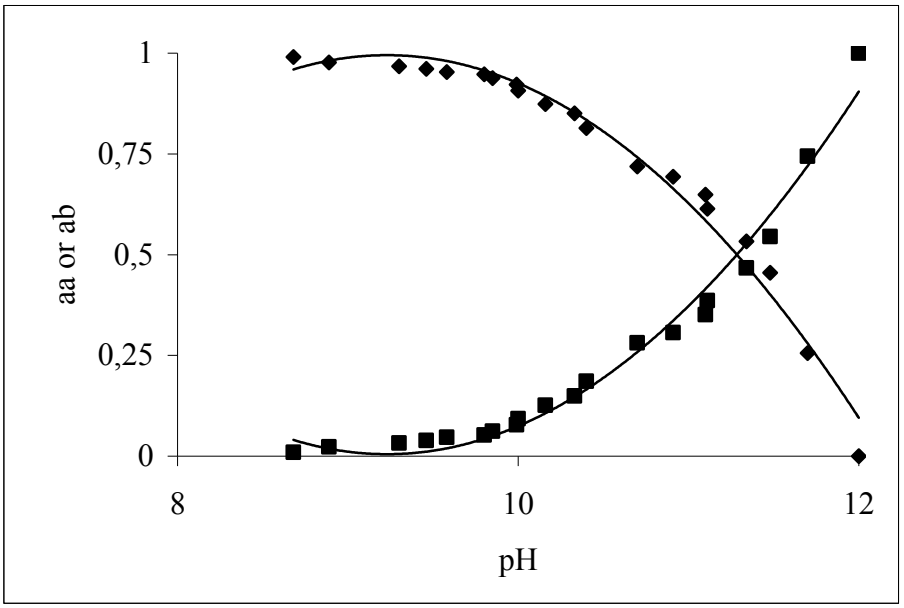

Figure 3.4 Plots of α_a and α_b of HPTS against pH in RTIL-II

3.4.2 Excitation and emission spectra of HPTS in RTILs

The imidazolium ionic liquids have non-negligible absorption beyond 300 nm and unusual fluorescence the peak position of which keeps on shifting with changing excitation wavelength. This unusual fluorescence behavior is because of the presence of energetically different associated forms of the imidazolium ions (Scovazzo et al, 2004). We therefore investigated the possibility of interference of the intrinsic fluorescence of RTIL-I and RTIL-II with the emission of HPTS. Figure 3.5 I and II show the emission spectra acquired for RTIL-I and II and the acidic and basic forms of HPTS. The RTILs were excited at the excitation wavelength of the acidic and basic forms of HPTS. From Figure 3.5 it can be concluded that the observed fluorescence of the studied ionic liquids is negligible and does not limit the sensing ability of HPTS. Figure 3.6 and 3.7 show the pH induced fluorescence excitation (EX) and emission (EM) spectra of acidic form of HPTS in the explored RTILs.

The HPTS (C-2) in RTIL-I was in its acidic form and was titrated with 1 M tetrabuthyl ammonium hydroxide solution. HPTS in RTIL-I was excited at 404 nm and emission spectra were recorded (Figure 3.6 I). The excitation spectra were back scanned by exciting at the maximum emission wavelength, 428 nm. A relative signal change of 95% was obtained in the pH range 3.52–11.06. On addition of quaternary ammonium base the intensity of the signal of the emission spectra at 428 nm decreased whereas that at 519 nm increased. The emission spectra of the acidic form of HPTS had an isoemissive point at 490 nm in RTIL-I.

The HPTS (C-5) in RTIL-II was in its basic form and was titrated with 1 M perchloric acid solution. HPTS in RTIL-II was excited at 408 nm and emission spectra were recorded (Figure 3.6 II). The excitation spectra were back scanned by exciting at the maximum emission wavelength, 438 nm. A relative signal change of 85% was obtained in the pH range 10.90-2.00. On addition of 1 M perchloric acid, the intensity of the signal of the emission spectra at 438 nm increased whereas that at 518 nm decreased. The emission spectra of the acidic form of HPTS had an isoemissive point at 496 nm in RTIL-II.

The HPTS in RTIL-I (C-2) was also excited at 470 nm to obtain the emission spectra (Figure 3.7 I). The excitation spectra were recorded by exciting at 519 nm. On addition of quaternary ammonium base the intensity of the signal of the emission spectra at 519 nm and the intensity of the signal of the excitation spectra at 407 and 473 nm decreased. No isoemissive points were observed in the excitation and emission spectra when HPTS in RTIL-I was excited in the above mentioned wavelengths.

The HPTS in RTIL-II (C-5) was also excited at 480 nm to obtain the emission spectra (Figure 3.7 II). The excitation spectra were recorded by exciting at 520 nm. On addition of perchloric acid the intensity of the peak at 520 nm (emission spectra) and 480 nm (excitation spectra) decreased whereas that at 408 nm (excitation spectra) increased. An isobestic point was observed at 420 nm. The spectral characteristics and pKa of HPTS in phosphate buffer, ethylcellulose, RTIL-I, and RTIL-II at 25 °C are listed in Table 3.4.

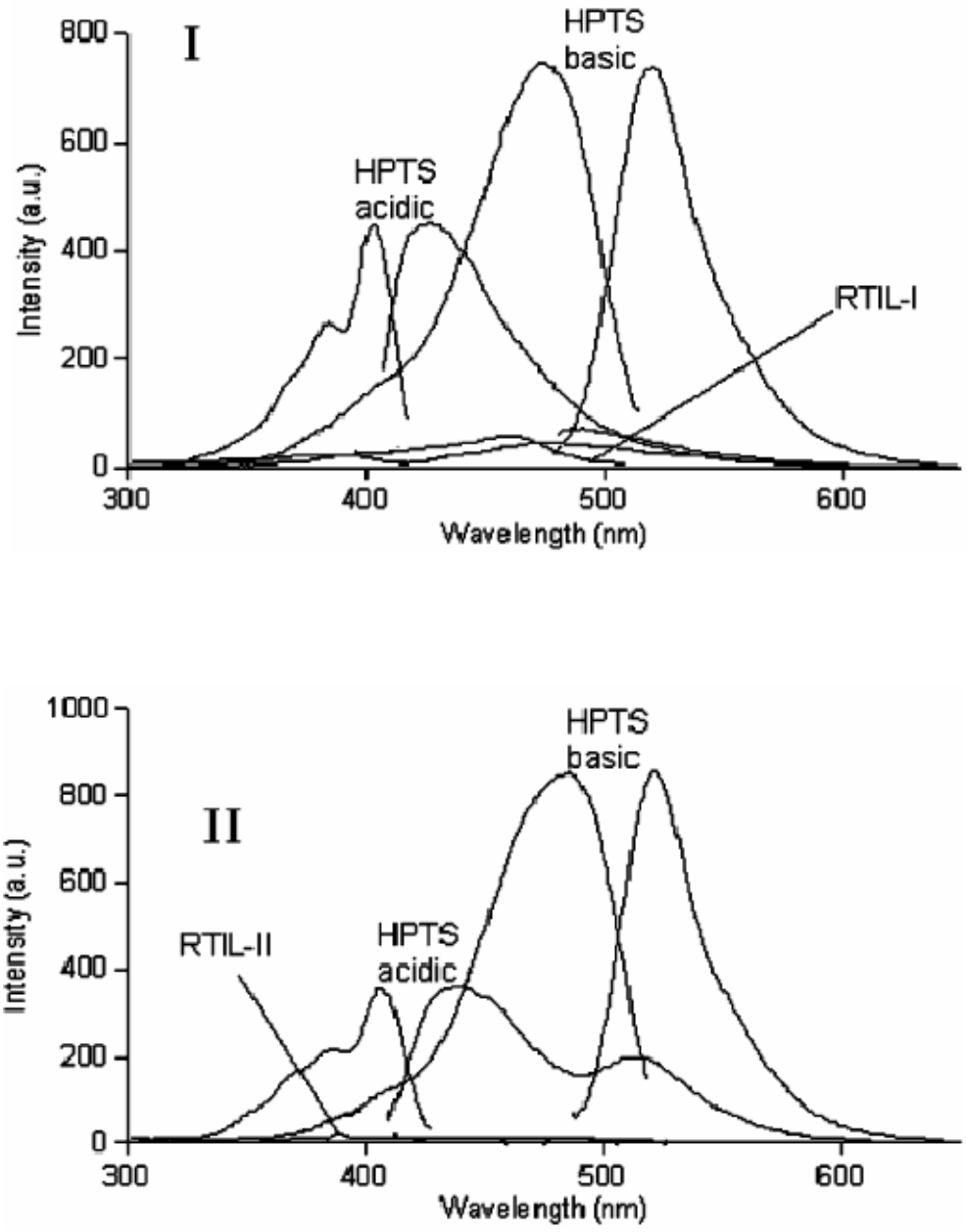

Figure 3.5 Emission spectra of RTIL-I and the acidic and basic forms of HPTS. **I** Basic form of HPTS in RTIL-I (λ^{ex}_{max} = 470 nm, λ^{em}_{max} = 519 nm), Acidic form of HPTS in RTIL-I (λ^{ex}_{max} = 404 nm, λ^{em}_{max} = 426 nm), RTIL-I excited at λ^{ex}_{max} =470 nm and λ^{em}_{max} =519 nm, RTIL-I excited at λ^{ex}_{max} = 404 nm and λ^{em}_{max} = 426 nm. **II** Basic form of HPTS in RTIL-II (λ^{ex}_{max} = 480 nm, λ^{em}_{max} = 520 nm), Acidic form of HPTS in RTIL-II (λ^{ex}_{max} = 406 nm, λ^{em}_{max} = 438 nm), RTIL-II excited at λ^{ex}_{max} =480 nm and λ^{em}_{max} =520 nm, RTIL-II excited at λ^{ex}_{max} = 406 nm and λ^{em}_{max} = 438 nm.

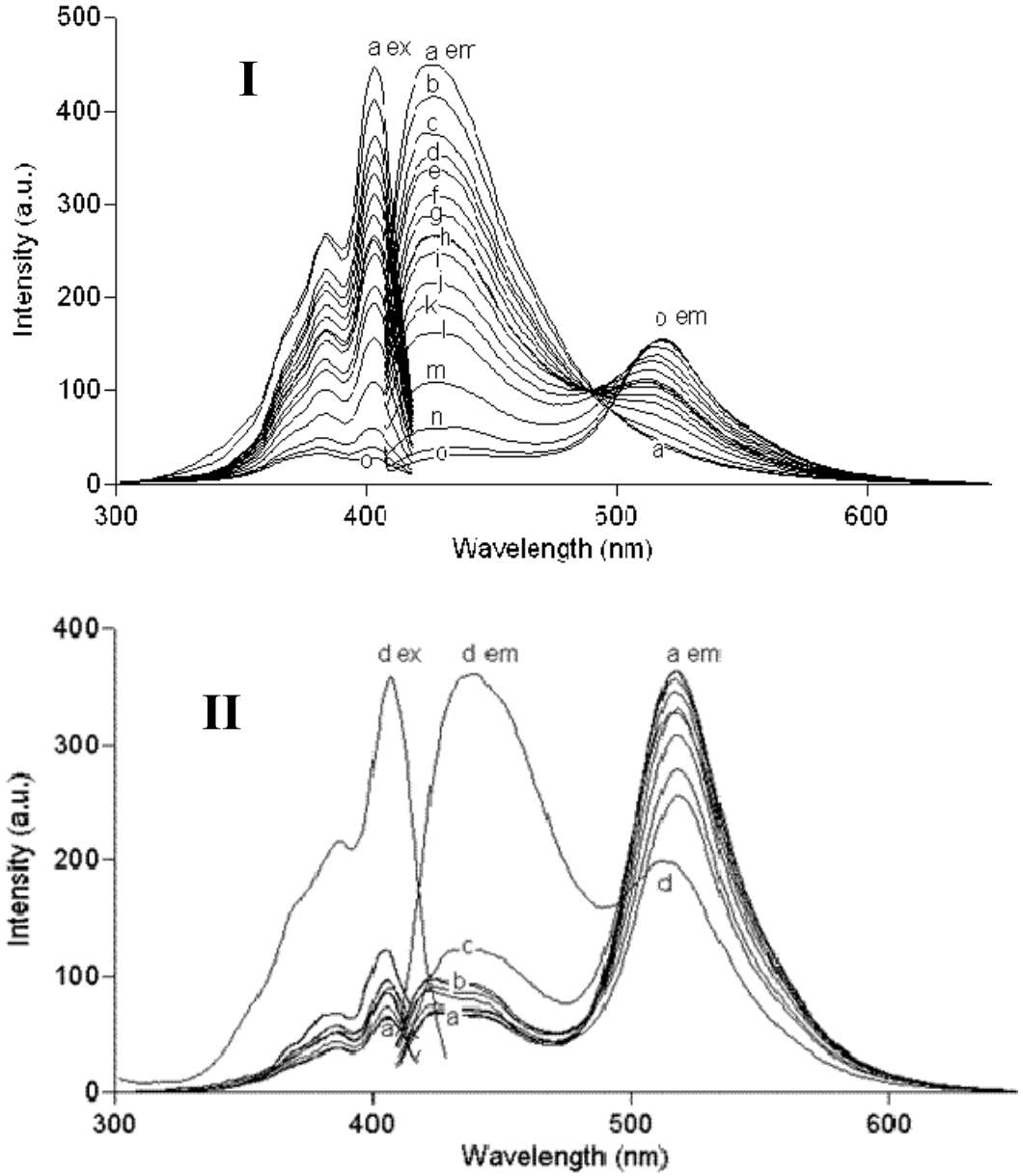

Figure 3.6 **I** Fluorescence spectra of HPTS in RTIL-I in the pH range 3.52–11.06 after micrometric titration with 1 mol L^{-1} TBAOH. Excitation spectra: ex 300–420 nm; em 427 nm; Emission spectra: ex 404 nm; em 410–640 nm; a, pH 3.52; b, pH 4.70; c, pH 5.67; d, pH 6.30; e, pH 6.96; f, pH 7.55; g, pH 8.00; h, pH 8.50; i, pH 8.74; j, pH 9.1; k, pH 9.36; l, pH 9.63; m, pH 9.93; n, pH 10.37; o, pH 10.68; p, pH 11.06. **II** Fluorescence spectra of 2×10^{-5} mol L^{-1} HPTS in RTIL-II in the pH range 10.90-2.00. Excitation spectra: ex 300–420 nm; em: 438 nm, Emission spectra: ex 408 nm; em 410–640 nm; a pH: 10.90-8.90; b, pH: 8.20-7.00; c, pH: 5.80; d, pH: 2.0

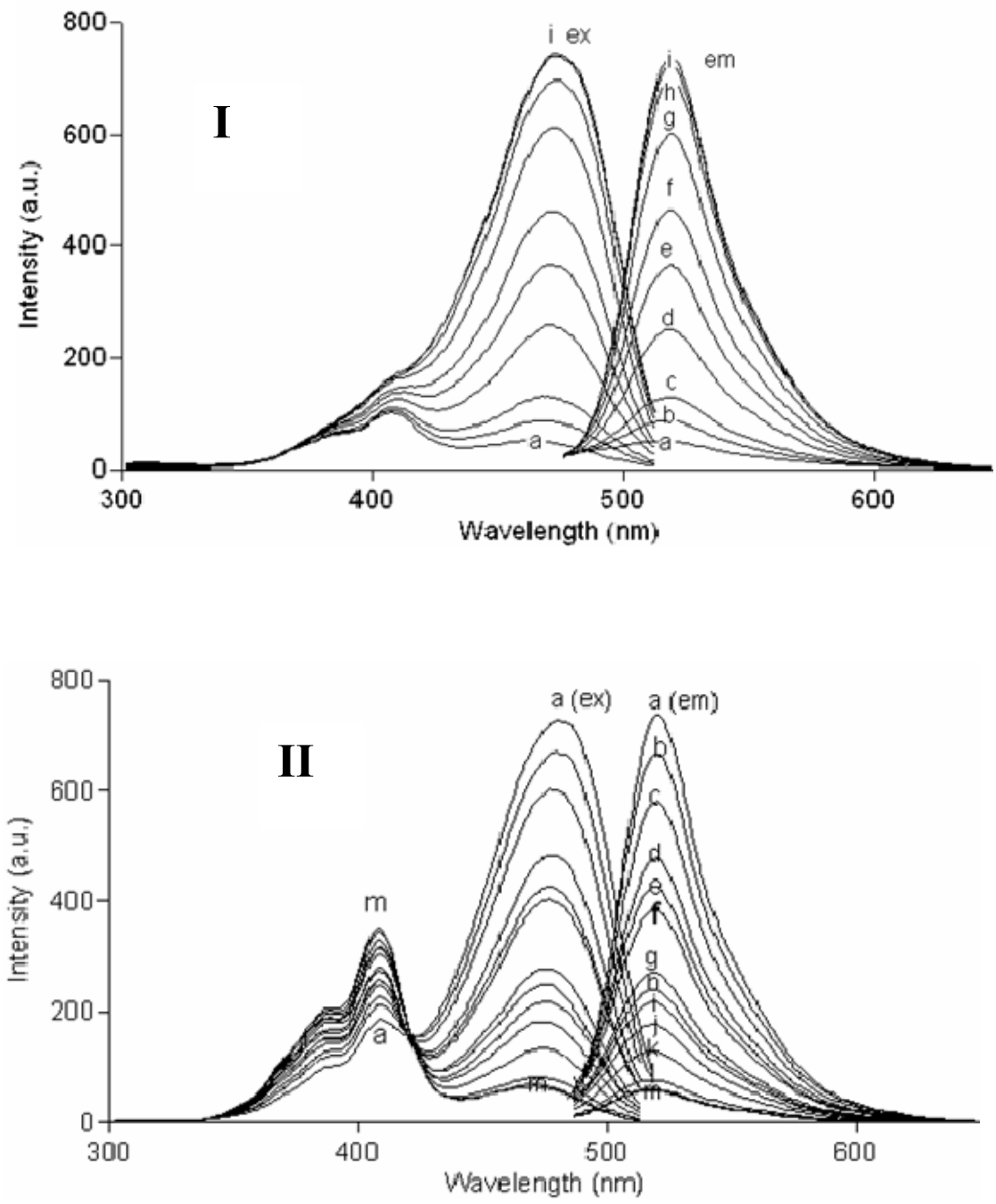

Figure 3.7 I Fluorescence spectra of 2×10^{-5} mol L^{-1} HPTS in RTIL-I in the pH range 10.70–8.35 after micrometric titration with 1 mol L^{-1} TBAOH. Excitation spectra: ex 300–510 nm; em 520 nm, Emission spectra: ex 470 nm; em 475–640 nm; a, pH 8.35; b, pH: 8.53; c, pH: 8.74; d, pH: 9.10; e, pH: 9.36; f, pH: 9.50; g, pH: 9.63; h, pH: 9.93; i, pH: 10.6 and 10.70.
IB Fluorescence spectra of 2×10^{-5} mol L^{-1} HPTS in RTIL-II Excitation spectra: ex 300–510 nm; em 520 nm, Emission spectra: ex 480 nm; em 485–640 nm; a, pH 12.00; b, pH 11.70; c, pH 11.50; d, pH 11.30; e, pH 11.10; f, pH 10.90; g, pH 10.70; h, pH 10.40; i, pH 10.30; j, pH 10.20; k, pH 10.00; l, pH 9.50; m, pH: 8.90 and 8.70.

Table 3.4 Spectral characteristics and pKa of HPTS in phosphate buffer, ethylcellulose, RTIL-I, and RTIL-II at 25 °C

Spectrophotometric properties	HPTS in phosphate solution	HPTS in ethylcellulose film	HPTS in RTIL-I	HPTS in RTIL-II
Absorption, λmax Acidic form	404, 382(s), 368	404, 382(s), 368	365, 380, 403	403
Basic form	454, 392(s), 368	460, 404(s), 368	365, 380, 470	480
Isobestic point (nm)	416	415	412	413
Excitation, Acidic form	404, 382, 368(s)	402, 382(s), 369	404, 385, 367(s)	406, 387, 370(s)
Basic form	457, 395, 369(s)	468, 458(s), 402	370 473, 407(s)	481, 408, 387(s)
Emission, Acidic form	510	429	426, 519	438, 518
Basic form	510	515	519	520
Isoemissive point (nm)	EX 417 EM 510	- -	EX – EM 490 (acidic)	EX 420 (basic) EM 496 (acidic)
pKa	7.31	8.43	9.50	11.20

(s) denotes shoulder on peak

3.4.3 Dissolved CO_2 sensing studies

Standard solutions were prepared freshly from 1 mol L^{-1} $NaHCO_3$ stock solution before the measurements. CO_2-free standard solutions were prepared with doubly distilled water after boiling and bubbling with nitrogen; they were stored in closed containers. Microliter volumes of (10 μL) of standard solutions of $NaHCO_3$ were added to the sensing agent-containing cuvette, mixed and the changes in fluorescence intensity caused by addition of different concentrations of dissolved CO_2 were measured. All the experiments were performed at room temperature (25 °C). Figure 3.8 I and II show the emission and excitation spectra of HPTS in RTIL-I and RTIL-II after exposure to HCO_3^- solutions. Isobestic points were not observed in either of the

ionic liquid media after addition of HCO_3^- ions. Use of water-miscible RTILs enables uptake of water molecules and direct addition of HCO_3^- solutions to the sensing medium. 10 microliters of standard HCO_3^- solutions were added by using a micro syringe onto the sensing agent, so dilution was avoided. The linearized calibration plots of sensor compositions C-3 and C-6 are shown in Figure 3.9 and 3.10. The calibration plot for the sensor in RTIL-I (C-3) can be described by the equation y = 284.3 x + 0.4635, correlation coefficient 0.9949. The dynamic working range in RTIL-I is between 8.0×10^{-6} and 2.0×10^{-2} mol L^{-1} HCO_3^-. The calibration plot for the sensor in RTIL-II (C-6) is logarithmic and can be described by the equation y = -3.1847x + 11.355, correlation coefficient 0.9912. The dynamic working range in RTIL-II covers the concentration range 8.0×10^{-4}–1.2×10^{-2} mol L^{-1} HCO_3^-.

Use of the RTILs as matrix materials results in distinct advantages over previously reported dissolved CO_2 sensors—excellent stability and quite long storage lifetimes. The dynamic working range achieved for measurement of dissolved CO_2 with both ILs is in accordance with the literature. The lifetime of our sensor is currently 212 days, which is quite good compared with previous carbon dioxide sensors (Bültzingslöwen et al., 2002; Ertekin et al., 2003; Malins & MacCraith, 1998; Müller & Hauser, 1996; Neurauter et al., 1999; Weigl & Wolfbeis, 1995). In most previous sensor designs quaternary hydroxides were added into the sensing cocktail as a counter ion to increase sensitivity and lifetime, and enhancement has been reported because of the presence of quaternary hydroxides (Bültzingslöwen et al., 2002; Ertekin et al., 2003; Mills et al., 1992; Neurauter et al., 1999; Weigl & Wolfbeis, 1995; Wolfbeis et al., 1998). These quaternary hydroxides are indeed capable of activating the fluorescence of dyes in media of low polarity. In our sensors tetrabutylammonium hydroxide (TBAOH) was used as an internal buffering system. TBAOH stabilizes the deprotonated form of the dye in the matrix and, with the trace amount of water, provides the sensing chemistry. The excess TBAOH is neutralized by atmospheric carbon dioxide, forming a hydrogen carbonate buffer in the matrix and this can be used to tune the sensitivity and to improve the storage stability of the sensor. The optimum TBAOH concentration in the matrix was found

to be 130 μL mL^{-1} and 25 μL mL^{-1} for RTIL-I and RTIL-II, respectively. The functioning of the RTIL-based sensing cocktail as a colorimetric sensor for CO_2 can be depicted by the equilibrium reaction:

$$Dye^- \text{ (color A)} + xH_2O + CO_{2(g)} \rightleftharpoons HCO_3^- + (x\text{-}1)\ H_2O + DyeH \text{ (color B)}$$

Here, color A is the color of the unprotonated form of HPTS in the RTILs, which is phosphorescent green, and color B is the color of the protonated form, which is pale yellow. Calculated H_2CO_3 concentrations (the sum of hydrated CO_2 (aq) and real H_2CO_3) and corresponding pCO_2 values in solutions prepared from $NaHCO_3$ are listed in Table 3.5. Concentrations were calculated by use of the equations below:

$$CO_{2\ (g)} + H_2O \rightleftharpoons H_2CO_3 \qquad \log K_H = -1.41$$

$$H_2CO_3 \rightleftharpoons H^+ + HCO_3^- \qquad \log Ka_1 = -6.35$$

$$HCO_3^- \rightleftharpoons H^+ + CO_3^{2-} \qquad \log Ka_2 = -10.38$$

where K_1 is the Henry's coefficient of gaseous CO_2 in water. Ka_1 and Ka_2 are the first and second acid-dissociation constants of carbonic acid (Stumm & Morgan, 1981; Mills et al., 1992). In HCO_3^- solution the relationship between the $[H_2CO_3]$ and proton concentration is:

$$[H_2CO_3] = ([H^+]^3 + [H^+]^2[Na^+] - K_w [H^+]) / (Ka_1[H^+] + 2\ Ka_2) \quad (3.3)$$

where Kw is the water dissociation constant, and $[Na^+]$ is the concentration of sodium ions present.

For $NaHCO_3$ solutions the $[H^+]$ can be determined from the following formula (Gündüz, 1993);

$$[H^+] = \sqrt{\frac{Ka_1.Ka_2.C + Ka_1.Kw}{C + Ka_1}} \qquad (3.4)$$

where C is the concentration of the $NaHCO_3$.

The $[H_2CO_3]$ can also be calculated by the following formula:

$$[H_2CO_3] = \frac{[HCO_3^-][H^+]}{Ka_1} = \frac{C.[H^+]}{Ka_1} \quad (3.5)$$

Partial pressures of $CO_2(g)$ was calculated by the following equation:

$$pCO_2(g) = [H_2CO_3]/K_H \quad (3.6)$$

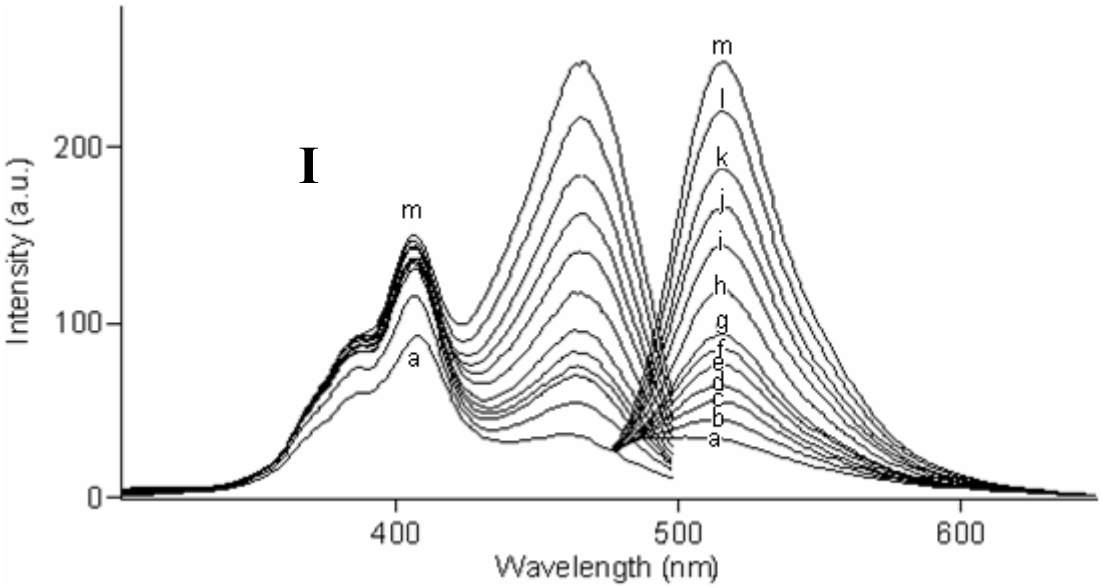

Figure 3.8 HPTS after addition of HCO_3^- solutions. I In RTIL-I; HCO_3^- concn. (mol L^{-1}): a, 0; b, 8.0×10^{-7}; c, 8.0×10^{-6}; d, 8.0×10^{-5}; e, 2.0×10^{-3}; f, 3.2×10^{-3}; g, 4.4×10^{-3}; h, 6.8×10^{-3}; i, 9.2×10^{-3}; j, 1.2×10^{-2}; k, 1.4×10^{-2}; l, 1.7×10^{-2}; m, 1.9×10^{-2}. II In RTIL-II; HCO_3^- concn (mol L^{-1}): a, 0; b, 4.0×10^{-6}; c, 4.0×10^{-5}; d, 4.0×10^{-4}; e, 8.0×10^{-4}; f, 1.2×10^{-3}; g, 1.6×10^{-3}; h, 2×10^{-3}; i, 2.4×10^{-3}; j, 2.8×10^{-3}; k, 3.6×10^{-3}; l, 4.4×10^{-3}; m, 5.2×10^{-3}; n, 6.8×10^{-3}; o, 7.6×10^{-3}; p, 8.4×10^{-3}; r, 10^{-2} , 1.2×10^{-2}

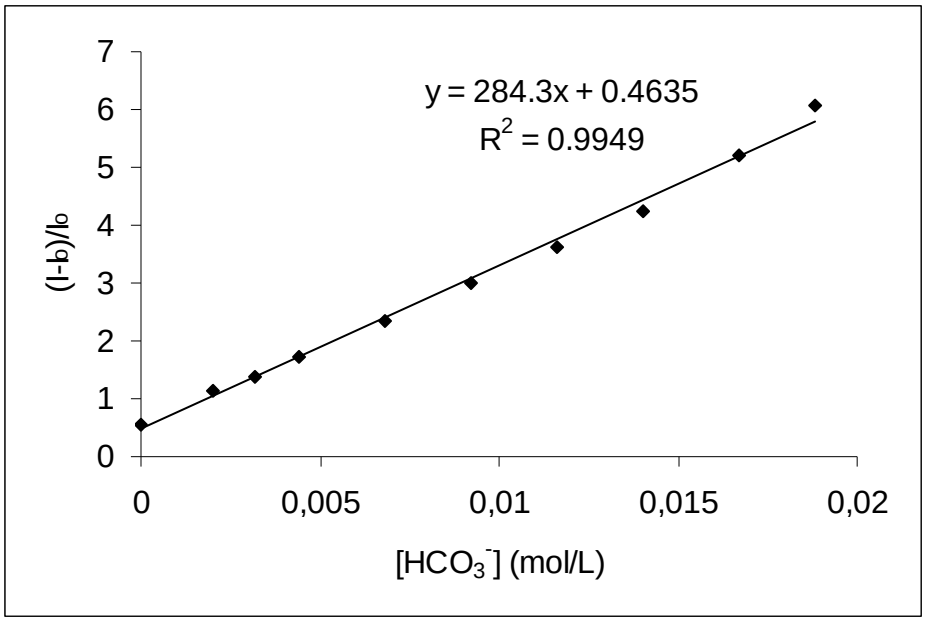

Figure 3.9 Calibration graph of HPTS in RTIL-I after addition of HCO_3^- solutions

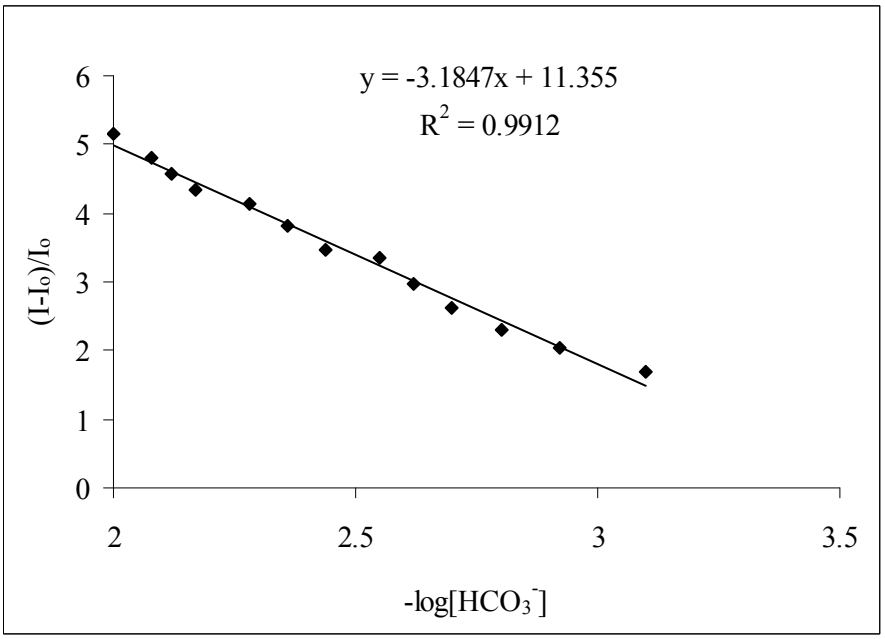

Figure 3.10 Calibration graph of HPTS in RTIL-II after addition of HCO_3^- solutions

Table 3.5 Calculated concentrations of $[H_2CO_3]$ and the corresponding pCO_2 in solutions prepared with $NaHCO_3$

Total $NaHCO_3$ (mol L^{-1})	$[H_2CO_3]$ (mol L^{-1})	pCO_2 in RTILs (atm)
2×10^{-6}	1.95×10^{-7}	5.02×10^{-6}
2×10^{-5}	6.97×10^{-7}	1.79×10^{-5}
2×10^{-4}	2.79×10^{-6}	7.17×10^{-5}
2×10^{-3}	2.33×10^{-5}	5.98×10^{-4}
2×10^{-2}	1.86×10^{-4}	4.78×10^{-3}

3.4.4 Gaseous CO_2 sensing studies

Gaseous CO_2 and N_2 were mixed in the concentration range 0–100% in a gas diluter (Sonimix 7000A gas blending system). The output flow rate of the gas mixture was maintained at 250 mL min^{-1}. Gas mixtures were introduced into the sensor agent-containing cuvette via a diffuser needle under ambient conditions either directly or after humidification of the gas by bubbling through water at 25 °C.

With the sensor compositions tested good sensitivity to gas-phase carbon dioxide and large relative signal changes were obtained (Table 3.6). Plots of $(I_0-I)/I_0$ against amount (%) of carbon dioxide in the gas mixture are shown in Figures 3.13 and 14 for RTIL-I and RTIL-II, respectively. The response and recovery-related data of the sensing cocktails with RTIL-I and RTIL-II were acquired by recording the emission intensity signals during exposure to 0.0–10% CO_2 and 0–60% CO_2, respectively. The response of the sensors was hyperbolic, with greater sensitivity at low carbon dioxide concentrations, which is typical of this type of pCO_2 sensor [1, 3, 9]. The RTIL-II-based sensor had a wider dynamic range (0–60% pCO2) than the RTIL-I based sensor (0–10% pCO_2), with resolution of ±2%. $(I_0-I)/I_0$ is the intensity ratio of the protonated (I) and deprotonated (I_0) forms of the indicator. These sensor compositions resulted in quite high relative signal changes of approximately 90% and 75% in the direction of a decrease in emission intensity at λ^{em}_{max} =519 nm (RTIL-

I) and λ_{max}^{em} =520 nm (RTIL-II) on exposure to CO_2 when excited at 470 nm and 480 nm, respectively.

The τ_{90} response times (the time to achieve 90% of the overall signal change) in-RTIL-I and II were in the range 1–2 min on exposure to 0.0–10% CO_2 and 0–60% CO_2, respectively. The initial signal intensities for the cocktails containing RTIL-I could be completely recovered after switching in the concentration range 0.0–10% CO_2 and no drift was observed even after the 9th cycle. Between the 1st and 10th cycles the level of reproducibility of upper signal levels was 540.89±1.76 (n=10). The regeneration time was 10 min. The signal intensities for the RTIL-II-containing cocktails were not fully reversible on going from 60% CO_2 to 100% N_2. In the concentration range 0.0–60% 6% hysteresis was observed between the 1st and 6th cycles. After the 6th cycle (between the 6th and 8th cycles) no hysteresis was observed (Figure 3.11). The response and recovery time, between one and ten minutes, includes the equilibration time for the protonation- deprotonation reaction and the dead volume of the gas tubes, rather than the true response time of the sensor composition. The volume of RTIL used has an important effect on these times. The system used here was for characterization purposes only, and a significantly lower cuvette volume or a micro flow cell is required for evaluation of the true response time. The rate of sensor chemistry is kinetically determined by a combination of the association–dissociation equilibrium of the indicator and the interaction of the analyte gas with the trace amount of water bound within the water-miscible RTILs [25]. These processes, occurring in the viscous RTILs, are slow compared with diffusion of gas through the sensing membrane. The long recovery time can also be attributed to the lower solubility of the regeneration agent, N_2, in ionic liquid media. The literature reveals that N_2 is poorly soluble in RTILs. The ratio of the solubility of CO_2 to that of N_2 in butylmethylimidazolium hexafluorophosphate ([bmim][PF_6]) was found to be greater than 374 [23].

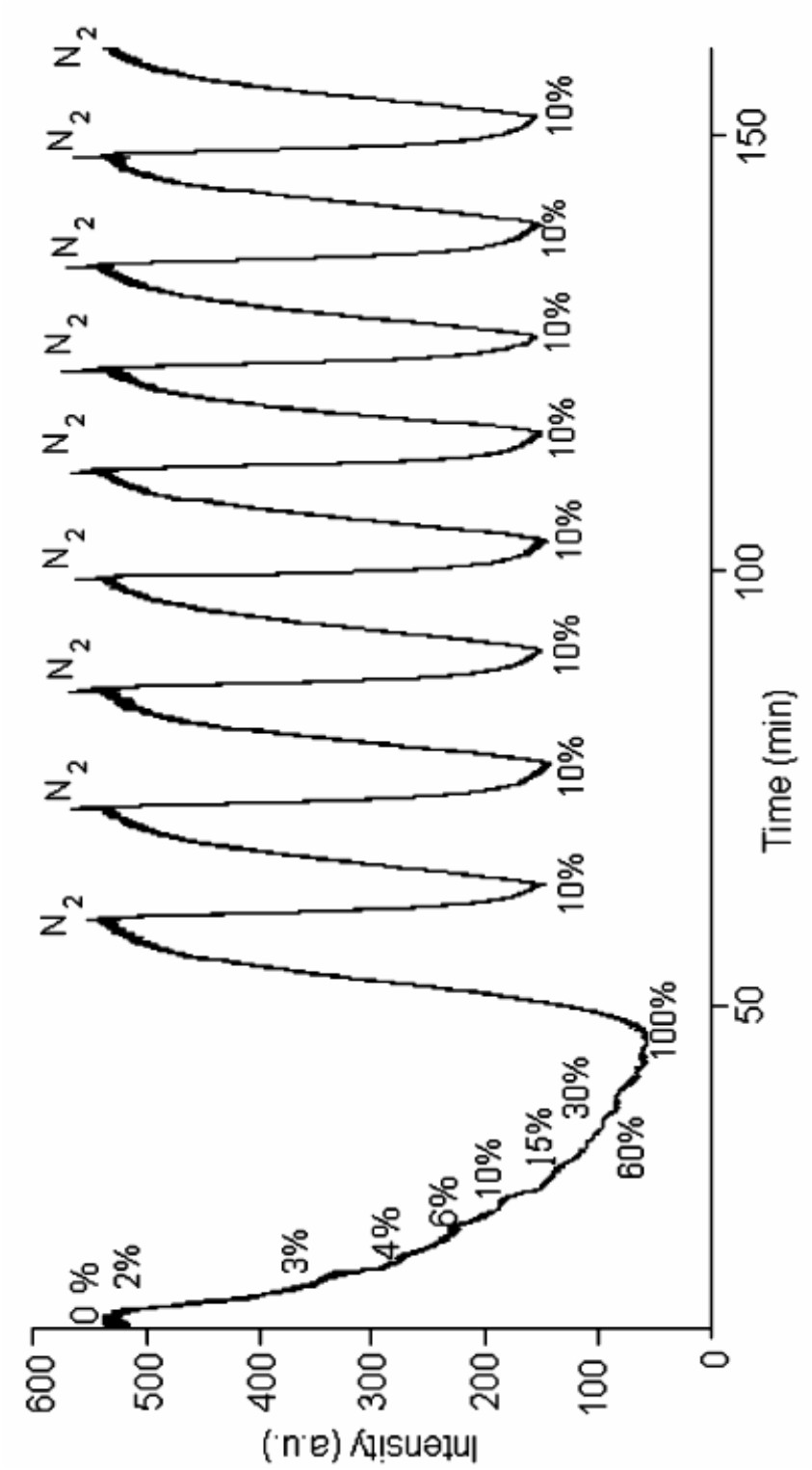

Figure 3.11 Emission-based response of HPTS in RTIL-I to gaseous CO_2

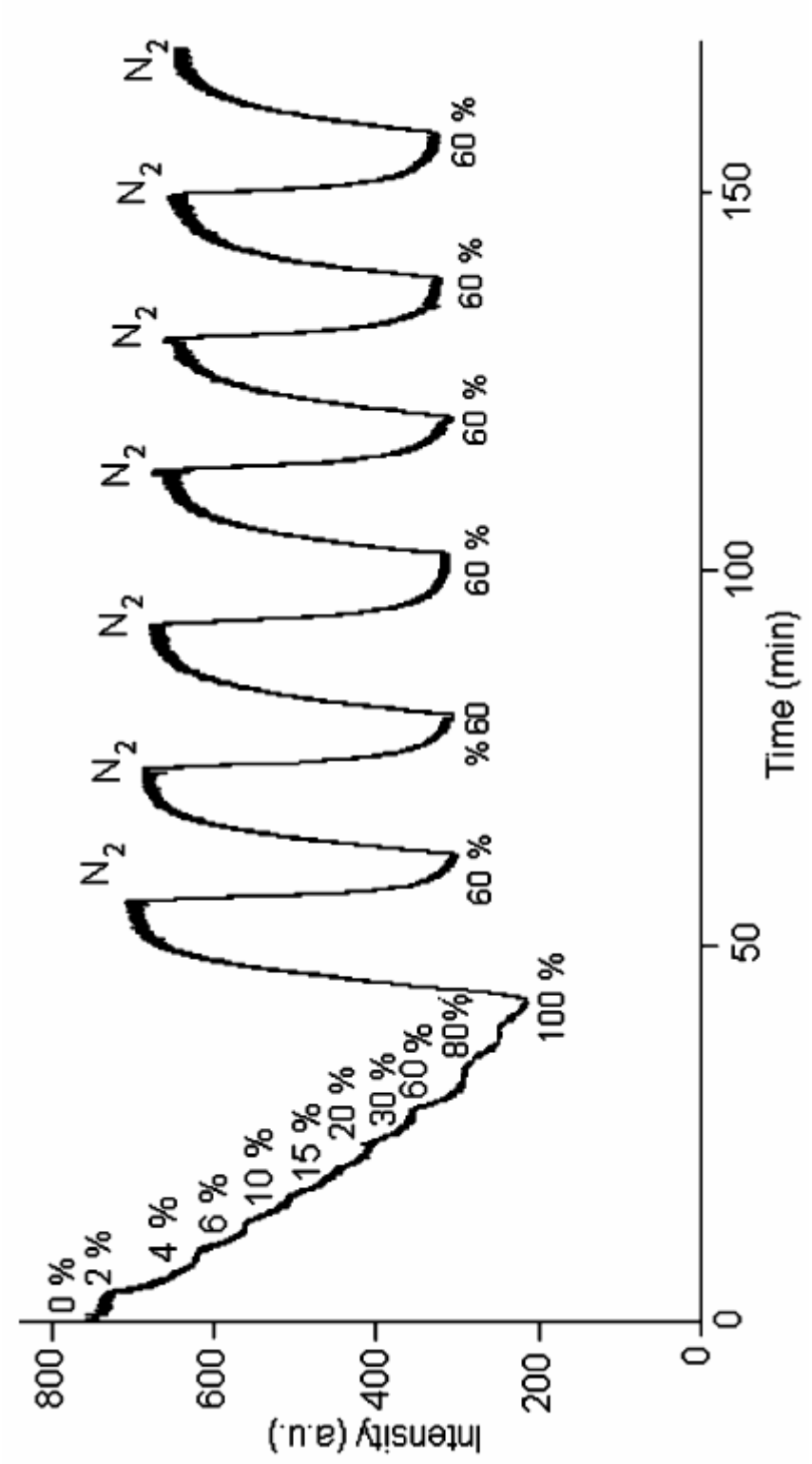

Figure 3.12 Emission-based response of HPTS in RTIL-II to gaseous CO_2

Table 3.6 Fluorescence intensities of HPTS in RTIL-I and RTIL-II when exposed to different % CO_2(g) (I_0 is the intensity at 0 % CO_2(g) and I is the intensity at any % CO_2(g), $(I_0-I)/I_0$ is the relative signal change.)

RTIL-I			RTIL-II		
% CO_2	I	$(I_0-I)/I_0$	% CO_2	I	$(I_0-I)/I_0$
0	541	0	0	759	0
2	345	0.362	2	735	0.032
3	275	0.492	4	627	0.174
4	230	0.575	6	570	0.2494
6	184	0.660	10	511	0.327
10	138	0.745	15	461	0.393
15	111	0.795	20	410	0.456
20	98	0.819	30	356	0.531
30	81	0.851	60	266	0.650
60	70	0.871	80	220	0.710
80	59	0.891	100	193	0.746
100	52	0.904			

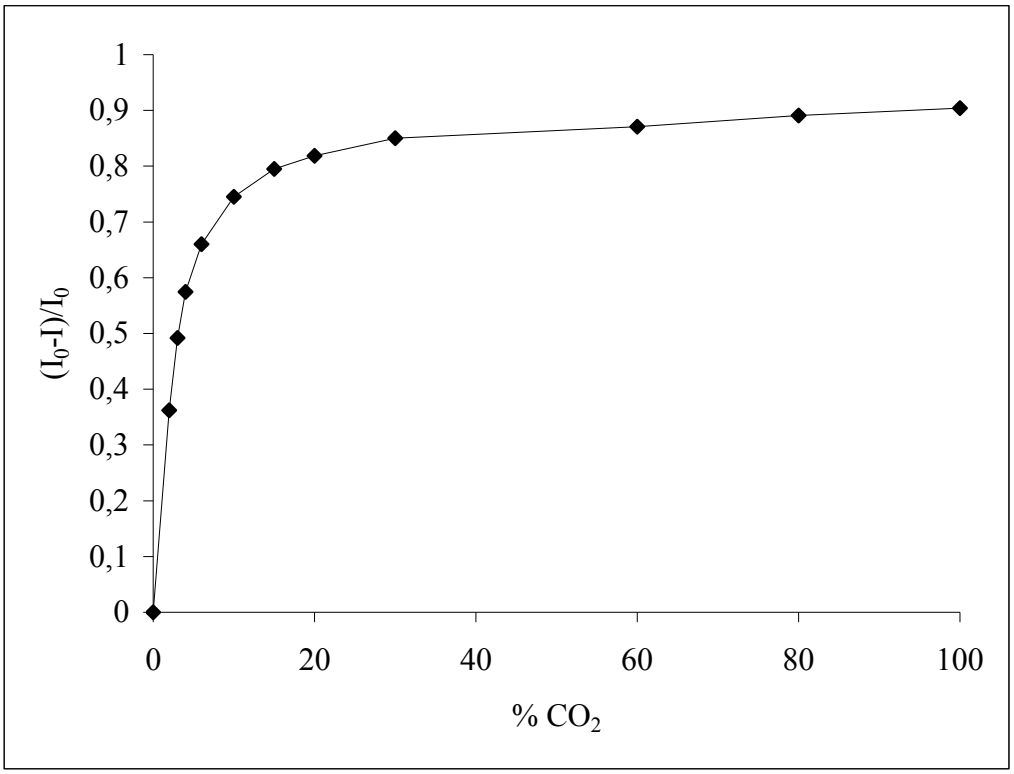

Figure 3.13 Calibration plot of the emission based response of HPTS in RTIL-I to gaseous CO_2.

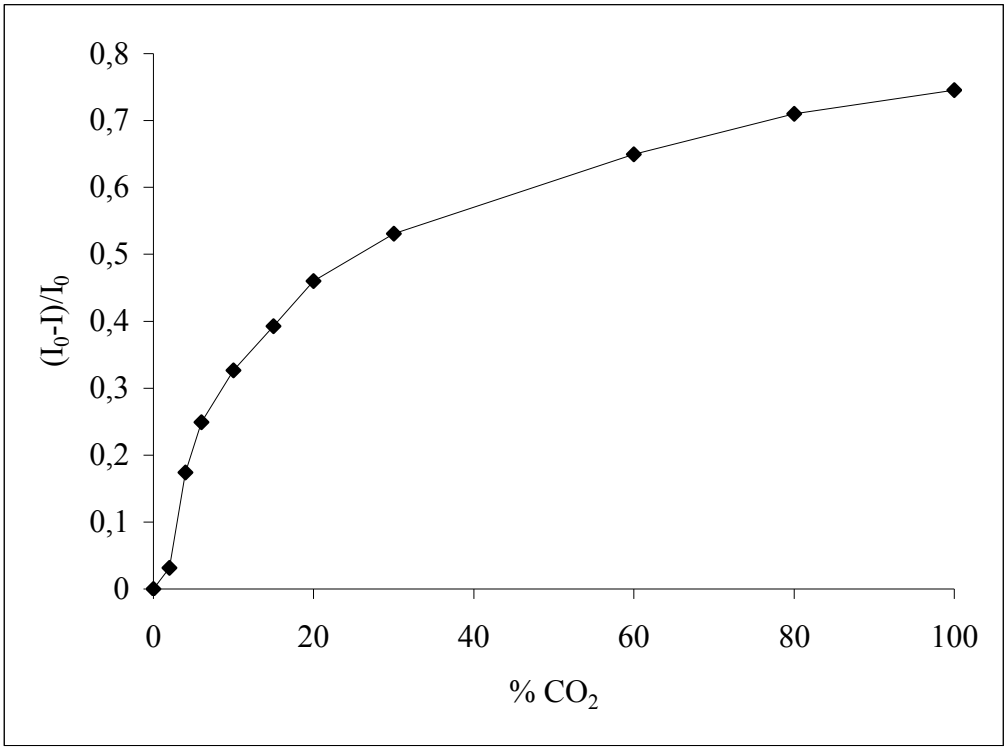

Figure 3.14 Calibration plot of the emission based response of HPTS in RTIL-II to gaseous CO_2.

3.4.5 Effect of humidity and sensor stability

To evaluate the effect of the trace water content of the water-miscible RTILs used, we performed experiments with or without humidification of gaseous CO_2. The sensor compositions used had reversible sensitivity towards CO_2 at 0% humidity, indicating there is still sufficient moisture (traces of water in the ionic liquid) within the matrix to facilitate a response to the analyte gas. This behavior was found to be highly reproducible and we therefore concluded that for the ionic liquid media studied no humidification was necessary for the sensor to work. When the sensing cocktails were stored in sealed cuvettes protected from sunlight for approximately 7 months no decrease in the sensitivity was observed for RTIL-I and only a slight decrease was observed for RTIL-II after 103 days (9% drift in fluorescence intensity). Figure 8 illustrates the stability of the sensors during storage for 212 days under ambient laboratory conditions. This was good news for us, because most of the popular ethylcellulose- based CO_2 sensors using HPTS have very short time stability, even when kept in a desiccator. The cross sensitivity of the cocktail compositions to

acidogenic species, for example H_2S and SO_2, was not tested. Ionic liquid media are known to have high selectivity and solubility for CO_2, however. The detection limits (concentrations of CO_2 or HCO_3^- giving a signal equal to the blank signal plus three times the standard deviation of the blank) were 1.4% for gaseous CO_2 and 10^{-8} mol L^{-1} for HCO_3^-. For measurement of gaseous CO_2 the detection limit was limited by the sensitivity of the gas-diluter system. The compatibility of the components of the sensor with solid-state optics (in particular fiber optics and LEDs) might be useful for construction of inexpensive and fieldavailable instruments.

3.5 Conclusions

In this chapter, two new RTIL-based carbon dioxide sensors are reported. RTIL-I and RTIL-II can be effectively used as alternative matrix materials to conventional solvents and solid matrices in emission-based CO_2 sensing studies with HPTS. An important feature of the sensor is its excellent long-term stability and repeatability over a period longer than seven months. Ionic liquids (ILs) are discussed as green solvents. Several unique properties of the ILs, mainly their reversible CO_2 solubility and selectivity, negligible vapor pressure, dye-dissolution properties, water-miscible characteristics, and optical transparency, make them promising matrix materials for CO_2 sensor design. ILs combine the attractive physical properties of solid and liquid phases and can be useful in construction of inexpensive and fieldavailable reservoir-type sensor design. The compatibility of the sensor component(s) with solidstate optical components (in particular LEDs and fiber optics) also makes them promising optical sensor matrix materials.

CHAPTER FOUR

ROOM TEMPERATURE IONIC LIQUIDS AS OPTICAL SENSOR MATRIX MATERIALS FOR GASEOUS AND DISSOLVED CO_2

4.1 Experimental Studies

In this chapter, a new optical sensor prepared by the simple immobilization of the modified bromothymol blue (Figure 4.1) into water miscible room temperature ionic liquids; 1-methyl-3-butylimidazolium tetrafluoroborate (RTIL-I) and 1-methyl-3-butylimidazolium bromide (RTIL-II) have been investigated.

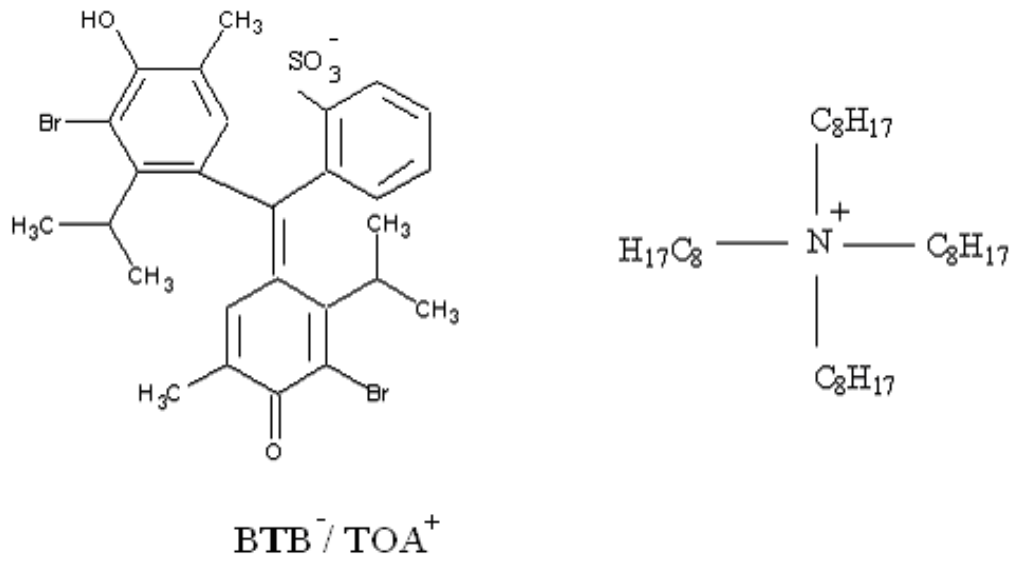

Figure 4.1 Schematic structure of BTB^-/TOA^+ ion pair.

Sensing cocktails were prepared by dissolving either the sodium salt or the ion pair form of the indicator dye in two different ionic liquids. Cocktail 1 contains 0.014 mg of ion pair form in 1 mL of ionic liquid (1-methyl-3-butylimidazolium tetrafluoroborate) and 80 μL of tetraoctylammonium hydroxide (TOAOH). Cocktail 2 was the same as cocktail 1 but does not contain TOAOH. Other cocktail compositions were given in Table 4.1.

Table 4.1 Compositions of cocktails employed as CO_2 sensing agent.

Coctail no.	Ionic liquid	Dye	Additive
C-1	RTIL-I (1 mL)	BTB^-/TOA^+ (9.74×10^{-5} M)	TOAOH (80 uL)
C-2	RTIL-I (1 mL)	BTB^-/TOA^+ (9.74×10^{-5} M)	-
C-3	RTIL-I (1 mL)	BTB^-/TOA^+ (1.95×10^{-5} M)	TOAOH (80 uL)
C-4	RTIL-II(1 mL)	BTB^-/TOA^+ (1.95×10^{-5} M)	-
C-5	RTIL-I (1 mL)	Na-BTB (9.74×10^{-5} M)	TOAOH (80 uL)
C-6	RTIL-II (1 mL)	Na-BTB (1.95×10^{-5} M)	TOAOH (160 uL)

BTB^-/TOA^+ and Na-BTB are Bromothymol Blue/Tetraoctylammonium and Sodium Bromothymol Blue respectively.

4.2 Results and Discussion

4.2.1 Dissociation constant (pK_a) of indicator dye in RTILs

The knowledge of dissociation constant (pK_a) of BTB in RTILs is of fundamental importance in order to provide information on chemical reactivity range of the indicator dye. Indicators with pK_a values between 6.8 and 10.0 are essential for sensitive pCO_2 optodes. In order to evaluate the availability of BTB^-/TOA^+ ion pair in the RTILs for CO_2 sensing, determination of the acidity constant has been performed. pH induced absorption spectra of the cocktail composition were recorded in the pH range of 8.70-10.49 in both of the ionic liquids. Dye dopped-RTIL-II was titrated with 0.5 M HCl, and after each addition, pH values of the media were recorded (Figure 4.2). Here a relative signal change of approximately 65% has been reached. Figure 4.3 shows the plot of absorbance intensity of BTB in RTIL-II versus measured pH values. In RTIL-I, BTB exhibited very similar results. pKa values were found as 9.68 and 9.74 for RTIL-I and II, respectively. Given pKa values were calculated by using non-linear fitting algorithm of Gauss–Newton–Marquardt method,

$$pKa = pH+\log [(A_x-A_b)/(A_a-A_x)]$$

where A_a and A_b are the absorbance intensities of acidic and basic forms and A_x is the intensity at a pH near to the midpoint (Werner & Wolfbeis, 1993). The calculated pKa values reveal that the BTB^-/TOA^+ ion pair can be used as absorption based CO_2 indicator when doped into RTILs.

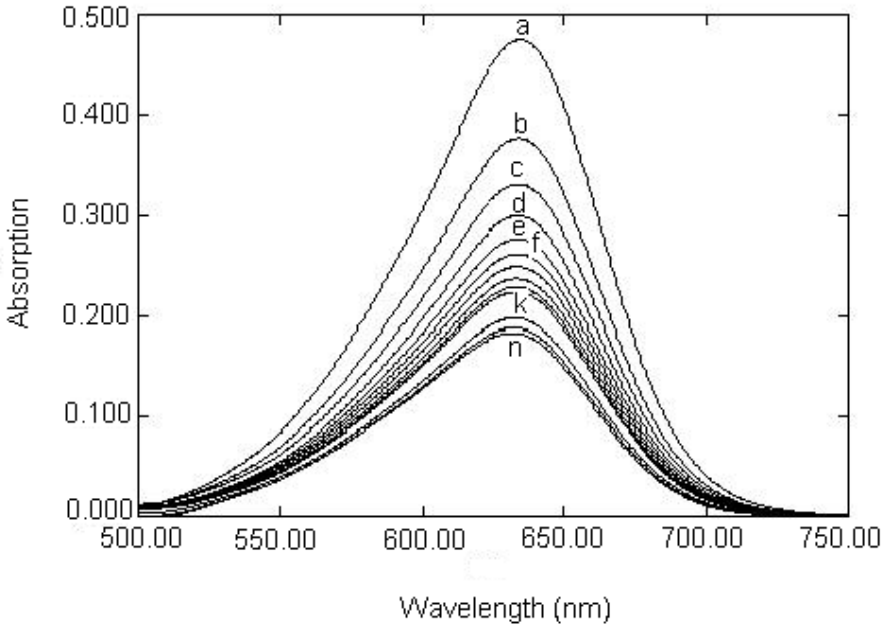

Figure 4.2 pH induced absorption spectra of the BTB in RTIL-II after titration with 0.5 M HCl in pH range of 8.70-10.49. (a) pH=10.49, (b) 10.00, (c) 9.80, (d) 9.53, (e) 9.45, (f) 9.37; 9.29; 9.23, (k) 9.18; 8.95; 8.80 (n) 8.70 in RTIL-II.

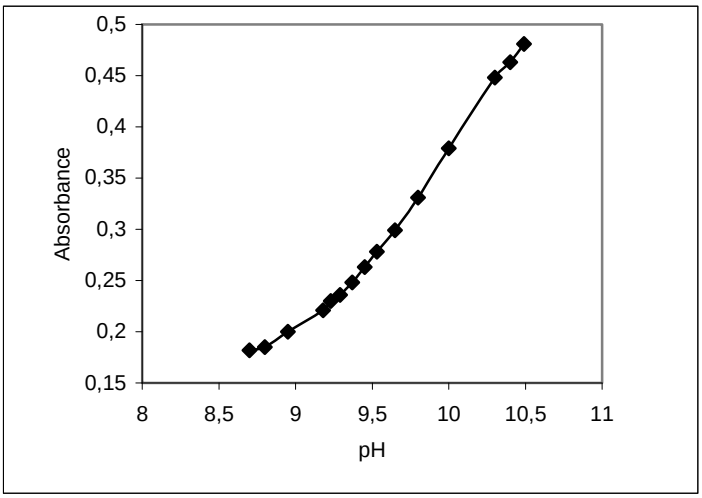

Figure 4.3 Plot of absorbance versus measured pH in the pH range of 8.70-10.49 (the pH values of 10.49; 10.30; 10.00; 9.80; 9.53; 9.45; 9.37; 9.29; 9.23; 9.18; 8.95; 8.8; 8.7 are taken)

4.2.2 Gaseous CO_2 sensing studies

CO_2 and N_2 gases were mixed in the concentration range of 0-100 % in a home made gas mixing chamber by controlling the gas flow rates with sensitive flow-meters. The output flow rate of the gas mixture was maintained at 500 mL min^{-1}. Gas mixtures were introduced into the sensor agent containing cuvette via a diffuser needle under atmospheric conditions.

The representative absorption spectrum of Cocktail 1 as a function of pCO_2 and related calibration graph are illustrated in Figure 4.4 and Figure 4.5, respectively. $(A_0-A)/A_0$ is the intensity ratio of protonated (A) and deprotonated (A_0) forms of the indicator. The linearized calibration plot of the sensor composition (C-1) can be described by the equation of $y = 0.0034x + 0.2855$ and the correlation coefficient of $R^2 = 0.9645$. Since hydration of CO_2 and subsequent protolysis is essential for the functionality of the sensor, we blew CO_2 gas through the water during the gas-phase studies. The sensor compositions exhibited relative signal changes around 60% (61-54%) in the direction of a decrease in absorption intensities at λ_{max}^{abs} =628 nm (RTIL-I) and λ_{max}^{abs} = 636 nm (RTIL-II) upon exposure to CO_2. The long wavelength absorption band of the BTB^-/TOA^+ ion pair exhibited a slight red shift (8 nm) from RTIL-I to II. Except the small red shift, both of the ionic liquids exhibited similar response to gaseous CO_2. The best results have been obtained with cocktail compositions of C-1 and C-5.

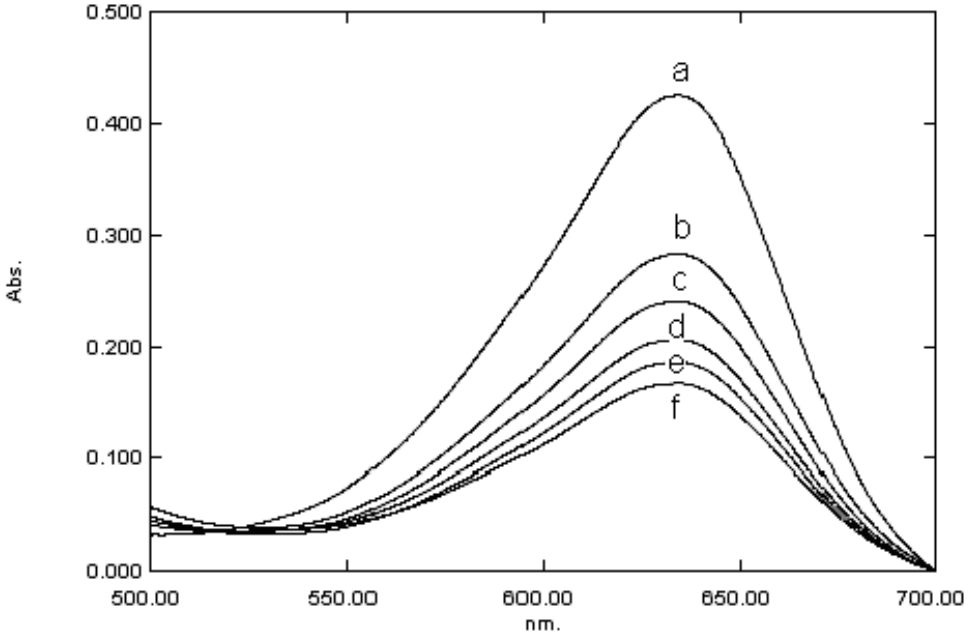

Figure 4.4 Absorption spectrum in RTIL-I after exposure to certain CO_2 partial pressures a) 0.0 %, b) 20 %, c) 40 %, d) 60 %, e) 80 %, f) 100 % pCO_2.

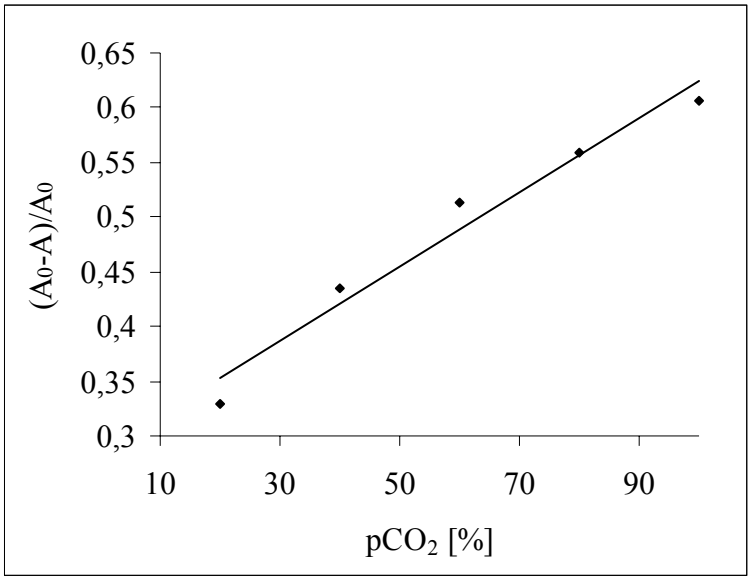

Figure 4.5 Linearized calibration curve of the sensor composition C–1 after exposure to CO_2 in the partial pressure range of a) 0.0–100 % pCO_2

4.2.3 Dissolved CO_2 sensing studies

Standard solutions were prepared freshly from a 1 M $NaHCO_3$ stock solution prior to the measurements. Dilute solutions of sodium hydrogencarbonate were used to form dissolved CO_2 calibration graphs. CO_2-free standard solutions were prepared

with doubly distilled water after boiling, bubbling with nitrogen, and kept in closed containers. Table 4.2 gives calculated H_2CO_3 concentrations [the sum of hydrated CO_2 (aq) and real H_2CO_3] and corresponding pCO_2 values in solutions made up from $NaHCO_3$. 20 μL portions of standard solutions of $NaHCO_3$ were added into the sensing agent containing cuvette and mixed. The change in absorbance due to addition of different concentrations of dissolved CO_2 was measured. All the experiments were carried out at room temperature of 25 ± 1 ^oC.

How the RTIL based sensing cocktail may work as a colorimetric sensor for CO_2 can be explained by the following equilibrium reaction.

$$BTB^- \text{ (color A)} + xH_2O + CO_{2(g)} \leftrightarrow HCO_3^- + (x\text{-}1)H_2O + BTBH \text{ (color B)}$$

Here, color A is the color of the unprotonated form of the bromothymol blue in RTILs which is blue (turquoise) and color B is the color of the protonated form which is greenish yellow. For the preparation of the modified sensing agent (BTB^-/TOA^+) stoichiometric amounts of tetraoctylammonium bromide (in dichloromethane) and bromothymol blue solution (in water solution of 1% Na_2CO_3) were vigorously shaken in a separatory funnel for 5 min, extracted, and the organic phase was washed 3 times with 3 mL portions of a 0.1 M solution of NaOH. Finally, the ion pair was treated in rotary evaporator as reported by Weigl and Wolfbeis (1995).

In order to evaluate the effect of the RTIL matrix material to the dye performance, the absorption spectra of the BTB^-/TOA^+ ion pair both in ethanol and RTILs were recorded. From EtOH to RTIL, the blue shift at 420 nm has disappeared in both of the RTILs. The absorption maximum around 420 nm shifted to 414 nm, exhibiting a 6 nm blue shift. The absorption maximum around 625 nm exhibited a slight red shift and appeared at 628 nm. Figure 5.6 shows the absorption spectra of the BTB^-/TOA^+ ion pair in EtOH in comparison with in RTIL-I after addition of HCO_3^- solutions in the concentration range of 2×10^{-6}- 2×10^{-2} mol L^{-1}.

The relative signal changes of absorption spectra of the cocktails 1-6 were monitored after addition of certain concentrations of HCO_3^- solutions. The cocktail 1 (C-1), which contained 1-methyl-3-butylimidazolium tetrafluoroborate, exhibited the best response to different concentrations of HCO_3^- solutions in the direction of an increase in signal intensity at 628 nm. Due to the presence of the isobestic point at 512 nm, BTB^-/TOA^+ ion pair allows ratiometric measurements in RTIL-I. However, the isobestic point becomes unclear in RTIL –II (Figure 4.6).

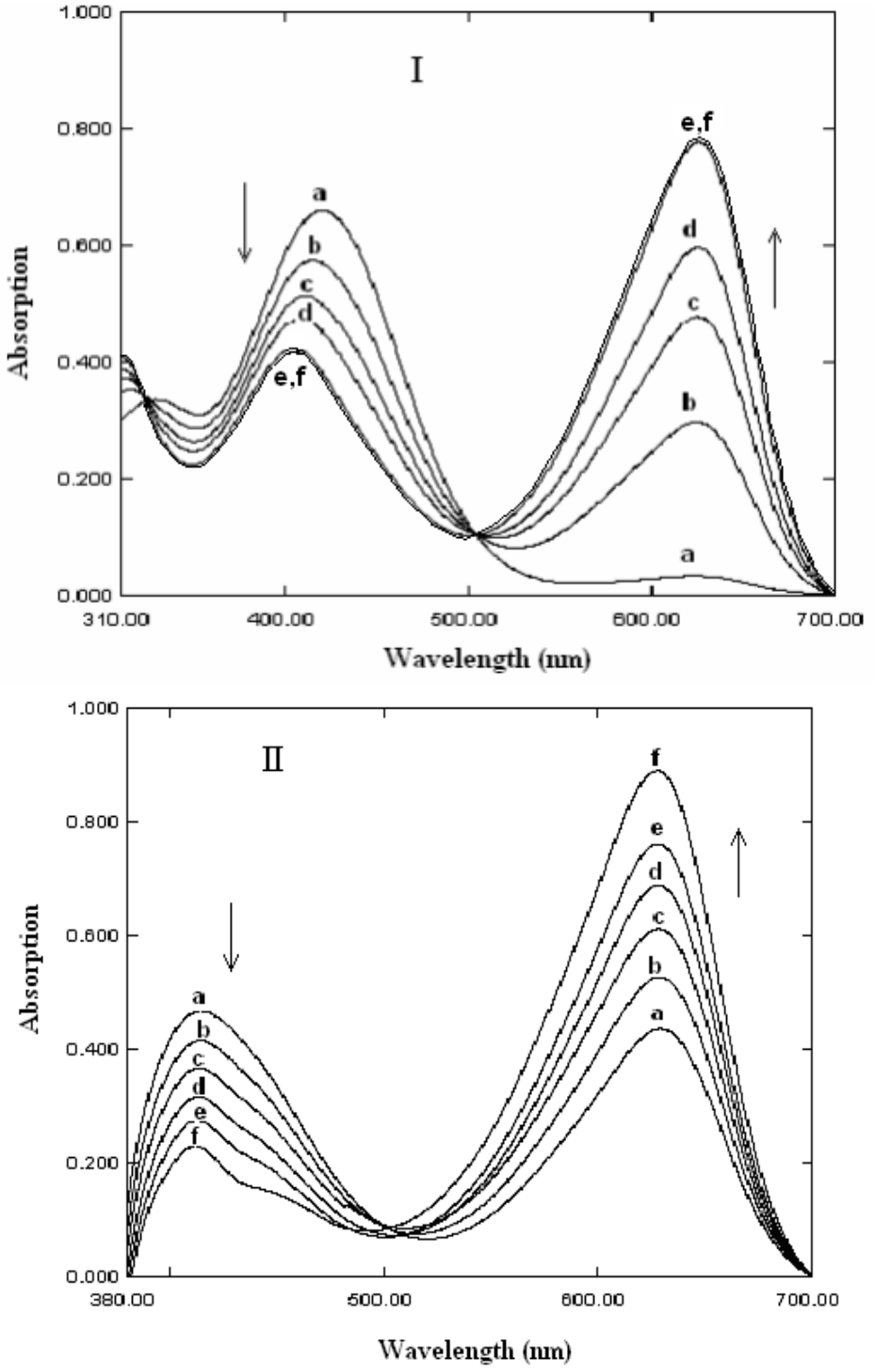

Figure 4.6 Absorption spectra of BTB^-/TOA^+ ion pair in EtOH (I) and in RTIL-I (II) after addition of HCO_3^- solutions in the concentration range of $2x10^{-6}$-$2x10^{-2}$ mol $L^{-1.}$ a: 0, b: $2x10^{-6}$, c: $2x10^{-5}$ d: $2x10^{-4}$ e: $2x10^{-3}$ f: $2x10^{-2}$ mol L^{-1}.

The linearized calibration curve of the sensor composition C-1 is shown in Figure 4.7. The calibration plot of the sensor can be described by the equation of y= -0.1818x + 1.2534 and the correlation coefficient of 0.9984. The dynamic working range is logarithmic and covers the concentration range of 1×10^{-6} - 2×10^{-2} mol L^{-1} [HCO_3^-].

In most of the sensor designs, TOAOH was added into the sensing cocktail as a counter ion in order to increase the sensitivity and lifetime, and an enhancement has been reported due to the presence of TOAOH (Müller & Hauser, 1996). However, we could not observe any significant enhancement in sensor response after addition of HCO_3^- solutions in the TOAOH containing cocktail compositions. In our case, the matrix material was basic enough, the initial pH of the matrix was around pH= 10.45, and the dye was completely in the deprotonated form. Besides the proper initial pH value, the water miscible RTILs also allow the uptake of water molecules and the direct addition of HCO_3^- solutions into the sensing medium.

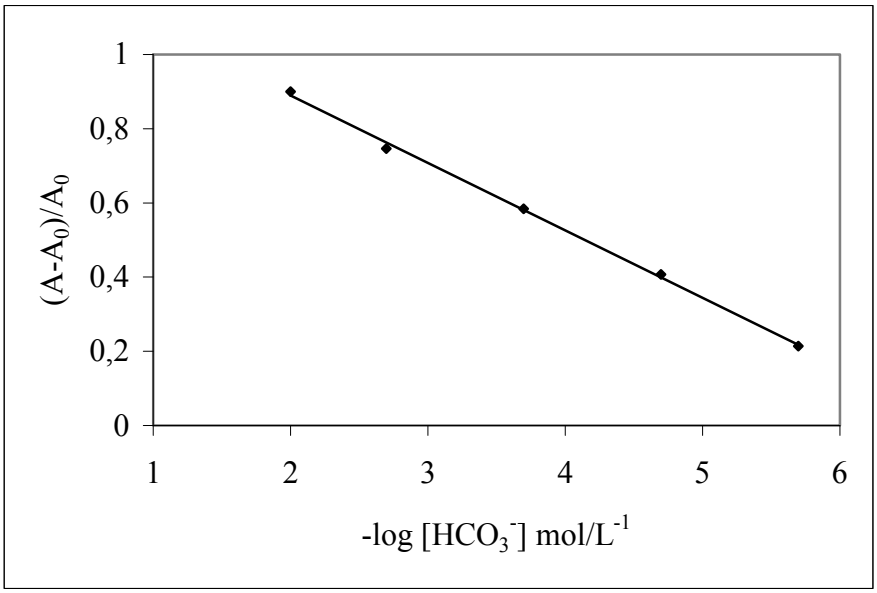

Figure 4.7 Sensor calibration curve in the concentration range of $2x10^{-6}$-$2x10^{-2}$ mol L^{-1} [HCO_3^-], λ^{Abs}_{max}= 628 nm.

4.2.4 Response, recovery and stability characteristics

The response and recovery related data of sensing cocktails were acquired by recording the absorbance intensity signals while exposing to 100% CO_2 and 100% N_2, respectively. The τ_{90} response times in-RTIL-I and II were 60 and 68 s, respectively. In the concentration range of 0.0-100% pCO_2, in the RTIL-I containing cocktails the regeneration could not be succeeded more than 67%. However, the initial signal intensities of the cocktails could be completely recovered after switching in the concentration range of 0.0-80% pCO_2. In the RTIL-II containing cocktails, regeneration performance was better than that of the RTIL-I containing ones. It was fully reversible on going from 100% CO_2 to 100% N_2, and no hysterisis was observed during the experiments. The τ_{90} response times of the sensor compositions were 60 and 126 s for C-4, C-6 and C-1, C-2, C-3, C-5, respectively. When the cocktail solution was stored in sealed brown bottles away from sunlight over a period of 1 month, no drift in the sensitivity was observed. Figure 4.8 exhibits the response behaviour of the C-4 in the partial pressure range of 0.0-100% pCO_2.

At each time the reagent phase was regenerated with pure gaseous nitrogen (99.99%). Between 1st and 6th cycles, the level of reproducibility of upper signal levels was 0.435 ± 0.014 (n=6). The average regeneration time under batch conditions was about 2.5 min for all compositions.

The detection limits (the concentration of the pCO_2 or $[HCO_3^-]$ giving a signal equal to the blank signal, plus three standard deviation of the blank) were 1.4 % for gaseous and 10^{-6} M $[HCO_3^-]$ for dissolved CO_2.

The independence of the cocktail compositions from pH or other acidogenic species like H_2S was not tested. However, CO_2 is known to dissolve selectively in ionic liquids.

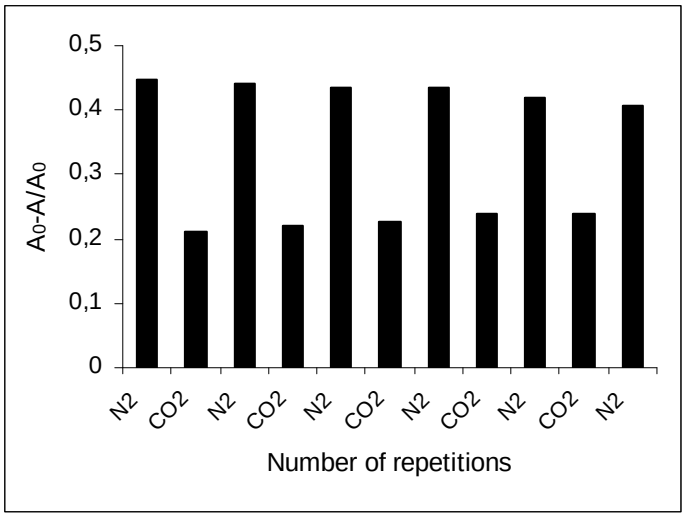

Figure 4.8 The reproducibility of sensor (C-4) after 6 times exposure to carbon dioxide in the partial pressure range of 0-100 % pCO_2.

4.3 Conclusions

Ionic liquids (ILs) are discussed as green solvents. Several unique properties of the ILs, mainly their negligible vapour pressure, reversible CO_2 solubility and selectivity, capability of dye dissolution, water-miscible characteristic and optical transparency, make them promising matrix materials for CO_2 sensor design. The lack of vapour pressure makes the ILs highly attractive for laboratory workers during gas processing. Additionally, due to their reversible CO_2 adsorption-desorption property, ILs can be used repeatedly instead of solvents. It should be remembered that our municipal water treatment facilities are not designed for removing of synthetic chemicals or solvents and typically only consist of sand bed filtration and disinfection.

As discussed earlier, the RTIL-I and RTIL-II could be effectively used as alternative matrix materials to conventional solvents and solid matrices in absorption based studies. ILs combine the attractive physical properties of solid and liquid phases and can be useful in construction of the inexpensive and field available reservoir type sensor design. The compatibility of the sensor composition(s) with the solid-state optical components (in particular LEDs and fiber optics) also makes them promising optical sensor matrix materials.

CHAPTER FIVE

PHOTOCHARACTERIZATION OF A NOVEL FLUORESCENT SCHIFF BASE AND INVESTIGATION OF THE UTILITY AS AN OPTICAL Fe^{3+} SENSOR in PVC MATRIX

5.1 Introduction

The discovery, design and synthesis of new organic fluorescent molecules and their interaction with cations, anions or biomaterials leads exciting advances in sensing, imaging and diagnostic. Owing to the active role in aquatic redox processes and medical analysis, iron is one of the most important elements in metabolic processes, environmental investigations and biological materials. Different dyes have been used for spectral iron detection either in immobilized or free form.

Pulido-Tofino, Barrero-Moreno & Perez-Conde (2000) used immobilized pyoverdin pigment (on controlled pore glass) which selectively reacts with Fe^{3+}. Zhang, Xie & Shi (1999) performed spectrophotometric determination of iron by using eriochrome cyanine-R as extractant and color-developing agent in organic solvents. Sarradin, Le Bris, Le Gall & Rodier (2005) applied ferrozine method to flow injection analysis (FIA) to perform iron analysis. The iron sensitive organic chromophores Phen Gren FL, Phen Gren SK and calcein has been intensely studied and commercialized by Molecular Probes™ Invitrogen Detection Technologies. Phen Gren FL and Phen Gren SK are cell membrane-permeable fluorescent diacetate derivatives of phenanthroline and are capable of detecting Fe^{2+}, as well as Cu^{2+}, Cu^{+}, Hg^{2+}, Pb^{2+}, Cd^{2+} and Ni^{2+} (Kuhn et al., 1995; Petrat, Rauen & de Groot, 1999). Picard, Epsztejn, Santambrogio, Cabantchik & Beaumont (1998) have exploited the fluorescence quenching of calcein at neutral pH to follow intracellular release of Fe^{2+} from transferin.

In the present work, newly synthesized DBS dye (Figure 5.1) has been characterized in different solvents and PVC, and, used for sensor preparation in PVC

matrix. The indicator molecule was synthesized and provided by Professor B. Çetinkaya from Ege University. Its possible use for optical sensing of $Fe^{3+}$and typical sensor characteristics such as dynamic working range, sensitivity, limit of detection, and selectivity have been investigated. The interferences of various cations on the response of Fe^{3+} also have been studied. The employed metal salts were given in Chapter 2.

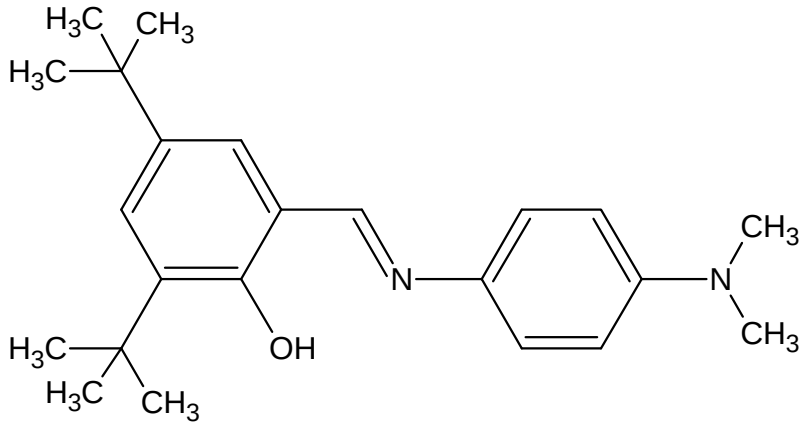

Figure 5.1 Schematic structure of the N-(4-dimethylaminophenyl)-3,5-di-*t*-butyl salicylaldimine (DBS) dye (MW= 352 g/mol).

5.2 Cocktail preparation protocols and emission-excitation spectra

The optode membranes were prepared to contain 120 mg of PVC, 240 mg of plasticizer, 0.5-2.0 mg of (DBS) dye (9.50×10^{-4}-3.78×10^{-3} M in the coctail), equivalent amount of potassium tetrakis (4-chlorophenyl) borate and 1.5 ml of THF. The prepared cocktails contained 33% PVC and 66% plasticizer by weight which is quite common.

The resulting cocktails were spread onto a 125 μm polyester support (Mylar TM type) in order to obtain the sensing films. Each sensing film was cut to 1.2 cm width and fixed diagonally into the sample cuvette and the excitation and fluorescence emission spectra were recorded. For the flow system experiments, the films were cut to 1 cm width and 1 cm long and placed into the before mentioned flow cell system (Chapter II, Section 2.2). Flow rate of the peristaltic pump was kept at 2.4 mL min^{-1}.

5.3 Results and discussion

5.3.1 Spectral data and photophysical constants

The florescent (DBS) dye exhibited excellent photostability in all of the solvents and PVC matrix employed. The absorption, emission and excitation spectra of the DBS dye were recorded in the solvents of different polarities and in PVC matrix. The gathered absorption spectra are shown in Figure 5.1. Absorption spectra related molar extinction coefficients and maximum absorption wavelengths of the dye in employed solvents and PVC are given in Table 5.1. Absorption wavelength of DBS, λ_{max}, in PVC is seen to be shifted about 10 nm compared to absorption λ_{max} in THF solution. Red shift of absorption of DBS may be related to enhanced conjugation in immobilized polymer phase by hindrance of rotational and vibrational motions.

Table 5.1 Absorption spectrum related data of DBS.

Dye	Solvent	ε (molar extinction coefficient, $cm^{-1}.M^{-1}$)	n (refractive index)	λ^{abs}_{max}
DBS	EtOH	32541	1.3590	385
DBS	DCM	32392	1.4241	389
DBS	THF	31850	1.4070	388
DBS	PVC	650755	1.5200	399

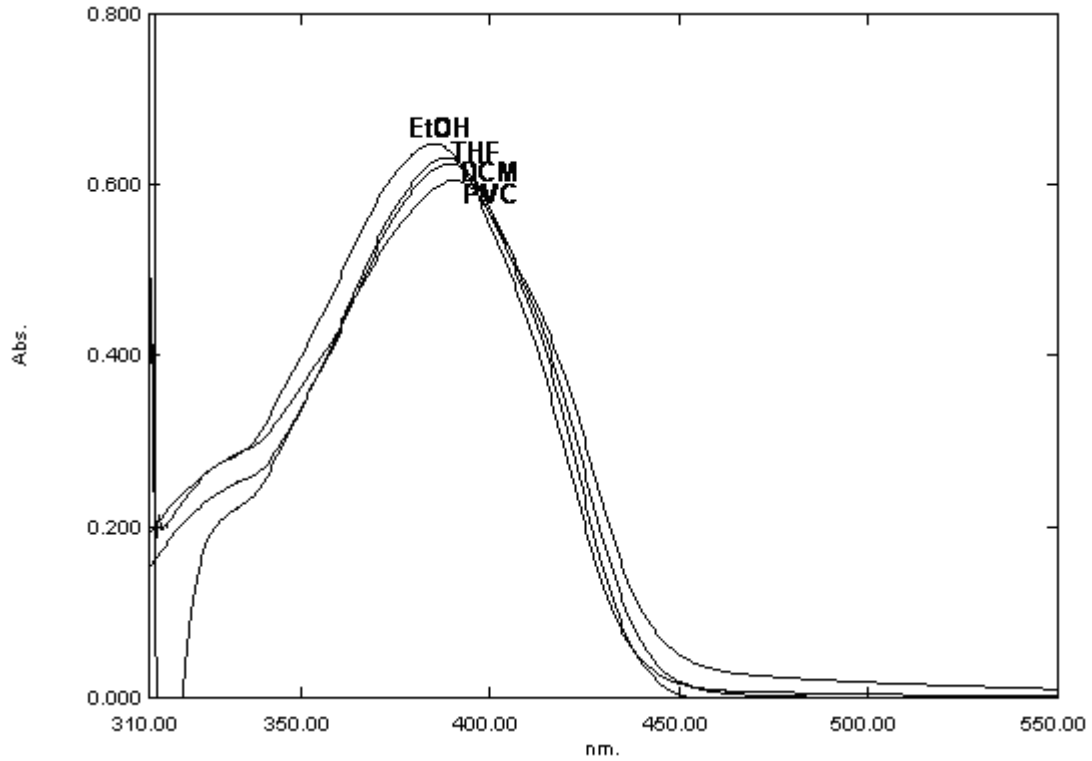

Figure 5.1 The absorption spectra of DBS dye in solvents of DCM, EtOH, THF and in PVC.

The excitation-emission spectra and the related data of the DBS are shown in Figure 5.2 and Table 5.2. In all of the employed matrices the Stoke's shift values, $\Delta\lambda_{ST}$ (the difference between excitation and emission maximum), calculated from the spectral data are quietly high. Stoke's shift is important for fluorescence and optical sensor studies because the high Stoke's shift value allows the emitted fluorescence photons to be easily distinguished from the excitation photons, leading to the possibility of very low background signals and permits the usage of DBS dye in the construction of fiber optic sensor.

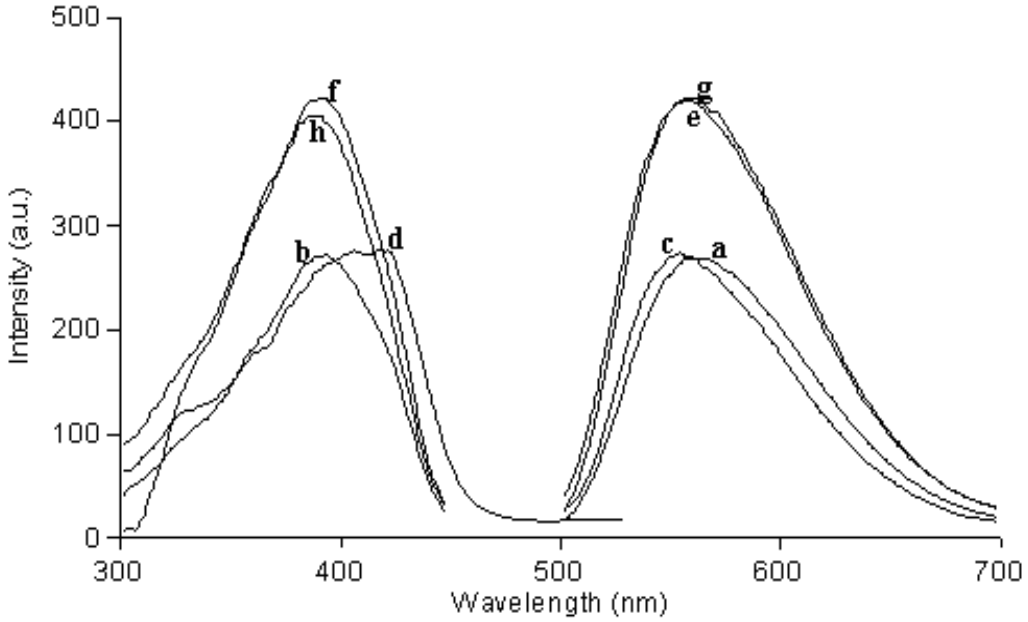

Figure 5.2 Emission and excitation spectra of DBS in different solvents and PVC: (a) emission in DCM; λ_{ex} = 395nm, λ^{em}_{max} = 562 nm (b) excitation in DCM; λ_{ex} = 562 nm, λ^{ex}_{max} = 394 nm (c) emission in PVC; λ_{ex} = 410 nm, λ^{em}_{max} = 554 nm (d) excitation in PVC; λ_{ex} = 554 nm, λ^{ex}_{max} = 418 nm (e) emission in EtOH; λ_{ex} = 390 nm, λ^{em}_{max} = 559 nm (f) excitation in EtOH; λ_{ex} = 559 nm, λ^{ex}_{max} = 388 nm (g) emission in THF; λ_{ex} = 390 nm, λ^{em}_{max} = 557 nm (f) excitation in THF; λ_{ex} = 557 nm, λ^{ex}_{max} = 390 nm.

Table 5.2 Emission and excitation spectra related data of DBS.

Dye	Matrix	λ_{ex} (excitation wavelength for emission)	λ_{ex} (excitation wavelength for excitation)	λ_{em} (maximum emission wavelength)	$\Delta\lambda_{ST}$ (Stoks Shift)	θ_F (Quantum Yield)
DBS	EtOH	388	559	559	171	0.0021
DBS	DCM	394	562	562	168	-
DBS	THF	390	557	557	167	-
DBS	PVC	410	554	554	136	0.0254

Promising spectral properties such as visible region excitation (410 nm) and emission wavelength (554 nm), high molar absorbtivity (650755 $cm^{-1}(mol/L^{-1})$) satisfactory quantum yield (0.0254) and high photostability (Figure 4.3) in immobilized form and intensity based response to Fe^{3+} cations encouraged this study using the DBS dye in optical sensor design for iron sensing.

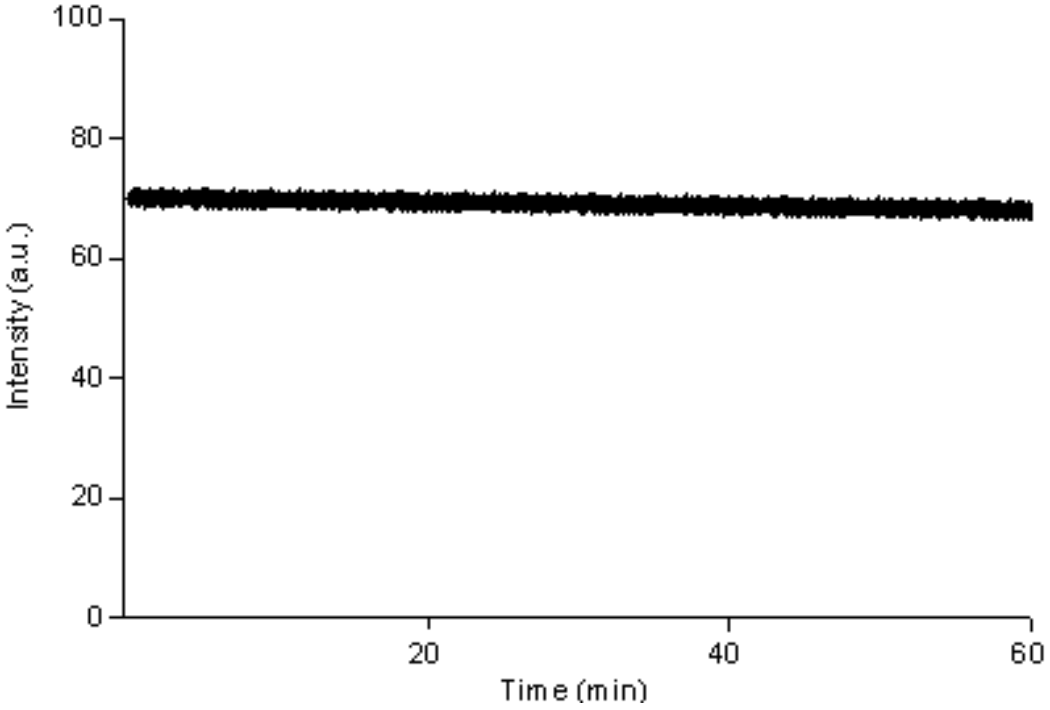

Figure 5.3 The photostability of DBS in PVC.

5.3.2 Quantum yield calculations

The fluorescence quantum yield of DBS in EtOH and PVC matrices was calculated by William's Method. The Williams method and the calculation of quantum yield values was explained in detail in Chapter 2. For this purpose, the emission spectra of five different concentrations of reference standard (HPTS) were recorded by exciting at 410nm and 390nm (Figure 5.4 and Figure 5.5). By similar way, the emission spectra of the five different concentrations of the DBS dye were recorded (Figure 5.6 and Figure 5.7). The integrated fluorescence intensities were plotted *vs* absorbance for the reference standard, and the dye. The ratio of gradients of the plots is important and proportional to the quantum yield. The linearized plots of the dye in EtOH and PVC matrices can be described by equations and the relevant

correlation coefficients of [y=2007x, R^2= 0.9922] and [y=76335x, R^2=0.9935], respectively. For quantum yield standard; HPTS, the equations are [y=971979x, R^2=0.9988] and [y=3910150x, R^2=0.9999] for EtOH and PVC, respectively. The data are also shown in Table 5.3. Fluorescence quantum yield of DBS in PVC, Q_f = 0.0254, has increased about 12-fold, with respect to Q_f of DBS in EtOH, and, molar extinction coefficient of DBS in PVC matrix, ε =650755, has increased about 20-fold, with respect to ε of DBS in DCM. These data can be taken as proofs that the dye molecule DBS fluoresces better in immobilized PVC matrix.

Table 5.3 Quantum yield related data for DBS in EtOH and PVC matrices.

Dye	DBS (in EtOH)	HPTS (in acidic water)	DBS (in PVC)	HPTS (in acidic water)
Excitation wavelength, λ_{ex}	390 nm	390 nm	410 nm	410 nm
rafractive index, n	1.3590	1.3328	1.5200	1.3328
Equations of plots	y=2007x	y=971979x	y=76335x	y=3910150x
Gradients of the plots	2007	971979	76335	3910150
Quantum yields	0.0214 (calculated)	1	0.0254 (calculated)	1

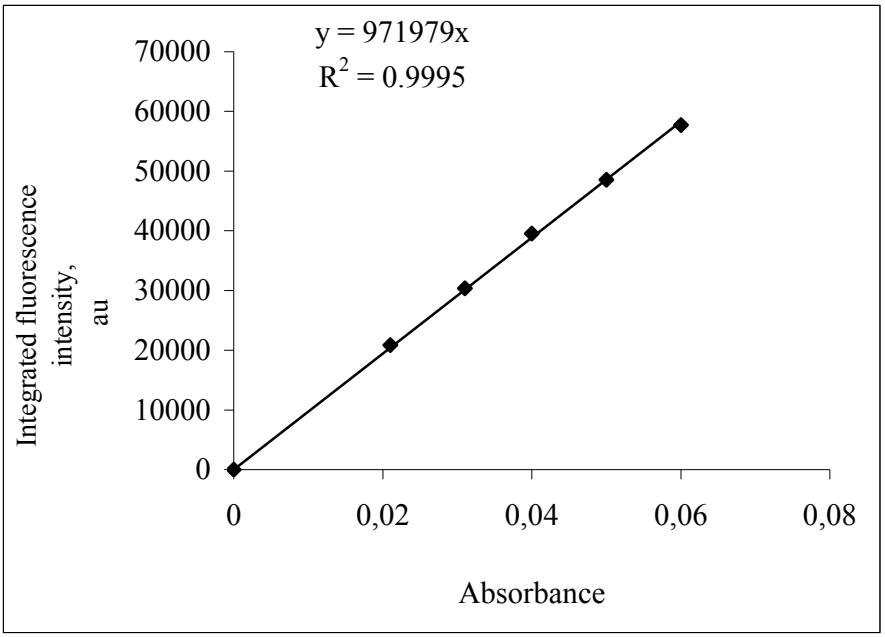

Figure 5.4 The integrated fluorescence intensities *vs* absorbance values of HPTS in water (excitation at 390 nm).

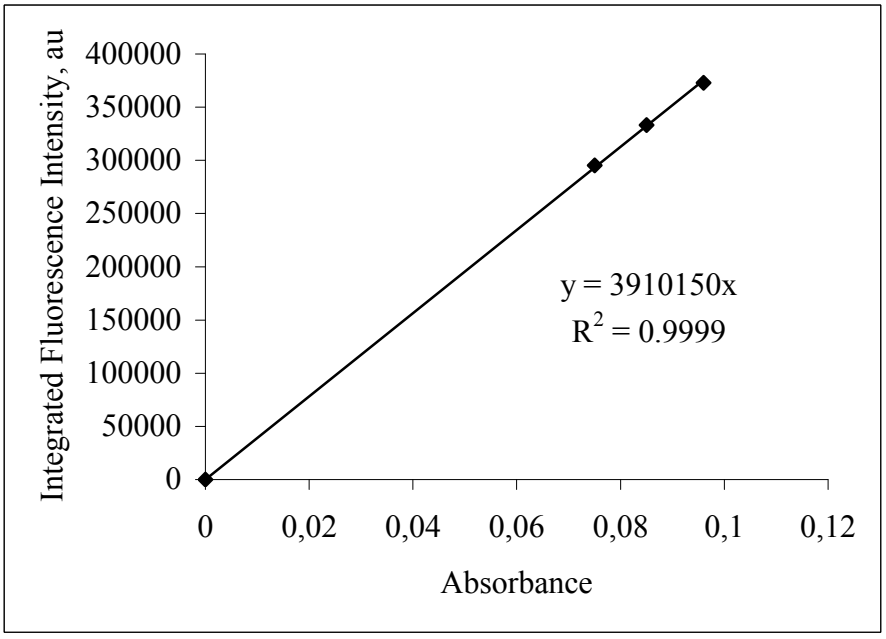

Figure 5.5 The integrated fluorescence intensities *vs* absorbance values of HPTS in distilled water (ex at 410 nm; correction factor of 12.5 is used in the quantum yield calculations).

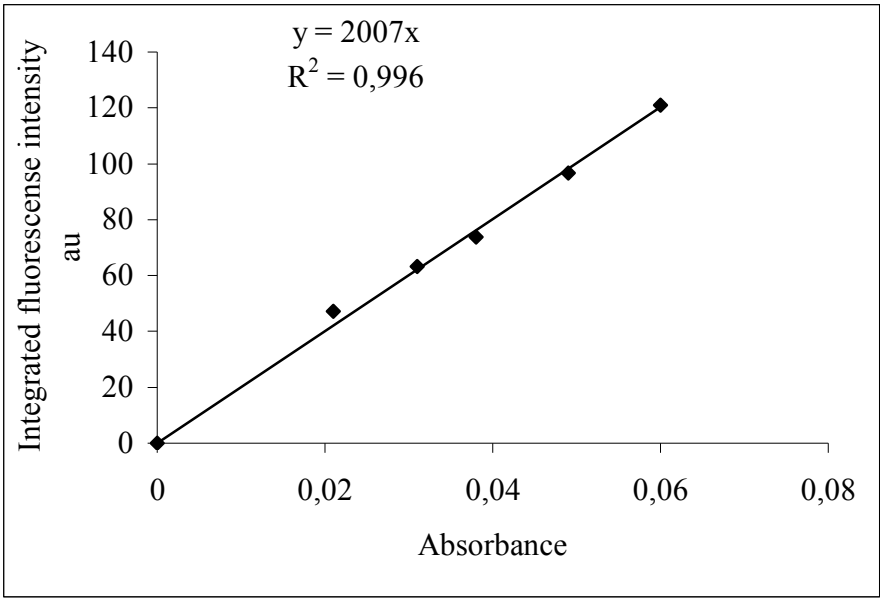

Figure 5.6 The integrated fluorescence intensities *vs* absorbance values of DBS dye in EtOH (excitation at 390 nm).

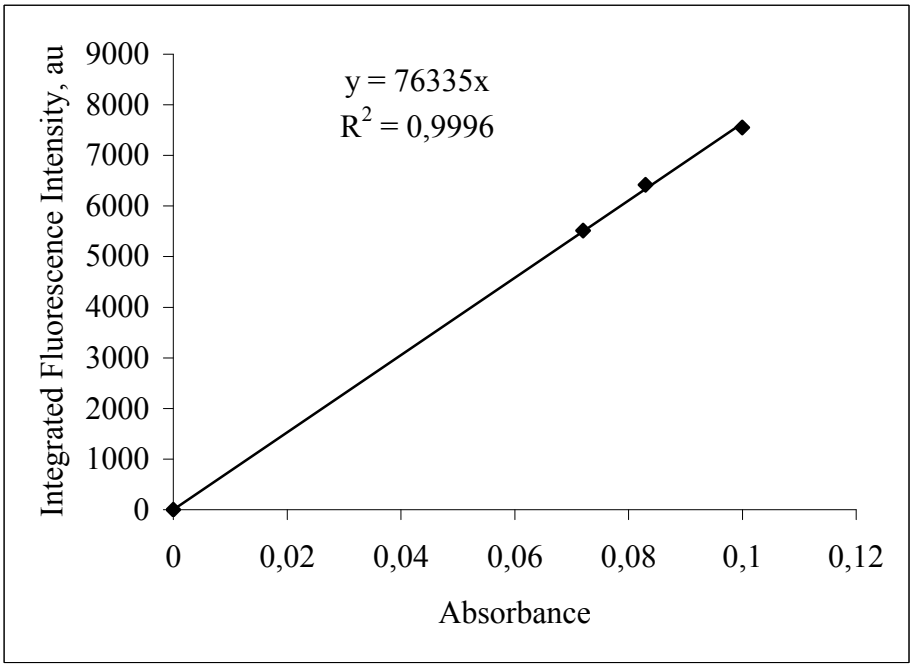

Figure 5.7 The integrated fluorescence intensities *vs* absorbance values of DBS dye in PVC matrix (ex. at 410 nm).

5.3.3 pH dependence of DBS dye

The pH dependence of the dye doped membrane was investigated in buffered solutions in the pH range of 3.0-9.0 iron free and Fe^{3+} containing solutions. Buffer solutions were prepared with 0.01 M CH_3COOH, 0.01 M NaH_2PO_4 or 0.01 M BES. The preparation procedures for the buffer solutions were given in Chapter 2. The emission maximum of the DBS dye at 559 nm decreases as the pH of the buffer varies from 9.0 to 3.0. The pH dependence of the dye is probably due to the protonation-deprotonation equilibria of the terminal hydroxyl and the central nitrogen groups. Figure 4.8 shows the pH dependency of the membrane in Fe^{3+} free buffer solutions in the pH range of 3.0-9.0. The pK_a value of the immobilized indicator is calculated to be pK_a= 5.57 by using non linear fitting algorithm of Gauss-Newton-Marquardt method.

$$pK_a = pH + \log [(I_x - I_b)/(I_a - I_x)] \qquad (5.1)$$

where I_a and I_b are the intensities of acidic and basic forms and I_x is the intensity at a pH near to the pKa.

pKa = 5.5 + log[(71-109)/(39-71)]
pKa = 5.5 + log [1.18]
pKa = 5.57

Figure 5.9-13 shows the pH dependent response of the sensor slide to different concentrations of Fe^{3+} (10^{-9}, 10^{-8}, 10^{-7}, 10^{-6} and 10^{-4} M) at different pH values (pH=6.5, 6.0, 5.5 and 5.0). Around pH=5, membrane was highly sensitive to Fe^{3+}. Therefore pH=5.0 was chosen as optimum working pH.

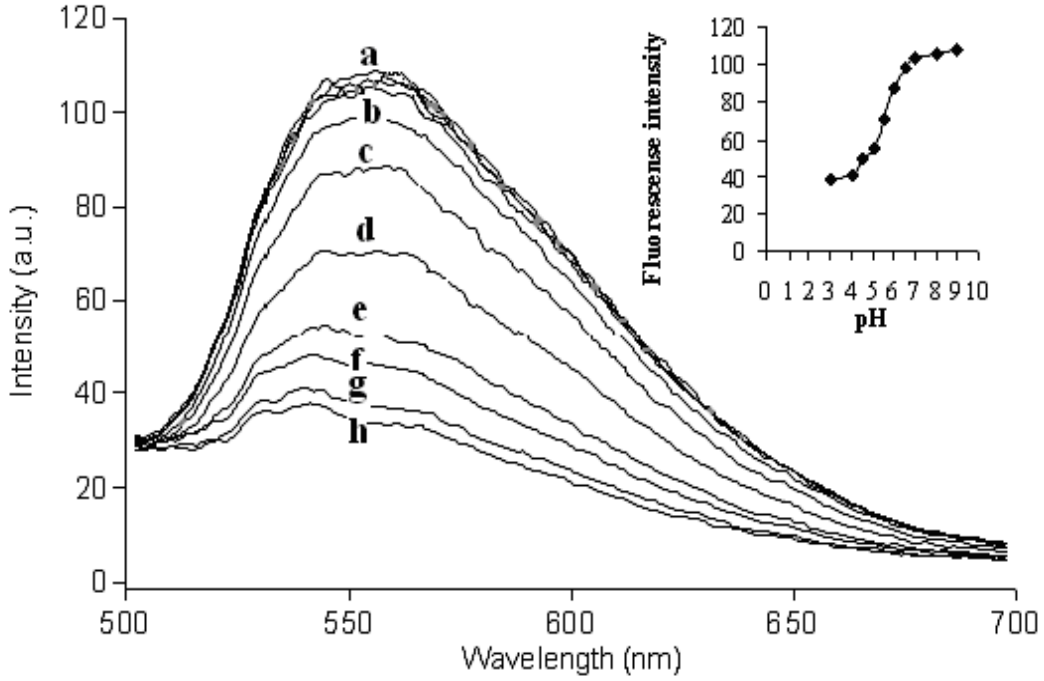

Figure 5.8 pH induced emission spectra of the DBS membrane after exposure to buffer solutions of (a) pH=9.0-7.0 (b) pH=6.5 (c) pH= 6.0 (d) pH= 5.5 (e) pH= 5.0 (f) pH= 4.5 (g) pH= 4.0 (h) 3.0 (pKa=5.57).

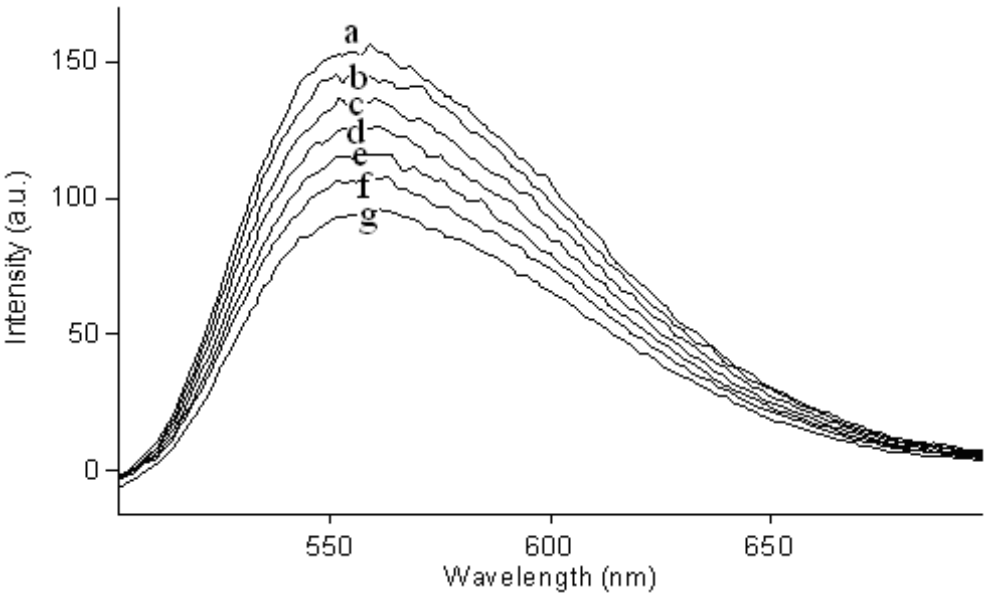

Figure 5.9 Emission based signal change of DBS dye doped membrane to different concentrations of Fe^{3+} at pH=6.5. (a) pH=6.5 iron free BES buffer (b) 10^{-9} M (c) 10^{-8} M (d) 10^{-7} M (e) 10^{-6} M (f) 10^{-5} M (g) 10^{-4} M Fe^{3+} (38% relative signal change).

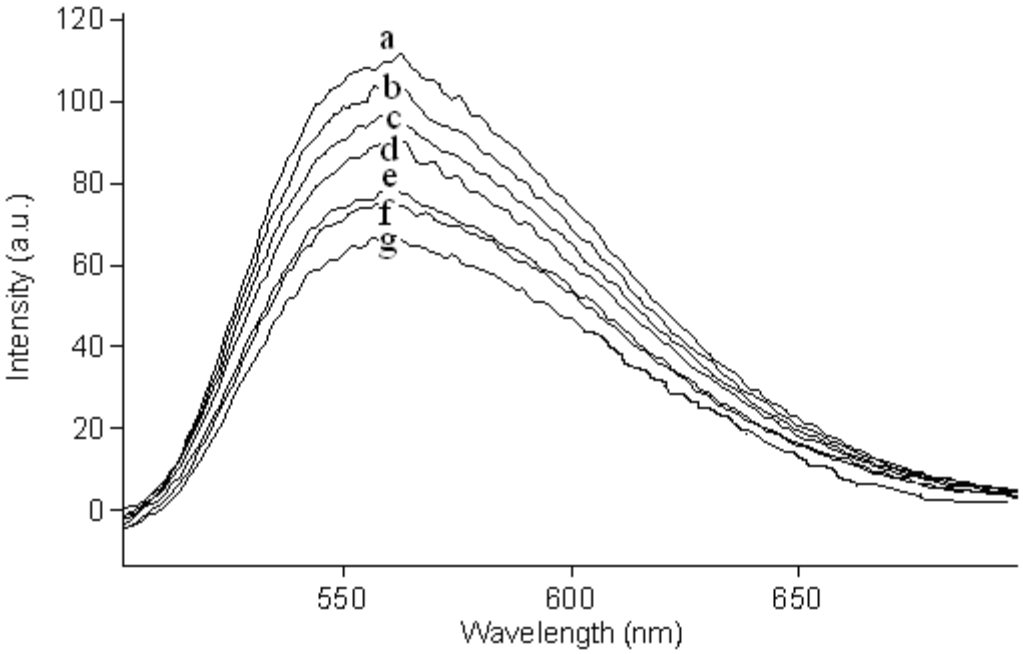

Figure 5.10 Emission based signal change of DBS dye doped membrane to different concentrations of of Fe^{3+} at pH=6.0. (a) pH=6.0 iron free BES buffer (b) 10^{-9} M (c) 10^{-8} M (d) 10^{-7} M (e) 10^{-6} M (f) 10^{-5} M (g) 10^{-4} M Fe^{3+} (41% relative signal change).

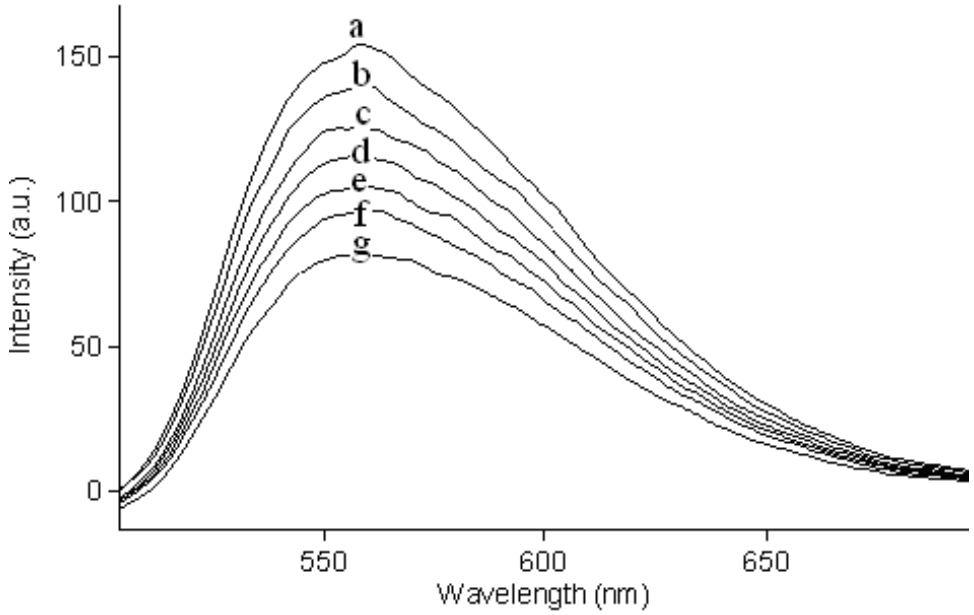

Figure 5.11 Emission based signal change of DBS dye doped membrane to different concentrations of of Fe^{3+} at pH=5.5. (a) pH=5.5 iron free BES buffer (b) 10^{-9} M (c) 10^{-8} M (d) 10^{-7} M (e) 10^{-6} M (f) 10^{-5} M (g) 10^{-4} M Fe^{3+} (47% relative signal change).

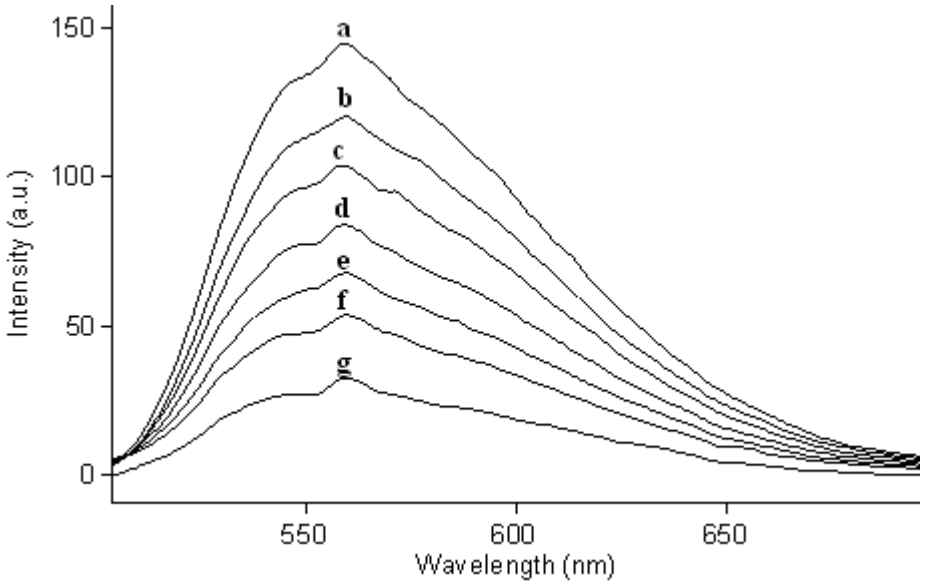

Figure 5.12 Emission based signal change of DBS dye doped membrane to different concentrations of of Fe^{3+} at pH=5.0. (a) pH=5.0 iron free BES buffer (b) 10^{-9} M (c) 10^{-8} M (d) 10^{-7} M (e) 10^{-6} M (f) 10^{-5} M (g) 10^{-4} M Fe^{3+} (74% relative signal change).

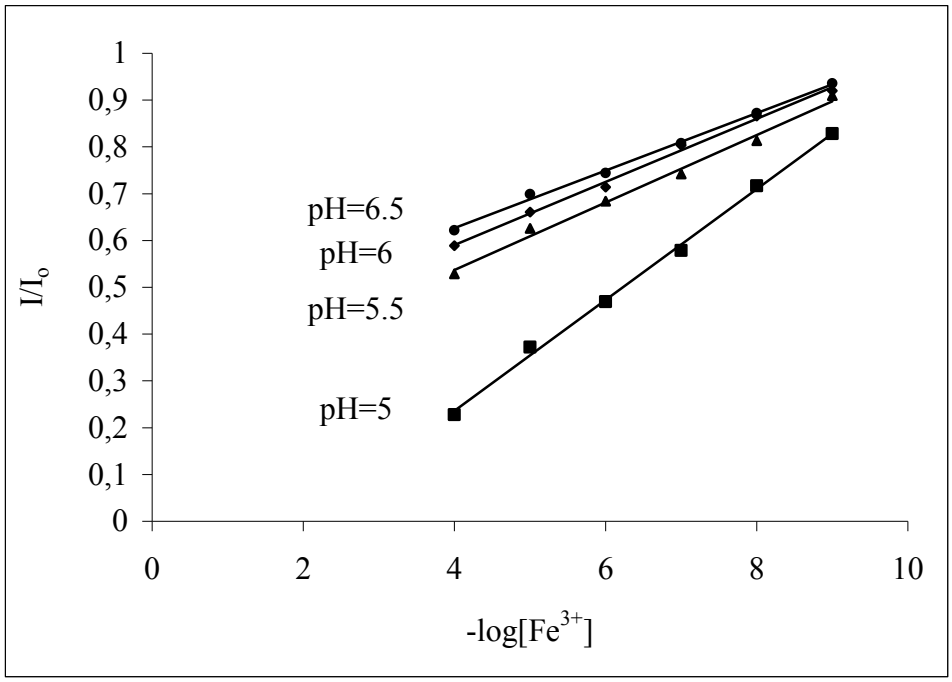

Figure 5.13 pH dependent response of the DBS dye doped membrane to Fe^{3+} at pH=6.5, 6.0, 5.5 and 5.0.

5.3.4 Response to Fe^{3+} ions

The membrane exhibited remarkable fluorescence intensity quenching on exposure to Fe^{3+} ions at pH=5.0 while the effects of the other responding ions (Cu^{2+}, Sn^{2+} and Hg^{2+}) were less pronounced. The dynamic response to Fe^{3+} ions were monitored as a change in the relative fluorescence intensity at 559 nm as the membrane was exposed to buffer solutions containing different concentrations of Fe^{3+}. Spectral response and characteristic calibration curves for Fe^{3+} obtained for three different concentrations of dye in the membrane are shown in Figure 5.14-17 respectively.

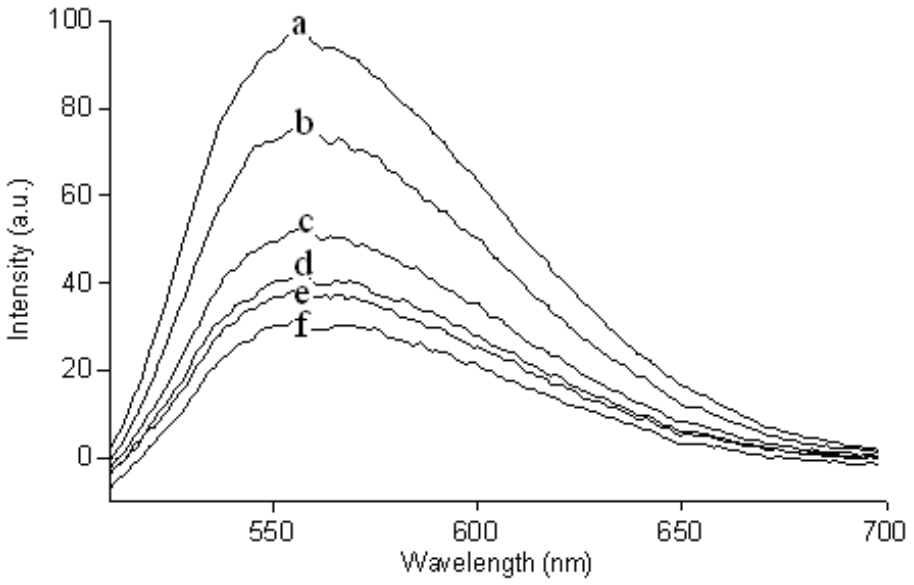

Figure 5.14 Emission spectra of sensor membrane (0.5 mg dye) in BES buffered solutions at pH=5.0 after exposure to different concentrations of Fe^{3+} ions (a) pH=5.0 iron free BES buffer (b) 10^{-9} M (c) 10^{-8} M (d) 10^{-7} M (e) 10^{-6} M (f) 10^{-4} M Fe^{3+}.

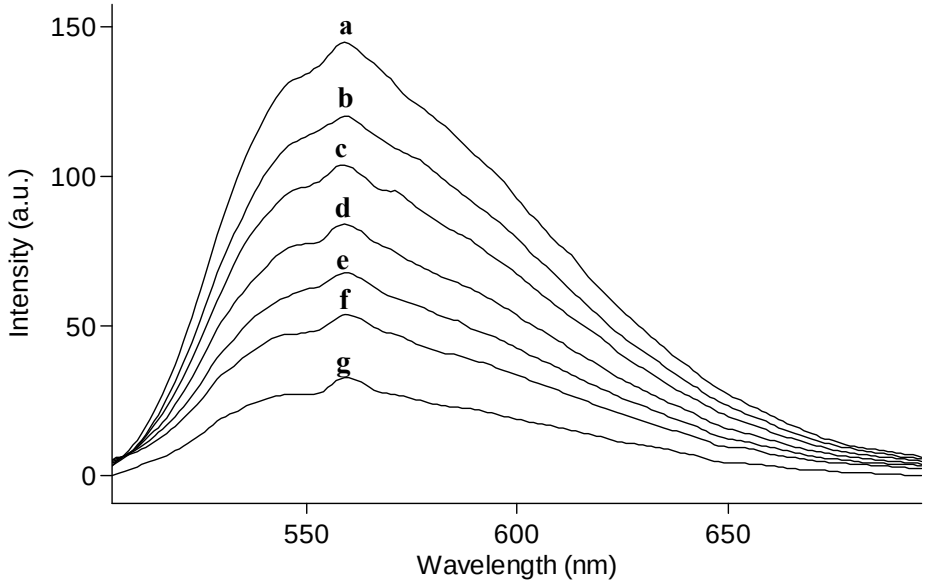

Figure 5.15 Emission spectra of sensor membrane (1 mg dye) in BES buffered solutions at pH=5.0 after exposure to different concentrations of Fe^{3+} ions. (a) pH=5.0 iron free BES buffer (b) 10^{-9} M (c) 10^{-8} M (d) 10^{-7} M (e) 10^{-6} M (f) 10^{-5} M (g) 10^{-4} M Fe^{3+}.

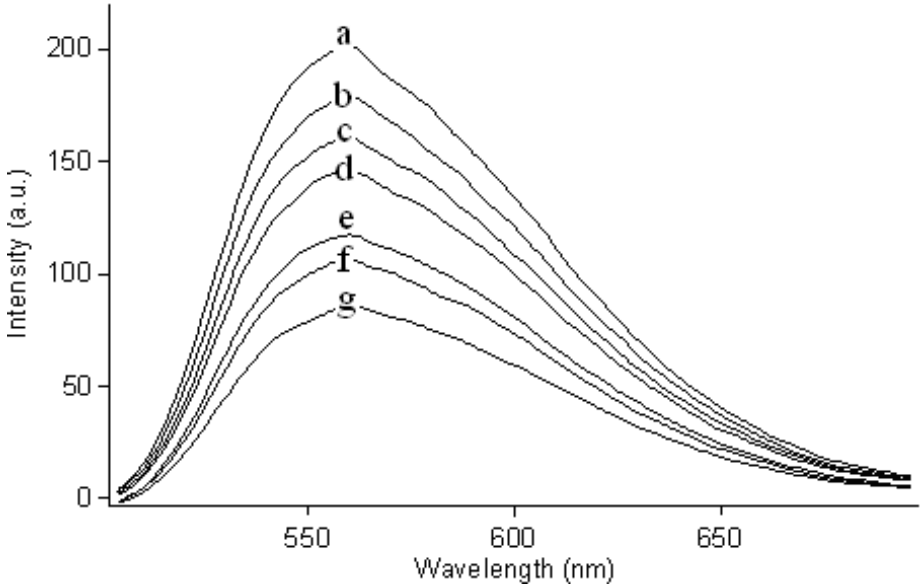

Figure 5.16 Emission spectra of sensor membrane (2 mg dye) in BES buffered solutions at pH=5.0 after exposure to different concentrations of Fe^{3+} ions (a) pH=5.0 iron free BES buffer (b) 10^{-9} M (c) 10^{-8} M (d) 10^{-7} M (e) 10^{-6} M (f) 10^{-5} M (g) 10^{-4} M Fe^{3+}.

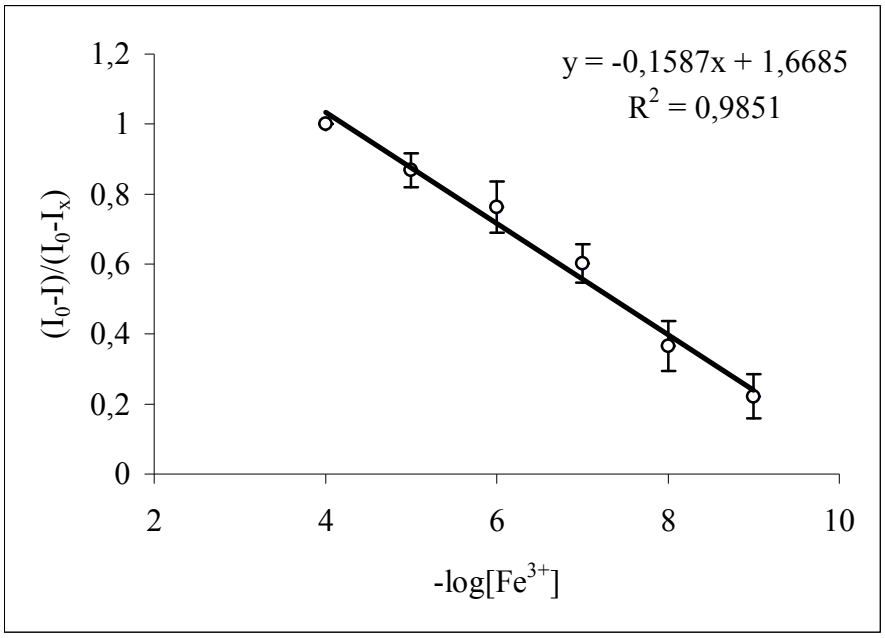

Figure 5.17 Linearized calibration curve of DBS membrane after exposure to Fe^{3+} solutions at pH=5.0 (the sensor films were prepared from cocktail containing 1 mg of DBS dye).

The determination of two oxidation states of iron; Fe^{2+} and Fe^{3+} was also tested. However no significant separate spectral response for the ionic forms of Fe^{2+} and Fe^{3+} was observed. Figure 5.18 shows the non-linearized comparative response of the DBS membrane to Fe^{2+} and Fe^{3+}.

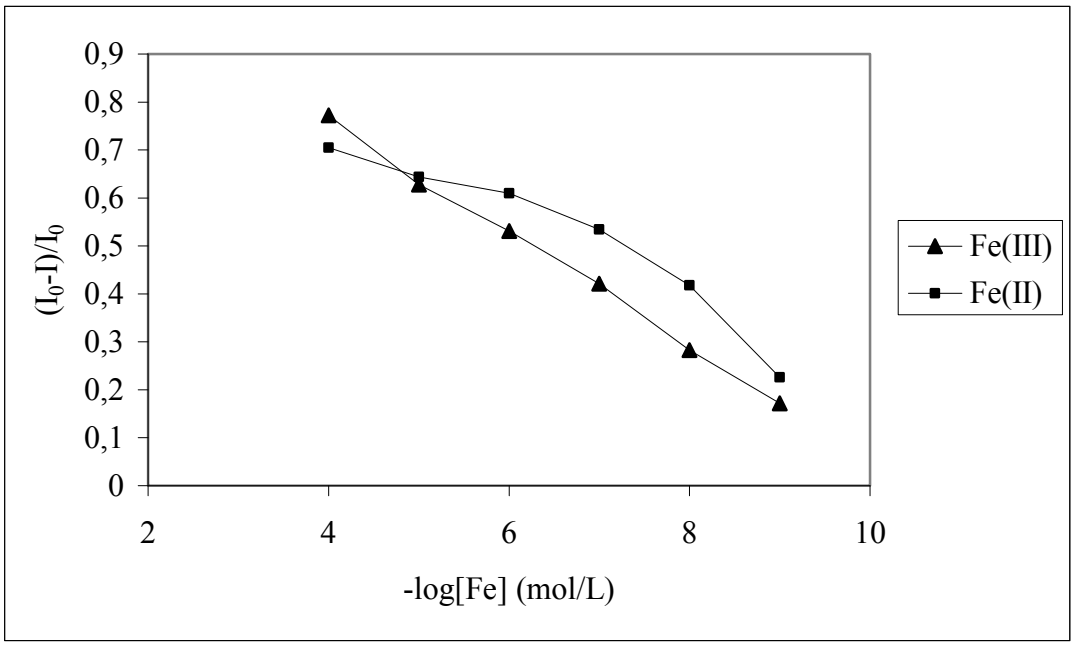

Figure 5.18 Response of the DBS membrane to Fe^{2+} and Fe^{3+} in the concentration range of 10^{-9}-10^{-4} M at pH=5.0.

5.3.5 Response and reproducibility

The DBS doped membrane exhibited a 77 % relative signal change in direction of decrease in fluorescence intensity when exposed to Fe^{3+} in the concentration range of 10^{-9}-10^{-4} M at pH 5.0. Regeneration was also accomplished at pH=5.0 in 0.1 M BES buffer solution with 100% efficiency.

The detection limit which is the concentration of analyte producing an analytical signal equal to three times of the standard deviation of the blank signal was found to be 10^{-9} M for Fe^{3+}.

Response time (τ_{90}) changed between 3 and 8 min for 10^{-9} M and 10^{-4} M Fe^{3+} respectively. The sensor was fully reversible and no drifts were observed after the fifth cycle (Figure 5.19). The reproducibility of the optical responses was assessed by repeatedly introducing a sample of 10^{-5} M Fe^{3+} in buffer at pH 5.0 and a 0.1 M BES buffer at pH 5.0. Between the 1st and 5th cycles, the level of reproducibility of the upper signal level achieved was quite good with a SD of 154.16 ± 1.33.

PVC matrix is one of the most durable matrices for aqueous media. Due to the lipophilic characteristics of the DBS dye and compatibility with PVC matrix, leaching from membrane to aqueous media has not been subject.

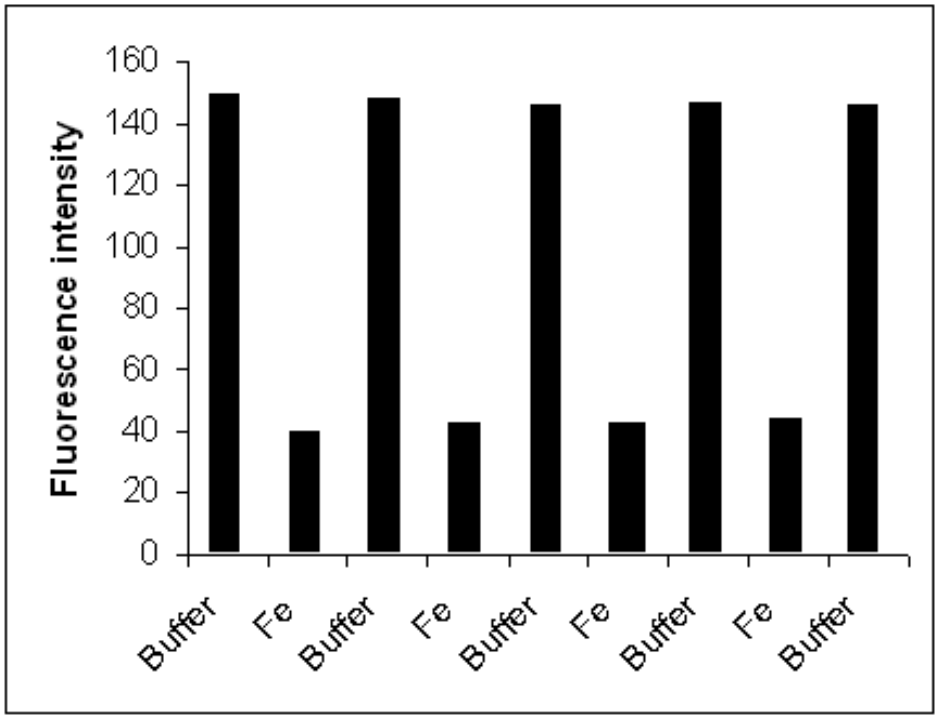

Figure 5.19 Response curve of the DBS membrane to Fe^{3+} for the concentrations of 0.0 and 10^{-5} M at pH=5.0. Reproducibility of the upper signal level is 154.16 ± 1.33 for 5 measurements.

5.3.6 Selectivity studies

The dye response to different metal ions was investigated in 1mM iron free metal ion solutions (Co^{2+}, Cu^{2+}, Ni^{2+}, Fe^{3+}, Cd^{2+}, Zn^{2+}, Pb^{2+}, Mn^{2+}, Mg^{2+}, Sn^{2+}, Cr^{3+} and Hg^{+}) at pH 5.0 in separate solutions. The membrane exhibited remarkable spectral change on exposure to 10^{-3} M Cu^{2+} and Sn^{2+} ions at pH 5.0, while the effects of other metal ions (Co^{2+}, Ni^{2+}, Cd^{2+}, Zn^{2+}, Pb^{2+}, Mn^{2+}, Mg^{2+}, $Cr^{3+}$and Hg^{2+}) were negligible (Figure 5.20). The relative signal intensity changes were 52.0% and 25.2% for Cu^{2+} and Sn^{2+} respectively.

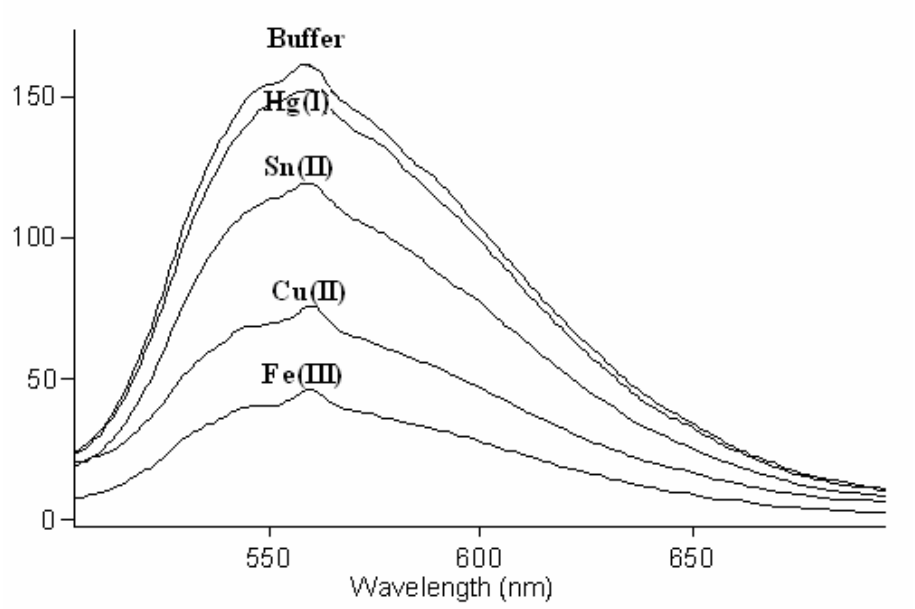

Figure 5.20 Emission spectra of DBS membrane in the presence of 1 mM Fe^{3+}, Cu^{2+}, Sn^{2+} and Hg^{2+} ions at pH 5.5 in separate solutions.

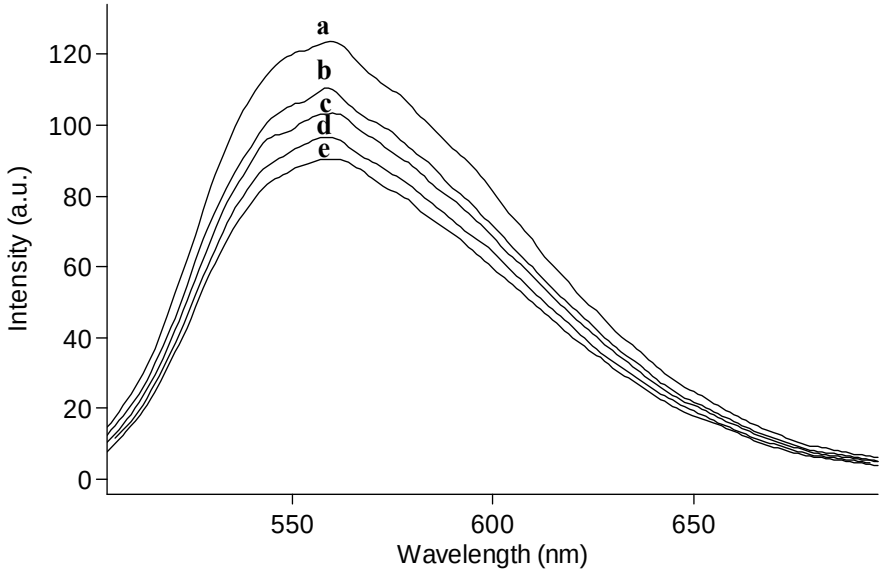

Figure 5.21 Emission spectra of sensor membrane (1 mg dye) in BES buffered solutions at pH=5.0 after exposure to different concentrations of Cu^{2+} ions. (a) pH=5.0 copper free BES buffer (b) 10^{-9} M (c) 10^{-8} M (d) 10^{-6} M (e) 10^{-4} M Cu^{2+} .

Figure 5.21 shows the emission spectra of sensor membrane (1 mg dye) in BES buffered solutions at pH=5.0 after exposure to different concentrations of Cu^{2+} ions in the concentration range of 10^{-9}-10^{-4} M. Figure 5.22 shows comparative response of DBS dye to Fe^{3+} and Cu^{2+}. The linearized plots reveal that the slope of the Fe^{3+}calibration curve is 5 times higher than the Cu^{2+}calibration curve.

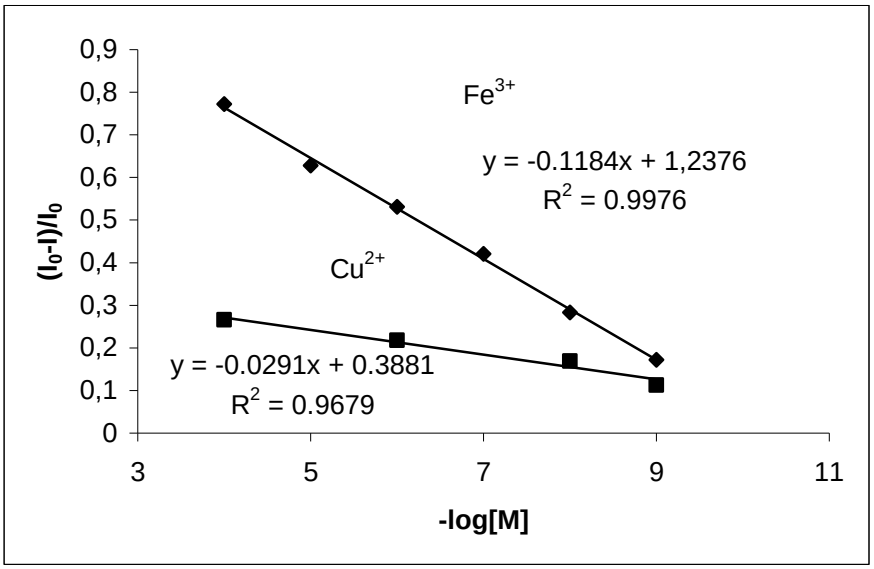

Figure 5.22 Linearized response of DBS dye to Fe^{3+} and Cu^{2+} at pH=5.0.

5.3.7 Effect of salinity

The iron concentration–dependent spectral response of sensor membrane is affected by the ionic strength of the buffer solution. By making the ionic strength of the buffer solution 135 mM with NaCl, the relative signal change of the emission spectrum of the sensor in contact with this solution decreased by around 50%. Calibration curve of the membrane in BES-buffered and 135 mM NaCl–containing solutions at pH 5.0 is shown in Figure 5.23.

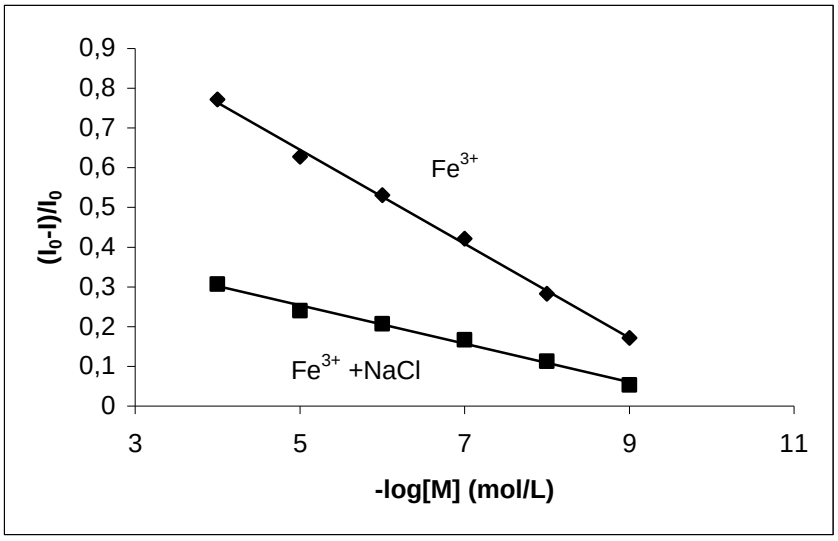

Figure 5.23 Calibration curve of the DBS membrane in BES-buffered and 135 mM NaCl–containing solutions at pH 5.0.

5.4 Conclusions

The selective determination of Fe^{3+} was accomplished by use of the newly synthesized DBS dye in plasticized PVC matrix. No significant response at the working wavelength was observed from other potential heavy metal interferents. The membrane responds to Fe^{3+} by changing fluorescence intensity reversibly at 554 nm when excited at 410 nm, and is sensitive to Fe^{3+}in the 10^{-9}-10^{-4} M range for an average exposure time of 5 min. The membranes are sensitive to pH as well, and the determination of Fe^{3+} should be performed in buffered solutions, ideally at pH 5.0. The fluorescent DBS dye can be offered as an optical Fe^{3+} sensor due to the visible excitation (410 nm) and emission wavelength (554nm), high molar absorbtivity (650755 $cm^{-1}M^{-1}$) and satisfactory quantum yield (0.0254) in immobilized form.

CHAPTER SIX

CHARACTERIZATION OF A NEWLY SYNTHESIZED FLUORESCENT BENZOFURAN DERIVATIVE AND USAGE AS A SELECTIVE FIBER OPTIC SENSOR FOR Fe^{3+}

6.1 Introduction

The monitoring of trace levels of iron has raised interest since iron plays an important role in metabolic processes, biological materials and environmental samples. The speciation analysis of iron is also important to understand the biochemical cycling in metabolic processes as well as in the ocean or atmosphere. Most investigations of iron have been limited to the determination of its total dissolved concentration, and relatively little is known about its oxidation state. Among a variety of analytical techniques including UV–Vis spectrophotometry, atomic absorption spectroscopy (AAS) and spectrofluorimetry for the measurement of iron (II) and iron (III), only a few approaches have been developed to quantify the different oxidation state species of iron in a sample. On the other hand, the discovery, design and synthesis of new organic fluorescent molecules and their interaction with cations, anions or biomaterials lead exciting advances in sensing, imaging and diagnostic.

The iron sensitive organic chromophores Phen Gren FL, Phen Gren SK and calcein has been commercialized by Molecular Probes^{TM} Invitrogen Detection Technologies and studied by Petrat, Rauen & Groot (1999) and Kuhn et al. (1995). Phen Gren FL and Phen Gren SK are cell membrane-permeable fluorescent diacetate derivatives of phenanthroline and are capable of detecting Fe^{2+}, as well as Cu^{2+}, Cu^{+}, Hg^{2+}, Pb^{2+}, Cd^{2+} and Ni^{2+}.

Picard et al. (1998) have exploited the fluorescence quenching of calcein at neutral pH to follow intracellular release of Fe^{2+} from transferin.

Pulido-Tofino et al. (2000) used immobilized fluorescent pyoverdin pigment (on controlled pore glass) which selectively reacts with Fe(III) in the 3-200 μg L^{-1}conentration range.

Pons, Forteza & Cerdà (2005) offered an optical fiber reflectance sensor for the determination and speciation analysis of Fe(III) and total iron in fresh and seawater samples. They formed Fe (III)–thiocyanate complex which is spectrophotometrically detected at 480 nm.

In a recent work, Abbaspour et al. (2006) offered a sensor array for speciation of iron(II), iron(III) and full-range pH monitoring using a simple colorimetric method as an appropriate alternative for optodes. They used ionophores 4-methyl-2,6-bis (hydroxymethyl)phenol (or its halo-derivatives) and 1,10- phenanthroline for determination of Fe(III) and Fe(II), respectively.

In this study, newly synthesized fluorescent benzofuran derivative Bis(7-methoxybenzofuran-2-il)ketoxime (BFK) (Figure 6.1) has been characterized in different solvents and in PVC and the successful use of a fluorescent benzofuran derivative in construction of selective poly vinyl chloride (PVC)-based fiber optic Fe (III) sensor have been reported. Typical sensor characteristics such as dynamic working range, sensitivity, limit of detection, and selectivity have been investigated. The interferences of various cations on the response of Fe^{3+} also have been studied. The fluorescent benzofuran derivative Bis(7-methoxybenzofuran-2-il)ketoxime (BFK) has been used for the first time as sensing agent in the optical sensor design.

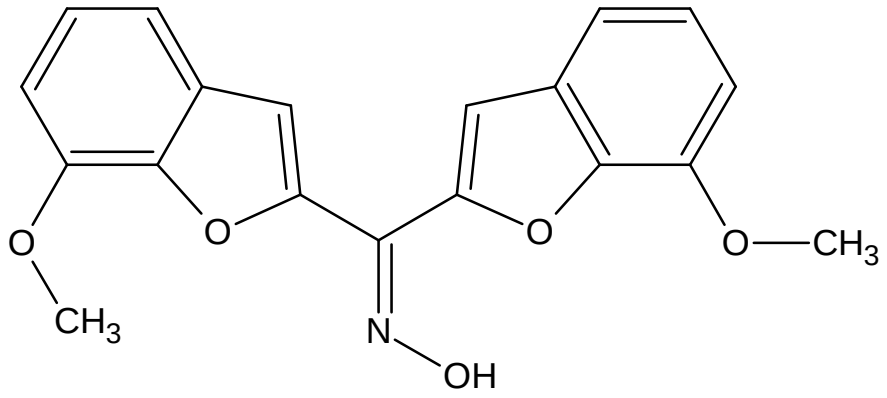

Figure 6.1 Schematic structure of the Bis(7-metoksi-1-benzofuran-2-il)ketoksim (BFK) dye.

6.2 Experimental

The excitation and fluorescence emission spectra were recorded in different solvents of absolute ethanol, tetrahydrofuran (THF), dichloromethane (DCM), and toluene and in solid polymer matrices of polyvinyl chloride (PVC) and ethyl cellulose (EC).

Buffer components; acetic acid/acetate, phosphate and metal salts (iron(III) nitrate and ammonium iron(II) sulphate hexahydrate) were of analytical grade (Merck and Fluka). Doubly distilled water was used throughout the studies. 0.1 M stock solutions of Fe^{2+}, Fe^{3+} and other metal cations were prepared from respective metal nitrates, sulphates or chlorides and diluted with 5.0×10^{-3} M buffers of demanded pH. The preparation of the buffer solutions and the used metal salts were given in Chapter 2.

6.2.1 Preparation of the sensor membrane films

The optode PVC membranes were prepared to contain 120 mg of PVC, 240 mg of plasticizer, 1.0 mg of BFK dye (25 mmol dye/kg polymer), equivalent amount of potassium tetrakis (4-chlorophenyl) borate and 1.5 ml of THF. The prepared cocktails contained 33% PVC and 66% plasticizer by weight which is quite common (Seiler & Simon, 1992; Bakker & Simon, 1992; Lerchi et al., 1992; Morf, Seiler, Rusterholz & Simon, 1990). The EC membranes were prepared to contain 100 mg

of EC, 200 mg of plasticizer, 1.0 mg of BFK dye (25 mmol dye/kg polymer), equivalent amount of potassium tetrakis (4-chlorophenyl) borate and 1.5 ml of THF.

The resulting cocktails were spread onto a 125 μm polyester support (Mylar TM type) in order to obtain the sensing films as given in Chapter 2. The most important function of the polyester is to act as a mechanical support because the thin PVC or EC films are impossible to handle. The polyester support is optically fully transparent, ion impermeable and exhibits good adhesion to PVC. The films were kept in a desiccator in the dark. This way the photostability of the membrane was ensured and the damage from the ambient air of the laboratory was avoided. Each sensing film was cut to 1.2*3.0 cm size and fixed diagonally into the sample cuvette and the excitation and fluorescence emission spectra were recorded. For spectral characterization of the PVC and Ethyl Cellulose (EC) doped BFK, excitation and corrected emission spectra of the films were recorded.

The pH values of the solutions were checked using a digital pH meter (WTW) calibrated with standard buffer solutions of Merck. All of the experiments were carried out at room temperature; 25 ± 1 ^{o}C. Quinine sulphate; Fluka AG 22640, was used as reference for fluorescence quantum yield calculations of the benzofuran derivative.

6.2.2 Instrumentation

Metal response measurements were carried out with fibre optic coupler, fibre optic probe (2m) and solid sample tip accessories constructed on the spectrofluorometer. The tip of the bifurcated fiber optic probe was interfaced with a sensing film in a buffer containing home made 300 μL flow cell. For the flow system experiments, the films were cut to 1 cm width and 1 cm long and placed into the before mentioned flow cell system (Chapter II, Section 2.2). Flow rate of the peristaltic pump was kept at 9.9 mL min^{-1}. Analyte solutions or buffers were transported by the pump via tygon tubing of 2.06 mm i.d. Analyte solutions were introduced into the flow cell with a microsyringe.

6.3 Results and discussion

6.3.1 Spectral characterization studies in solution phase

In order to perform the spectral characterization of the BFK, absorption, excitation, and corrected emission spectra were recorded in the solvents of DCM, EtOH, THF and toluene. Spectral data of reference standard quinine sulphate were acquired in 0.05 M H_2SO_4. In the employed solvents (DCM, EtOH, THF and toluene) the BFK was excited at 301, 303, 302, and 304 nm, respectively and the emission spectra were recorded. In order to obtain the excitation spectra, the BFK was excited at 428, 430, 427 and 424 nm, respectively and back scanned in the range of 420-250 nm. The emission spectra were corrected using commercially available silica ground of Cary-Eclipse. The Stoke's shift values, absorption, excitation and emission wavelengths and quantum yields were extracted from the spectral data (Figure 6.2 and 6.3, Table 6.1).

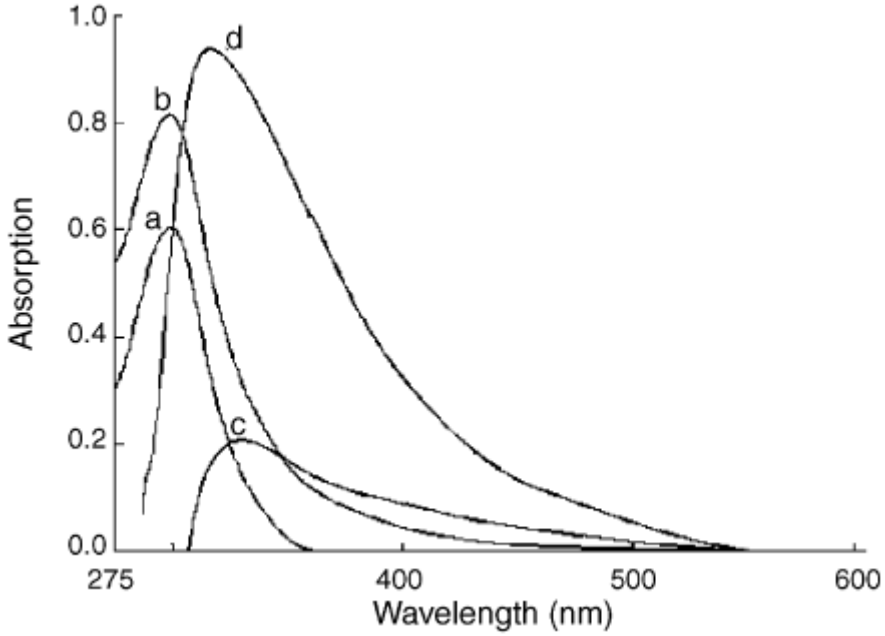

Figure 6.2 Absorption spectra of BFK dye: (a) in EtOH (λmax = 300 nm), (b) in EtOH, in presence of 10^{-4}M Fe^{3+} (λmax = 300 nm), (c) in PVC, in the form of thin film (λmax = 330 nm), and (d) in PVC, in presence of 10^{-4} M Fe^{3+} (λmax = 314 nm).

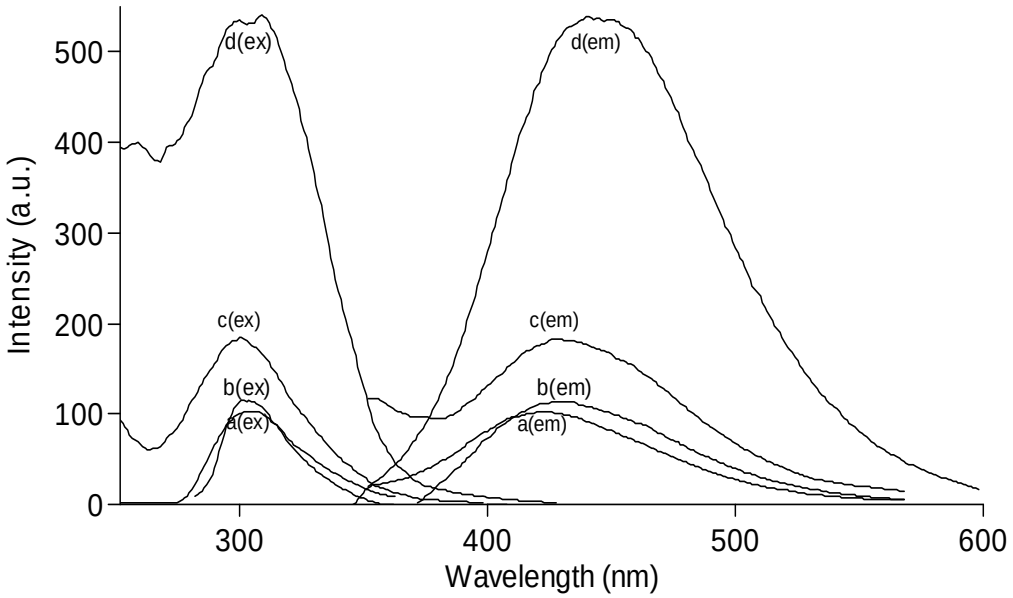

Figure 6.3 Excitation and corrected emission spectra of the 10^{-6}M BFK in a: Toluene (λ_{ex} = 304, λ_{em} = 424 nm), b: THF (λ_{ex} = 302, λ_{em} = 427nm), c: DCM (λ_{ex} = 301, λ_{em} = 428 nm) and d: EtOH (λ_{ex} = 303, λ_{em} = 430 nm).

Table 6.1 Spectral characterization of BFK dye (λ_{ex} : excitation wavelength in nm, λ_{em} : emission wavelength in nm, $\Delta\lambda_{ST}$: Stoke's shift and θ_F : Quantum yield)

Compound	Solvent	λ_{ex} (excitation wavelength)	λ_{em} (emission wavelength)	$\Delta\lambda_{ST}$ (Stoke's shift)	θ_F (Quantum yield)
BFK	DCM	301	428	127	0.00508 (in DCM)
	EtOH	303	430	127	
	THF	302	427	127	
	Toluene	304	424	120	
	PVC	340	414	74	0.0155
	EC	325	398	73	0.0398

6.3.2 Spectral characterization studies in solid phase

For spectral characterization of the PVC and Ethyl Cellulose (EC) doped BFK, excitation and corrected emission spectra of the films were recorded. BFK was excited at 325 and 340 nm in EC and PVC respectively (Figure 6.4).

For fiber optic studies the appropriate size of the sensor films were cut, attached to the fiber tip (6 mm diameter) and immersed into the buffer containing flow cell. Flow rate of the peristaltic pomp was kept at 9.9 mL min^{-1}. Solutions were transported by an Ismatec peristaltic pump via tygon tubing of 2.06 mm i.d. The contact between the sensor membrane and the buffer provides a constant fluorescence signal. During fiber optic measurements the fluorescent intensity was monitored at 414 nm and recorded versus time. Iron determinations were carried out pumping analyte solutions into buffer solutions of desired pH. The Fe^{3+} solution pumped for 2 min was responsible for the observed relative signal change.

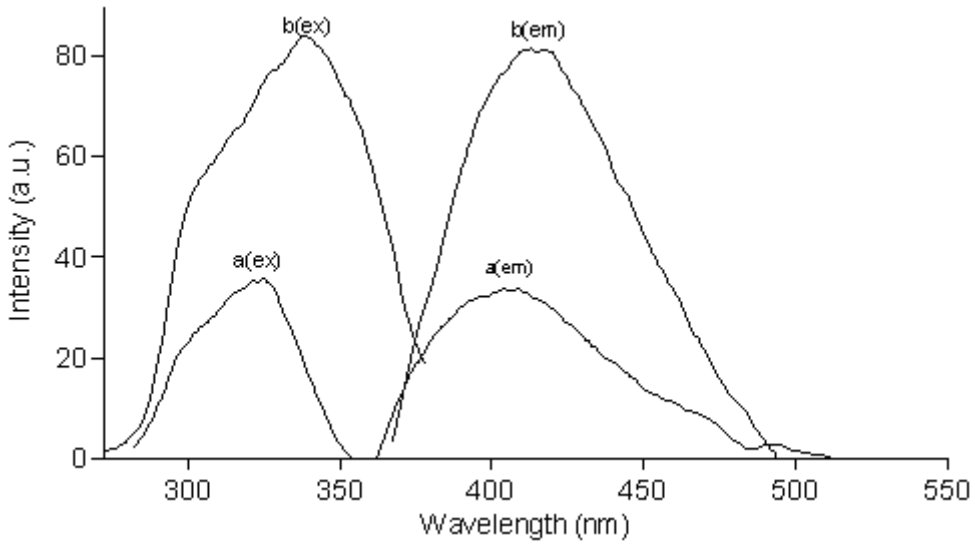

Figure 6.4 Excitation and corrected emission spectra of the 10^{-6}M BFK dye a: in PVC (λ_{ex} = 340, λ_{em} = 414nm), b: EC (λ_{ex} = 325, λ_{em} = 398 nm).

6.3.3 Fluorescence quantum yield calculations

The UV-Vis absorbance and corrected emission spectra of nine different concentrations of reference standard (quinine sulphate solution, in sulphuric acid; Fluka AG 22640, >99%, ϕ_F =0.54) and BFK compound were recorded for fluorescence quantum yield calculations. The integrated fluorescence intensities were plotted *vs* absorbance for the reference standards and the BFK compound in PVC and EC matrices (Figure 6.5). The gradients of the plots are proportional to the quantity of the quantum yield of the studied molecules. The equations of the plots are y = 160442x; R^2 = 0.9998 for reference standard, y = 93621x; R^2 = 1 for BFK dye in EC and y = 35406x; R^2 = 0.9984 for BFK dye in PVC. Quantum yield (ϕ_F) values were calculated according to the given equation in Chapter 2 as 0.00508 in DCM, 0.0155 in PVC and 0.0398 in EC.

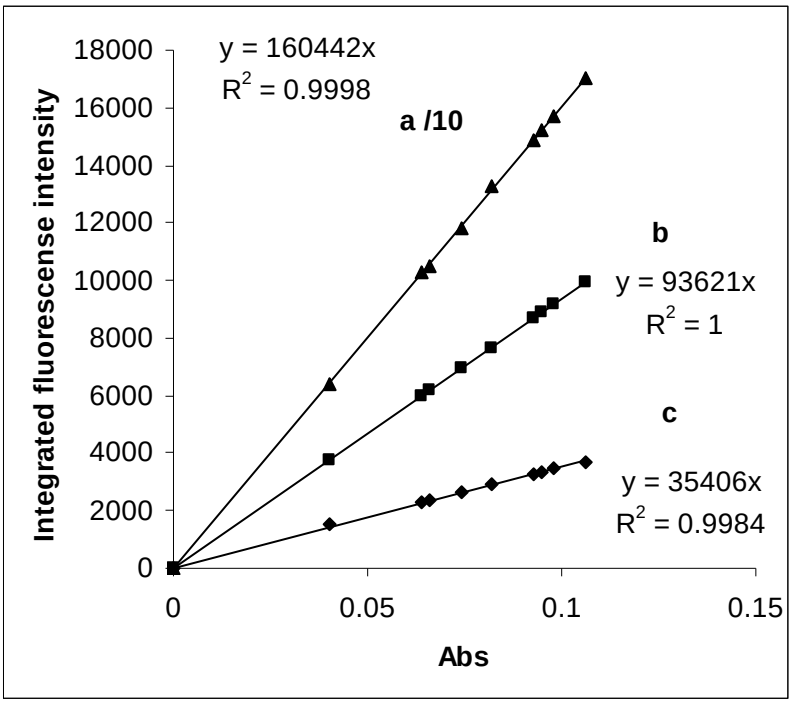

Figure 6.5 The integrated fluorescence intensities *vs* absorbance **a**: for the reference standard; quinine sulphate in H_2SO_4 **b:** the BFK dye in EC **c:** BFK dye in PVC matrices.

6.3.4 Choice of matrix material and dye

According to the data given in Table 6.1, the BFK compound exhibited quite high quantum yield in plasticized PVC. In comparison to EC, the BFK dye exhibited higher excitation wavelength and Stoke's shift value in PVC. Although, the quantum yield efficiency of BFK is higher in EC, due to the higher water uptake and swelling tendencies of EC, the PVC matrix was chosen as cocktail material for further studies.

In all of the employed matrices the Stoke's shift values of BFK dye, $\Delta\lambda_{ST}$ calculated from the spectral data are quite high. Stoke's shift is important for fluorescence and optical sensor studies because the high Stoke's shift value allows the emitted fluorescence photons to be easily distinguished from the excitation photons, leading to the possibility of very low background signals and permits the usage of BFK dye in the construction of fiber optic sensor.

The BFK dye was used in optical sensor design for Fe^{3+} sensing because of its promising spectral properties like quite high quantum yield in immobilized form (0.0155 in PVC and 0.0398 in EC), high photostability, selective intensity based response to Fe^{3+} in presence of Fe^{2+} and other cations, and pH induced stability.

6.3.5 pH dependence of BFK dye

The pH dependence of the dye doped membrane was investigated in buffered iron free solutions in the pH range of 7.0-2.5. Buffer solutions were prepared with 5.0×10^{-3} M CH_3COOH, 5.10^{-3} M NaH_2PO_4. The immobilized BFK dye did not exhibit significant pH dependence. Fig. 6.6 shows the pH dependency of the sensor membrane in iron free buffer solutions in the pH range of 7.0-2.5.

Optimum conditions of pH were investigated separately at constant concentrations of Fe^{2+} and Fe^{3+}ions. The analytical signal (I_0-I/I_0) produced by the Fe^{3+} was approximately 10 fold of the signal produced by Fe^{2+} in the pH range of

4.0-6.0 (Figure 6.7). Therefore, pH 6.0 was selected as the optimum pH for Fe^{3+} determination for the concentration range of $[Fe^{3+}] = 1.0\times10^{-6}$- 8.0×10^{-4} M.

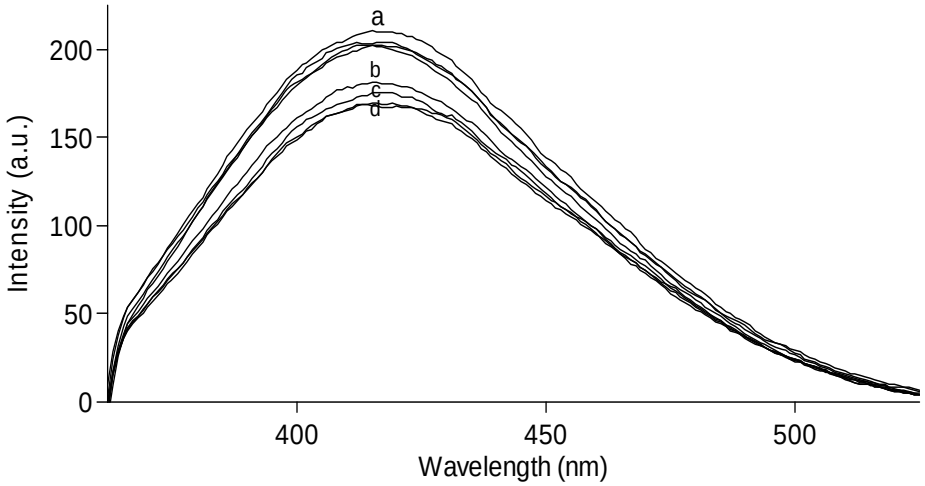

Figure 6.6 Intensity based pH response of BFK dye in iron free solutions in the pH range of 7.0-2.5. a: pH= 7.0, 6.0, 5.0, 4.5, b: pH= 4.0, c: pH=3.5, d: pH=3.0, 2.5.

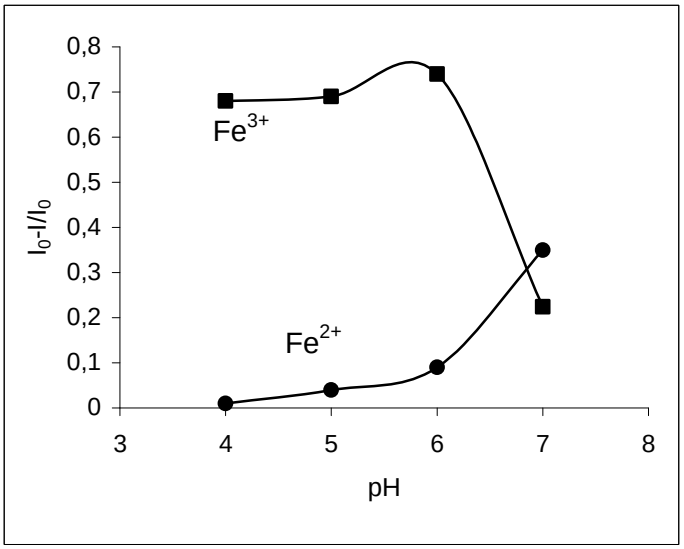

Figure 6.7 Effect of pH on relative fluorescence intensity of immobilized BFK dye in fixed Fe^{2+} and Fe^{3+} concentrations (5.0×10^{-4} M).

6.3.6 Response to Fe^{3+} ions

The dye-doped membrane exhibited remarkable fluorescence intensity quenching upon exposure to Fe^{3+} ions at pH=6.0 while the effects of Fe^{2+} and other responding ions (Cu^{2+}, Ca^{2+}, Hg^{+}, Pb^{2+}, Al^{3+}, Cr^{3+}, Mn^{2+}, Mg^{2+}, Sn^{2+}, Cd^{2+}, Co^{2+} and Ni^{2+}) were less pronounced. Upon exposure to iron concentrations from 1.0×10^{-6} to 8.0×10^{-4} M, the membrane exhibited an 86% relative signal change in direction of decrease in fluorescence intensity (Figure 6.8).

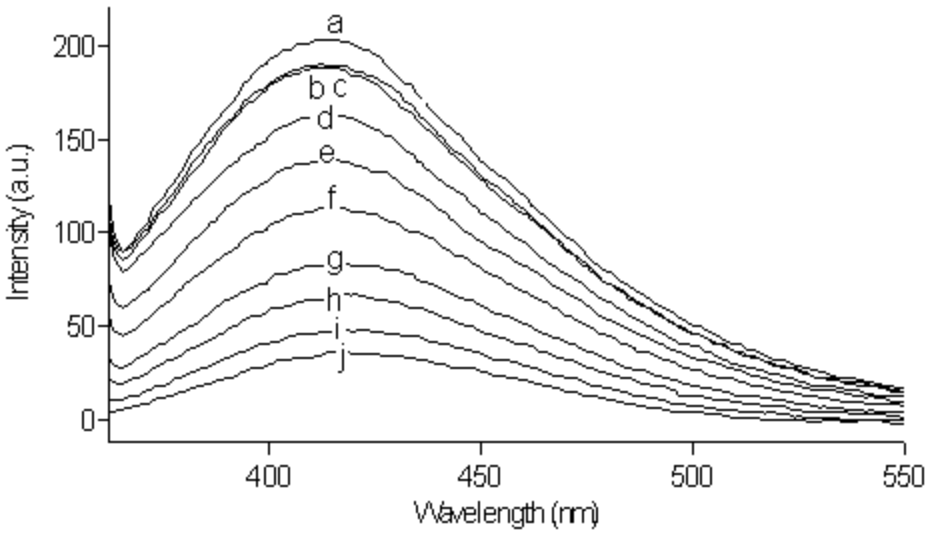

Figure 6.8 Intensity based response of sensor membrane after exposure to certain concentrations of Fe^{3+}. a: 10^{-6} b: 3.0×10^{-6}, c: 1.3×10^{-5}, d: 2.6×10^{-5}, e: 3.9×10^{-5}, f: 1.43×10^{-4}, g: 2.86×10^{-4}, h: 4.49×10^{-4}, i: 5.72×10^{-4}, j: 8.0×10^{-4}.

The data on Figure 6.9 represent results of five replicate measurements each prepared using the same cocktail composition. Error bars show the standard deviation (S.D.) between 2 and 5%. The slightly sigmoidal shape of the calibration curve is in agreement with the literature (Morf, Seiler, Rusterholz & Simon, 1990). In the concentration range of 10^{-6}–8.0×10^{-4} M a quite good linear correlation was obtained with R^2 value of 0.9668 for Fe^{3+}.

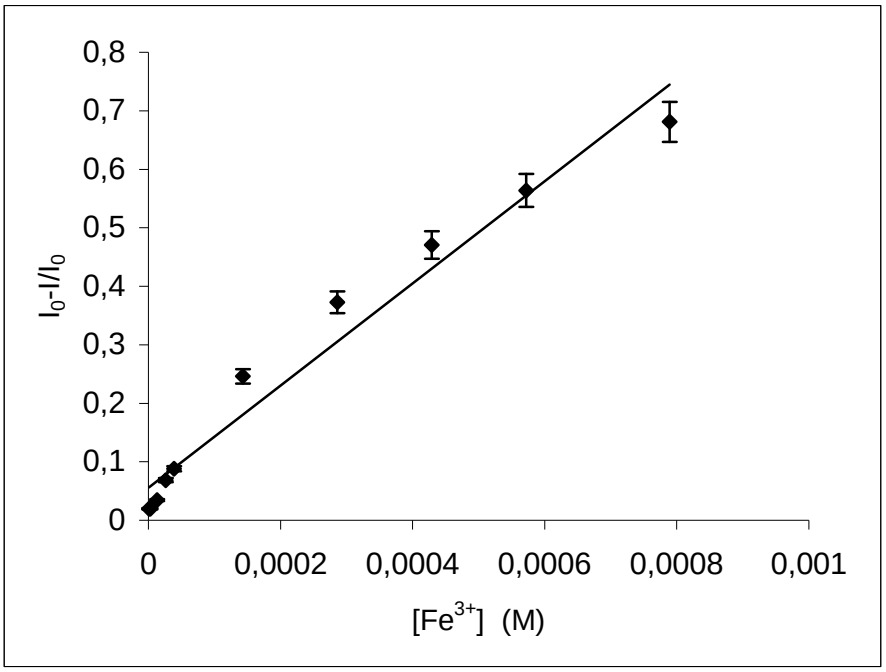

Figure 6.9 Calibration plot of Fe^{3+} selective composition in the concentration range of 1.0×10^{-6}–8.0×10^{-4} M in acetic acid/acetate buffered solutions at pH 6.0. Data presented are mean of five sets of measurements.

6.3.7 Selectivity studies

Figure 6.10 summarizes a selectivity comparison of Fe^{3+} over Fe^{2+} in separate solutions at pH 6.0. According to the figure, since I_0-I/I_0 =0.5 can not be reached by Fe^{2+} , it can be concluded that, the BFK dye was effectual in reversible binding of Fe^{3+} but ineffectual in binding Fe^{2+} and other possible interfering ions (Cu^{2+}, Ca^{2+}, Hg^{+}, Pb^{2+}, Al^{3+}, Cr^{3+}, Mn^{2+}, Mg^{2+}, Sn^{2+}, Cd^{2+}, Co^{2+}, Ni^{2+}) in immobilized form. The selective uptake of Fe^{3+} over Fe^{2+} by the membrane may partly be attributed to the Pearson's HSAB principle. Theory states that "*hard* [Lewis] acids prefer to bind to *hard* [Lewis] bases and that *soft* [Lewis] acids prefer to bind to *soft* [Lewis] bases to give complexes. Fe^{3+} ion is a harder acid in the sense of hard-soft acid-base (HSAB) theory than Fe^{2+}, Cu^{2+}, Hg^{+}, Pb^{2+}, Sn^{2+}, Cd^{2+}, Co^{2+} and Ni^{2+} (Pearson, 1973).

The O- and N- donor Lewis bases on the BFK dye are in the category of hard Lewis bases and are probably responsible for the binding of Fe^{3+} ions. Although Fe^{3+}

is in the same category with Ca^{2+}, Al^{3+}, Cr^{3+}, Mn^{2+}, Mg^{2+} in Pearson's classification, the other cations do not interact with the dye. The selective and strong response of BFK dye to Fe^{3+} can also be attributed to the strong quencher characteristic of Fe^{3+}. The fluorescence was quenched to a greater extent by Fe^{3+} than by Fe^{2+} and other possible interferent cations; Cu^{2+}, Ca^{2+}, Hg^{+}, Pb^{2+}, Al^{3+}, Cr^{3+}, Mn^{2+}, Mg^{2+}, Sn^{2+}, Cd^{2+}, Co^{2+} and Ni^{2+}.

The LOD for Fe^{3+} was defined as the concentration at which the signal is equal to the blank signal plus 3σ and found to be 6.0×10^{-7} M. At constant pH (pH=6.0), the response is reproducible. The photostability and chemical stability in the polymer matrix (at least 3 months) was satisfactory.

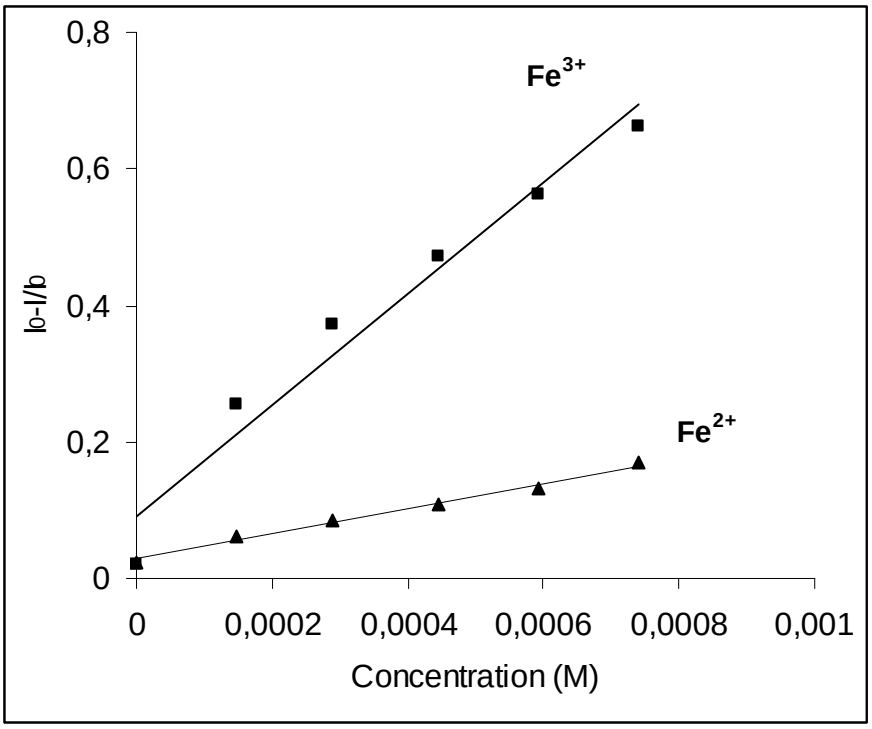

Figure 6.10 Fluorescence intensity based response of immobilized BFK dye to Fe^{3+} and Fe^{2+} ions in separate solutions at pH 6.0.

6.3.8 Response and reproducibility

The time based response data of the sensor membrane for the determination of Fe^{3+} was acquired in the concentration range from 1.36×10^{-5} to 9.9×10^{-4} M (Figure

6.11). The sensor was fully reversible within the dynamic working range and the average response time (τ_{90}) is 30 sec. under flow conditions.

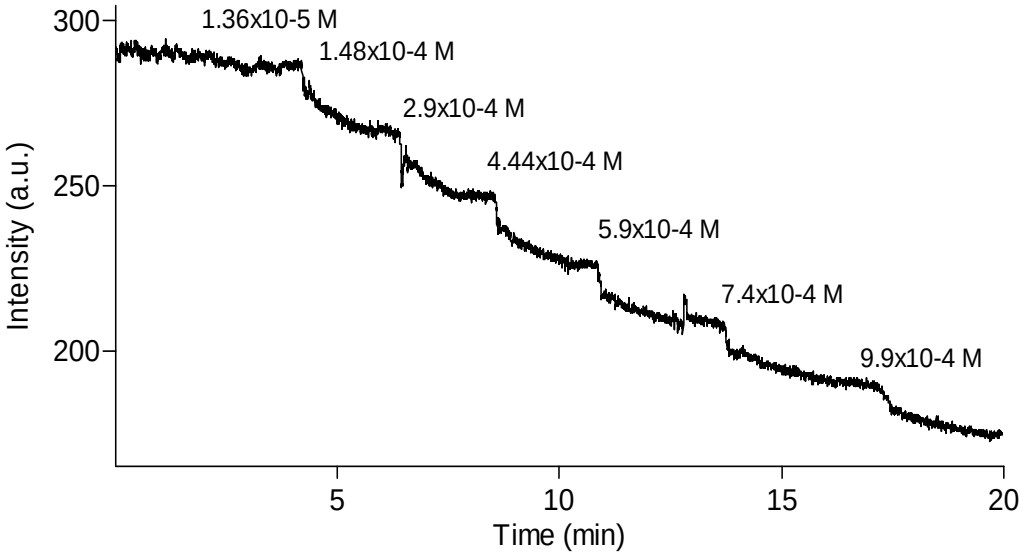

Figure 6.11 Time dependent response of the sensor membrane after injection of certain concentration of Fe^{3+} solutions.

Regeneration experiments were carried out in 0.1 M EDTA, 0.1 M HCl and 10^{-4} M HCl solutions, respectively. Approximately 100 % regeneration performance was succeeded with 10^{-4} M HCl and with EDTA solution but only 80 % recovery could be obtained in 0.1 M HCl. For further regeneration treatments 10^{-4} M HCl was preferred. The sensor was fully reversible and only a slight drift of the upper signal level has been observed after the 6th cycle. The reproducibility of the optical responses was assessed by repeatedly introducing a sample of 5.0×10^{-4} M Fe^{3+} in 5.0×10^{-3} M acetic acid/acetate buffer at pH 6.0.and a 10^{-4} M HCl solution. Between the 1st and 5th cycles, the level of reproducibility achieved was quite good with a RSD of 203.60 ±1.14 (Figure 6.12).

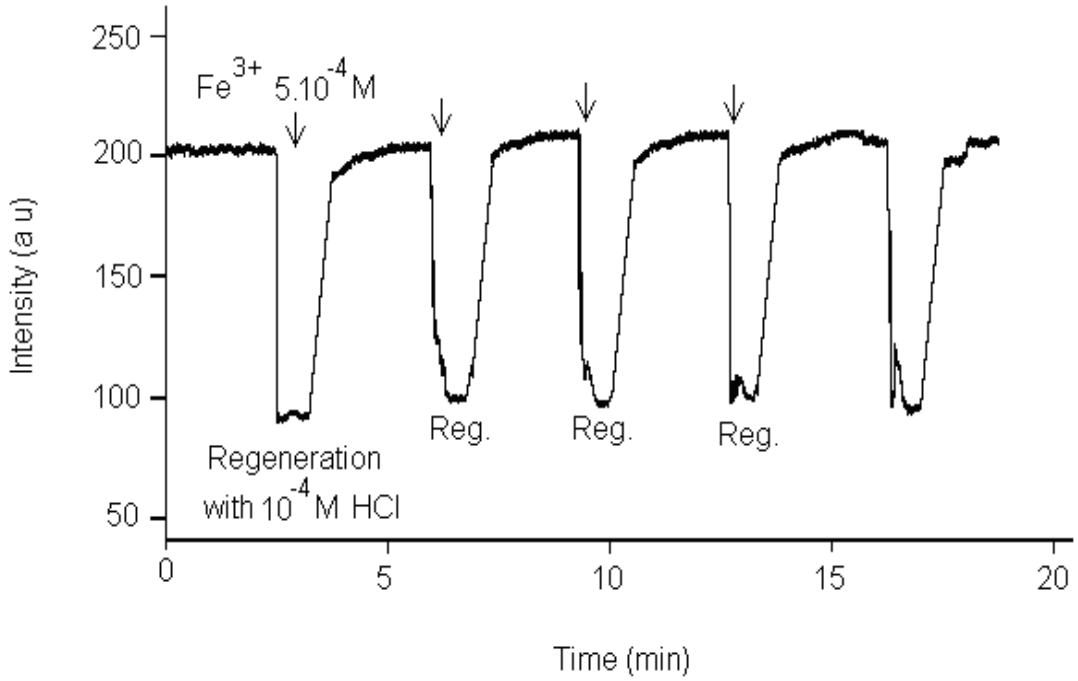

Figure 6.12 Response characteristics of the sensor film in an alternating concentration of Fe^{3+} 5.0×10^{-4} M of 10^{-4} M HCl solution.

6.4 Conclusion

We demonstrate that, newly synthesized fluorescent benzofuran derivative can be used for selective and reversible Fe^{3+} sensing, in plasticized PVC matrix. The dye was quenched to a greater extent by Fe^{3+} than by Fe^{2+} and other possible interferent cations; Cu^{2+}, Ca^{2+}, Hg^{+}, Pb^{2+}, Al^{3+}, Cr^{3+}, Mn^{2+}, Mg^{2+}, Sn^{2+}, Cd^{2+}, Co^{2+} and Ni^{2+}. In the present fiber optic based studies, the dynamic working range has been determined as 1.0×10^{-6}–8.0×10^{-4} M Fe^{3+}. Offered dye may be an alternative to fluorescent Fe^{3+} indicators excited with UV Light. The sensor was fully reversible within the dynamic working range and the average response time (τ_{90}) is 30 sec. under flow conditions. The LOD for Fe^{3+} was found to be 6.0×10^{-7} M. At constant pH (pH=6.0), the response is reproducible. The photostability and chemical stability in the polymer matrix (at least 3 months) was satisfactory.

CHAPTER SEVEN

OXYGEN SENSING PROPERTIES OF TRIS(BIPYRIDINE)RUTHENIUM(II) DOPED IN SOL-GEL MATRIX TOGETHER WITH IONIC LIQUIDS

7.1 The sol-gel process (Lobnik, 1998)

The sol-gel process allows the preparation of glass films where indicator chemistry can be incorporated. The production of ceramic materials and glassy networks is based on the polymerisation of suitable precursors at low temperature. The increasing popularity of sol-gels in sensor applications results from the processing versatility. There are a number of variables which effect the hydrolysis and condensation rates and hence the microstructure of the sol-gel glass. The detailed microstructure of sol-gel glasses depends on parameters such as nature and concentration of the catalyst, water/sol-gel precursor ratio (R) and precursor type, nature of the solvent, ageing time, ageing temperature, drying time and drying temperature. The process can be adapted for formation of thin sensor layers. At the sol stage, thin glass films can be formed by dip-coating or spin-coating. These films are porous and are used for sensor applications.

Components of the sol-gel cocktail are the sol-gel precursor, water, a catalyst, the indicator and a solvent such as ethanol. The sol-gel precursors are mostly low molecular weight alkoxysilanes such as tetramethoxysilanes (TMOS) and tetraethoxysilanes (TEOS) which are not miscible with water. Mixing these components causes hydrolysis of the ester, silanol-ester condensation, and silanol-silanol condensation of the precursors. In this process, the alkoxy groups hydrolyze and the hydroxy groups condense.

This general reaction scheme can be seen in equations 7.1, 7.2 and 7.3.

$$Si(OR)_4 + H_2O \rightarrow Si(OR)_3OH + ROH \quad \text{(hydrolysis)} \quad (7.1)$$

$$Si(OR)_3OH + Si(OR)_4 \rightarrow Si(OR)_3\text{ -O- }Si(OR)_3 + ROH \quad \text{(condensation)} \quad (7.2)$$

$$R\text{-}Si\text{-}OH + HO\text{-}Si\text{-}R \rightarrow R\text{-}Si\text{-}O\text{-}Si\text{-}R + H_2O \quad \text{(condensation)} \quad (7.3)$$

7.1.1 Hydrolysis and condensation reactions

The hydrolysis reaction (Eq. 7.1), through the addition of water, replaces alkoxide groups (-OR) with hydroxyl groups (-OH). Subsequent condensation reactions (Eqs. 7.2 and 7.3) involving the silanol groups (Si-OH) produce siloxane bonds (Si-O-Si) plus the by-products water or alcohol. Under most conditions, condensation begins before hydrolysis is complete. However, conditions such as, pH, H_2O/Si molar ratio (R), and catalyst can force completion of hydrolysis before condensation begins (Keefer, 1990). Additionally, because water and alkoxides are immiscible, a mutual solvent such as an alcohol is utilized. With the presence of this homogenizing agent, alcohol, hydrolysis is facilitated due to the miscibility of the alkoxide and water (Prassas & Hench, 1984).

The first phase in the process is the formation of the “sol”. A sol is a colloidal suspension of solid particles in a liquid. Colloids are solid particles with diameters of 1-100 nm. As the number of siloxane bonds increases, the individual molecules are bridged and jointly aggregate in the sol. After a certain period, the colloidal particles and condensed silica species link to form a “gel” - an interconnected, rigid network with pores of submicrometer dimensions and polymeric chains whose average length is greater than micrometer. After the sol-gel transition, the solvent phase is removed from the interconnected pore network. If removed by conventional drying such as

evaporation, so-called “xerogels” are obtained, if removed via supercritical evacuation; the product is an “aerogel” (Figure 7.1).

“Ageing” is the process that takes place after mixing precursor, water, solvent and catalyst to form a sol, but before coating, in the case of coating sols. Ageing or pre-polymerisation of the sol causes aggregation due to hydrolysis and condensation reactions, and consequently an increase in viscosity. During this step, the sol is allowed to stand either at room temperature or at a higher temperature for a period of time during which hydrolysis and condensation reactions cause aggregation and cross-linking.

The “gel point” is defined as the point at which the entire solid mass becomes interconnected. The physical characteristics of the gel network depend upon the size of particles and extent of cross-linking prior to gelation.

Acid-catalysis leads to a more polymeric form of gel with linear chains as intermediates. Base-catalysis yields colloidal gels where gelation occurs by cross-linking of the colloidal particles.

Sol-gel glass is ion-permeable due to residual hydroxy groups and its porosity, and can be used to optically measure pH by entrapping (caging) conventional pH indicator dyes in the material. Often, water soluble indicator dyes do not have to be chemically modified for immobilisation because due to their size they are retained in the pores of the sol-gel glass and do not wash out.

Ormosils (organically modified siloxanes) represent hybrid systems in which several precursor types such as organotrialkoxysilanes or diorganodialkoxysilane precursors ($R.Si(OR)_3$ or $R.2Si(OR)_2$, respectively) are combined in which R. represents a non-hydrolyzable organic substituent (e.g. methyl or phenyl). The substituent R. can also be a reactive aminopropyl group which allows subsequent covalent binding of indicators. Ormosils are not as hydrophilic and brittle as conventional sol-gel glass. If the content of alkyl chains R. increases, then the

material turns hydrophobic and ion-impermeable. Nevertheless, due to its gas permeability, it can be used for sensing acidic or basic gases which permeate the material and react with indicator dyes (e.g. by protonation/deprotonation of pH indicators).

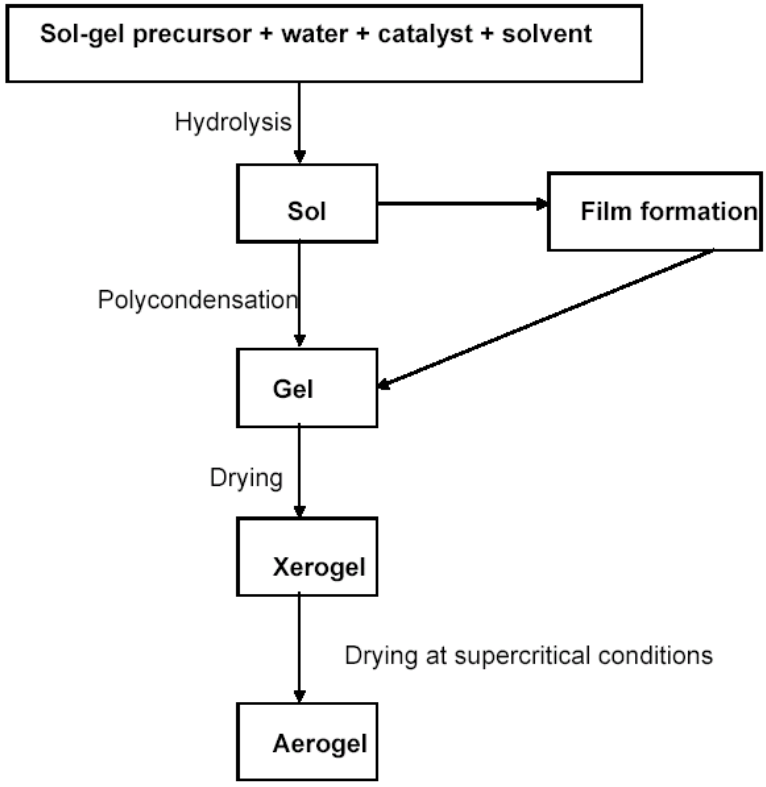

Figure 7.1 Sol gel process
(taken from http://www2.uni-jena.de/~c1moge/Mohr/ASCOS2002.pdf).

.

7.1.1.1 Hydrolysis

Although hydrolysis can occur without addition of an external catalyst, it is most rapid and complete when they are employed. Mineral acids (HCl) and ammonia are mostlly used, however, other catalysts are acetic acid, KOH, amines, KF, and HF (Brinker & Scherer, 1990).

With weaker bases such as, ammonium hydroxide and pyridine, measurable speeds of reaction were produced only if large concentrations were present. Therefore,

compared to acidic conditions, base hydrolysis kinetics is more strongly affected by the nature of the solvent (Aelion, Loebel & Eirich, 1950). Figure 7.2 shows the pH rate profile for hydrolysis reaction in aqueous solution.

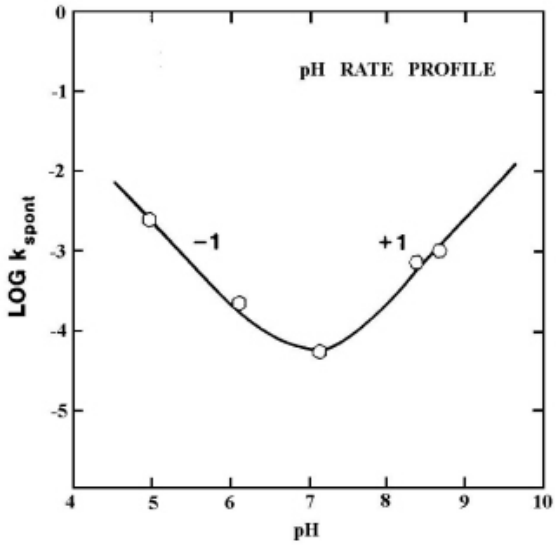

Figure 7.2 pH rate profile for hydrolysis in aqueous solution

(taken from http://www.psrc.usm.edu/mauritz/solgel.html).

Acid-Catalyzed Mechanism

Under acidic conditions, it is likely that an alkoxide group is protonated in a rapid first step. Electron density is withdrawn from the silicon atom, making it more electrophilic and thus more susceptible to attack from water. This results in the formation of a penta-coordinate transition state with significant SN2-type character (Brinker & Scherer, 1990). The transition state decays by displacement of an alcohol and inversion of the silicon tetrahedron, as seen in Figure 7.3.

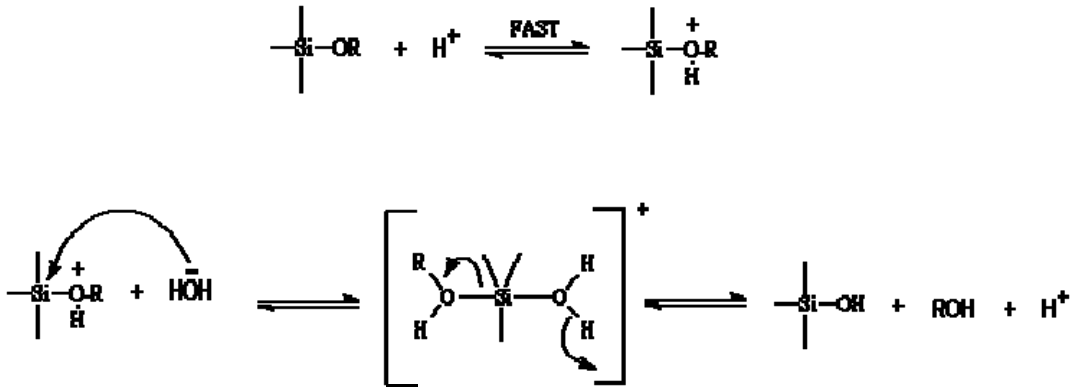

Figure 7.3 Acid-Catalyzed Hydrolysis (taken from http://www.psrc.usm.edu/mauritz/solgel.html)

H_2O/Si Molar Ratio (R)

From equation 7.1, an increased value of R is expected to promote the hydrolysis reaction. The most obvious effect of the increased value of R is the acceleration of the hydrolysis reaction. Additionally, higher values of R caused more complete hydrolysis of monomers before significant condensation occurs. Differing extents of monomer hydrolysis should affect the relative rates of the alcohol- or water-producing condensation reactions. Generally, with understoichiometric additions of water ($R << 2$), the alcohol producing-condensation mechanism is favored, whereas, the water-forming condensation reaction is favored when $R \geq 2$ (Assink & Kay, 1998).

Although increased values of R generally promote hydrolysis, when R is increased while maintaining a constant solvent:silicate ratio, the silicate concentration is reduced. This in turn reduces the hydrolysis and condensation rates, resulting in longer gel times. This effect is evident in Figure 7.4 which shows gel times for acid-catalyzed TEOS systems as a function of R and the initial alcohol: TEOS molar ratio (Klein, 1985). Finally, since water is the by-product of the condensation reaction (Eq. 7.3), large values of R promote siloxane bond hydrolysis (reverse of Eq. 7.3).

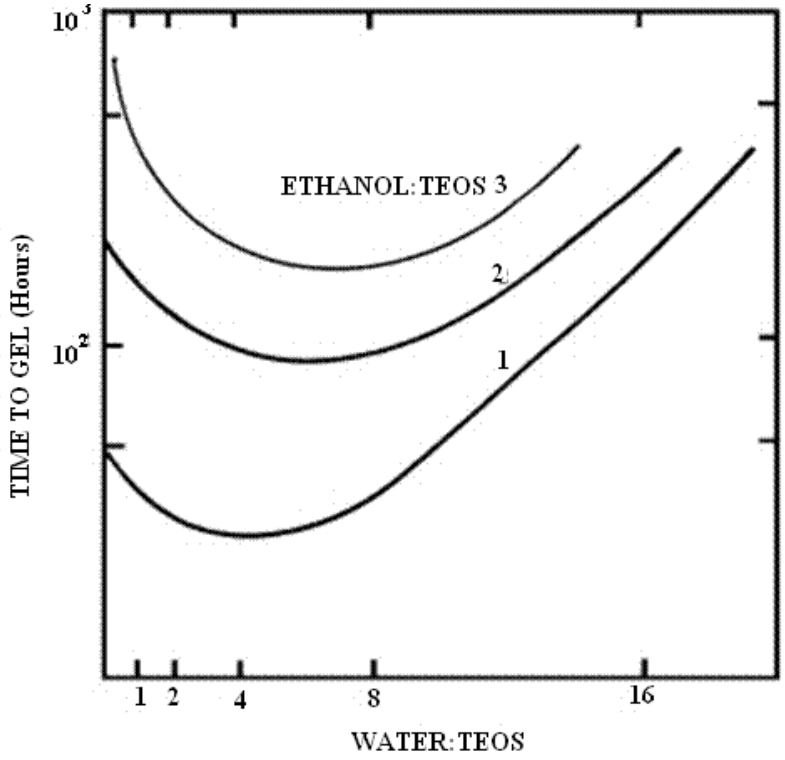

Figure 7.4 Gel times as a function of H_2O: TEOS ratio, R.

(taken from http://www.psrc.usm.edu/mauritz/solgel.html)

7.1.1.2 Condensation

Polymerization to form siloxane bonds occurs by either an alcohol-producing or a water-producing condensation reaction. It has been shown by Engelhardt, Altenburg, Hoebbel & Wieker (1977) that a typical sequence of condensation products is monomer, dimer, linear trimer, cyclic trimer, cyclic tetramer, and higher order rings.

As with hydrolysis, condensation can proceed without catalyst, however, their use in organosiloxanes is highly helpful. It has been shown that condensation reactions are acid and base specific (Pohl & Osterholtz, 1985). In addition, Iler (1979) has shown that under more basic conditions, gel times are observed to increase. Condensation reactions continue to proceed, however, gelation does not occur.

Acid-Catalyzed Mechanism

It is generally believed that the acid-catalyzed condensation mechanism involves a protonated silanol species. Protonation of the silanol makes the silicon more electrophilic and thus susceptible to nucleophilic attack. The most basic silanol species (silanols contained in monomers or weakly branched oligomers) are the most likely to be protonated. Therefore, condensation reactions may occur preferentially between neutral species and protonated silanols situated on monomers, end groups of chains, etc. (Brinker & Scherer, 1990).

7.2. Introduction

Optical oxygen sensors have many advantages such as zero oxygen destruction, no interference from exterior electromagnetic field and no need for a reference electrode (Choi & Xiao, 1999; Xu, McDonough, Langsdorf, Demas & DeGraff, 1994). Sol gel films are widely used as chemical optic sensor matrix materials because they have many advantages such as being chemically inert, optically transparent, photochemically and thermally stable and mechanically strong. However, some further investigations are still expected to improve the performances of O_2 sensing sol-gel films. For this purpose, there are some investigations icluding the modification of sol-gel membranes by changing the sensitive dye, parameters of sol-gel process (the sol-gel precursor type, the molar ratio of water:precursor (R), pH, catalyst type, catalyst concentration, ageing time, ageing temperature, drying time, drying temperature) or by the addition of some chemicals into the sol coctail. The $Ru(bpy)_3^{2+}$ complex was selected in this study as the photosensitizer dye because of its attractive characteristics such as strong visible absorption, high photochemical stability, relatively high luminescence and long lifetime of metal-to-ligand charge transfer (MLCT) excited states. Ding, Li, Zhang, Lei & Li (2006) improved optical sensor properties by modifying the molecular structure of Ru(II) complex with the addition of organically modified precursors (ORMOSILs). ORMOSILs are transparent, tolerate high temperatures, and are not biodegraded. They have found that the oxygen sensor based on Ru(II) complex modified by esterification demonstrated excellent linear calibration relationship and improved

long-term stability. ORMOSILs have been used as immobilisation matrix for many other optical sensors (Iwamoto and Mackenzie, 1995; Lev et al., 1995; Shahriari et al., 1997), including well-functioning oxygen microsensors (Klimant et al., 1999). There are also some studies including the change of entrappment of the dye into the sol-gel matrix. These studies are mostly for minimizing leaching of the fluorophore. Zhang, Li, Lei, Li & Lu, 2006 prepared sol–gel derived thin films containing covalently grafted $Ru(bpy)_3^{2+}$ fragments and detected dissolved oxygen with greatly improved anti-leaching and stability.

Furthermore, the oxygen permeability of the prepared sol-gel membranes is of major concern for the development of oxygen sensitive sol-gel films. There are also a few studies which investigated the effect of surfactants added into the sol-gel coctail to the porous structure and the O_2 sensing capability of the films. Garcia, Fernandez & Diaz-Garcia (2004) have studied the spectroscopic properties of $Ru(bpy)_3^{2+}$ doped in sol–gel matrices, both in the presence and absence of charged and non-charged surfactants, for dissolved oxygen in hexane. They have found increased response to hexane dissolved oxygen in sol–gel material in presence of surfactants as additives, due to favourable electrostatic interactions of surfactant counterions.

Matos, Fernandes, Guerreiro, Barata, Ramos et al. (2006) obtained different porous structure xerogels with the addition of different surfactants. They told that the addition of non-ionic surfactant does not influence the morphology and porous size distribution; in contrast, anionic and cationic surfactants have an important role on pore size distribution.

Boonamnuayvitaya, Tayamanon, Sae-ung & Tanthapanichakoon (2005) synthesized a porous media produced by a sol–gel method together with surfactants. They have obtained the highest surface area mesoporous silica material by using a cationic surfactant.

The above mentioned studies indicating the increase in the O_2 sensitivity with the addition of cationic and anionic surfactants into the sol-gel composition encouraged

us to improve O_2 sensing properties of classical acid catalysed sol-gel membranes by adding ionic liquids as ionic surfactants. ILs are constituted of cations/anions and are still in the liquid state at the ambient temperature. Besides, there are some studies for the usage of ionic liquids as surfactants mostly in aqueous media (Miskolczy, Sebök-Nagy, Biczok & Gokturk, 2004; Behera, Dahiya, & Pandey, 2006); Vanyur, Biczok & Miskolczy, 2006; Fernandez, Held, Willing & Breuer, 2004). To our knowlege, there are no studies including the effect of ionic liquids to the O_2 sensitivity of the sol-gel derived membranes.

7.3 Experimental

The O_2 sensitive fluorescent dye, tris (2, 2'-bipyridyl) ruthenium (II) chloride ($Ru(bipy)_3^{2+}$) was supplied from Aldrich (99.5% purity). The commercial ionic liquid, 1-ethyl-3-methylimidazolium tetrafluoroborate (RTIL-III) was supplied from Fluka. The ionic liquid of 1-methyl-3-(triethoxysilanebutyl) imidazolium tetrafluoroborate (RTIL-IV) was supplied from Dr. H. Türkmen and was synthesized in the laboratories of University of Ege. The structures of the ionic liquids and the dye were given in Figure 7.5.

The sol–gel materials were prepared by modification of a reported method of Lobnik, 1998 and Mcevoy, Mcdonagh & Maccraith, 1997. The sols were prepared by the acid catalyst method from a solution containing TEOS, HCl-acidified water, ethanol, $Ru(bipy)_3^{2+}$ complex, Triton X-100 and or ionic liquid (RTIL-III or RTIL-IV). The ionic liquid amount, the acid amount and the R (mol ratios of water/TEOS) values were varied and the effect to the oxygen sensitivity was examined. The compositions of the sols and the gelation times were given in Table 7.1. The molar ratios of TEOS, ethanol and water were either 1:1:4 (R=4) or 1:1:2 (R=2). Firstly, TEOS and EtOH were added into a clean glass bottle and were stirred for 10 minutes. After, the HCl-acidified water and the Ru(II) complex dissolved in EtOH was added and the mixture was stirred continually to promote the hydrolysis and condensation reactions. Triton X-100 was added into the sol and the mixture was further stirred for 20 min. The concentration of Ru(II) complex was 10^{-3} M in the sol.

Triton X-100 was added in order to improve the homogeneity of the silica sol-gel and to give a crack-free monolith. The sol gel was also prepared by the addition of different ionic liquids with the same method. In all cases the solutions were aged at room temperature in open glass vials. Glass slides were used as solid support onto which the sol-gel was cast by manual dip-coating technique. Prior to casting, the glass surface was activated by treatment with concentrated HNO_3 for 24 h, washed with distilled water, and then ethanol. After the coating, the slides were left to dry at room temperature or at 70 ^oC for at least 18 hours before any measurement. By that way, the condensation reactions and the sol-gel formation was expected to be completely finished. Finally, optically transparent thin films were obtained and the adhesion of the ionic liquids to the sol was found to be excellent.

For the gas phase measurements, oxygen (99.9%) and nitrogen (99.99%) were mixed at different concentrations by the Sonimix 7000A gas mixing system (See Section 2.3) and passed directly to the sealed beaker. 1 min. was waited between changes in the N_2/O_2 concentration to ensure that a new equilibrium point had been established. Constant luminescence intensity was the evident of the equilibrium. The O_2 concentrations were accurate to 0.1%.

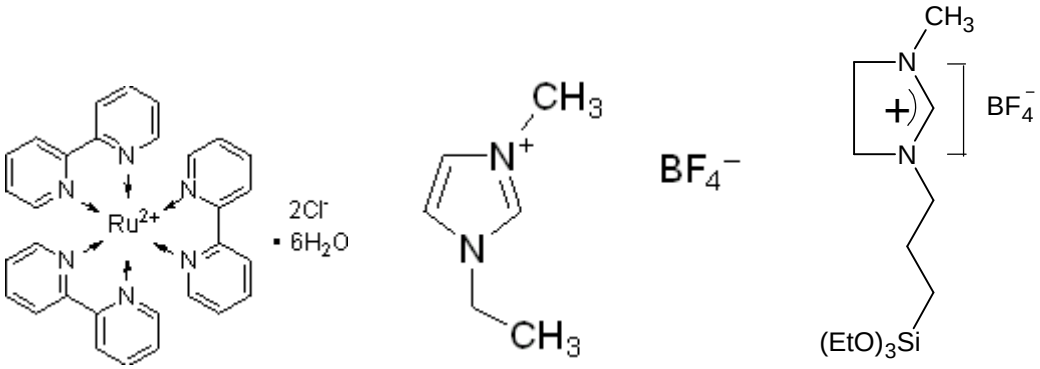

$Ru(bipy)_3^{2+}$ RTIL-III RTIL-IV

Figure 7.5 Structure of the ruthenium dye and the ionic liquids.

Table 7.1 Compositions of the cocktails used as O_2-sensing agents

Cocktail name	TEOS (mL)	EtOH (mL)	Acidified water (μL)	Triton-X 100 (μL)	Ionic liquid	Gelation time (min.)	Cocktail pH
sol-1	1.07	1.07	386 [a]	120	-	20	<1.0
sol-2	1.07	1.07	386[a]	120	RTIL-III (40μL)	25	1.0
sol-3	1.07	1.07	386[a]	120	RTIL-III (120 μL)	30	2.0
sol-4	1.07	1.07	386[a]	120	RTIL-IV (120 μL)	40	<1.0
sol-5	1.07	1.07	386 [b]	120	-	120	5.0
sol-6	1.07	1.07	386[b]	120	RTIL-III (120 μL)	360	5.5
sol-7	1.07	1.07	386[b]	120	RTIL-III (200 μL)	420	6.0
sol-8	1.07	1.07	193[c]	120	-	90	4.0
sol-9	1.07	1.07	193[c]	120	RTIL-III (40μL)	90	4.0
sol-10	1.07	1.07	193[c]	120	RTIL-III (120 μL)	120	4.5
sol-11	1.07	1.07	193[c]	120	RTIL-III (200 μL)	180	5.0

[a] 386 refers to 338 μL water and 48 μL concentrated HCl (R=4)
[b] 386 refers to 338 μL water and 48 μL 0.1 M HCl (R=4)
[c] 193 refers to 193 μL 0.1 M HCl (R=2)

7.4 Results and discussion.

7.4.1 Absorption and emission spectra

The absorption, excitation, and corrected emission spectra of ruthenium complexes were recorded for different films prepared from the above mentioned cocktails. In order to obtain the excitation spectra, the Ruthenium complex was excited at its maximum emission wavelengths. Figure 7.6 shows the absorption spectra of $Ru(bipy)_3^{2+}$ in the employed sol-gel membranes (sol-1, sol-2, sol-3). The three absorption spectra show an intense band between 410-470 nm which can be assigned to the metal ligand charge transphere (MLCT) ($t_{2g}(Ru) \rightarrow \pi^*(L)$) transition, and a smaller band at 380 nm originated from metal centered (MC) d–d transition (Cook, Lewis, McAuliffe, Skarda, Thomson, Glasper & Robbins, 1984; Belser, Daul

& Zelewsky, 1981; Ferguson & Herren, 1983; Kober & Meyer, 1982). It is known from the literature that the MLCT band of $Ru(bipy)_3^{2+}$ gives an absorption maxium at 447 nm in water. In the case of immobilization in sol-1, it can be seen from the figure that the MLCT absorption band blue-shifts by 9 nm and gives a maxium at 438 nm. By the addition of 40, 120 and 200 μL of ionic liquid into the sol-gel coctail (sol-2, sol-3 and sol 11), the MLCT band blue-shifts and becomes at 434, 430 and 428 nm, respectively.

It is well established that solvent can play a key role in infuencing the absorption and emission spectra of ruthenium polypyridyl complexes (Hush & Reimers, 1998; Brunschwig, Cruetz & Sutin, 1998). The detailed photophysical study of $Ru(bipy)_3^{2+}$ has revealed that strongly electron donating solvents can both perturb the energy of the emitting 3MLCT state and the structure of the acceptor ligand and electron deficient groups can play a significant role in controlling the photophysical behaviour of ruthenium(II) polypyridyl complexes (Andrew et al., 2001). Figure 7.7 shows the absorption spectra of $Ru(bipy)_3^{2+}$ in sol-4 and the RTIL-IV solution in EtOH. As shown in figure, the absorption features of $Ru(bipy)_3^{2+}$ complex entrapped in sol-4 is significantly changed from that observed in ethanol, indicating that there is probably an interaction between the complex and the RTIL-IV in the energetically ground state. Ionic liquids are ionic salts containig the positive charged imidazolium group and the negative charged tetrafluoroborate anion. Because of this, they increase the polarity and the ionic strength of the media that they are dissolved in giving rise to some shifts in the absorption spectra of $Ru(bipy)_3^{2+}$. In the case of sol-4 (with RTIL-IV), this change is more significant because RTIL-IV gives an absorption spectrum covering a wide range between 300-500 nm. This range covers the absorption range of $Ru(bipy)_3^{2+}$ and causes the disappereance of ruthenium peak.

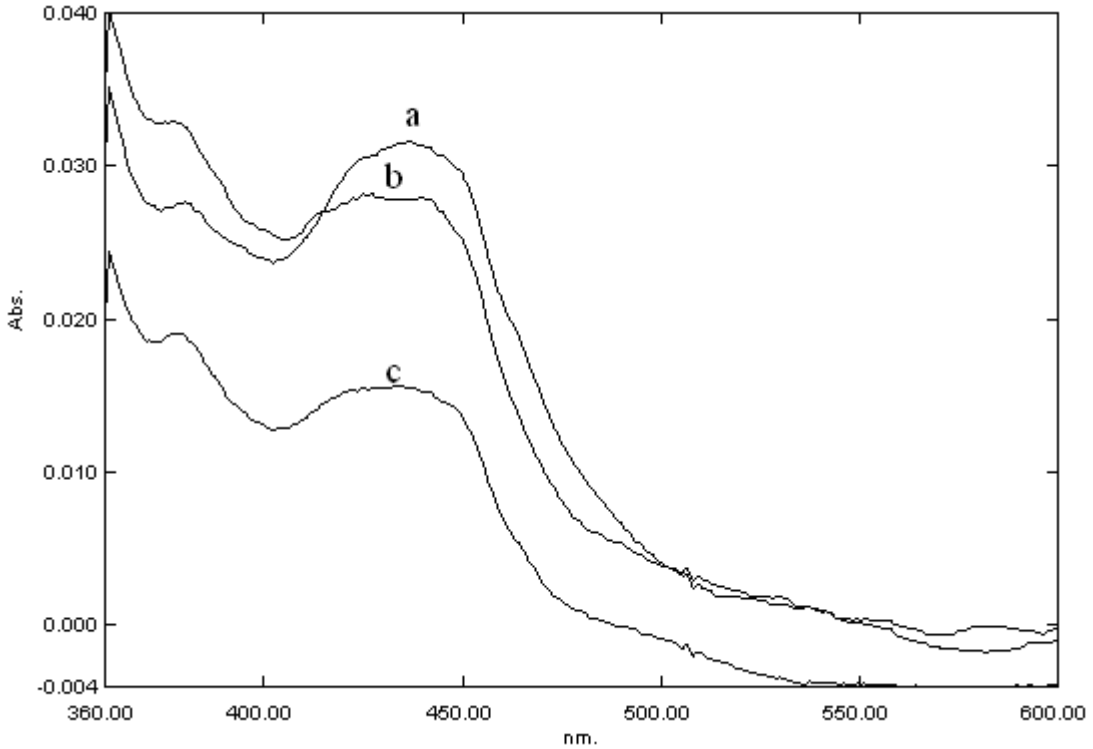

Fig 7.6 Absorption spectra of $Ru(bipy)_3^{2+}$ a) in sol-1 b) in sol-3 c) in sol-2.

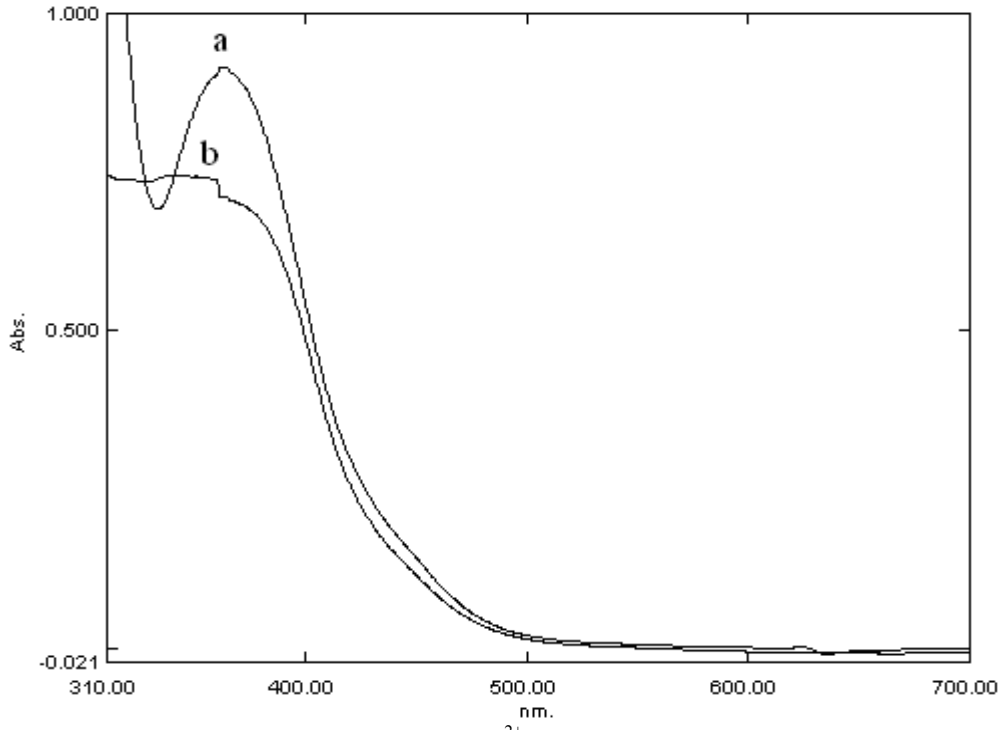

Fig 7.7 Absorption spectra of a) $Ru(bipy)_3^{2+}$ in sol-4 b) RTIL-4 in EtOH.

Figure 7.8 shows the fluorescence emission spectra of $Ru(bipy)_3^{2+}$complex immobilized in different sol-gel matrices. We can see from the figure that the emission spectra of $Ru(bipy)_3^{2+}$show a broad band ranging from 530 to 750 nm. The broadband fluorescence emission arises from ligand to metal charge transfer excited state. The maximum emission wavelength in aqueous solutions shows a blue shift of 17 nm from 607 to 590 nm when the complex is immobilized within the sol–1 derived thin film. This result is matching with the literature. Maruszewski, Jasiorski, Salamon & Strek (1999) say the band shifts from 608 nm in aqueous solution to 587 nm in bulk sol–gel silicates. Innocenzi, Kozuka & Yoko (1997) have also reported blue shift of the entrapped complex emission maximum for the doped thin films. The authors suggest that the luminescence maxima blue shifts are caused by 'rigidochromism' related to decreased rotational freedom of the entrapped molecules interacting with the solvent molecules filling the network of gel pores and or the network itself. In contrast by the addition of ionic liquid in the sol-gel matrix (sol-2, 40 uL RTIL-III), this blue shift is only 7 nms from 607 to 600 nms and with the increase in the amount of the ionic liquid (sol-3, 120 μL RTIL-III and sol 11, 200 μL RTIL-III), there is no blue shift. The maximum emission wavelength in sol-3 was identical with the one in aqueous solutions at 607 nm and in sol-11 was at 610 nm. However in the case of sol-4, the addition of RTIL-IV in the sol-gel matrix didn't change the maxium emission wavelength (590 nm, same with sol-1) but significantly decreased the fluoresence intensity of ruthenium complex. The decrease in the fluoresence intensity of $Ru(bipy)_3^{2+}$ also proves the above discussed energy transphere between the RTIL-IV and the ruthenium complex. The maximum emission and excitation wavelengths of the $Ru(bipy)_3^{2+}$ in different sol-gel matrices were given in Table 7.2. The Stocks shift values in the table were calculated from the spectral data and are 127, 135, 125, 145, 152, 132 and 152 nm for the Ru (II) complexes in water, sol-1, sol-2, sol-3, sol-4, sol-8 and sol-11, respectively. Large Stoke's shift is desirable for fluorescence and solid state component containing optical sensor studies because the high Stoke's shift values allow the emitted fluorescence photons to be easily distinguished from the excitation photons, leading to the possibility of very low background signals. The presence of RTIL-III caused an increase between 10-18 nm in the Stoke's shift of ruthenium complex.

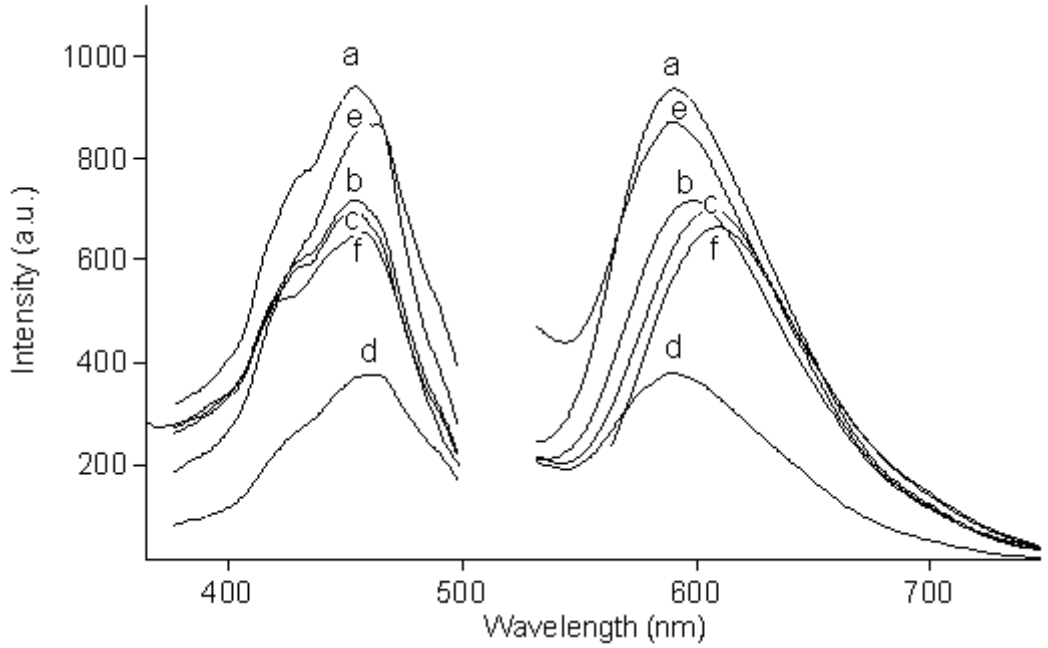

Figure 7.8 Excitation and corrected emission spectra of the $Ru(bipy)_3^{2+}$ dye a: in sol-1 (λ_{ex} =455, λ_{em} = 590nm), b: in sol-2 (λ_{ex} = 455, λ_{em} = 600 nm), c: in sol-3 (λ_{ex} = 455, λ_{em} = 606 nm), d: in sol-4 (λ_{ex} =465, λ_{em} = 590 nm), e: in sol-8 (λ_{ex} = 459, λ_{em} = 591 nm), f: in sol-11(λ_{ex} =458, λ_{em} = 610 nm)

Table 7.2 Absorption and emission related data of $Ru(bipy)_3^{2+}$ dye in different matrices.

Coctail name	$\lambda_{max\ (Abs.)}$, nm	$\lambda_{max\ (ex.)}$, nm	$\lambda_{max\ (em.)}$, nm	Stoke's shift
water	447	450	607	127
Sol-1	438	455	590	135
Sol-2	363	465	590	125
Sol-3	434	455	600	145
Sol-4	430	454	606	152
Sol-8	440	459	591	132
Sol-11	428	458	610	152

7.4.2 O_2 sensing studies

Immobiliziation methods in the sol-gel process include covalent binding, physical entrapment, electrostatic binding and adsorption. The covalent binding method offers the most effective entrapment and minimal leaching. However, the method is not as simple as the physical entrapment method and mostly used in applications in

which immobilization by covalent binding is obligatory to prevent the leach out of the dye especially in in-vivo biomedical sensing. In this study, physical entrapment method is used for the immobilization of dye in the sol-gel matrix. The preference of this method was its sufficient stability and reproducibility and simplicity. In this method, the ruthenium dye was added to the sol-gel coctail at the start of the process before coating. By that way, the network of the sol-gel grows around the dye molecules and encapsulates the dye molecules in cages of nanometers scale.

Oxygen as a triplet molecule is able to quench efficiently the fluorescence and phosphorescence of certain luminophores. Ruthenium complexes are from these complexes and collision of an oxygen molecule with the fluorophore in its excited state leads to a non-radiative transfer of energy. This effect is called "dynamic fluorescence quenching". The degree of fluorescence quenching relates to the frequency of collisions, and therefore to the concentration, pressure and temperature and the sensor matrix material.

In order to make accurate oxygen measurements, a calibration procedure is nesassary. The Linear (Stern-Volmer) algorithm requires at least two standards of known oxygen concentration.

The fluorescence intensity can be expressed in terms of the Stern-Volmer equation where the fluorescence is related quantitatively to the partial pressure of oxygen:

$$I_0/I = K_{SV}.pO_2 + 1 \qquad (7.4)$$

I_0 is the intensity of fluorescence at zero pressure of oxygen, I is the intensity of fluorescence at a pressure p of oxygen, *Ksv* is the Stern-Volmer constant

For a given media, and at a constant total pressure and temperature, the partial pressure of oxygen is proportional to oxygen mole fraction.

The *Stern-Volmer constant (Ksv)* is primarily dependent on the chemical composition of the ruthenium complex. However, the *Stern-Volmer constant* does

vary among probes, and it is temperature dependent. All measurements should be made at the same temperature as the calibration experiments or temperature monitoring devices should be used. In this study, all of the experiments were done at room temperature of 25 ± 1 ^{o}C. The oxygen sensitivity is proportional to Ksv, which in turn, is proportional to the oxygen permeability and diffusion coefficient of the sol gel film. The diffusion eficiency of oxygen is related to the microstucture of the sol-gel membrane whereas the microstructure of the porous sol-gel glass is dependent to molar water: silisium ratio (R), pH, precursor type, nature of catalyst, aging time, aging temperature, drying time and drying temperature. In this study, the precursor used was TEOS, the R value was 2 or 4, and the process was acid catalysed with the mineral acid of HCl. The aging time was dependent to the cocktail composition and between 20-420 minutes at room temperature and the films were left to dry for 18 hours either at room temperature or at 70 ^{o}C in an oven before the gas phase measurements. The R value is usually preferred as 4 than 2 in order to prevent the leaching of the dye especially for dissolved oxygen studies. In our case, we concentrated on the gas phase studies and executed the experiments both with the cocktails at R=4 and R=2 value. In this study, Triton X-100 was used alone or together with ionic liquids as surfactants in the preparation of the sol-gel glasses in order to reduce the risk of fracture and increase the sensor sensitivity. Room-temperature ionic liquids are promising nonvolatile, nonflammable, environmentally friendly alternatives to conventional organic solvents and are known as green solvents (Wasserscheid & Keim, 2000). Despite their widespread applications in chemical synthesis, homogeneous catalysis, electrochemistry and separation techniques, it was also shown that they could be either used to modify in a controlled fashion the properties of the conventional micelles or just themselves as miscelles. (Wasserscheid & Welton, 2003; Welton, 2004; Vanyur, Biczok & Miskolczy, 2007). Also surfactant behavior and possibility of surfactant self-assembly within ILs have been invested by many research groups (Matos et al., 2006). The usage of surfactants in the sol-gel process reduces the interfacial energy and thereby decreases the capillary stress. Another opportunity of addition of ionic liquids into the sol-gel glass is their coimmobilization with enzyme in silica can increase the activity and

stability of enzyme and can develop further studies on biochemical sensors with sol-gel glasses together with ionic liquids.

7.4.2.1 O_2 sensing studies with cocktails of R=2

The sol-gel glasses from sol-8 were prepared in different ways in order to optimize the drying time, aging time and aging temperature. The spectra of oxygen response of the sol-gel glasses prepared from cocktails of sol-8a, b and c (R=2) are shown in Figures 9, 10 and 11, respectively. The aging time was 90 min., drying temperature was 70 ^{o}C and the drying time was 18 hours for sol-8 a. The aging time differs for sol-8 b and was 60 min and the drying temperature differs for sol-8 c and was 25 ^{o}C. It can be seen from the figures that the increase of the aging time and the drying temperature increases the O_2 sensitivity.

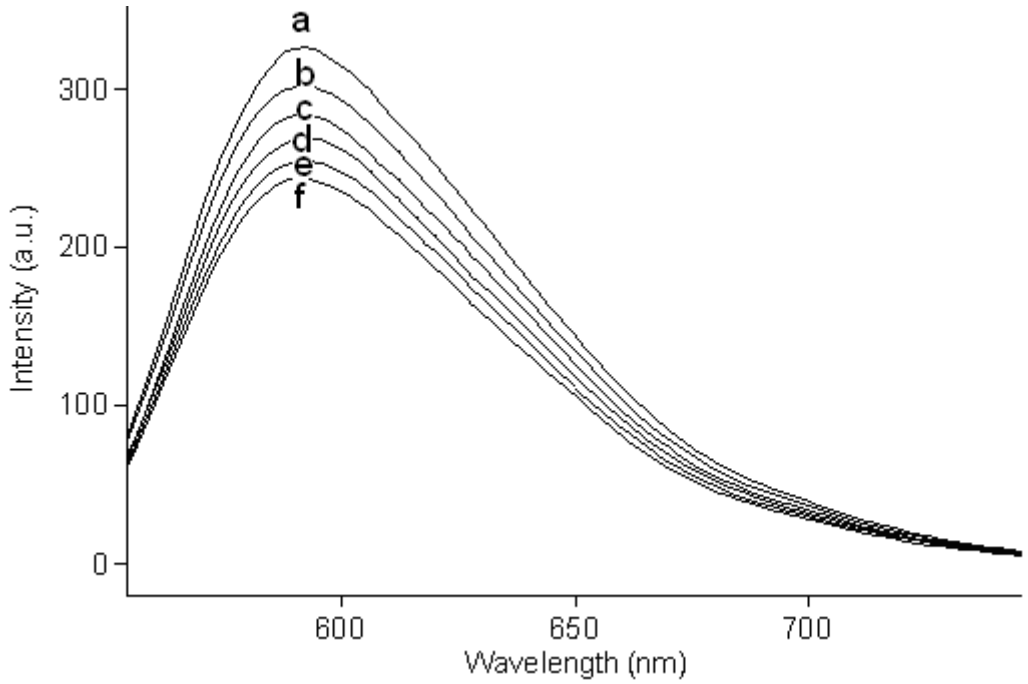

Figure 7.9 Response of sol-8 a to O_2 (g) (a) 0% O_2 (b) 20 % O_2 (c) 40 % O_2 (d) 60 % O_2 (e) 80 % O_2 (f) 100 % O_2 (The aging time was 90 min., drying temperature was 70 ^{o}C and the drying time was 18 hours)

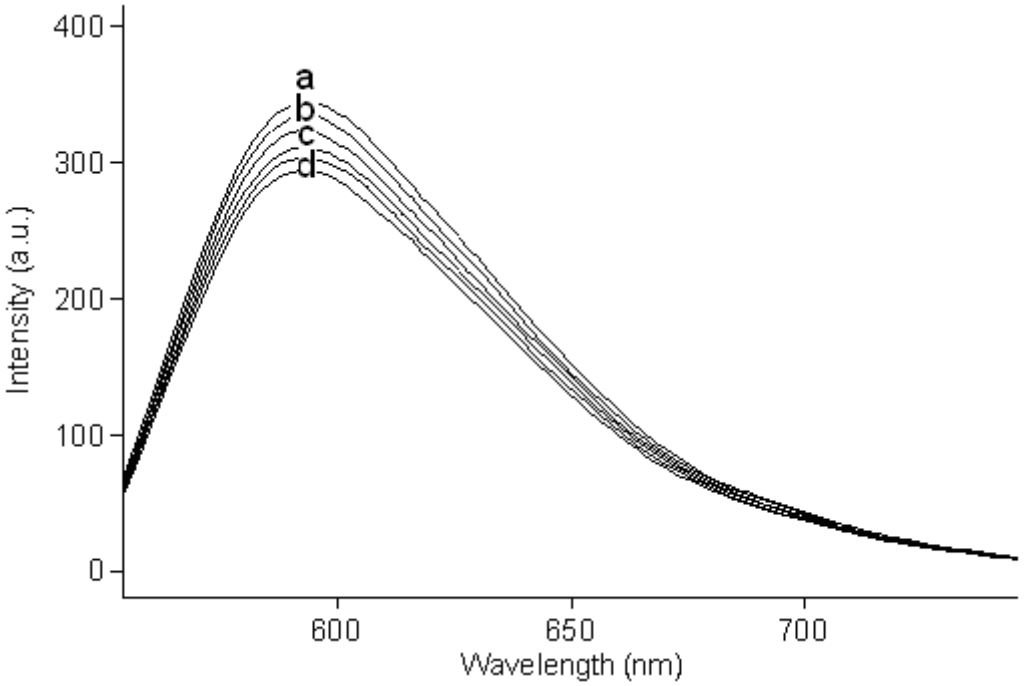

Figure 7.10 Response of sol-8 b to O_2 (g) (a) 0% O_2 (b) 20 % O_2 (c) 40 % O_2 (d) 60, 80, 100 % O_2 (The aging time was 60 min., drying temperature was 70 ^oC and the drying time was 18 hours)

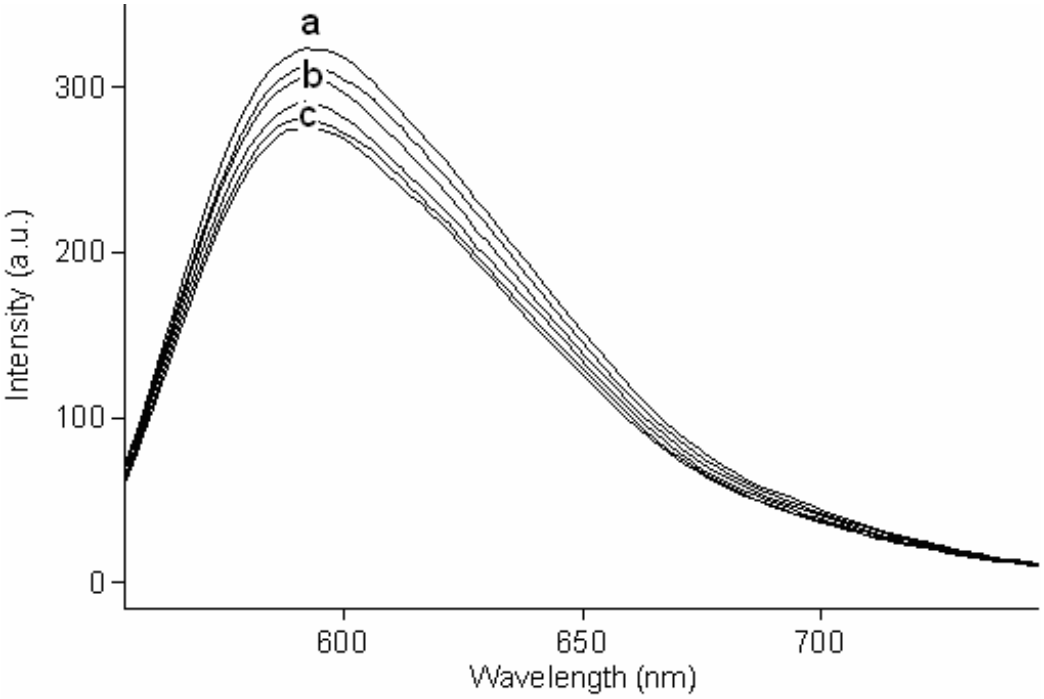

Figure 7.11 Response of sol-8 c to O_2 (g) (a) 0% O_2 (b) 20, 40 % O_2 (c) 60, 80, 100 % O_2 (The aging time was 60 min., drying temperature was 25 ^oC and the drying time was 18 hours)

The oxygen sensing properties of the sensing agent were characterised by I_0/I_{100} value and Stern-Volmer quenching constant. The I_0/I_{100} ratio was found to be 1.32, 1.18 and 1.17 for sol-8 a, sol-8 b and sol-8 c. The Stern Volmer plot is derived by using the Stern-Volmer equation (Eq. 7.4). The plots for sol-8 a, b and c exhibited considerable linearity at oxygen concentrations in the range of 0-100 % and can be described with the equations, y = 0.0032 x + 1; R^2 = 0.9984, y = 0.0019x + 1; R^2 = 0.9870 and y = 0.0018x + 1; R^2 = 0.9898, respectively (Figure 7.12). The error bars represent the standart deviation of the mean of 3 different measurements. The high linearity of the plot reveals that, only one type of quenching; dynamic quenching occurs throughout the gas measurements. The Stern-Volmer constant (K_{SV}) was found to be the highest and 0.0032 in the case of sol-8a and the further studies were carried out for the conditions in which drying temperature was 70 ^oC and the drying time was 18 hours. However, the aging time couldn't be taken as 90 min. for all cocktails because; the aging time varies with the cocktail composition.

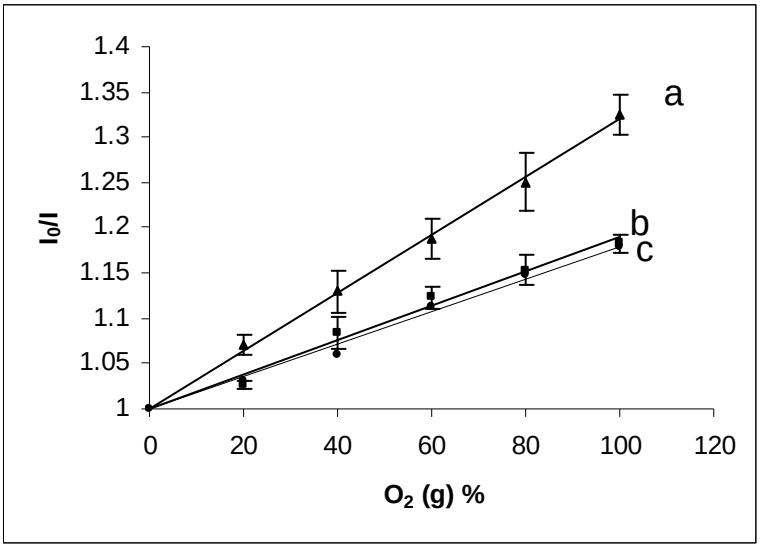

Figure 7.12 Stern Volmer Plot for sol-8 (a: aging time: 90 min., drying temperature: 70 ^oC; drying time: 18 hours) b: aging time: 60 min., drying temperature: 70 ^oC, drying time: 18 hours; c: aging time: 90 min., drying temperature: 25 ^oC, drying time: 18 hours)

By the addition of 40, 120 and 200 µL ionic liquid to sol-8, we obtain sol-9, sol-10 and sol-11, respectively. It can be concluded from the results that, addition of the ionic liquid into the sol-gel increased the O_2 sensitivity of the films (Figure 7.13-15). The relative signal change when exposed to 100 % of O_2 gas was increased from 25% (sol-8; no ionic liquid) to 41 % (sol-10; 120 µL ionic liquid). The Stern Volmer constants for sol-9, sol-10 and sol-11 were found to be 0.0027, 0.0072 and 0.0710 (Figure 7.16). When we added 200 µl ionic liquid (sol-11), the O_2 sensitivity didn't change any more, on the contrary the gelation time increased and the transparancey of the glass films decreased.

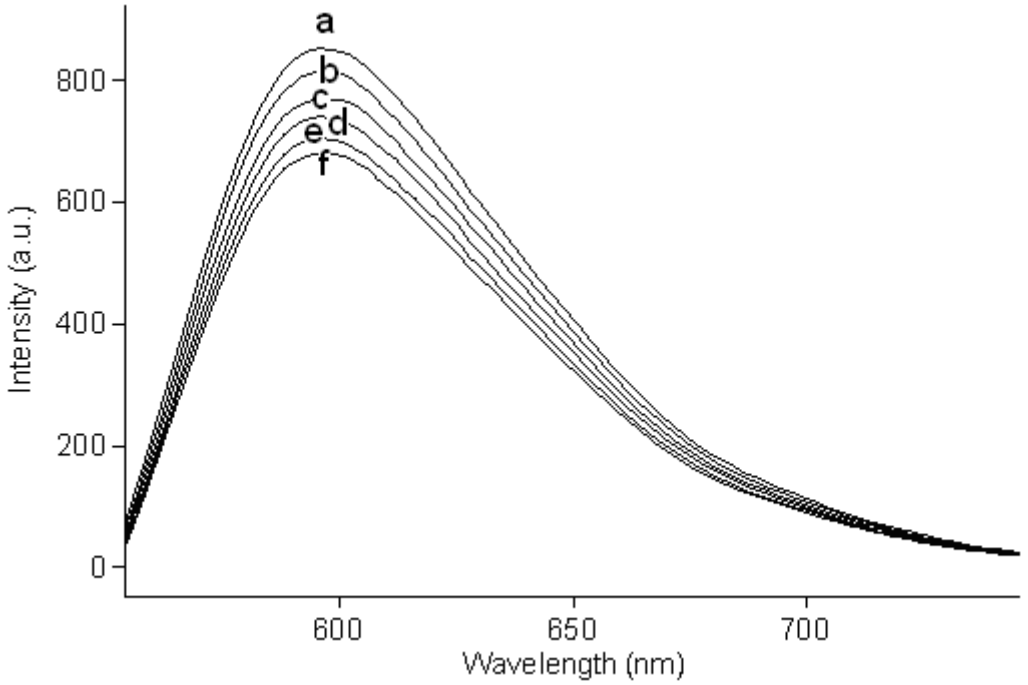

Figure 7.13 Response of sol-9 to O_2 (g) (a) 0% O_2 (b) 20 (c) 40% (d) 60% (e) 80% (f) 100 % O_2

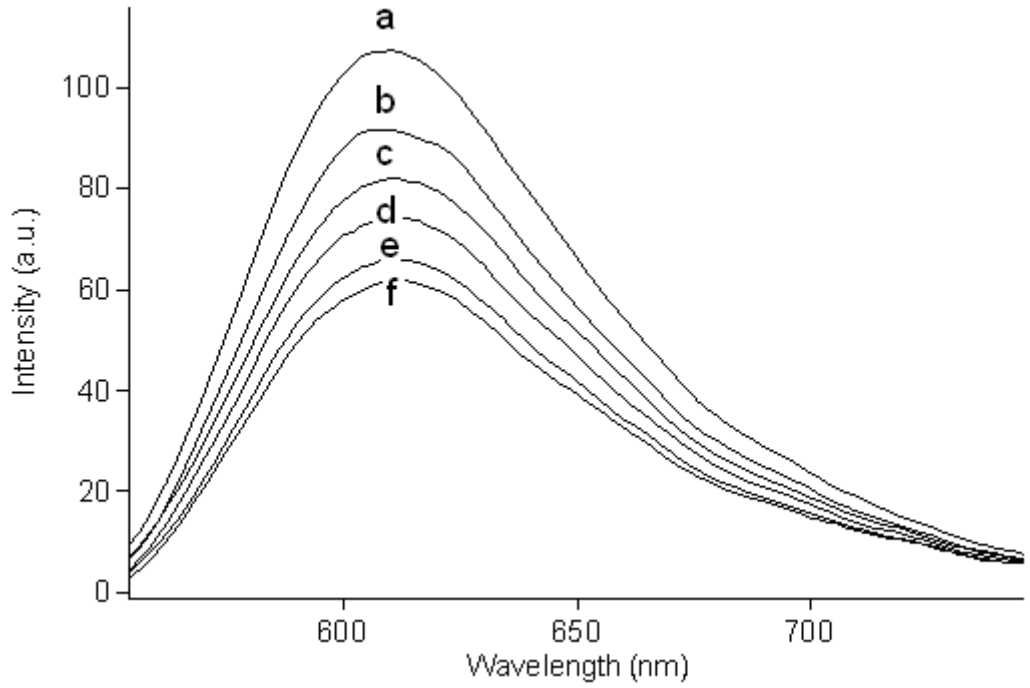

Figure 7.14 Response of sol-10 to O_2 (g) (a) 0% O_2 (b) 20 (c) 40% (d) 60% (e) 80% (f) 100 % O_2

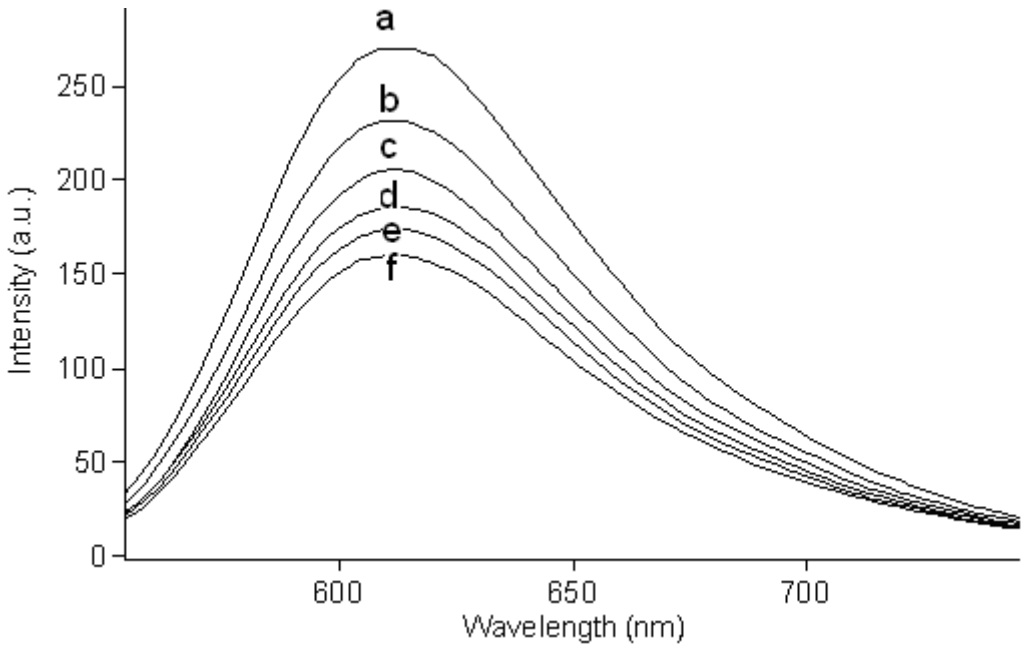

Figure 7.15 Response of sol-11 to O_2 (g) (a) 0% O_2 (b) 20 (c) 40% (d) 60% (e) 80% (f) 100 % O_2

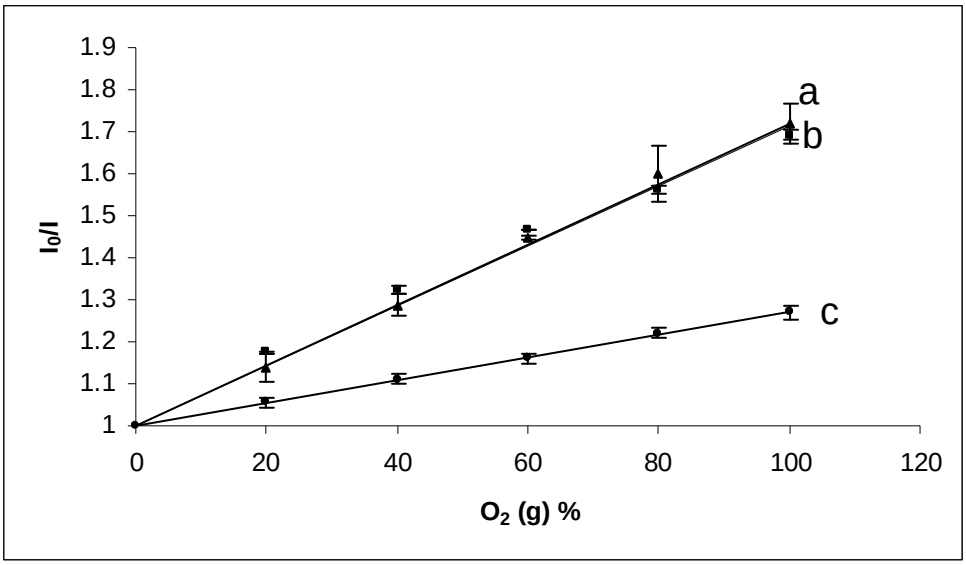

Figure 7.16 Stern Volmer Plot for (a) sol-10 (b) sol-11 and (c) sol-9

7.4.2.2 O_2 sensing studies with cocktails of R=4

Under similar aging conditions, when the R value is higher (e.g. R=4), the hydrolysis and condensation reactions are faster forming a denser more cross linked structures with smaller pores. These smaller pores entrap the dye molecules better and prevent the leaching. However, the oxygen sensitivity decreases because of the difficulty of gas diffusion into the small pores. The relative signal change when exposed to 100 % of O_2 gas can only be achieved at 10 % in the case of sol-1 (R=4). The relative signal change when exposed to 100 % of O_2 gas was achieved at 10%, 20%, 35% and 14% with the films prepared from sol-1, sol-2, sol-3 and sol-4, respectively (Figure 7.17-19). It can be concluded from the results that, addition of the ionic liquid into the sol-gel increases the O_2 sensitivity of the films and RTIL-III is more effective for increasing the sensitivity. The addition of 40 μL RTIL-III (sol-2) increased the relative signal change from 10% to 20 %. In the case of 120 μL (sol-3) ionic liquid, the relative signal change was 35%. The I_0/I_{100} ratio was found to be 1.48 for sol-3. The Stern Volmer plot for sol-3 exhibited considerable linearity at oxygen concentrations in the range of 0-100 % and can be described with the equation, y = 0.0047x + 1 and regression coefficient; R^2 = 0.9958 (Figure 7.20). The Stern-Volmer constant (K_{SV}) was found to be 0.0047.

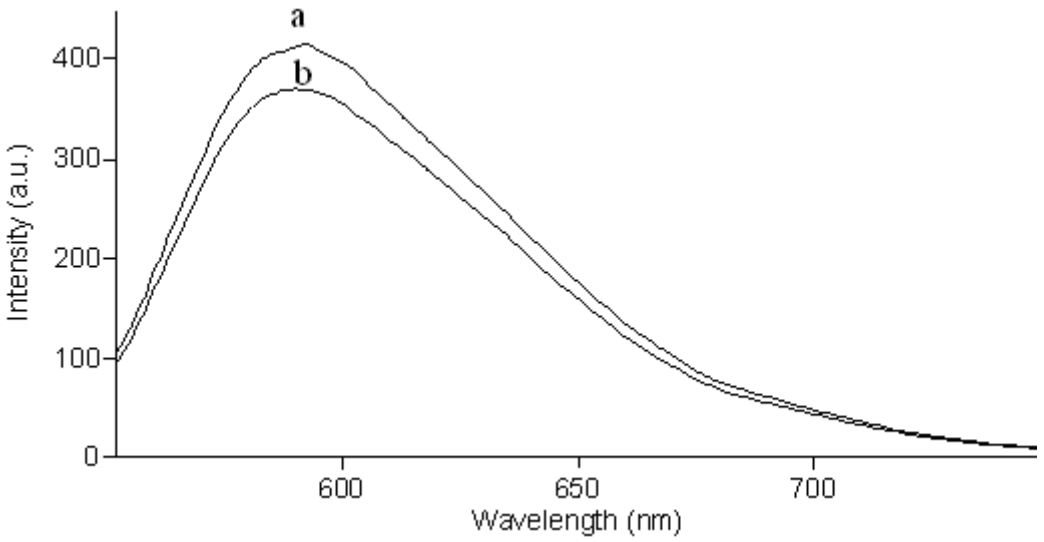

Figure 7.17 Response of sol-1 to O_2 (g) (a) 0% O_2 (b) 100 % O_2 (relative signal change is 10%)

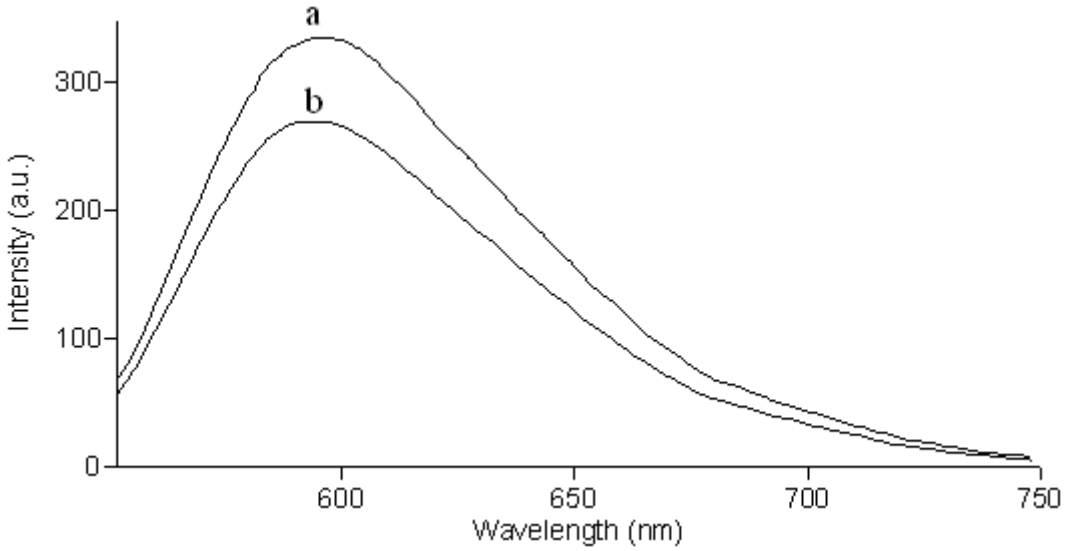

Figure 7.18 Response of sol-2 to O_2 (g) (a) 0% O_2 (b) 100 % O_2 (relative signal change is 20%)

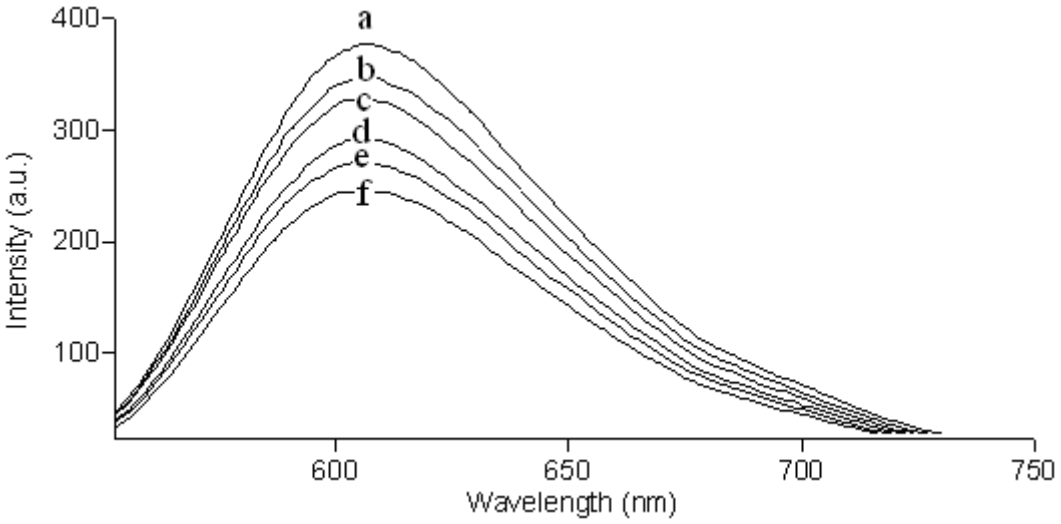

Figure 7.19 Response of sol-3 to O_2 (g) (a) 0% O_2 (b) 20 (c) 40% (d) 60% (e) 80% (f) 100 % O_2

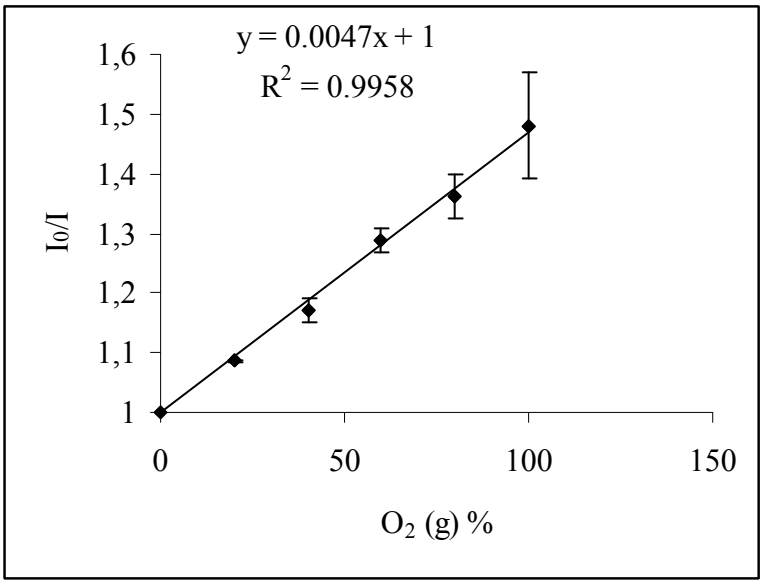

Figure 7.20 Stern Volmer Plot for sol-3

The cocktails were also prepared by using a lower amount of acid (sol-5, sol-6 and sol-7) in order to investigate the possible effect of acidity to the O_2 sensitivity. The relative signal change when exposed to 100 % of O_2 gas was achieved at 20%, 32% and 40% with the films prepared from sol-5, sol-6 and sol-7, respectively (Figure 7.16-18). We obtained the same result that; addition of the ionic liquid into the sol-

gel increased the O_2 sensitivity of the slides. The relative signal changes of sol-1 and 3 (the acid catalyser was added from concentrated HCl) were vey similar with the ones of sol-5 and 6 (the acid catalyser was added from 0.1 M HCl) indicating that the acid concentration does not influence very much the sensitivity of the films in both cases. However, from the data in Table 7.1, we see that by the addition of increasing amounts of ionic liquid, the gelation time changes at a significant rate. The addition of 200 μL ionic liquid increases the gelation time from 2 hours (sol-5) to 7 hours (sol-7). It is told by Iler (1979) that the rate and extent of the hydrolysis reaction is most influenced by the strength and concentration of the acid-or base catalyst. Also, Aelion et al. (1950) found that all strong acids behave similarly, whereas weaker acids require longer reaction times to achieve the same extent of reaction. By the addition of ionic liquid into the sol-gel cocktail, the acidity character of the cocktail was decreased and the pH changed from 5.0 to 6.0. As a result, the gelation time (aging time) increases. However, the sensitivity of the films didn't change in a significant rate because the solubility of silica is quite low below pH 2, formation and aggregation of primary silica particles occur together and growth of a network contributes little to growth after particles exceed 2 nm in diameter. Thus, developing gel networks are composed of exceedingly small primary particles which doesn't permit the gas diffusion so much (Brinker & Scherer, 1990). Between pH 2 and pH 6 condensation rates are proportional to [-OH] concentrations. Further growth occurs by addition of lower molecular weight species to more highly condensed species and aggregation of the condensed species to form chains and networks. The solubility of silica in this pH range is again low and particle growth stops when the particles reach 2-4 nm in diameter (Keefer, 1990). So, below pH 2.0 and between pH 2.0-6.0, the particle diameter of the sol-gel network was vey near and was between 2-4 nm and the diffusion of the gas can be obtained in a limited rate. The resulting pHs of the cocktails were in the range of pH=1-2 for sol-1-3 and pH=5.0-6.0 for sol-5-7. The Stern Volmer plot for sol-7 also exhibited considerable linearity at oxygen concentrations in the range of 0-100 % and can be described with the equation, $y = 0.0066x + 1$ and regression coefficient; $R^2 = 0.9962$. The Stern-Volmer constant (K_{SV}) was found to be 0.0066 (Figure 7.24).

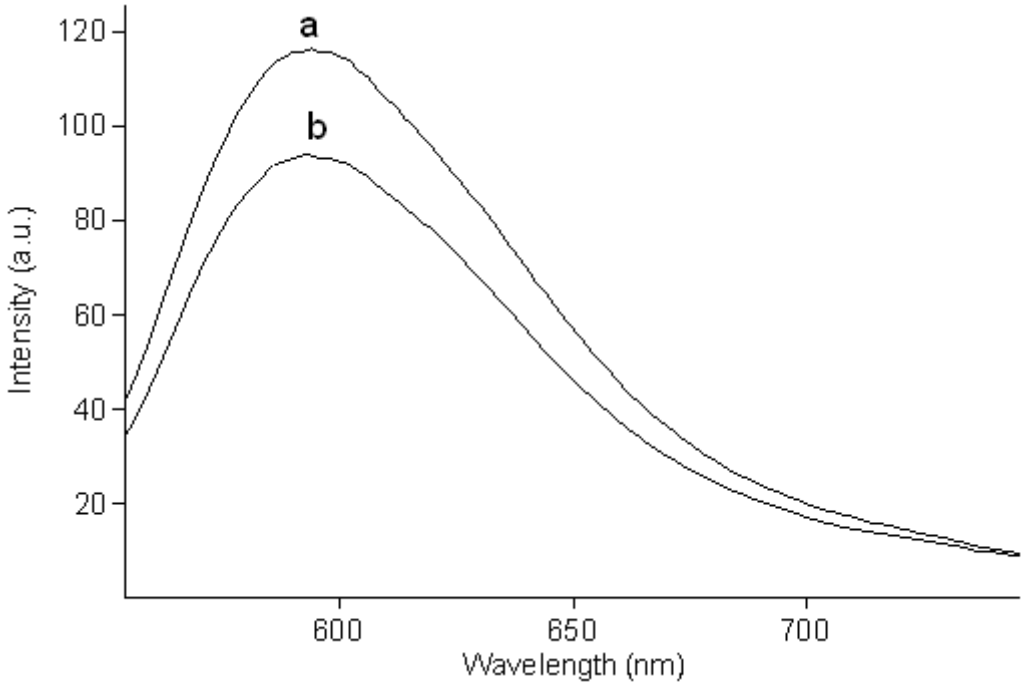

Figure 7.21 Response of sol-5 to O_2 (g) (a) 0% O_2 (b) 100 % O_2 (relative signal change is 20%)

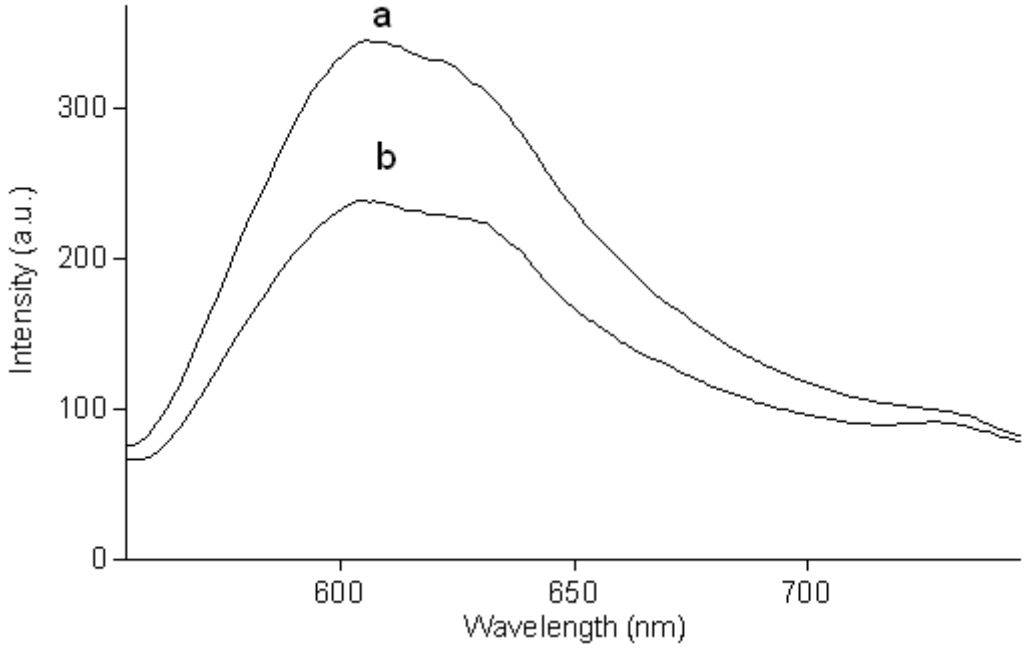

Figure 7.22 Response of sol-6 to O_2 (g) (a) 0% O_2 (b) 100 % O_2 (relative signal change is 32%)

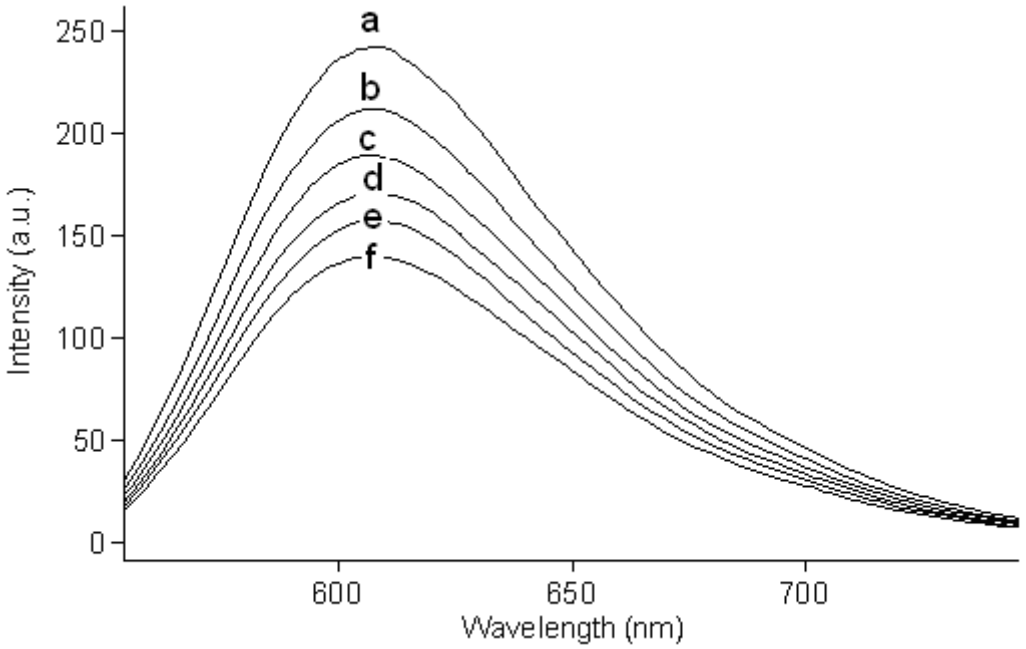

Figure 7.23 Response of sol-7 to O_2 (g) (a) 0% O_2 (b) 100 % O_2 (relative signal change is 42%)

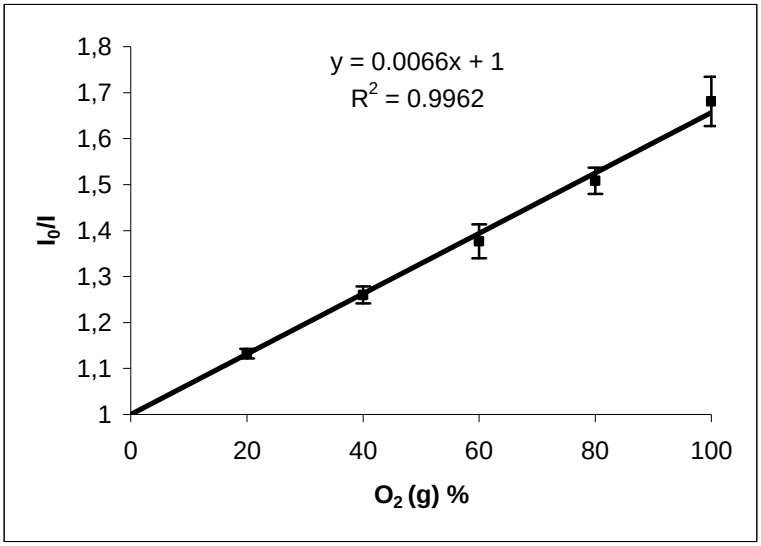

Figure 7.24 Stern Volmer Plot for sol-7

As a result, in all of the experiments either with R=2 or R=4 it was seen that the ionic liquid increased the O_2 sensitivity to some extent. Surfactants of different charge were used in the literature to investigate their effect on the oxygen sensitivity of the sol–gels (Garcia, Fernandez & Diaz-Garcia, 2004). They have found that in the case of the non-ionic surfactant Triton X-100, where electrostatic interactions are

absent, no improved response for oxygen was observed. When the charged surfactants (e.g. SDS and CTAB) were used, the relative signal changes increased. They have explained this increase with the favourable electrostatic interactions of the anionic surfactant, SDS counterions with the $Ru(bipy)_3^{2+}$ complex and that of the cationic surfactant, CTA^+ counter ions with the silicon atom which holds higher electron density than those of tetralkoxysilanes due to inductive effects (Schuber & Husing, 2000). These electrostatic interactions can reduce repulsive forces, stabilize the transition state during the sol–gel process and allow the network to become less open. The addition of charged surfactants, SDS, CTAB or ionic liquids during the sol–gel preparation allows the sol–gel particles to approach each other without large electrostatic barriers. This may enhance the rate of condensation (the rate-determining step in acid media) which results in a denser and porous sol–gel structure. A key parameter that influences oxygen sensitivity is therefore, the film porosity. Generally, an increase in the film porosity is indicative of a higher diffusion coefficient of the O_2 gas into the matrix and explains the higher O_2 sensitivity when the ionic liquids are added into the sol.

It is said before that, the porosity and the O_2 sensitivity of the films could be improved by the application of many modifications including the (R), pH, precursor type, nature of catalyst, aging time, aging temperature, drying time and drying temperature. By the addition of ionic liquids into the media we can control all of these parameters except one which is the last pH of the sol. Besides, the charged surfactant character of the ionic liquids, they have acid-base characteristics. The acidity properties of an ionic liquid are esentially determined by the nature of its anion. The RTIL-III has an anionic BF_4^- in its structure which is a neutral anion. It should be also noted that the cation of the ionic liquid has also an effect on the acidity character of the ionic liquid. For RTIL-III, the cationic part is the imidazolium cation which has a weak Lewis acidity character (Wassercheid & Kleim, 2000). Due to that, the pH of the RTIL-III was 5 which was slightly acidic. In the construction of sol-gel films, we have used the acid-catalysed method and added acidified water (pH<1) into TEOS/EtOH solution. In the sol-gel coctails which didn't contain any ionic liquid, the last pH of the sol was lower and consequently resulted

in weakly branched structures with small pores and a lessened O_2 sensitivity. In the case of sol-gel cocktails which contained ionic liquid; RTIL-III; the last pH of the sol was higher than the one without ionic liquid. The higher pH results with larger pores and higher O_2 sensitivity which is matching with our results.

7.4.3 Response and regeneration

Figure 7.25 and 7.26 illustrates the response characteristics of the RTIL-III containing sol-3 and sol-10 in an alternating atmosphere of O_2. Response time is defined as the time taken to attain 90 % of its original signal intensity (τ_{90}) when the gas is changed. The response times for oxygen sensing of sol-3 (R=4) after exposure to 100 % and 0 % O_2 were quite fast and found to be 14 s. The recovery time was 25 s. In case of seven replicate measurements, standard deviation of upper signal level was found to be 805 ± 4. In case of sol-2 (R=2), the response time decreased and was 5 and 10 seconds after exposure to 100 % and 0 % O_2, respectively. After exposure to 100 % and 0 % O_2 by four replicate measurements, standard deviation of upper signal level was found to be 316 ± 4.

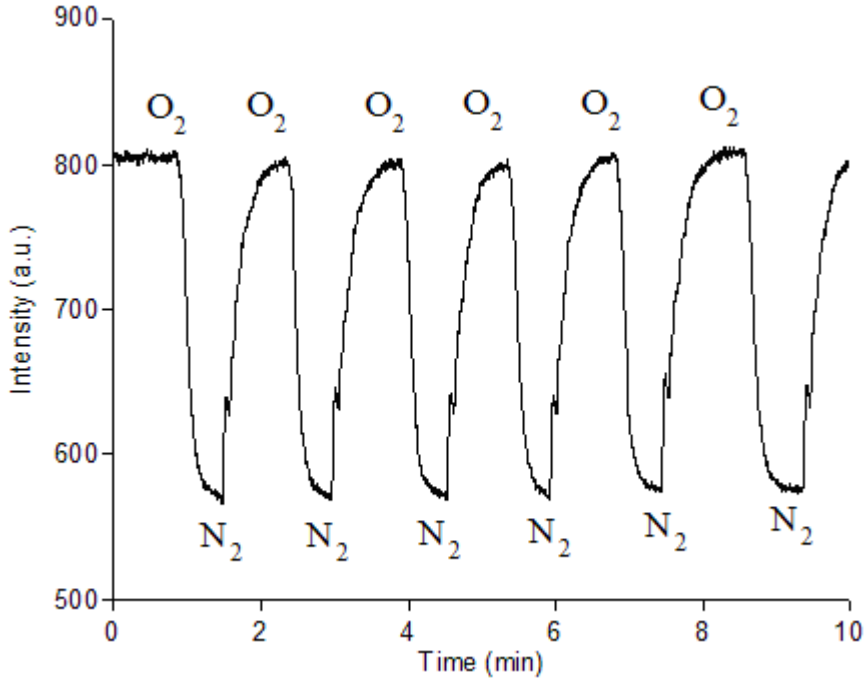

Figure 7.25 Response kinetics of sol-3.

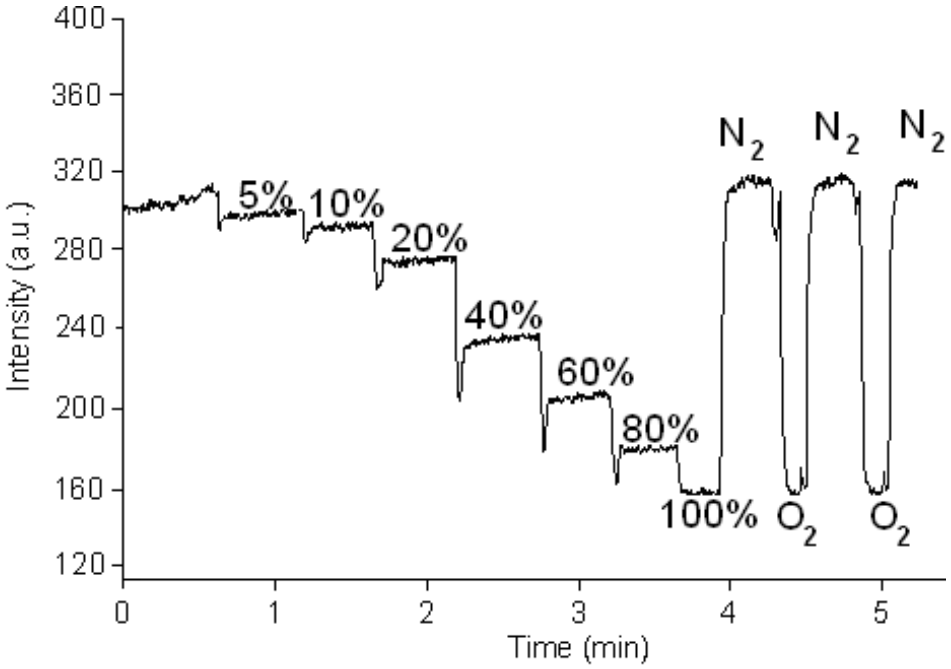

Figure 7.26 Response kinetics of sol-10.

7.5. Conclusion

The oxygen sensitive dye of tris (2, 2'-bipyridyl) ruthenium (II) chloride was characterised in conventional and ionic liquid modified sol-gel matrices. It has been found that the adition of RTIL-III has increased the O_2 sensitivity and created a more smooth, crackles surface structure.In case of sol-2 (R=2), the response time decreased and was 5 and 10 seconds after exposure to 100 % and 0 % O_2, respectively.

CHAPTER EIGHT
CONCLUSIONS

In the first part of this work (In Chapter 3 and 4), two newly developed RTIL-based carbon dioxide sensors were reported.

In Chapter 3, the characterization of a new optical CO_2 sensor based on the change in the fluorescence signal intensity of 8-hydroxypyrene-1,3,6-trisulfonic acid trisodium salt (HPTS) in green chemistry reagents—room temperature ionic liquids (RTILs) was described. This is the first time that RTILs, 1-methyl-3-butylimidazolium tetrafluoroborate (RTIL-I) and 1-methyl-3-butylimidazolium bromide (RTIL-II), have been used as matrix materials with HPTS in an optical CO_2 sensor. It should be noted that the solubility of CO_2 in water-miscible ionic liquids is approximately 10 to 20 times that in conventional solvents, polymer matrices, or water. The response of the sensor to gaseous and dissolved CO_2 has been evaluated. The luminescence intensity of HPTS at 519 and 521 nm decreased with the increasing concentrations of CO_2 by 90 and 75% in RTIL-I and RTIL-II, respectively. The response times of the sensing reagents were in the range 1–2 min for switching from nitrogen to CO_2, and 7–10 min for switching from CO_2 to nitrogen. The signal changes were fully reversible and no significant hysteresis was observed during the measurements. The stability of HPTS in RTILs was excellent and when stored in the ambient air of the laboratory there was no significant drift in signal intensity after 7 months.

In Chapter 4, a new optical CO_2 sensor based on the spectrophotometric signal changes of the bromothymol blue/tetraoctylammonium (BTB−/TOA+) ion pair in room temperature ionic liquids (RTILs) has been proposed. In the first stage of the study, determination of the acidity constant (p*K*a) of the modified BTB has been performed in the employed ionic liquids. In the second stage, response of the sensor composition to gaseous and dissolved CO_2 has been evaluated. The detection limits were 1.4 % for gaseous, and 10^{-6} M [HCO_3^-] for dissolved CO_2. The regenerated ionic liquid has been used for CO_2 sensing without any loss of efficiency.

In Chapter 5 and 6, two original Fe^{3+} sensor designs were proposed, respectively. The photoluminescent properties of Fe^{3+} selective organic fluoroionophores, bis(7-methoxybenzofuran-2-il)ketoxime (BFK) and N-(4-dimethylaminophenyl)-3,5-di-t-butyl salicylaldimine (DBS) were investigated in different solvents (dichloromethane, tetrahydrofuran, toluene and ethanol) and in polymer matrices of polyvinylchloride (PVC) and ethyl cellulose (EC) by using absorption and emission spectrometry. The response to Fe^{3+} ions was evaluated in terms of the effect of pH, ionic strength and cross sensitivity to other cations.

In Chapter 5, the selective determination of Fe^{3+} was accomplished by use of the newly synthesized DBS dye in plasticized PVC matrix. The fluorescent DBS dye can be offered as an optical Fe^{3+} sensor due to the visible excitation (410 nm) and emission wavelength (554 nm), high molar extinction coefficient (650755 cm^{-1} M^{-1}), large Stoke's shift (136 nm) and satisfactory quantum yield (0.0254) in immobilized form. The membranes are sensitive to pH as well, and the determination of Fe^{3+} was performed in buffered solutions at pH 5.0.

The DBS doped membrane exhibited a 77 % relative signal change in direction of decrease in fluorescence intensity when exposed to Fe^{3+} in the concentration range of 10^{-9}-10^{-4} M at pH 5.0. The detection limit was found to be 10^{-9} M for Fe^{3+}.

Response time (τ_{90}) changed between 3 and 8 min for 10^{-9} M and 10^{-4} M Fe^{3+}, respectively.

The membrane exhibited remarkable fluorescence intensity quenching on exposure to Fe^{3+} ions at pH=5.0 while the effects of the other responding ions (Cu^{2+}, $Sn2^{+}$ and Hg^{2+}) were less pronounced. The determination of two oxidation states of iron; Fe^{2+} and Fe^{3+} was also tested. However no significant separate spectral response for the ionic forms of Fe^{2+} and Fe^{3+} was observed.

The iron concentration–dependent spectral response of sensor membrane is affected by the ionic strength of the buffer solution. By making the ionic strength of

the buffer solution 135 mM with NaCl, the relative signal change of the emission spectrum of the sensor in contact with this solution decreased by around 50%.

In chapter 6, newly synthesized fluorescent benzofuran ketoxime (BFK) dye, have been used for selective and reversible Fe^{3+} sensing, in plasticized PVC matrix. In the employed solvents (DCM, EtOH, THF and toluene) the BFK was excited at 301, 303, 302, and 304 nm, respectively and the emission spectra were recorded. BFK dye exhibited promising spectral properties like quite high quantum yield in immobilized form (0.0155 in PVC and 0.0398 in EC),

The dye-doped membrane exhibited remarkable fluorescence intensity quenching upon exposure to Fe^{3+} ions at pH=6.0 while the effects of the Fe^{2+} and other responding ions (Cu^{2+}, Ca^{2+}, Hg^{+}, Pb^{2+}, Al^{3+}, Cr^{3+}, Mn^{2+}, Mg^{2+}, Sn^{2+}, Cd^{2+}, Co^{2+} and Ni^{2+}) were less pronounced.

In the present fiber optic based studies, the dynamic working range has been determined as 1.0×10^{-6} to 8.0×10^{-4} M Fe^{3+}. The membrane exhibited a 86% relative signal change in direction of decrease in fluorescence intensity (Figure 6.7). A quite good linear correlation was obtained with R^2 value of 0.9668 for Fe^{3+}. The LOD for Fe^{3+} was found to be 6.0×10^{-7} M. At constant pH (pH=6.0), the response is reproducible. The photostability and chemical stability in the polymer matrix (at least 3 months) was satisfactory.

The sensor average response time (τ_{90}) is 30 sec. under flow conditions. The sensor was fully reversible and only a slight drift (1.56 %) of the upper signal level has been observed after the 6th cycle. Between the 1st and 5th cycles, the level of reproducibility achieved was quite good with a RSD of 203.60 ±1.14% (Figure 6.11).

In the 7th Chapter, the oxygen sensitive dye of tris (2, 2'-bipyridyl) ruthenium (II) chloride was characterised in conventional and ionic liquid modified sol-gel matrices. It has been found that the adition of RTIL-III has increased the O_2 sensitivity and created a more smooth, crackles surface structure.

REFERENCES

Abbaspour, A., Mehrgardi, M. A., Noori, A., Kamyabi, M. A., Khalafi-Nezhad, A. & Soltani Rad, M. N. (2006). Speciation of iron(II), iron(III) and full-range pH monitoring using paptode: A simple colorimetric method as an appropriate alternative for optodes. *Sens. Actuators B,* 113 (2), 857-865.

Adrian, W., Mark, B. S. & Novartis, A. G. (2002). *Optical carbon dioxide sensors.* US Patent 6338822.

Aelion, R., Loebel, A. & Eirich, F. *J.* (1950). Hydrolysis of Ethyl Silicate. *Am. Chem. Soc*., 72, 5705-5712.

Aki, S. N. V. K., Mellein, B. R., Saurer, E. M. & Brennecke, J. F. (2004). High-Pressure Phase Behavior of Carbon Dioxide with Imidazolium-Based Ionic Liquids. *J. Phys. Chem. B.* 108 (52), 20355–20365.

Alderete, J. E., Olstein, A.D, Furlong, S. C. (1998). *Optical carbon dioxide sensor and associated methods of manufacture.* US Patent 5714121.

Anthony, J. L, Maginn, E. J., Brennecke, J. F. (2001). Solution thermodynamics of imidazolium-based ionic liquids and water. *J. Phys. Chem. B*, 105 (44), 10942–10949.

Anthony, J. L., Maginn, E. J. & Brennecke, J. F. (2002). Solubilities and thermodynamic properties of gases in the ionic liquid 1-*n*-Butyl-3-methylimidazolium hexafluorophosphate. *J. Phys. Chem. B,* 106 (29), 7315–7320.

Amao, Y. & Nakamura, N. (2004). Optical CO_2 sensor with the combination of colorimetric change of α-naphtholphthalein and internal reference fluorescent porphyrin dye**.** *Sensors and Actuators B*, 100 (3), 347-351.

Andrew, K.N. &, Worsfold, P.J. (1994). Comparison of multivariate calibration techniques for the quantification of model process streams using diode-array. *Analyst*, 119, 1541-1569.

Assink, R. A. & Kay, B. D. J. (1988). Sol-gel kinetics I. Functional group kinetics. *Non-Crystalline Solids*., 99 (2-3), 359-370.

Baker, S. N., Baker, G. A., & Bright, F. V. (2002) Temperature-dependent microscopic solvent properties of dry and wet 1-butyl-3-methylimidazolium hexafluorophosphate: correlation with ET(30) and Kamlet-Taft polarity scales. *Green Chem.* 4, 165–169.

Bakker, E. & Simon, W. (1992). Selectivity of ion-sensitive bulk optodes. *Anal. Chem.*, 64 (17), 1805-1812.

Baldini, F., Falai, A., De Gaudio, A. R., Landi, D., Lueger, A.; Mencaglia, A. et al. (2003). Continuous Monitoring of Gastric Carbon Dioxide with Optical Fibres. *Sensors and Actuators B*, B90 (1-3), 132-138.

Baltus, R. E., Culbertson, B.H., Dai, S., Luo, H., & DePaoli, D. W. (2004). Low - pressure solubility of carbon dioxide in room temperature ionic liquids measured with a quartz crystal microbalance. *J. Phys.Chem. B*., 108, 721-727.

Bates, E. D, Mayton, R. D., Ntai, I. & Davis, J. H. (2002). CO_2 capture by a task-specific ionic liquid. *J. Am. Chem. Soc.,* 124, 926-927.

Beer, P.D. (1998). Transition-Metal receptor Systems for the Selective Recognition and Sensing of Anionic Guest Species. *Acc. Chem. Res*. 31 (2) 71-80.

Behera, K., Dahiya, P. & Pandey, S. (2006). Effect of added ionic liquid on aqueous Triton X-100 micelles. *J. Colloid Interface Sci.* doi:10.1016/j.jcis.2006.11.009.

Belser, P., Daul, C. & Zelewsky, A. (1981). On the assignment of the MLCT transition in the $Ru(bpy)_3^{2+}$ complex ion. *Chem. Phys. Lett.* 79, 596–598.

Benniston, A. C., Mackie, P. R., Farrugia, L. J., Smith, G., Teat, S. J. & McLean, A. J. (2001). Detailed photophysical properties of a functionalized ruthenium(II) polypyridyl complex: through-space solvent effects. *New J. Chem*., 25, 458-464.

Blanchard, L. A., Hancu, D., Beckman, E. J., Brennecke, J. F. (1999). Green processing using ionic liquids and CO2. *Nature*, 399 (6731), 28–29.

Blanchard, L. A., Gu, Z. J. & Brennecke, F. (2001). High-pressure phase behaviour of ionic liquid/CO_2 systems. *J. Phys. Chem. B*, 105, 2437-2444.

Bonhote, P., Dias, A. P., Armand, M., Papageorgiou, N. & Gratzel, M. (1996). Hydrophobic, highly conductive ambient-temperature molten salts. *Inorg. Chem.,* 35, 1168-1178.

Boonamnuayvitayaa*,* V., Tayamanona, C., Sae-ungb, S., Tanthapanichakoonc, W. (2006). Synthesis and characterization of porous media produced by a sol–gel method. *Chemical Engineering Science,* 61, 1686 – 1691.

Brennecke, J. F. & Maginn, E. J. (2001), Ionic liquids: innovative fluids for chemical processing. *AICHE J.*, 47, 2384–2389.

Brinker, C. J. & Scherer, G.W. (1990). *Sol-Gel Science: The Physics and Chemistry of Sol-Gel Processing.* Academic Press: New York.

Brunschwig, B. S., Cruetz, C. & Sutin, N. (1998). Electroabsorption spectroscopy of charge transfer states of transition metal complexes. *Coord. Chem. Rev*., 177, 61-79.

Bültzingslöwen, C., McEvoy, A. K., McDonagh, C., MacCraith, B. D., Klimant, I., Krause, C. & Wolfbeis, O. S. (2002). Sol-Gel Based Optical Carbon Dioxide Sensor Employing Dual Luminophore Referencing for Application in Food Packaging Technology. *Analyst*, 127 (11), 1478-1483.

Buzzeo, M.C., Hardacre, C., & Compton, R. G. (2004). Use of room temperature ionic liquids in gas sensor design. *Anal. Chem.,* 76 (15), 4583-4588.

Cadena, C. Anthony, J. L., Shah, J. K., Morrow, T. I., Brennecke, J. F. & Maginn, E. J. (2004). Why is CO_2 so soluble in imidazolium based ionic liquids? *Am. Chem. Soc.,* 126, 5300-5308.

Camper, D., Scovazzo, P., Koval, C. & Noble, R. (2004). Gas solubilities in room temperature ionic liquids. *Ind. Eng. Chem. Res.,* 43, 3049-3054.

Cao, N. W., Shakin, C. M. & Sun, W. D. (1992). Quasiparticle properties of the quarks of the Nambu–Jona-Lasinio model**.** *Phys. Rev. C,* 46, 2535 – 2546.

Carmichael, A. J. & Seddon, K. R. (2000). Polarity study of some 1-alkyl-3-methylimidazolium ambient-temperature ionic liquids with the solvatochromic dye Nile red. *J. Phys. Org. Chem.,* 13, 591–595.

Choi, M.M.F. & Xiao, D. (1999). Linear calibration function of. luminescence quenching-based optical sensor for trace. Oxygen. *Analyst,* 124, 695-698.

Cook, M.J., Lewis, A.P., McAuliffe, G.S., Skarda, V., Thomson, A.J., Glasper, J.L. & Robbins, D.J. (1984). Luminescent metal complexes. Part 1. Tris-chelates of substituted 2,2-bipyridyls with ruthenium(II) as dyes for luminescent solar collectors, *J. Chem. Soc., Perkin Trans.* 2, 1293–1301.

Dhami, S., Mello A. J., Rumbles, G., Bishop, S. M., Phillips, D. & Beeby, A. (1995). Phthalocyanine fluorescence at high concentration: dimers or reabsorption effect? *Photochem. Photobiol.*, 61, 341.

Ding, J., Li, B., Zhang, H., Lei, B. & Li, W. (2006). Oxygen-sensing properties of ormosil hybrid materials doped with ruthenium(II) complexes via a sol–gel process *Mater. Lett.*, doi:10.1016/j.matlet.2006.11.106.

Draxler, S. Lippitsch, M.E. & Leiner, M. J. P. (1993) Optical pH Sensors Using Fluorescence Decaytime. *Sensors and Actuators B,* 11, 421.

Egami, C., Suzuki, Y., Sugihara, O., Fujimura, H. & Okamoto, N. (1997). Wide range pH fiber sensor with congored-and methylred-doped cladding. *Jpn. J. Appl. Phys.* 36, 2902-2905.

Engelhardt, V. Q., Altenburg, W., Hoebbel**,** D. & Wieker, W. (1977). Si-NMR spectroscopy of silicate solutions. IV. investigations on the condensation of monosilicic acid. *Anorg. Allg. Chem.*, 428 (1), 43-52.

Ensafi, A. A. & Aboutalebi, A. (2005). A versatile stable cobalt optical sensor based on pyrogallol red immobilization on cellulose acetate film. *Sensors & Actuators, Chemicals B*, 105 (2), 479-485.

Ensafi, A. A. & Bakhshi, M. (2003). New Stable Optical Film Sensor Based on Immobilization of 2-Amino-1-Cyclopentene-1-Dithiocarboxylic Acid on Acetyl Cellulose Membrane for Ni(II) Determination, *Sensors and Actuators B: Chemicals*, 96 (1-2), 435-440.

Ertekin, K., Klimant, I.,Neurauter, G. & Wolfbeis, O. S. (2003). Characterization of a Reservoir-Type Capillary Optical Microsensor for pCO2 Measurements. *Talanta*, 59 (2), 261-267.

Ferguson, J. & Herren. F. (1983). A model for the interpretation of the electronicspectra of the complex-ion $M(bpy)_3^{2+}$ (M = Fe, Ru, Os) in D3 and D2 sites. *Chem. Phys.* 76, 45–59.

Fernandez, A. M., Held, U., Willing, A. & Breuer, W. H. (2005). New green surfactants for emulsion polymerization. *Progress in Organic Coatings,* 53, 246–255.

Fuller, J., Carlin, R. T., Delong, H. C. & Haworth, D. (1994). The properties of ionic liquids. *Chem. Commun.,* 299-300.

Furlong, S. C. (1997). *Simultaneous dual excitation/single emission fluorescent sensing method for pH and pCO_2.* US Patent 5672515.

Galster, H. (1991). *pH Measurements: Fundamentals, Methods, Applications, Instrumentatio.* Weinhein,VCH: Germany.

Gankema, H., Lugtenberg, R.J.W., Engbersen, J.F.J., Reinhoudt, D. N, Moller, M. (1994). Cross-linkable polar siloxane copolymers for ion detection devices. *Advanced Materials,* 6 (12): 944-947.

Garcia, E. A., Fernandez, G. R. & Diaz-Garcia M.E. (2004). Tris(bipyridine)ruthenium(II) doped sol–gel materials for oxygen recognition in organic solvents. *Microporous and Mesoporous Materials*, 77, 235–239.

Göpel, W. & Schierbaum, K.D. (1995). SnO_2 sensors: Current status and future prospects. *Sensors and Actuators B,* 26, 1–12.

Göpel, W., Reinhardt, G. & Rösch, M. (2000). Trends in the development of solid state amperometric and potentiometric high temperature sensors. *Solid State Ionics*, 136-137 (2): *519-531.*

Grant, S. A. & Glass, R.S. (1997). Development of a fiber optic pH sensor to monitor stroke patients. *Sensors and Actuators B,* 45, 35-42.

He, X. & Rechnitz, G.A. (1995). Linear response function for fluorescence-based fiber-optic CO_2 sensors. *Anal. Chem.,* 67, 2264-2268.

Hisamoto, H., Miyashita, N., Watanabe, K., Nakagawa, E., Yamamoto, N. & Suzuki, K. (1995). Ion sensing film optodes: disposable ion sensing probes for the determination of Na^+, K^+, Ca^{2+} and Cl^- concentrations in serum. *Sens. Act. B*., 29 (1-3) 378-385.

Hisamoto, H., Nakagawa, E., Nagatsuka, K., Abe, Y., Sato, S., Siswanta, D., Suzuki, K. (1995). Silver Ion Selective Optodes Based on Novel Thia Ether Compounds. *Anal. Chem.* 67, 1315-1317.

Holbrey, J. D. & K. R. Seddon (1999). Ionic liquids, Review. *Clean Products and Processes ,* 223-236.

Hush, N. S. & Reimers, J. R. (1998). Solvent effects on metal to ligand charge transfer excitations. *Coord. Chem. Rev*., 177, 37-60.

Iler, R. K. (1979). *The Chemistry of Silica*., Wiley: New York.

Innocenzi, P., Kozuka, H. & Yoko, T. (1997). Fluorescence properties of $Ru(bpy)^{2+}_3$ complex incorporated in sol-gel derived silica coating films. *J. Phys. Chem.* B, 101, 2285-2291.

Iwamoto, T. & Mackenzie, J. D., (1995). Ormosil coatings of high hardness. *Journal of Materials Science*, 30, 2566– 2570.

Jacquemin, J., Gomes, M. F. C., Husson, P. & Majer, V. (2006). Solubility of carbon dioxide, ethane, methane, oxygen, nitrogen, hydrogen, argon, and carbon monoxide in 1-butyl-3-methylimidazolium tetrafluoroborate between temperatures 283 K and 343 K and at pressures close to atmospheric. *J. Chem. Thermodyn*., 38 (4), 490–502.

Kamps, A. P. S., Tuma, D., Xia, J. & Maurer, G. (2003). Solubility of CO_2 in the ionic liquid [bmim][PF_6]. *Chem. Eng. Data*, 48, 746-749.

Keefer, K. D. (1990). *Silicon Based Polymer Science: A Comprehensive Resource*; eds. Zeigler, J. M. & Fearon, F. W. G. ACS Advances in Chemistry Ser. No. 224, American Chemical Society: Washington, DC, pp. 227-240.

Kelts, L. W., Effinger, N. J. & Melpolder, S. M. J. (1986). Sol-gel chemistry studied by ^{1}H and ^{29}Si nuclear magnetic resonance. *Non-Crystalline Solids*., 83 (3), 353-374.

Klein, L.C. (1985). Sol-Gel Processing of Silicates. *Ann. Rev. Mater. Sci.*, 15, 227-248.

Klimant, I., Ruckruh, F., Liebsch, G., Stangelmayer, A. & Wolfbeis, O., 1999. Fast response oxygen micro-optodes based on novel soluble Ormosil glasses. *Mikrochimica Acta*, 131, 35– 46.

Kober, E.M. & Meyer, T.J. (1982). Concerning the absorption spectra of the ions $M(bpy)_3^{2+}$ (M = Fe, Ru, Os; bpy = 2,2'-bipyridine). *Inorg. Chem.* 21, 3967–3977.

Koelling, M., Hecht, H. & Holst, G.A. (2002). Simple plastic fiber based optode array for the in-situ measurement of ground air oxygen concentrations.- in: Advanced Environmental Sensing Technology II.- Tuan Vo-Dinh, Stephanus Böttgenbach (Eds.), *Proceedings of SPIE*, 4576, 75-86.

Kuhn, B., Hoyland, S., Zhang, C. C. & Haugland, R. P. (1995). Fluorescent ion indicators for detecting heavy metals. *Proc SPIE-Int'l Soc. Opt. Eng*., 2388, 238-244.

Kuswandi, B. (2000). Optical Chemical Sensors for the Determination of Heavy Metal Ions: A mini review**.** *Jurnal ILMU DASAR,* 1 (2), 18 – 29.

Lakowicz, J. R. (1993). *Principles of Fluorescence Spectrocopy.* Plenum Press: New York and London.

Lau, R. M., Rantwijk, F., Seddon, K. R. & Sheldon, R. A. (2000). Lipase-catalyzed reactions in ionic liquids. *Org. Lett. 2*, 4189-4191.

Lee, Y. G. & Chou, T. C. (2004). Ionic liquid ethanol sensor. *Biosens. Bioelectron.,* 20, 33-40.

Leiner, M. J. P., Wolfbeis, O. S. O.S. Wolfbeis (Editor), Fiber Optic Chemical Sensors and Biosensors, Vol. I., CRC Press, Boca Raton, FL, 1991, p. 359.

Lerchi, M., Bakker, E., Rusterholz, B. & Simon, W. (1992). Lead-selective bulk optodes based on neutral ionophores with subnanomolar detection limits. *Anal. Chem.*, 64 (14), 1534-1540.

Lerchi, M., Reitter, E., Simon, W., Pretsch, E.,Chowdhury, D.A. & Kamata, S. (1994). Bulk optodes based on neutral dithiocarbamate ionophores with high selectivity and sensitivity for silver and mercury cations. *Anal. Chem.* 66: 1713-1717.

Lev, O., Tsionsky, M., Rabinovich, L., Glezer, V., Sampath, S., Pankratov, I. & Gun, J. (1995). Organically modified sol–gel sensors. *Analytical Chemistry,* 67, 22–30.

Liang, C., Yuan, C. Y., Warmack, R. J., Barnes, C. E., & Dai, S. (2002). Ionic liquids: a new class of sensing materials for detection of organic vapors based on the use of a quartz crystal microbalance. *Anal. Chem.,* 74 (9), 2172-2176.

Liu, J.F., Jönsson, J.A., Jiang, G.B. (2005). Application of ionic liquids in analytical chemistry. *Trends Anal. Chem.* 24, 20-27.

Lobnic, A. (1998). Optical characterization of sol-gels and their application to chemical sensors. Ph.D thesis. Graz.

MacCraith, B.D., Ruddy, V., Potter, C., O'Kelly, B. & McGilp, J.F. (1991). Optical waveguide sensor using evanescent wave excitation of fluorescent dye in sol-gel glass. *Electron. Lett.*, 27, 1247.

Malins, C. & MacCraith, B. D. (1998). Dye-doped organically modified silica glass for fluorescence based carbon dioxide gas detection. Analyst, 123 (11), 2373–2376.

Maruszewski, K., Jasiorski, M., Salamon, M. & Strek, W. (1999). Physicochemical properties of Ru bpy entrapped in silicate 3 bulks and fiber thin films prepared by the sol–gel method. *Chemical Physics Letters*, 314, 83–90.

Matos, I., Fernandes, S., Guerreiro, L., Barata, S., Ramos, A. M., Vital, J. & Fonseca, I. M. (2006). The effect of surfactants on the porosity of carbon xerogels. Microporous and Mesoporous Materials 92, 38–46.

Mayr, T. (1999). Neutral carrier based fluorosensor for silver (I) ions. Diploma Thesis, Graz.

Mcevoy, A. K., McDonagh, C. & MacCraith, B. D. (1997). Optimization of sol-gel derived silica films for optical oxygen sensing. Journal of sol-gel science and technology, 8, 1121-1125.

Mills, A., Chang, Q. & McMurray, N. (1992). Equilibrium study on colorimetric plastic film sensors for carbon dioxide. *Anal. Chem.,* 64, 1383-1389.

Miskolczy, Z., Sebok-Nagy, K., Biczok, L. & Gokturk, S. (2004). Aggregation and micelle formation of ionic liquids in aqueous solution. *Chemical Physics Letters,* 400, 296–300.

Mohr, G. J. (23th August, 2006).*A general introduction into optical sensor materials and recognition mechanism.online.* 18th January, 2007, http://www2.uni-jena.de/~c1moge/Mohr/ASCOS2002.pdf).

Morf, W.E., Seiler, K., Rusterholz, B. & Simon, W. (1990). Design of a novel calcium-selective optode membrane based on neutral ionophores. *Anal. Chem.*, 62, 738.

Motellier, S., Michels, M. H., Dureault, B. & Toulhoat, P. (1993). Fibre optic pH sensor for in situ applications. *Sensors and Actuators B*, 11, 467-473.

Mukundan, R., Brosha, E. L., Brown, D.R. & Garzon, F.H. (1999). Ceria-Electrolyte-Based Mixed Potential Sensors for the Detection of Hydrocarbons and Carbon Monoxide, Electrochemical and Solid State Letters, 2(8): 412-414.

Muller, C., Hitzmann, B., Schubert, F. & Scheper, T. (1997). Optical chemo- and biosensors for use in clinical applications. *Sensors Actuators B*, 40, 71–77.

Müller, B. & Hauser, P.C. (1996). Fluorescence optical sensor for low concentrations of dissolved carbon dioxide. *Analyst,*121, 339-343.

Neurauter, G., Klimant I. & Wolfbeis, O. S. (1999). Microsecond Lifetime-Based Optical Carbon Dioxide Sensor Using Luminescence Resonance Energy Transfer. *Anal. Chim. Acta*, 382, 67-75.

Neurauter, G., Klimant, I. & Wolfbeis, O. S. (2000). Fiber-Optic Environment. *J. Anal. Chem.*, 366, 481-487.

Oehme, I. & Wolfbeis, O.S. (1997). Fundamental Review: Optical Sensors for Determination of Heavy Metal Ions. *Mikrochim. Acta*, 126, 177-192.

Oter, O., Ertekin, K., Topkaya, D. & Alp, S. (2006a). Room temperature ionic liquids as optical sensor matrix materials for gaseous and dissolved CO_2. *Sensors and Actuators B*: *Chemical*, 117 (1): 295-301.

Oter, O., Ertekin, K., Topkaya, D. & Alp, S. (2006b). Emission based optical carbon dioxide sensing with HPTS in green chemistry reagents: room temperature ionic liquids. *Analytical and Bioanalytical Chemistry*, 386, 1225-1234.

Park, S., Kazlauskas, R. (2003). Biocatalysis in ionic liquids—advantages beyond green technology. *Curr. Opin. Biotechnol*., 14, 432–437.

Parker, C. A. (1968). *Photoluminescence of Solutions*. Elsevier: Amsterdam.

Pearson, R. G. (1973). *Hard and Soft Acids and Bases*. (eds. Dowden, Hutchinson and Ross), Stroudsburg.

Petrat, F., Rauen, U. & de Groot, H. (1999). Determination of the chelatable iron pool of isolated rat hepatocytes by digital fluorescence microscopy using the fluorescent probe, phen green SK. *Hepatology*, 29(4),1171-1179.

Picard, V., Epsztejn, S., Santambrogio, P., Cabantchik, Z. I. & Beaumont, C. (1998*)*. Role of ferritin in the control of the labile iron pool in murine erythroleukemic cells. *J Biol Chem.*, 273 (25),15382-15386.

Pohl, E. R. & Osterholtz, F. D. (1985). *Molecular Characterization of Composite Interfaces*; eds. Ishida, H. & Kumar, G., Plenum: New York, p. 157.

Pons, C., Forteza, R. & Cerdà, V. (2005). Optical fibre reflectance sensor for the determination and speciation analysis of iron in fresh and seawater samples coupled to a multisyringe flow injection system. *Anal. Chim. Acta,* 528 (2) 197-203.

Prassas, M. & Hench, L. L. (1984). *Ultrastructure Processing of Ceramics, Glasses, and Composites.* eds. Hench, L. L & Ulrich, D. R., John Wiley & Sons: New York, pp. 100-125.

Pulido-Tofino, P., Barrero-Moreno, J. M & Perez-Conde, M. C. (2000). A flowthrough fluorescent sensor to determine Fe(III) and total inorganic iron. *Talanta*, 51 (3), 537-545.

Rantwijk, F., Lau, R. M., & Sheldon, R. A. (2003). Biocatalytic transformations in ionic liquids. *Trends Biotechnol.,* 21, 131–138.

Reichardt, C. (1988). *Solvents and Solvent Effects in Organic Chemistry.* (6th ed.) VCH: Weinheim.

Yang, Z. & Pan, W. (2005). Ionic liquids: Green solvents for nonaqueos biocatalysis. *Enzyme and Microbial Technology,* 37,19–28.

Yang, L. & Saavedra, S.S. (1995). Chemical Sensing Using Sol-Gel Derived Planar Waveguides and Indicator Phases. *Anal. Chem.* 67, 1307-1314.

Yafuso, M. & Suzuki, J. K. (1989). *Gas sensors*, US Patent 4824789.

Sarradin, P. M., Le Bris, N., Le Gall, C. & Rodier, P. (2005). Fe analysis by the ferrozine method: Adaptation to FIA towards in situ analysis in hydrothermal environment. *Talanta*, 66 (5), 1131-1138.

Schmidt, W. (1994). *Optische Spektroskopie*. VCH: Weinheim.

Scovazzo, P., Camper, D., Kieft, J., Poshusta, J., Koval, C. & Noble, R. D. (2004). Regular Solution Theory and CO_2 Gas Solubility in Room-Temperature Ionic Liquids *Ind. Eng. Chem. Res.*, 43 (21), 6855–6860.

Seddon, K. R, Stark, A., & Torres MJ. (2000) Influence of chloride, water, and organic solvents on the physical properties of ionic liquids. *Pure Appl. Chem.*, 72, 2275–2287.

Seiler, K. & Simon, W. (1992). Theoretical aspects of bulk optode membranes. *Anal. Chim. Acta*, 266, 73-87.

Schubert, U. & Husing, N. (2000). *Synthesis of Inorganic Materials*, Wiley-VCH, Wien.

Shahriari, M.R., Murtagh, M.T. & Kwon, H.C. (1997). Ormosil thin films for chemical sensing platforms. *Proceedings of SPIE,* 3105, 40– 51.

Shimizu,Y. & Egashira, M. (1999). Basic aspects and challenge of semiconductor gas sensors. *MRS Bull.*, 24 (6), 18–24.

Song, A., Parus, S. & Kopelman, R. (1997). High-performance fiber-optic pH microsensors for practical physiological measurements using a dual-emission sensitive dye. *Anal Chem.* 69 (5), 863–867.

Stumm, W. & Morgan, J. J. (1981). *Aquatic Chemistry*. (2nd ed.), Wiley: New York.

Sweeny, B. K. & Peters, D. G. (2001). Cyclic voltammetric study of the catalytic behavior of nickel(I) salen electrogenerated at a glassy carbon electrode in an ionic liquid (1-butyl-3-methylimidazolium tetrafluoroborate, $BMIM^{+}BF_4^{-}$). *Electrochemistry Commun.* 3 (12), 712-715.

Szmacinski, H. & Lakowicz, J. R. (1993). Optical measurements of pH using fluorescence lifetimes and phase-modulation fluorometry. *Anal. Chem*., 65, 1668-1674.

Tan, W., Shi, Z.-Y. & Kopelman, R. (1992). Development of. submicron chemical fibre oplic sensors. *Anal. Chem.* 64, 2985-2990.

Tan, W., Shi, Z., Smith, S., Birnbaum, D. & Kopelman, R. (1992). Submicrometer intracellular chemical optical fiber sensors. *Science,* 258, 778-781.

Thompson, R. B. & Lakowicz, J. R. (1993). Fibre optic sensor based on phase fluorescence lifetimes. *Anal Chem*., 65, 835-856.

Xu, W.Y., McDonough, R.C., Langsdorf, B., Demas, J.N. & DeGraff, B.A. (1994). Oxygen Sensors based on luminescence quenching: Interaction of metal complexes with the polymersupports. *Anal. Chem,* 66, 4133-4141.

Xu, Z., Rollins, A., Alcala, R. & Marchant, R.E. (1998). A novel fiber optic pH sensor incorporating carboxy SNAFL-2 and fluorescent wavelength-ratiometric detection. *Journal of Biomedical Materials Research,* 39, 9-15.

Vanyur, R., Biczok, L. & Miskolczy, Z. (2007). Micelle formation of 1-alkyl-3-methylimidazolium bromide ionic liquids in aqueous solution. *Colloids Surf. A: Physicochem. Eng. Aspects*, doi:10.1016/j.colsurfa.2006.11.049.

Velapoldi, R. A. & Tonnesen, H. H. (2004). Corrected emission spectra and quantum yields for a series of fluorescent compounds in the visible spectral region. *Journal of fluorescence*, 14 (4), 465-472.

Wang, R., Okajima, T., Kitamura, F., & Ohsaka, T. (2004). A Novel O2 Gas Sensor Based on Supported Room Temperature Ionic Liquid Membrane-Coated Electrodes. *Electroanalysis,* 16 (1-2), 66-72.

Wassercheid, P. & Kleim, W. (2000). Ionic liquids-new solutions for transition metal catalysis. *Angew. Chem.* Int., 39, 3772-3789.

Wasserscheid, P. & Welton, T. (Eds.) *Ionic Liquids in Synthesis*. Wiley–VCH, Weinheim, 2003.

Weigl, B. H. & Wolfbeis, O. S. (1995). New Hydrophobic Materials for Optical Carbon Dioxide Sensors Based on Ion Pairing. *Anal. Chim. Acta.* 302 (2/3), 249-254.

Welton, T. (1998). Room temperature ionic liquids, solvents for synthesis and catalysis. *Chem. Rev.*, 99, 2071-2083.

Welton, T. (2004). Ionic liquids in catalysis. *Coord. Chem. Rev*. 248, 2459–2477.

Werner, T. & Wolfbeis, O. S. (1993). Optical sensor for the pH 10–13 range using a new support material. *Anal. Chem.,* 346, 564-568.

Williams, A. T. R., Winfield S. A. & Miller, J. N. (1983). Relative fluorescence quantum yields using a computer controlled luminescence spectrometer. *Analyst*, 108, 1067.

Wolfbeis, O. S. (Ed.) (1991). Fiber Optic Chemical Sensors and Biosensors. *CRC Press: London.*

Wolfbeis, O. S., Kovacs, B., Goswami, K. & Klainer, S. M. (1998). Fiber-optic fluorescence carbon dioxide sensor for environmental monitoring. *Microchim. Acta.* 129 (3/4), 181-188.

Wolfbeis, O. S. & Schaffar, B. P. H. (1987). An Ion-selective Optrode for Potassium. *Anal. Chim. Acta.,* 198, 1-12.

Yamazoe, N. & Miura, N. (1996). Prospect and Problems of Solid Electrolyte-Based Oxygenic Gas Sensors. *Journal of Solid State Ionics*, 86-88 (Part II): 987-993.

Zhang, Z. X., Xie, Y. Y & Shi, Y. (1999). Spectrophotometric Determination of Iron Using Eriochrome Cyanine R As Extractant with Phase-Separation. *Spectroscopy and Spectral Analysis,* 19 (2), 241-243.

Zhang, H., Li, B., Lei, B., Li, W. & Lua, S. (2006). Preparation and oxygen sensing properties of a sol–gel derived thin film based on a covalently grafted ruthenium(II) complex. *Sens. Actuators B: Chem.* doi:10.1016/j.snb.2006.09.036.